

Charles University
Faculty of Science

University of Bordeaux
ED 304, Sciences and environment

Study program:
Anthropology and Human Genetics

Study program:
Biological Anthropology



université
de **BORDEAUX**

Mgr. Rebeka Rmoutilová

**VIRTUAL RECONSTRUCTION, INTERESTS AND CONTRIBUTION TO THE
PALEOBIOLOGICAL STUDIES OF FOSSIL HUMANS**

**Virtuální rekonstrukce, její význam a přínos k paleobiologickému studiu fosilního
člověka**

**Outils de la reconstruction virtuelle, intérêts et apports pour l'étude paléobiologique
des Hommes fossiles**

Dissertation

Supervisors: Prof. RNDr. Jaroslav Brůžek, Ph.D.

Bruno Maureille, Ph.D., DR

Consultant: Doc. RNDr. Jana Velemínská, Ph.D.

Prague 2020

Student declaration

Hereby I declare that I worked out this thesis independently, using only the listed resources and literature, and I did not present it to obtain another academic degree.

Prohlašuji, že jsem závěrečnou práci zpracovala samostatně a že jsem uvedla všechny použité informační zdroje a literaturu. Tato práce ani její podstatná část nebyla předložena k získání jiného nebo stejného akademického titulu.

In Prague, 9. 12. 2019

Signature:

Supervisor declaration

On behalf of all the co-authors, I declare that Mgr. Rebeka Rmoutilová substantially contributed to all presented publications. For her first-author publications, she designed experiments, performed data analyses, interpreted results, and prepared manuscripts.

Jménem všech spoluautorů prohlašuji, že Mgr. Rebeka Rmoutilová zásadně přispěla ke všem publikacím, jež jsou nedílnou částí této disertační práce. U publikací, kde je první autorkou, samostatně designovala a prováděla experimenty, analýzy dat, interpretaci výsledků a přípravu manuskriptů.

In Prague, 9. 12. 2019

Signature:

ACKNOWLEDGEMENT

I am very grateful to my supervisors for their patience during all the years of my thesis. I thank Jaroslav Brůžek for his innumerable encouragements to keep working despite my doubts and for his full engagement despite whatever it cost him. And I thank Bruno Maureille who was always patiently listening to all I wanted to discuss despite my level of spoken French. I am equally grateful to Jana Velemínská for letting me be a part of the 3D lab and for her trust.

I would not be able to proceed with my dissertation without Pierre Guyomarc'h, Yann Heuzé and Renaud Lebrun who introduced me to the methods of virtual reconstruction, showed me available software, and encouraged me in using R and scripting. I am also grateful to Ronan Ledevin who made the additional micro-CT scans of Regourdou and who helped in with some technical things.

Furthermore, I thank Asier Gómez-Olivencia, Martin Hora, Karen Rosenberg and Vito Sparacello for their help and discussions and for their very kind and friendly approach. In addition, I am grateful to Asier and Martin for their comments to this manuscript.

I also thank my colleague, Anežka, that we could share together various problems during those many years of studies. I am very grateful to Lenka Červenková for her helpfulness and for her perfect order that was exemplary for me. I thank the people who stayed in PACEA during the three years (Claire, Caroline, Dany, Antony, Vito, Irene, Mikel, Eline) – they were always very kind during my stays in Bordeaux and were helping me in various ways.

My great personal thanks belong to my husband who always tried to understand my “anthropological” problems and was very supportive when we were together or in different countries. I also thank my family whose “view from the outside” was sometimes encouraging, sometimes disappointing, keeping me balanced. I greatly thank Annick for letting me stay with her in her comfortable house in Bordeaux where I could always return not feeling lonely.

I thank to the following institutions for their support of my project: Grant Agency of Charles University (grant number 1088217) and Irene Levi Sala CARE Archaeological Foundation.

I am grateful to following institutions and their researchers and curators who allowed me to study fossil material deposited in their care and for providing 3D digitized material:

Musée National de Préhistoire in Les Eyzies-de-Tayac, Musée de l'Homme, Landesmuseum in Bonn and Tel Aviv University. Digitized material from the Krapina site was provided to my supervisor via NESPOS database. I thank Vitale Sparacello for the 3D models of Upper Paleolithic pelves and Asier Gómez-Olivencia for conveying me the surface model of the La Chapelle 1 right coxal bone.

ABSTRACT

Preservation is a major obstacle in paleoanthropological studies. Since 1990s virtual methods have become an important part of anthropological research helping to overcome preservation problems in two principle ways: they improve extraction of information from a fragmentary material, and they permit a more objective reconstruction of fragmentary and incomplete remains. This thesis has focused on the virtual reconstruction of two fossil specimens: the modern human cranium from the Upper Paleolithic site of Zlatý kůň (ZK; Czech Republic) and the Neandertal Regourdou 1 (R1) pelvis (France). The reconstruction of the ZK cranium allowed us to revise sex attribution and analyze morphological affinity. Based on the secondary sex diagnosis, the ZK individual was most probably a female and exhibits a great affinity to Early Upper Paleolithic population. The R1 pelvis shows considerable asymmetry that was first analyzed on the sacrum in comparison with healthy modern humans and Neandertals. The asymmetry exceeds normal variation observed in the extant population and could have related to asymmetrical load dissipation. Therefore, the asymmetry was considered in the subsequent preliminary pelvic reconstruction which allowed us to assess sex of the individual and to analyze transverse dimensions of the pelvic canal and orientation of the sacrum in the pelvis. Based on the newly available sexually dimorphic traits, the R1 individual was probably a male. Transverse canal diameters indicate slightly wider outlet than in modern males, but they show similar relationship as in other archaic humans. Regarding the high degree of correlation between sacral orientation and lumbar lordosis, R1 had slightly higher lumbar lordosis angle (close to modern mean) than has been proposed for most of other Neandertals. This slightly extends the previously suggested Neandertal range of variation, which, however, still remains in the lower portion of modern human variation. In other presented studies, we focused on sex estimation from fragmentary remains and compatibility of 3D data digitization techniques. Specifically, we proposed a method for sex estimation from the posterior ilium and adjusted the visual method of Brůžek (2002) to the use on fragmentary material. Finally, we compared two different 3D scanners and their outcomes. They did not significantly differ with regard to subsequent anthropological analyses (sex and age estimation), but they may provide differential results in highly structured areas.

Keywords: virtual reconstruction, geometric morphometrics, sexual dimorphism, skull, pelvis, Neandertals

ABSTRAKT

Zachovalost kosterního materiálu je hlavní překážkou paleoantropologických studií. Virtuální metody se od 90. let 20. století staly důležitou součástí antropologického výzkumu, přičemž značně pomáhají překonat problémy zachovalosti, a to dvěma hlavními způsoby: zlepšují extrakci informací z fragmentárního materiálu a umožňují objektivnější rekonstrukci fragmentárních a nekompletních nálezů. Tato práce se zaměřila na virtuální rekonstrukci dvou fosilních nálezů: lebky moderního člověka Zlatý kůň (ZK; Česká republika) ze svrchního paleolitu a neandertálské pánve Regourdou 1 (R1) z Francie. Rekonstrukce lebky ZK nám umožnila revidovat pohlavní diagnózu a analyzovat její morfologickou afinitu. Na základě sekundární pohlavní diagnózy byl jedinec ZK s vysokou pravděpodobností žena a lebka vykazuje afinitu k rané svrchně paleolitické populaci. Pánev R1 vykazuje značnou asymetrii, která byla nejprve analyzována na křížové kosti v porovnání se zdravými moderními lidmi a neandertálci. Asymetrie výrazně překračuje variabilitu pozorovanou v současné populaci a mohla souviset s asymetrickým přenosem zátěže. Výrazná asymetrie byla proto zohledněna při následné rekonstrukci pánve, která nám umožnila posoudit pohlaví jedince a analyzovat transversální rozměry pánevního kanálu a orientaci křížové kosti. Na základě nově dostupných pohlavně dimorfních znaků byl jedinec R1 pravděpodobně muž. Rozměry kanálu naznačují mírně širší východ než u moderních mužů, ale vykazují podobný vztah jako u dalších archaických nálezů. Vzhledem k vysoké korelaci mezi orientací křížové kosti a bederní lordózou měl R1 mírně vyšší úhel bederní lordózy (blízký modernímu průměru), než bylo navrženo pro většinu ostatních neandertálců. To rozšiřuje dříve navržený interval hodnot u neandertálců, který však stále zůstává v dolní části variability moderního člověka. V dalších prezentovaných studiích jsme se zaměřili na odhad pohlaví z fragmentárních nálezů a testování kompatibility různých technik digitalizace 3D dat. Konkrétně jsme navrhli metodu pro odhad pohlaví z posteriorní části ilia a upravili vizuální metodu Brůžka (2002) k použití na fragmentární materiál. Nakonec jsme porovnali dva různé 3D skenery a jejich výstupy. S ohledem na následné antropologické analýzy (odhad pohlaví a věku) se výstupy obou skenerů významně nelišily, ale skenery mohou poskytnout rozdílné výsledky ve více strukturovaných oblastech.

Klíčová slova: virtuální rekonstrukce, geometrická morfometrie, pohlavní dimorfismus, lebka, pánev, neandertálci

RÉSUMÉ

La préservation est un obstacle majeur dans les études paléoanthropologiques. Depuis les années 1990, les méthodes virtuelles sont devenues un élément important de la recherche anthropologique aidant à surmonter les problèmes de préservation de deux manières principales : elles améliorent l'extraction d'informations à partir de matériel fragmentaire et elles permettent une reconstruction plus objective des fossiles fragmentaires et incomplets. Cette thèse s'est concentrée sur la reconstruction virtuelle de deux spécimens fossiles: le crâne humain moderne du site du Paléolithique supérieur de Zlatý kůň (ZK ; République tchèque) et le bassin néandertalien de Regourdou 1 (R1 ; France). La reconstruction du crâne de ZK nous a permis de réviser la diagnose sexuelle et d'analyser son affinité morphologique. Selon la diagnose sexuelle secondaire, l'individu de ZK était très probablement une femme et le crâne présente une grande affinité avec la population de la période ancienne du Paléolithique supérieur. Le bassin de R1 montre une asymétrie considérable qui a été analysée sur le sacrum en comparaison avec un échantillon moderne d'individus sains et un échantillon néandertalien. L'asymétrie dépasse considérablement la variation dans la population récente et elle aurait pu être liée à une transmission déséquilibrée du poids. Par conséquent, l'asymétrie a été prise en compte dans la reconstruction pelvienne qui a permis d'évaluer le sexe de l'individu et d'analyser les dimensions transversales du canal pelvien et l'orientation du sacrum. Sur la base des caractères sexuels disponibles, l'individu de R1 était probablement un homme. Les dimensions du canal pelvien indiquent une sortie légèrement plus large que chez les hommes modernes, mais ils montrent une relation similaire à celle d'autres spécimens archaïques. En considérant la corrélation forte entre l'orientation de sacrum et la lordose lombaire, R1 avait l'angle de lordose lombaire légèrement plus élevé (proche de la moyenne moderne) que celui proposé pour la plupart des autres Néandertaliens. Cela étend légèrement l'intervalle de variation néandertalienne précédemment suggérée, qui reste cependant dans la partie inférieure de la variation moderne. Dans d'autres études présentées, nous nous sommes concentrés sur l'estimation du sexe à partir de restes fragmentaires et l'analyse de compatibilité des techniques de numérisation des données 3D. Plus précisément, nous avons proposé une méthode d'estimation du sexe à partir de l'ilium postérieur et nous avons ajusté la méthode visuelle de Brůžek (2002) à l'utilisation sur un matériel fragmentaire. Enfin, nous avons comparé deux scanners 3D et leurs

résultats. Ils ne diffèrent pas de manière significative en ce qui concerne les analyses anthropologiques (estimation du sexe et de l'âge), mais ils peuvent fournir des résultats différentiels par rapport au détail dans des parties plus structurées.

Mots clés : reconstruction virtuelle, morphométrie géométrique, dimorphisme sexuel, crâne, bassin, Néandertaliens

LIST OF ABBREVIATIONS

(cal) BP ... calibrated years before present

CT ... computed tomography

DNA ... deoxyribonucleic acid

DSP ... *Diagnose sexuelle probabiliste*

GM ... geometric morphometrics

GPA ... Generalized Procrustes analysis

ICP ... Iterative closest point

ky ... thousand years

LGM ... Last Glacial Maximum

LL ... lumbar lordosis

MRI ... magnetic resonance imaging

PI ... pelvic incidence

post-LGM ... after the Last Glacial Maximum

pre-LGM ... before the Last Glacial Maximum

R1 ... Regourdou 1

SH ... Sima de los Huesos

SI(J) ... sacroiliac (joint)

SVM ... Support Vector Machine

TPS ... thin plate spline

ZK ... Zlatý kůň

LIST OF FIGURES

Figure 1. Effect of position <i>in situ</i> and movements of stratigraphic layers on shape of the fossil	6
Figure 2. Steps of Generalized Procrustes Analysis	8
Figure 3. Criteria for semilandmark sliding.....	10
Figure 4. The effect of landmark number on the warping of the reference specimen	18
Figure 5. Central European sites with most important human skeletal remains from the Magdalenian or Final Paleolithic	25
Figure 6. Regourdou 1 (R1) pelvic remains.....	38
Figure 7. Alignment of the R1 right ischial fragment to the ilium	41
Figure 8. Colormap of distances between preserved complementary parts of the superimposed ilia of R1	42
Figure 9. Estimation of the incomplete right acetabulum of R1	43
Figure 10. Removal of fractures and gaps in the R1 ilia.....	44
Figure 11. Summary of the reconstruction of both coxal bones of R1	45
Figure 12. Male (M) and female (F) forms of visual traits from the method of Brůžek (2002).....	47
Figure 13. Linear dimensions from DSP (Brůžek et al., 2017)	47
Figure 14. Definition of pelvic incidence angle (PI) and lumbar lordosis angle	48
Figure 15. Comparison of outcomes of different SIJ assemblies in R1	51
Figure 16. 3D printed models of the R1 sacrum and right coxal bone assembled together.	53
Figure 17. Final state of the R1 pelvic reconstruction	53
Figure 18. Visual sex traits in R1 following Brůžek (2002).....	59
Figure 19. Analysis of shape in pelvic inlet and outlet.....	62
Figure 20. Inlet and outlet transverse diameters	63

LIST OF TABLES

Table 1. Different types of landmarks used in geometric morphometrics.....	7
Table 2. List of adult pelvic remains from the Neandertal lineage.....	33
Table 3. Comparative specimens	39
Table 4. Summary of different assemblies of sacroiliac joint.	50
Table 5. Linear dimensions of the reconstructed Regourdou 1 pelvis in comparison with the previous reconstruction.....	55
Table 6. Scoring of Neandertal sexual traits.....	56
Table 7. Linear dimensions of the Neandertal specimens for sex diagnosis	57
Table 8. Sex estimates of Neandertal specimens based on the visual and metrical methods with summary of congruency with literature data.	58
Table 9. Summary of pelvic linear dimensions	61
Table 10. Variation of pelvic incidence angle	64
Table 11. Estimated lumbar lordosis angle.....	65

TABLE OF CONTENTS

ACKNOWLEDGEMENT	iii
ABSTRACT.....	v
ABSTRAKT	vi
RÉSUMÉ	vii
LIST OF ABBREVIATIONS.....	ix
LIST OF FIGURES	x
LIST OF TABLES.....	xi
TABLE OF CONTENTS.....	xiii
1 Introduction	1
1.1 Objectives.....	3
1.2 Dissertation structure	4
2 Taphonomy.....	5
3 Geometric morphometrics and information extraction	7
4 Virtual reconstruction.....	10
4.1 Fragment reassembly	11
4.2 Estimation of missing parts.....	12
4.3 Retrodeformation	15
4.4 Evaluation of reconstruction reliability.....	16
5 Comparability of digitization techniques	19
5.1 Comparative studies	21
6 Summary of presented articles	24
7 Preliminary reconstruction of the Regourdou 1 pelvis.....	31
7.1 Material	32
7.2 Methods.....	40
7.2.1 Reconstruction.....	40
7.2.2 Analysis.....	46
7.3 Results.....	49
7.3.1 Sacroiliac joint assembly.....	49
7.3.2 Validation of the reconstruction.....	54

7.3.3	Sex diagnosis.....	55
7.3.4	Comparative analysis	60
7.4	Discussion and conclusions.....	66
7.4.1	Pelvic reconstruction	66
7.4.2	Sex diagnosis in Neandertals.....	68
7.4.3	Pelvic canal dimensions	70
7.4.4	Spinopelvic alignment.....	72
8	Conclusion	75
9	Perspectives	76
	SHRNUTÍ (Czech Summary)	77
	RÉSUMÉ (French Summary)	82
	BIBLIOGRAPHY	87
	APPENDICES	106
A.	List of presented publications	106
B.	List of other published work	107
	Conference abstracts.....	107
	Publications in other periodicals and monographies	107
C.	Presented publications.....	108
	Virtual reconstruction of the Upper Palaeolithic skull from Zlatý Kůň, Czech Republic: Sex assessment and morphological affinity	108
	A case of marked bilateral asymmetry in the sacral alae of the Neandertal specimen Regourdou 1 (Périgord, France).....	149
	Geometric morphometric and traditional methods for sex assessment using the posterior ilium.....	175
	Impact of 3D surface scanning protocols on the Os coxae digital data: Implications for sex and age-at-death assessment	185
	A method of sexing the human os coxae based on logistic regressions and Bruzek's nonmetric traits.....	195

1 Introduction

Preservation is a major obstacle in paleoanthropological studies limiting inclusion of fragmentary and incomplete fossil specimens to a wider range of analyses. Recently, emphasis has been put on the reconstruction of fossils in order to increase reliability and objectivity of the reconstruction process and subsequent scientific interpretations (Gunz et al., 2009). Traditionally, reconstruction was performed by an experienced researcher often using original fossil remains (White and Folkens, 2005). Not only that the fossil remains were in many cases further damaged by this procedure (Thompson and Illerhaus, 1998; Ponce de León and Zollikofer, 1999), but physical reconstruction is inherently based on personal impressions and experience leading to hardly reproducible outcomes.

In 1990s, a new approach called virtual reconstruction was introduced in response to this problem (Kalvin et al., 1992, 1995; Zollikofer et al., 1995). Development of new tools in anthropology followed increased availability of medical imaging methods, such as computed tomography (CT), that produce digitized copies of physical objects (Spoor et al., 2000a). Therefore, a methodological framework combining digitized 3D data and computer tools was developed to address reconstruction of taphonomically damaged specimens in a more concise and reproducible way (Zollikofer and Ponce de León, 2005). In contrast to physical reconstruction, virtual approach is based not only on anatomy but also on mathematical and geometrical principles providing an exact protocol that can be repeated by an independent researcher. Although subjectivity cannot be completely eliminated during the reconstruction process, the new approach minimizes its effect and allows examination of multiple possible forms (Weber and Bookstein, 2011). Finally, the reconstructed specimen can be transferred back to the real world and it can serve for educational or exhibition purposes (Garas et al., 2018; Bastir et al., 2019) as a means of mediating scientific research to the public (Rahman et al., 2012; Schlager and Wittwer-Backofen, 2015; Profico et al., 2019a).

Nonetheless, the reconstruction of missing parts has natural limitations, and thus it is necessary to maximize information that is possible to extract from fragmentary or few fossil remains (Zollikofer et al., 1998; Bräuer et al., 2004). To give an example, this trend is evident in sex estimation methods. As sex is an important parameter associated with physical and behavioral differences, many studies are interested in morphological variability and behavioral patterns related to sex in past populations (Fruyer, 1980; Kuhn and Stiner, 2006; Villotte et al., 2010; Hora and Sladek, 2014; Estalrich and Rosas, 2015;

Sládek et al., 2016; Sparacello et al., 2017). Although there is a general agreement that sex diagnosis is most reliable from the pelvis due to different selection pressures in males and females (Stewart, 1984; Rosenberg and Trevathan, 2002; Brůžek and Murail, 2006; Fischer and Mitteroecker, 2017), pelvic remains are not always sufficiently preserved. Therefore, methods of sex estimation need to be adjusted to differential states of preservation of pelvic remains and new methods need to be created and tested on other skeletal regions (Brůžek et al., 1996; Brůžek, 2002; Murail et al., 2005).

Imaging techniques and geometric morphometrics (GM) methods greatly help in respect of studying fragmentary remains. GM is a set of tools that permits statistical analyses of form and shape (Bookstein, 1991). It is based on configurations of landmarks that conserve geometrical relationships of studied objects and permit comprehensible visualization of shape changes. In addition, 3D imaging techniques used in medical diagnostics penetrate the object and they allow studying hidden or inaccessible structures (Weber et al., 2001; Braga et al., 2019). Combined with GM methods, this set of tools improves information extraction from structures that could not be adequately analyzed with methods of traditional morphometrics (Zollikofer et al., 1998; Bräuer et al., 2004).

In summary, virtual methods help to overcome the problem of preservation in two main ways: first, imaging techniques and new morphometric methods extract more information from partial bone fragments (Zollikofer et al., 1998; Bräuer et al., 2004); second, virtual methods of reconstruction enable a more reproducible way of reconstructing incomplete specimens in order to include them in a wider range of analyses (Zollikofer, 2002; Gunz et al., 2009). However, new methods and techniques go hand in hand with new problems and questions that must be addressed in order to keep results reproducible (Slizewski et al., 2010; Mestekova et al., 2015; Mullins and Albanese, 2018).

1.1 Objectives

The main focus of this dissertation is on the virtual reconstruction of two fossil specimens: the Upper Paleolithic cranium Zlatý kůň (ZK) from the Czech Republic (Vlček, 1956; Svoboda et al., 2002) and the Neandertal pelvis Regourdou 1 (R1) from France (Piveteau, 1959; Meyer et al., 2011; Maureille et al., 2015a). Despite completely different chronological and taxonomical attributions, both specimens are fragmentary and incomplete and need to be reconstructed before addressing specific questions that relate to research history of these specimens or their broader evolutionary context.

We enter the issue of virtual reconstruction with the Zlatý kůň cranium which is advantageous, as the virtual methodological framework has originally been established on skulls in particular. Zlatý kůň, unlike majority of its contemporary specimens, was discovered in the Bohemian part of the Czech Republic. With regard to the history of this specimen, we aim to perform the reconstruction with two particular objectives: revise its sex diagnosis and analyze its morphological affinity in comparison with Upper Paleolithic human populations.

Regourdou 1 has one of the most complete pelvises from European Neandertals. However, the pelvis shows a considerable asymmetry most noticeable in the sacrum. To better understand this asymmetry, the sacral morphology is quantitatively analyzed prior to the pelvic reconstruction. Subsequent preliminary pelvic reconstruction is aimed at revising sex diagnosis of this specimen and at exploring newly available pelvic canal dimensions and relative orientation of the sacrum within the pelvis.

Our secondary aims relate to the use of 3D imaging and GM methods in addressing questions of sex diagnosis from fragmentary material and reliability of different digitizing methods. Focusing on the former aim, we analyze accuracy of sex estimation from the posterior ilium, which is usually better preserved in archeological record than the ischio-pubic region. For this purpose, we also revise previously suggested sexual dimorphism in shape of the iliac auricular surface, and we compare traditional and geometric morphometric approaches in the estimation of sex. In addition, we perform a revision of the visual method introduced by Brůžek (2002) that takes into account differential preservation of skeletal remains. Simultaneously, we test visual assessment of sexually dimorphic traits on digitized skeletal material. Finally, as the virtual approach largely depends on 3D data that can be acquired by various techniques, we compare two surface scanners and examine their impact on anthropological analyses of sex and age.

1.2 Dissertation structure

The dissertation is compiled from five published articles and is supplemented by an unpublished section on the preliminary reconstruction of the Regourdou 1 pelvis. The next chapters address major contributions of virtual methods following the two principal paths introduced above so that the reader is acquainted with the current methodological framework that is particularly important for virtual reconstruction of fossils. We start by explaining origin of various taphonomical disturbances, and we continue with the use of geometric morphometrics methods for information extraction from fragmentary remains. Special focus is given to the explanation of methods of virtual reconstruction and their reliability. Finally, we address questions regarding the compatibility of different 3D digitization techniques. After the theoretical background, in chapter 6 we summarize contributions of the articles that are attached to the thesis (Appendix A and C). The following chapter presents the unpublished reconstruction of the R1 pelvis that is accompanied with sufficient theoretical context and methodological background. Final chapters summarize main contributions of the thesis and explain future perspectives.

2 Taphonomy

The preservation of fossil remains can be influenced by various processes before and especially after death of an organism. For fossil specimens, diagenetic changes occurring after deposition of the dead body into the lithosphere are of special importance (Lyman, 1994). As a whole, the diagenetic process depends on many factors such as bone material, climate, depositional mode, sediment character and time span (Lyman, 1994); all of them contribute to the alteration of the bone content: organic matter is gradually removed and mineral content can be dissolved, replaced or enriched depending on specific chemical elements (Henderson et al., 1983). These structural alterations change physical properties of the bone that can even result in a change of its form (Fernandez-Jalvo and Andrews, 2016).

Generally, post-depositional processes can lead to four principal disturbances that have a direct impact on the specimen's representation and the choice of a reconstruction technique (Weber and Bookstein, 2011):

- type 1 = fragmentation,
- type 2 = incompleteness,
- type 3 = plastic deformation,
- type 4 = extrinsic material.

Fragmentation and incompleteness are very common in paleoanthropological and archeological material. While the bone loses both its organic and mineral content, it becomes less resistant to external forces. Furthermore, the overlying sediments become more compact with increasing time and press the bone with a greater weight (Lyman, 1994). This can have two consequences depending on the bone's mechanical properties: fracture or deformation (Zollikofer and Ponce de León, 2005). After fracturing, fragments are dislocated, but they do not show apparent deformation.

Plastic deformation results from the de- and re-mineralization processes during fossilization which in long-term action may considerably change bone geometry while the integrity remains intact (Figure 1). As such, deformation is rather associated with fossilized material covered with thicker layer of sediments that exerts greater pressure (Zollikofer and Ponce de León, 2005). Potential relationship between *in situ* positioning and plastic deformation was also studied in archeological skulls from recent historical periods. However, the established relationship between the skull shape and the *in situ* position was more probably interpreted as though the position was a consequence of the original skull

shape (Jurda et al., 2015). As plastic deformation does not involve breakage, it must be distinguished from physiological or pathological condition (Fernandez-Jalvo and Andrews, 2016).

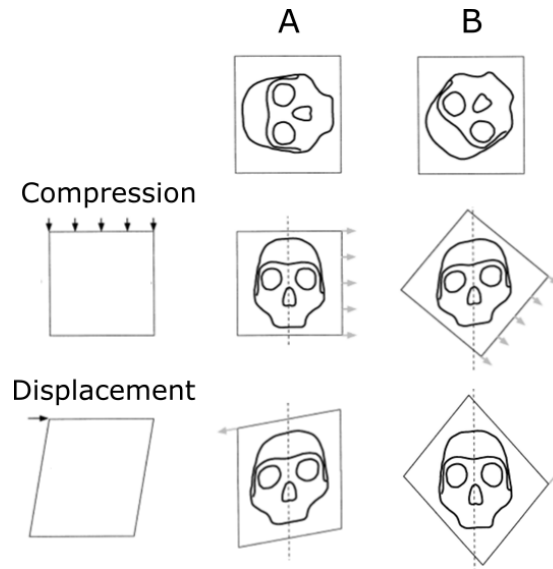


Figure 1. Effect of position *in situ* (A, B) and movements of stratigraphic layers (compression and displacement) on shape of the fossil. Compression in B and displacement in A result in a uniform shear that is possible to correct with symmetrization (adapted from Ponce De León and Zollikofer, 1999).

Special type of deformation is a so-called expanding matrix distortion or a brittle deformation; bone is fragmented into very tiny pieces whose integrity is maintained by matrix filling that expands in a nonlinear way (White, 2003; Arbour and Currie, 2012). In fact, it is a combination of type 1 and 4 defects.

The fourth type of disturbance is when an object or its parts are not accessible because they are covered by or embedded in a foreign material (Weber and Bookstein, 2011). This may happen during the time the fossil lies in sediments in the form of encrustation or cavity fillings (Lyman, 1994). However, it may also concern intentionally added material, such as plaster or clay, from previous physical reconstructions that often used coloring to match the color of the fossilized bone. Therefore, the added material cannot be reliably distinguished by naked eye (Thompson and Illerhaus, 1998; Nerudová et al., 2019). To disengage the studied object, foreign material can be removed virtually using a CT scan; the unwanted material can be recognized based on different density or homogeneity of the inner structure (Bräuer et al., 2004).

3 Geometric morphometrics and information extraction

Geometric morphometrics can be used to analyze differences in shape which result from various biological processes (Bookstein, 1991; Zelditch et al., 2004). In contrast to traditional morphometrics, GM depends on Cartesian coordinates of landmarks. Unlike linear measurements, coordinates provide spatial relationships within the configuration, and thus they preserve information on structure's shape allowing comprehensible visualization of results. Landmarks are points that are located at homologous positions across specimens, and they can be divided into several types based on their homology (Table 1). During a standard GM analysis, configurations of landmarks are superimposed using Generalized Procrustes Analysis (GPA) that separates shape and size components. GPA is an iterative process consisting of three steps (Figure 2): translation of objects so that the centroids are superimposed; scaling onto the unit size represented by centroid size of each object; rotation of objects while minimizing sum of squared distances between homologous landmarks (Zelditch et al., 2004). Finally, all specimens are superimposed and effects of differences in position, size and orientation are filtered out

Table 1. Different types of landmarks used in geometric morphometrics (following Bookstein, 1991; Gunz and Mitteroecker, 2013).

Landmark type	Group of landmarks	Homology	Definition
Type 1	Fixed	Anatomical	Juxtaposition of tissue types (0 degrees of freedom)
Type 2	Fixed	Geometrical	Extreme curvature (0 degrees of freedom)
Type 3	Fixed	Geometrical	Extreme distance (0 degrees of freedom)
Curve semilandmarks	Sliding	Geometrical	Landmark sliding along a curve (1 degree of freedom)
Surface semilandmarks	Sliding	Geometrical	Landmark sliding on a surface (2 degrees of freedom)

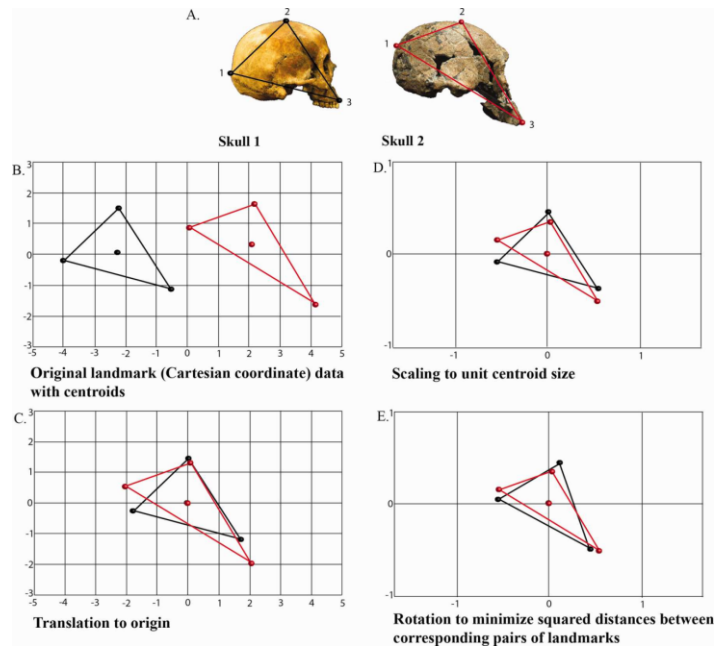


Figure 2. Steps of Generalized Procrustes Analysis illustrated on three cranial landmarks (from Baab et al., 2012).

Despite many advantages of analyzing landmark configurations, commonly used landmarks (types 1 to 3) are usually not evenly distributed over biological specimens (Zollikofer et al., 1998). This is an important shortcoming, as there are often large areas without any fixed landmarks, and thus common GM methods cannot convey any information from such regions. Therefore, several methods have appeared that can be used for structures lacking a great number of classical landmarks. They are so-called homology-free non-landmark methods that use registration of whole meshes (Dupej et al., 2014; Durrleman et al., 2014). These methods provide a general analysis of global geometry (Bruner, 2019) in a fairly short amount of time (Gunz and Mitteroecker, 2013). However, point homology across specimens is not always guaranteed as in landmark analyses, and for now, they are not adapted to fragmentary remains (Gunz and Mitteroecker, 2013; Bruner, 2019). Therefore, special landmarks called sliding semilandmarks were introduced that are more in control of the researcher. Using semilandmarks, one can exploit information from structures that were previously neglected due to the lack of consistent traditional examination or lack of classical landmarks (González et al., 2007; Anastasiou and Chamberlain, 2013; Velemínská et al., 2013; Braga et al., 2019). Moreover, they also serve for the purpose of virtual reconstruction of missing parts (Bookstein, 1997; Gunz et al., 2005; Gunz and Mitteroecker, 2013).

Sliding semilandmarks are points that are not biologically but geometrically homologous. Their position on the object is determined by a homologous curve or surface on which semilandmarks are located through a process called sliding after which they can be treated the same way as classical landmarks (Gunz and Mitteroecker, 2013). During sliding, semilandmarks change their positions according to minimization of differences between the current configuration and the reference configuration (a template or a sample mean). The difference between both configurations can be computed by two algorithms (Perez et al., 2006): Thin-Plate Spline (TPS) bending energy or GPA Procrustes distance. The TPS algorithm is a function defined for warping one object onto another while the measure of deformation expressed as bending energy is minimized (Bookstein, 1989). Procrustes distance is a square root of the sum of squared distances between corresponding landmarks of two superimposed configurations. Both criteria have different assumptions about the involved process and the differences are graphically represented in Figure 3. To calculate bending energy, a whole set of landmarks and semilandmarks is taken into account, and sliding of each semilandmark is influenced by sliding of the adjacent ones. On the other side, in Procrustes distance minimization, each semilandmark slides separately without any influence of adjacent semilandmarks. Thus, the former approach considers interlandmark relationships while the latter approach does not which can result in a malposition during sliding process (Bastir et al., 2019). It was empirically demonstrated that results from both sliding procedures slightly vary (Perez et al., 2006). Regarding the previously mentioned differences and consequences, the approach minimizing bending energy is generally more recommended in the context of biological studies as this approach leads to more smoothly interpolated geometry (Gunz et al., 2005; Gunz and Mitteroecker, 2013; Bastir et al., 2019).

Based on the TPS sliding, the procedure consists of two steps: sliding and projection. First, semilandmarks are relaxed and they are allowed to slide along the tangent or the tangent plane for curves or surfaces, respectively. By this process, they may lose their contact with the 3D surface, so they are projected back onto the curve or the surface (Gunz et al., 2005). By iterative manner, all points finally get to geometrically homologous positions.

In addition to the described use in shape analysis, the above mentioned algorithm of sliding that localizes semilandmarks onto their homologous positions is in its nature a missing data algorithm; curve semilandmarks are determined by a curve, but their position

on the curve is missing (1 degree of freedom); likewise, surface semilandmarks are determined by a surface, but they can move along the tangent plane (2 degrees of freedom). Missing landmarks have missing all three coordinates (3 degrees of freedom), and therefore they can be interpolated based on the available landmarks and semilandmarks using a complete reference specimen (Gunz et al., 2009; Gunz and Mitteroecker, 2013). This leads us to the topic of virtual reconstruction which will be described in the next section.

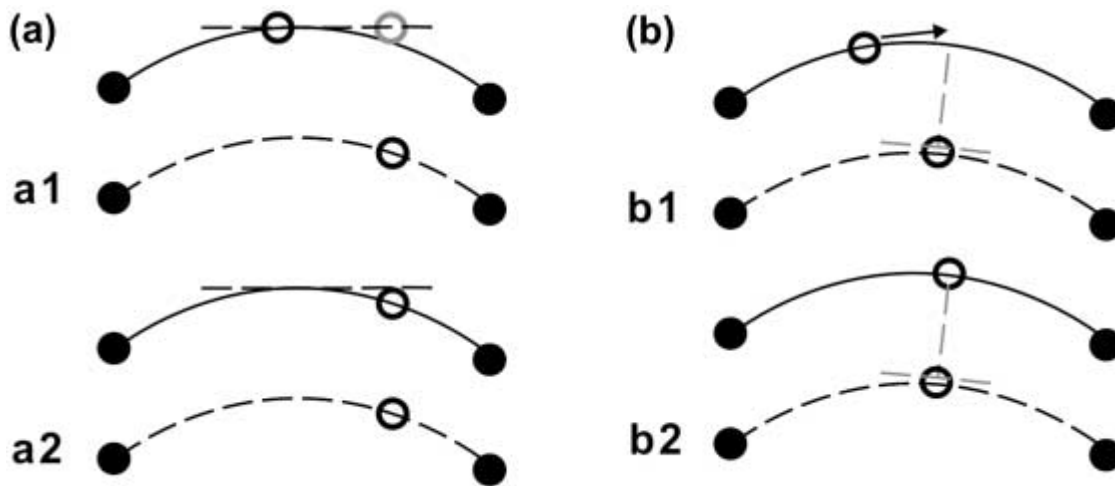


Figure 3. Criteria for semilandmark sliding: a) minimum bending energy, b) minimum Procrustes distance. Part 1 = semilandmark sliding relative to the template (dashed line), part 2 = final state (from Perez et al., 2006).

4 Virtual reconstruction

Virtual reconstruction is an approach combining digitized 3D data and computer tools to reconstruct fragmentary or incomplete specimens (Zollikofer and Ponce de León, 2005). In contrast to physical reconstruction, virtual approach is apart from anatomical rules also based on mathematical and geometrical principles. This ensures that the exact protocol can be recorded and reproduced and that results from differently designed protocols can be compared. Historically, the virtual approach is linked to the development of CT scanning. First virtual reconstructions of paleoanthropological specimens were performed in 1990s (Kalvin et al., 1992, 1995; Zollikofer et al., 1995) while they employed computer tools on CT scanned fossils and consisted mainly of anatomy-driven steps such as reassembly of

fragments, mirror-imaging and scaling of fragments from different individuals (Weber and Bookstein, 2011). Subsequently, mathematical and geometrical principles were implemented into the reconstruction of missing parts and correction of plastic deformation; these operations were mainly linked to the development of geometric morphometrics (Weber and Bookstein, 2011).

Techniques of virtual reconstruction are also employed in other domains than paleoanthropology. In forensic anthropology and paleopathology, they can clarify the origin of an injury, its cause, weapon identification, or injury treatment (Woźniak et al., 2012; Coutinho Nogueira et al., 2019; Nerudová et al., 2019). Virtual skeletal reconstructions are an initial stage for soft tissue reconstructions; e.g., facial reconstruction helps in forensic identification and it is also used to present historical and other interesting persons (Benazzi et al., 2009b; a; Nerudová et al., 2019). Lastly, virtual reconstruction is important for planning surgery procedures such as transplantations or bone replacement (Benazzi and Senck, 2011; Benazzi et al., 2011b).

With regard to their wide application, virtual methods are currently an extensively discussed topic in scientific publications. Solely to virtual reconstruction and virtual methods in anthropology, two monographies have already been fully devoted (Zollikofer and Ponce de León, 2005; Weber and Bookstein, 2011). They summarize the whole process from digitization to reconstruction and morphometric analysis. Therefore, in the following sections, we will briefly go through the main points that everybody should be appraised of, and we will focus on the research that have followed since those monographies came out.

4.1 Fragment reassembly

Different types of disturbances described in chapter 2 can be corrected by different approaches that are described in the following sections. When type 1 disturbance is present, it is usually advisable to start with its correction. We cannot use tactile senses in virtual environment. Therefore, it is sometimes more reliable to glue physical fragments together provided that their surface edges are sufficiently large. If this condition is not fulfilled or glued unit would be too fragile, virtual tools are an appropriate option.

Virtual reassembly can be performed manually, semi-manually or fully automatically. Manual reassembly follows anatomical constraints such as fracture lines or articulations

and dental occlusion (Benazzi et al., 2014; Amano et al., 2015). Using a complete reference as a placeholder, fragments may be aligned using an Iterative closest point (ICP) algorithm that overlaps the fragment with the reference (Li et al., 2011; Yin et al., 2011). The ICP algorithm translates and rotates a point cloud while minimizing the distance to the target point cloud by the least squares method (Besl and McKay, 1992; Zhang, 1994; Lynch, 2018). When the reconstructed object is very fragmentary, manual reassembly could cause large error, so special algorithms may be used that align fragments based on the correspondence of their fracture surfaces (Papaioannou et al., 2002). However, this approach is better applicable on fragmentary archeological artefacts from stone or ceramic rather than on fragmentary fossil remains that have often very thin fracture edges or the latter are abraded or eroded (Ogihara et al., 2015). Another algorithm may be more useful in osteological specimens; this method extrapolates the shape of neighboring fragments and aligns them based on the smoothness of the junction between them (Kikuchi and Ogihara, 2013; Amano et al., 2015).

Automatic reassembly has still many drawbacks related to low efficiency of registration of fragmentary elements to a single specimen (Lynch, 2018), and it is restricted to rather trivial cases (Jurda et al., 2019). Therefore, manual techniques are still commonly applied even in virtual environment, and special devices are sometimes used to imitate the dimensional reality that is lost on the desktop (Jurda et al., 2019).

Fragmentation is often coupled with missing regions, and therefore fragments may lack direct contact between themselves. To solve this problem, it is again possible to use a complete reference placeholder and reassemble fragments manually or using ICP algorithm (Li et al., 2011; Milella et al., 2015). Or, it is possible to digitally align fragments using landmarks which are placed on both fragments independently and one of the fragments is subsequently aligned based on a complete reference (Profico et al., 2019b). Whatever the method of alignment is, a reference used for the reassembly should be phylogenetically close, but sex and allometric effects may also be important (Profico et al., 2019b).

4.2 Estimation of missing parts

Missing parts are a common problem in paleoanthropological analyses, which is often solved by discarding specimens whose information is incomplete or by mean substitution. Analyzing metric dimensions is feasible with partial subsets of preserved specimens, but

other analyses such as GM require all specimens to have the same number of landmarks (Mitteroecker and Gunz, 2009). Moreover, biological specimens are physical objects whose morphology also needs visual inspection, and thus reconstruction of missing parts may provide us not only estimates of missing variables but also visual representations of studied specimens.

As majority of vertebrates are bilaterally symmetrical, missing regions can be either unilateral or bilateral. Unilaterally missing structures are most reliably reconstructed based on the other preserved side while a complete reference individual must be used for bilaterally missing regions.

Exploiting bilateral symmetry can be performed in several different ways using virtual tools (Gunz et al., 2009). A fragment can be reflected and moved to its appropriate position, or an object can be mirrored across an empirical midplane estimated from midsagittal landmarks. These operations create an exact mirrored copy of the original object and they only differ in the final position of the mirrored fragment on the incomplete side. However, simple reflection might not be an optimal solution when a specimen is characterized by a higher degree of physiological (not *post-mortem*) asymmetry (Benazzi and Senck, 2011). Third option can be applied when the incomplete side still contains a considerable preserved portion; the mirrored complete side is used as a template to be warped onto landmarks on the preserved portion. This results in a slightly different outcome that better fits the preserved morphology (Benazzi et al., 2009a; Gunz et al., 2009; Haile-Selassie et al., 2019) providing a higher accuracy than a simple reflection in specimens with a marked bilateral asymmetry (Benazzi and Senck, 2011).

When missing regions occur on both sides, complete reference specimens must be used to estimate such areas. Generally, there are two different methods to predict missing morphology: statistical and geometrical (Gunz et al., 2004). The statistical reconstruction works on the principle of interlandmark correlations which are involved in the multiple multivariate regressions model. Therefore, this method takes into account population variance and covariance, such as allometry and morphological integration, but it also requires a large sample of reference individuals, as every landmark coordinate is predicted separately (Gunz et al., 2004, 2009). On the other hand, the geometrical reconstruction is based on geometrical continuity and curvature smoothness with a reference specimen to be warped onto the incomplete while keeping minimum deformation in the TPS algorithm (Gunz et al., 2004). During this process, areas between preserved landmarks are

interpolated meaning that estimation of missing regions works best when the missing area is surrounded by preserved landmarks. For this method, only one reference specimen can be used which is advantageous for paleoanthropological reconstructions as fossil species are not usually represented by a large number of complete specimens. Prediction using TPS is always based on one specimen; this can be an average of multiple specimens or each specimen from a sample leading to multiple reconstructions.

To exploit maximum information, the preserved morphology must be sufficiently covered by landmarks. This is an important condition for both statistical and geometrical reconstructions, as close landmarks have higher covariance affecting the statistical reconstruction, and the TPS reliably predicts missing data close to the preserved morphology (Gunz et al., 2009). Therefore, sliding semilandmarks, described in chapter 3, are necessary for both methods as they allow one to capture morphology that does not possess any anatomical landmarks.

The estimation process concerns landmark coordinates or other variables, e.g., interlandmark distances (Neeser et al., 2009). To produce a visual reconstruction, another step is necessary via surface warping of a complete reference specimen onto the reconstructed configuration of landmarks. Reconstructed missing parts can be subsequently cut from the reference model and merged with the incomplete specimen. Perfect fit between the original and the new surface is important especially for subsequent 3D printing or in correcting skeletal defects in plastic surgery (Benazzi et al., 2011b). However, the new surface does not often perfectly match the original morphology, which pays for simple mirror-imaging as well as for TPS warping, and for this reason it is advisable to use computer-aided design techniques. These techniques improve continuity of the combined meshes and their effect on surface geometry is minimal (Benazzi et al., 2011b).

Apart from predicting positions of landmarks, there have been attempts to directly use whole point clouds which create surface meshes, and even whole volumes (Zheng and Lösch, 2013; Mahfouz et al., 2017). Between-mesh correspondence in the whole-mesh approach is solved by certain homologous surface features, such as bone tuberosities, that are automatically found and used to superimpose a fragment with a template (Mahfouz et al., 2017). However for now, this approach has been developed only on some bones without possibility of using own reference material which is limiting for paleoanthropological studies. The volumetric method should take into account not only

surface data but also data from each voxel, but this method has not yet been further developed (Zheng and Lösch, 2013).

4.3 Retrodeformation

Plastic or brittle deformations are more commonly corrected in paleontology (Angielczyk and Sheets, 2007; Boyd and Motani, 2008; Arbour and Currie, 2012; Hedrick and Dodson, 2013; Cuff and Rayfield, 2015), but they are also found in paleoanthropological specimens. Despite preserved object integrity, these deformations may have a significant effect on shape variability of fossil specimens (White, 2003; Angielczyk and Sheets, 2007; Hedrick and Dodson, 2013). Plastic deformation is a kind of defect that is not possible to correct physically and virtual methods are thus of great importance in solving this issue. Earlier, plastic deformations were corrected only in very flat 2D specimens, but retrodeformation methods started to be applied to 3D specimens too (Lautenschlager, 2016).

For correcting plastic deformation, chronological sequence of diagenetic changes leading to all observed defects has to be examined together with a documentation of the *in situ* position. This helps to identify place and time when the pressure of the overlaying sediments affected the fossil (Zollikofer, 2002). The outcome of deformation depends on the orientation of the fossil relative to the direction of compression (Figure 1) (Ponce de León and Zollikofer, 1999). This provides information whether the whole object is affected by deformation, or only its part, and an inverse transformation can subsequently be applied to retrodeform the specimen.

The easiest way of retrodeformation is by exploiting bilateral symmetry. This information can only be used in specific cases where only one side is distorted or when the whole form is distorted by a uniform shear (Gunz et al., 2009). While compression parallel or orthogonal to the midsagittal plane does not affect its overall symmetry, any other deformation results in shearing of the fossil (Ponce de León and Zollikofer, 1999). When the uniform shear is present, symmetry can be restored based on the principle of midsagittal landmarks being located in a single plane: distances from the plane to the bilateral landmarks should be symmetrical and connecting lines perpendicular to the midplane (Ogihara et al., 2006; Gunz et al., 2009; Tallman et al., 2014). This technique is based on the TPS deformation of the original landmark configuration onto the symmetrized

configuration. Until now, this technique has only been used with anatomical landmarks. However, the distribution and amount of landmarks affects the result of surface retrodeformation, so the techniques has recently been extended by symmetrical semilandmarks that are homogeneously distributed along curves and surfaces reaching better results in retrodeformation (Schlager et al., 2018).

Symmetrical distortion such as compression or stretching parallel or perpendicular to the midsagittal plane cannot be corrected based on this principle, since bilateral landmarks are equally far from the midplane and remain in 90° angle from the midplane (Ogihara et al., 2015). In some cases, it is possible to separate individual parts, reassemble them, and apply a retrodeformation function based on the original and newly positioned landmarks preserving continuity of the bone surface (Zollikofer, 2002; Benazzi et al., 2014). Another solution for such deformations is the use of a reference template onto which the deformed specimen or its part is warped (Ogihara et al., 2015). Comparing a deformed specimen to an undistorted one of the same species may help to assess direction of pressure in an attempt to simulate backward transformation. This operation does not necessarily lead to the true fossil shape, but it can help us to understand which parts were most affected by deformation (Arbour and Currie, 2012).

4.4 Evaluation of reconstruction reliability

Reconstruction of skeletal tissue is a process which attempts to bring a fossil variously affected by taphonomic conditions to the state *ante-mortem*. Although preservation state can be very variable, and therefore no single reconstruction protocol exists for every case, it is still possible to state main principles that should be maintained. First, every reconstruction should start with recovering the intrinsic information preserved in the fossil and use as much of this information as possible. Second, extrinsic information should be used to interpolate or extrapolate lost information that cannot be recovered from the preserved remains themselves (Zollikofer and Ponce de León, 2005).

Reconstruction accuracy is affected by many factors such as a type of the defect, its size and location, used methods, and a reference sample (Senck et al., 2013). Types 1 and 4 defects should ideally have a single solution if the object is complete but only fragmented or embedded in matrix. In types 2 and 3, reconstruction accuracy greatly depends on other

mentioned factors, and the result is always only an approximation (Weber and Bookstein, 2011).

Differential advantages and disadvantages specific for methods of missing parts reconstruction result in a predominant use of the TPS algorithm based on landmarks in the paleoanthropological context, since a large sample of reference specimens is not necessary (Grine et al., 2010; Benazzi et al., 2011a, 2014; Kranioti et al., 2011; Amano et al., 2015; Haile-Selassie et al., 2019). However, several works have demonstrated that the TPS function does not provide accurate estimates for missing data and that it sometimes works even worse than mean substitution (Neeser et al., 2009; Arbour and Brown, 2014). These studies used only very sparsely spaced anatomical landmarks and, as pointed out by Gunz et al. (2009), dense cover by sliding semilandmarks is crucial for TPS algorithm, as the least TPS bending causes convergence to the template form leading to striking resemblance with the template when the geometry is not sufficiently defined by landmarks (Figure 4). Other comparisons of TPS and regression methods showed decreasing accuracy with increasing distance from the preserved morphology in both methods. However, regression is able to reliably estimate large unilaterally missing regions, as it has access to the information about symmetry in contrast to TPS which provides biased estimation of unilateral defects influenced by a reference specimen (Gunz et al., 2004). Therefore, the use of TPS estimation in paleoanthropological studies is supported not only by the absence of need of large reference samples, but also by accurate results comparable to the statistical method, when applied appropriately. Ideally, TPS should be used for interpolation of smooth bilaterally missing regions in the vicinity of the preserved morphology (Gunz et al., 2009), and one should be cautious about extrapolation of projecting and more distant parts as the estimation tends to approach the reference specimen (Zollikofer and Ponce de León, 2005).

If the estimation of large missing defects is inevitable, two solutions are available: simulation or multiple estimations. Using simulation, we can quantify accuracy and reliability of missing region estimation on a complete specimen, while multiple estimations produce a range of possible forms based on the reference sample. However, the problem of a low number of reference specimens in paleoanthropology is re-encountered. The reference specimen should be from the same or morphologically close species (Senck et al., 2013; Teshima et al., 2015). It has been shown that sex or population origin has low effect on the reconstruction outcome in extant modern humans (Senck et al., 2013), but it

obviously depends on the location and size of the defect (Arbour and Brown, 2014), as skeletal structures are differentially integrated (Klingenberg, 2014), and thus preserved regions have limited capability of prediction. A degree of variation of multiple estimates indicates reconstruction reliability of a given structure, and, depending on the degree of structural integration and defect size, multiple estimates can still lead to a single conclusion (Gunz et al., 2009).

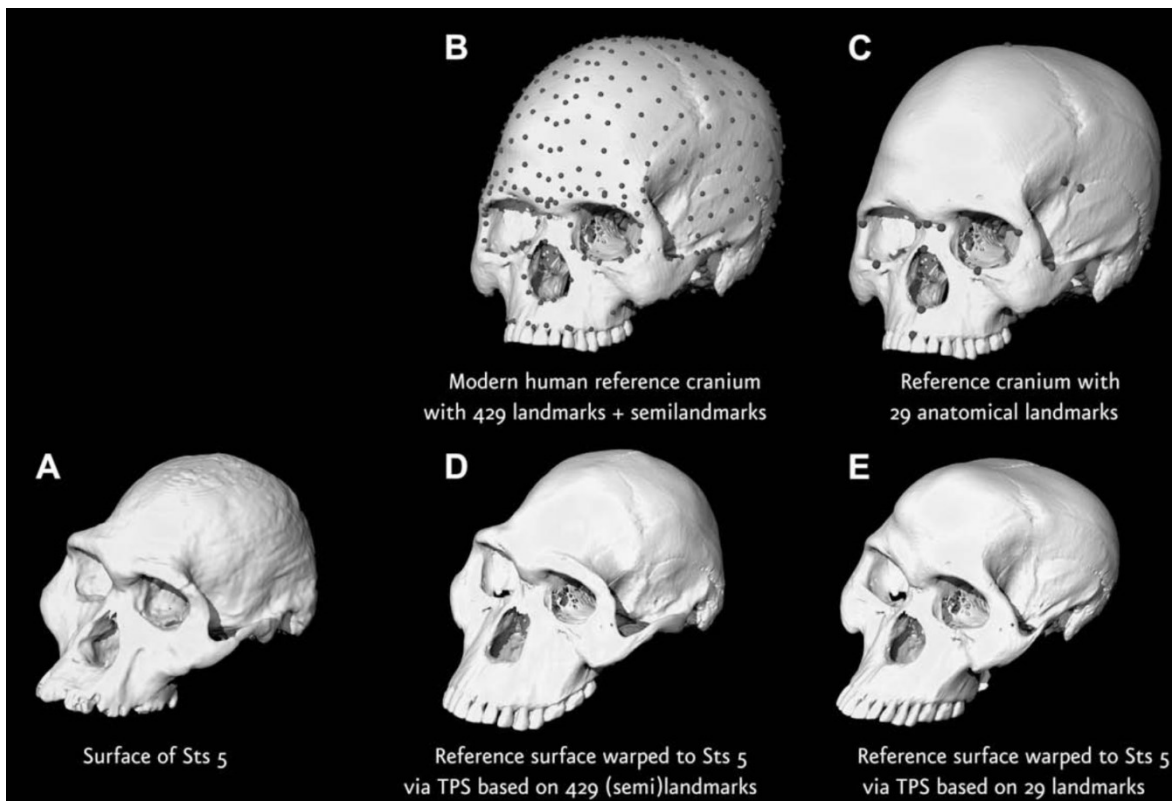


Figure 4. The effect of landmark number on the warping of the reference specimen (B, C) to the target (A). A high number of landmarks (B) results in a better fit (D) in contrast to a low number of landmarks (C, E) (adapted from Gunz et al., 2009).

Since complete fossil specimens are not abundant, it has been shown that interspecies reconstructions based on morphologically close contemporary species can be performed with sufficient reliability (Senck et al., 2015). However, if a fossil species shows a different pattern of integration, different extant taxa can be variously suitable for reconstructing different anatomical regions (Senck et al., 2015).

Every reconstruction involves assumptions that determine the reconstruction process and selection of suitable methods. Such assumptions follow taphonomical examination,

structural integration, symmetry, taxonomic attribution, sex or age, and they have to be considered in subsequent analyses (Gunz et al., 2009). Reconstruction should always exploit maximum from the preserved morphology and minimize reference-based reconstruction. However, when reconstructing an incomplete specimen, assumptions should not coincide with research hypotheses; otherwise, conclusions supporting our hypotheses would be weakened (Weber and Bookstein, 2011).

5 Comparability of digitization techniques

Data acquisition is usually an initial stage of morphological research and can be accomplished in different ways according to subsequent study aims. The existence of different techniques and devices causes differences between final outcomes that are further analyzed. Furthermore, despite the use of new analytical methods such as GM, traditional methods are still being used, but measurements of linear dimensions were defined on dry bones. To ensure research reproducibility, it is therefore important to examine these aspects and their potential effects. A specimen under study can be converted into the computer environment so that a virtual copy is created, or landmark coordinates can be simply acquired by means of a landmark digitizer (Weber et al., 2001). In this chapter, we will focus on the former means of digitization as it can substitute the original specimen in many aspects.

3D models can be acquired by different means as volumetric or surface data. The former approach relates to the development of conventional radiography in the medical research at the end of the 19th century. This method was very quickly adopted in the paleoanthropological research as an analytical tool for exploring inner structures (Spoor et al., 2000a). By extension into the third dimension within the computer environment, computed tomography was developed in the 1970s. This latter approach solves the spatial overlap and permits to observe individual structures in a complex 3D object (Weber and Bookstein, 2011). CT scanning is now an integral part of the paleoanthropological and paleontological research, as it avoids manipulation with the original object and potential damage (Zollikofer et al., 1998; Recheis et al., 1999; Sutton et al., 2016; Uldin, 2017).

CT imaging works on the basis of x-rays with electrons being emitted from a source and passed through the object. The object absorbs electrons based on its material density, and the attenuated signal of radiation is detected (Weber et al., 2001). Final CT scan consists of

a stack of 2D slices of certain thickness. Therefore, each pixel of the slice represents, in fact, a volume element called voxel that has a single value based on the attenuation coefficient displayed as a shade of grey (Spoor et al., 2000b). High density materials absorb larger portions of the x-ray resulting in high attenuation coefficients displayed by lighter shades of grey or white color. Resolution of the CT scan depends on several factors: radiation dose, size of the field of view and number of slices. Generally, medical CT scans reach lower resolution (the best around 0.4 mm), while industrial micro-CT scanners can achieve resolution between 1–200 μm providing insight into the bone microstructure, and thus they are often used in fossil specimens (Spoor et al., 2000b). Synchrotron facility can even reach $<1 \mu\text{m}$ resolution (Boyde, 2009). Radiation damage from CT scanning can be disregarded in fossil specimens except for synchrotron which can degrade ancient DNA impairing subsequent genetic studies (Immel et al., 2016) and potentially leading to choices in priorities regarding the analyses of fossil material (Hublin, 2015).

Magnetic resonance imaging (MRI) is another method used for medical diagnostics. This technique is based on the absorption and emission of high frequency radio waves by hydrogen nuclei when the atoms are subjected to a strong magnetic field. In common with CT, MRI generates volume of slices with various shades of grey, but in contrast to CT, MRI does not produce ionizing radiation and it is more suitable for imaging soft tissue which contains high proportion of water (Weber and Bookstein, 2011). The resolution of MRI is generally lower than that from CT, so it does not permit examination of smaller structural details. In conjunction with experimental studies, it provides valuable knowledge on biomechanical aspects in human evolution (Warrener et al., 2015).

Another means of creating 3D models is scanning the object's external morphology. This can be accomplished by photogrammetry or various 3D scanners. Photogrammetry is based on the alignment of a large number of photographs and calculation of their spatial positions. Collection of photographs is fast and does not need special equipment. In contrast, the computation phase is a very lengthy process which requires special software and high computer performance (Falkingham, 2012; Katz and Friess, 2014).

Use of scanners is based on the non-ionizing visible light that does not penetrate the object, thus restricting the outcome to the outer surface of the object (Friess, 2012). Surface scanners suitable for scanning small to medium sized objects (sufficient for most anthropological studies) work on a triangulation principle of detecting reflected visible light that is being projected onto the scanned object, thus resulting in a virtual point cloud

representing the original object (Tocheri, 2009; Friess, 2012). Two technologies are implemented in different scanner devices: laser and structured light. The latter is completely non-ionizing while the former can have ionizing effects based on the part of the light spectrum the laser is derived from (Friess, 2012).

5.1 Comparative studies

A digitized model is not an exact replica of the original model. The accuracy of the virtual copy in representing the original specimen is dependent on a variety of factors derived from the equipment, but also from the software and algorithms used for mesh alignment and processing (Tocheri, 2009). CT scanners are very costly and therefore they are not a standard equipment of every laboratory (Sutton et al., 2016). In fact, there are a few facilities per country that provide CT or micro-CT scanning for research purposes. Therefore, CT scanners are more standardized throughout studies compared to 3D surface scanners which are affordable by greater number of institutions, and thus there is greater variability among the devices.

Even though each scanner has its own resolution, this is hardly ever reached by surface scanners (Guidi et al., 2007), as the performance is influenced by environmental conditions, especially by other light sources, and color properties of the scanned object. Laser scanners are less affected by other light sources, since they are set to only acquire light of certain wavelength (Friess, 2012). In contrast, micro-CT is independent of these factors, and with its high resolution, it is often considered “gold standard” in comparative analyses (Slizewski et al., 2010; Marcy et al., 2018).

Scanner performance is usually evaluated on a uniform manufactured object without texture which is not totally indicative of suitability for osteological material (Friess, 2012). Furthermore, morphological assessment may also depend on the interaction between the somatosensory system and a physical or virtual object. For these reasons, many anthropological studies test the accuracy and precision of different 3D data acquisition techniques (Guidi et al., 2007; Fourie et al., 2011; Villa et al., 2015b; Algee-Hewitt and Wheat, 2016; Colman et al., 2019). These studies differ in material and means of performance evaluation. There are two general types of studies. The first group tests the accuracy of 3D data acquisition relative to a reference that is either more precise or considered a standard means of data acquisition (Slizewski et al., 2010; Fourie et al., 2011;

Algee-Hewitt and Wheat, 2016; Marcy et al., 2018; Mullins and Albanese, 2018; Perrone and Williams, 2019). The second group tests accuracy of scanners which are assumed to produce similar results based on technical parameters (Eder et al., 2013; Villa et al., 2015b). The effect of scanning is also usually evaluated with regard to specific methods of analysis or study aims (Marcy et al., 2018; Mullins and Albanese, 2018).

A large number of studies evaluate the effect of scanning using coordinates of landmarks or linear measurements which are commonly analyzed in morphological studies, and therefore the impact on such analyses needs to be quantified. The reference is usually a manual acquisition of measurements or landmarks using a caliper or a landmark digitizer directly on the bone; another option is micro-CT that is considered more precise (Slizewski et al., 2010; Marcy et al., 2018). Generally, landmarks and measurements show good reproducibility among different means of acquisition (manual, landmark digitizer, surface scanner, CT) (Fourie et al., 2011) except for highly complex anatomical structures where different scanners are more prone to inconsistent results (Eder et al., 2013). It was also suggested that different types of landmarks used in geometric morphometrics are variously reproducible across different sources of data, but studies do not show consistency in this aspect (Sholts et al., 2011; Algee-Hewitt and Wheat, 2016). This leads to an important fact that landmark digitization or measuring distances of a virtual object is undoubtedly different from that of a real object. In virtual environment, landmarks cannot be placed using tactile means but have to be located solely on a visual basis (Sholts et al., 2011). Moreover, standard osteological measurements were defined with regard to traditional measuring instruments (Martin, 1928; Bräuer, 1988) whose functions are sometimes difficult to reproduce in virtual environment. On the other hand, tools of computer-aided design software can serve to make landmarks and measurements more reproducible and comparable to standard definitions while substantially reducing observer error (Guyomarc'h et al., 2014; Reynolds et al., 2017).

Digitized surface models also provide more accurate estimates of certain geometrical properties such as surface area or volume (Tocheri, 2009), and they permit complex quantitative analyses of surface topography (Biwasaka et al., 2013; Villa et al., 2015b; Pampush et al., 2016; Winchester, 2016). These characteristics (especially the last-named) largely depend on the level of detail which can be very variable despite the fact that different scanners reach similar resolution (Guidi et al., 2007; Slizewski et al., 2010; Mathys et al., 2013). This discrepancy can be produced by different scanning protocols

(Sholts et al., 2010) or algorithms used for mesh generation (Klaas et al., 2011) and post-processing (Veneziano et al., 2018). As every scanner is typically sold with accompanying software performing the alignment of partial meshes, merging and basic mesh processing (Tocheri, 2009), these procedures may also influence detailed topography of the final model (Guidi et al., 2007). In consequence, scanners add a random noise to the mesh affecting its geometrical properties and topography. It has been suggested that smoothing filters can separate real anatomy from the error of each scanning instrument (Villa et al., 2015b; Veneziano et al., 2018). Decimation and smoothing tools are common post-processing operations (Friess, 2012; Bastir et al., 2019) employed in order to speed up manipulation or reduce artifacts and noise, but both tools can also cause a great information loss (Veneziano et al., 2018).

Regarding susceptibility of further analyses to differently acquired data, there is usually little or no effect on methods depending on measurements, landmarks, or surface topography (Mullins and Albanese, 2018; Perrone and Williams, 2019). However, lower resolution techniques may produce less reproducible results that should be taken into account especially in studies expecting little biological variation such as in the analysis of asymmetry (Marcy et al., 2018). Suitability of digitized models for analyses depending on morphological assessment has not yet been extensively studied. Naturally, delicate traits cannot be reliably observed on material with poor resolution (Colman et al., 2019), but in general, assessment of virtual material can give comparable results to those obtained from dry bones (Colman et al., 2019).

To sum up, digitizing error can come from various sources. Scanners operate on a different basis, they are associated with different software and algorithms, and final scans can be variously processed by researchers. All these factors cause smaller to greater differences and change mesh quality and topography. For macroscopic studies using scans acquired by different means seems acceptable if all the devices provide sufficient resolution for the smallest desired features (Weber, 2015). However, one should be cautious about combining different sources of scans in studies expecting little biological variation (Marcy et al., 2018) as scanners differ in the level of detail they are capable to capture (Guidi et al., 2007; Eder et al., 2013).

6 Summary of presented articles

First main focus of the thesis was on the virtual reconstruction of the Zlatý kůň cranium and subsequent morphometric analysis (**Rmoutilová et al., 2018**). The Upper Paleolithic specimen was discovered in 1950s, approximately 30 km southwest from Prague (Vlček, 1956). Skeletal remains only consist of the fragmentary skull and several fragments of ribs and vertebrae. Therefore, mainly cranial and mandibular remains had been analyzed and used in several comparative studies (Smith and Ranyard, 1980; Sládek et al., 2002; Lestrel et al., 2013). The specimen was identified as an adult female (Vlček, 1991; Wolpoff et al., 2006) despite previously described male features on the frontal bone (Vlček, 1956) when ZK had been considered to represent two individuals due to color differences of the fragments (Smith et al., 1982). In 2002, direct radiocarbon dating revealed an age of ~15.4 ky cal BP (Svoboda et al., 2002) moving the specimen from previously assumed Early Upper Paleolithic age to the Late Glacial period. Human skeletal remains are scarce in Central Europe from this period (Figure 5); a great portion of them are very fragmentary restricting morphological analyses, but at least ancient DNA sampling was possible in several cases (Posth et al., 2016).

In our study we reconstructed the ZK cranium using virtual methods in order to revise specimen's sex attribution and morphological affinity with regard to European Upper Paleolithic populations. The reconstruction protocol was designed in order to employ maximum of the preserved morphology. Overall, the process consisted of operations belonging to two groups: preserved morphology-based and reference-based reconstruction. The preserved morphology-based operations were fragment reassembly, TPS warping based on a mirrored template and simple mirroring; complete reference information was used in the estimation of a non-adjacent fragment position and in estimation of bilaterally missing regions.

As was discussed above, bilateral symmetry can be used in different ways in virtual reconstruction (Gunz et al., 2009). To reconstruct the left anterior portion of the calvarium, reflection with TPS was used, as there was a slight asymmetry in the specimen. Using landmarks and semilandmarks this approach exploited the preserved morphology on the left side which was supplemented by the aligned mandible. The mandible was aligned based on estimated cranial and mandibular midplanes and the right temporomandibular articulation. These criteria could not eliminate one degree of freedom, i.e., rotation along the transversal axis of the joints. However, this degree of freedom does not affect positions

of medial and lateral landmarks on the coronoid process used for TPS warping of the calvarium. This information ensured a congruity in the left temporomandibular articulation that is particularly important when transferring virtual objects into the real world via 3D printing.

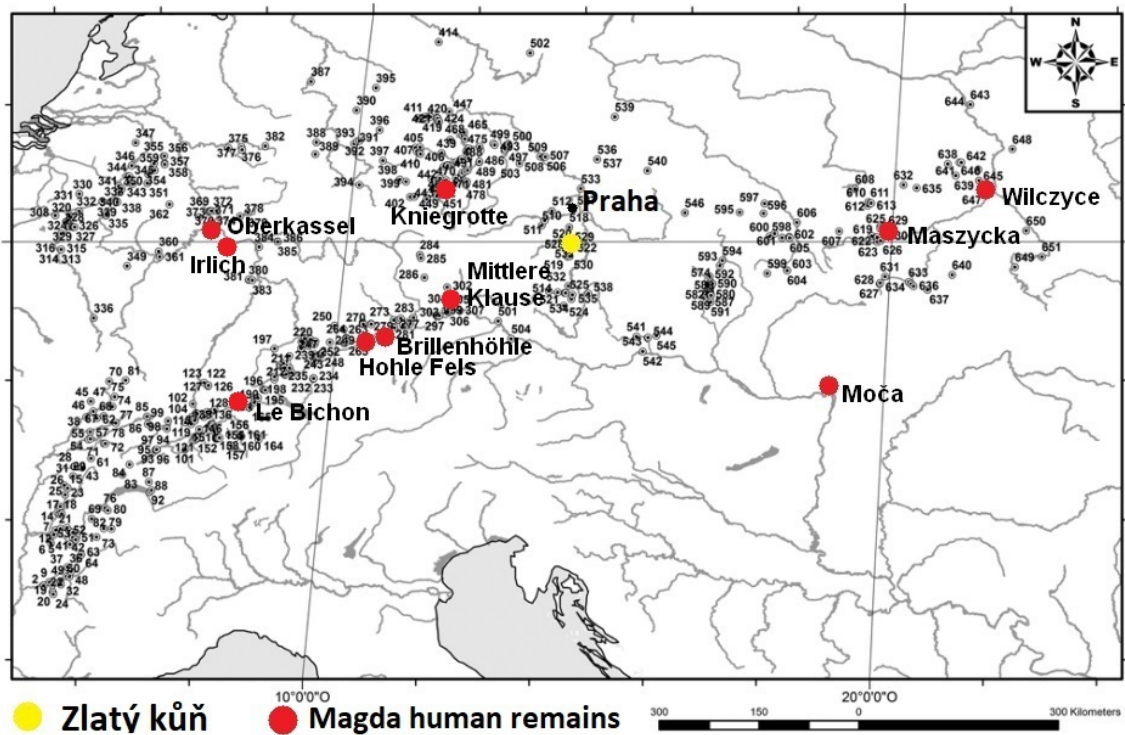


Figure 5. Central European sites with most important human skeletal remains from the Magdalenian or Final Paleolithic period projected on the map of Magdalenian assemblages (adapted from Maier, 2015; data from: Street et al., 2006; Irish et al., 2008; Šefčáková et al., 2011; Kozłowski et al., 2012; Maier, 2015).

Reflection using TPS was also employed in the reconstruction of the right zygomatic bone. Both zygomatic bones were aligned based on fracture lines and the continuity of the orbital margin. This increased information available for estimating position of the right maxilla that does not possess a direct connection with the rest of the cranium. For this step complete reference specimens were necessary. To assess reliability of the reconstruction, a set of multiple reconstructions was produced based on different subsets of reference specimens according to factors such as sex, chronology and morphological similarity. In all seven copies of the cranium, the right maxilla was mirrored across the estimated cranial midplane. Finally, the same reference subsets were used to estimate missing portions in the facial, temporal and basicranial regions completing all seven reconstruction versions.

Variation of the final reconstructions caused by different reference specimens was relatively small which allowed us to take average linear dimensions for subsequent analyses.

Using main cranial dimensions we addressed two questions of the ZK cranial morphology: sex attribution and morphological affinity. As has been shown, cranial shape is very population-specific (Musilová et al., 2019) and craniofacial sexual dimorphism changed over time (Frayer, 1980; Cieri et al., 2014). To sex the ZK specimen, we collected data on Upper Paleolithic specimens that were sexed by reliable techniques based on the pelvis, DNA, or secondary sex diagnosis (Murail et al., 1999). Using variables that best separated males and females, a linear discriminant model was created that successfully determined sex in 94% of the cross-validated reference sample (n=32). Moreover, with a posterior probability threshold of 0.95, sex was determined in 53% of the sample with no misclassification. By this tool, ZK was diagnosed as a female with a 0.98 posterior probability which can be considered very reliable.

Morphological affinity of the ZK cranium was examined using standardized log-shape variables filtering out differences due to size (Mosimann, 1970). In contrast to the radiocarbon dating (Svoboda et al., 2002), ZK showed great morphological affinity with a population that lived in Europe before the Last Glacial Maximum (LGM) that occurred 23 to 19 ky cal BP (Clark et al., 2009). The LGM was a dramatic climatic change that forced northern populations to southern refuge resulting in the abandonment of northern territories and subsequent re-settlement (Housley et al., 1997; Verpoorte, 2004). This had an impact on European populations changing their body constitution with regard to the climate (Straus, 1995; Churchill et al., 1999; Holt and Formicola, 2008), but populations also changed simply by genetic drift considering population bottleneck and the subsequent founder effect. Population turnover has been detected genetically (Pala et al., 2012; Fu et al., 2016; Posth et al., 2016) and also on craniometric variability of pre-LGM and post-LGM populations (Brewster et al., 2014). Given that the radiocarbon dating of ZK does not fulfill all suggested criteria for reliability (Housley et al., 1997) and given the lack of diagnostic artifacts, this result can be interpreted in many ways and real biological closeness to the pre-LGM population cannot be ruled out at this moment.

Thanks to the virtual reconstruction, we were able to extract new data and analyze general morphology of a fragmentary fossil specimen. We were able to address issues that have been discussed since the discovery of the specimen, but due to the preservation state

they could not have been analyzed in a complex way. For future studies involving this specimen, it is indispensable to revise its chronological dating. Depending on the results, this specimen can be very informative about population processes that occurred in Central Europe during the Upper Paleolithic.

This study can also be useful with regard to sexing Upper Paleolithic specimens. There were only two misclassified individuals in the cross-validated model with a threshold 0.5; one of them was a male individual Arene Candide (AC) 2. A posteriori we found that he had probably suffered from a hereditary form of rickets (Formicola, 1995; Sparacello et al., 2018). Unlike another individual in our sample affected by the same disease (AC3), pathological changes were also detected in the cranial shape of AC2 probably causing unsuccessful sex classification by our model. Using only non-pathological specimens, this model could be promising for sexing Upper Paleolithic specimens whose pelvic remains are not available.

Second main focus of this thesis related to the Regourdou 1 pelvis. Regourdou 1 is one of the most complete European Neandertal skeletons that was found in 1957 near the village Montignac-sur-Vézère in Dordogne (France) (Piveteau, 1959; Bonifay et al., 2007). Since 2008, new pelvic remains have been discovered during a revision of museum collections (Madelaine et al., 2008; Maureille et al., 2015a) making the R1 pelvis one of the best preserved pelvises of European Neandertals. However, based on the preliminary examination (Meyer et al., 2011), the sacrum shows considerable asymmetry. Therefore, we decided to first analyze a degree of the asymmetry in order to evaluate its importance for the reconstruction and possible impact on the individual (**Rmoutilová et al., in press**). The R1 sacrum was compared to modern healthy individuals (n=41) and other Neandertal sacra whose 3D models or literature data were available (n=6). Based on linear dimensions and landmarks, the asymmetry in length of sacral alae and orientation of sacral articular facets is substantial in R1 compared to both modern and Neandertal samples. In addition, we have provided a first quantitative analysis of the Neandertal sacra confirming previous descriptions that Neandertals had a relatively wide first sacral vertebra and a voluminous sacral canal opening.

With regard to the published literature (Scheuer and Black, 2000; Pitre and Lovell, 2010; Pfeiffer, 2011), the asymmetry in the sacral alae could have originated as a developmental abnormality during the intrauterine or postnatal period up to early childhood. As the sacrum plays a key role in weight transmission and posture (Pal, 1989),

there can be important implications related to load dissipation of the upper body onto the lower limbs. In addition, facet joint orientation is critical in maintaining stability of the spine with respect to shear forces (Noren et al., 1991) and asymmetrical orientation (facet tropism) is associated with degenerative vertebral diseases (Dai, 2001; Kim et al., 2013; Schleich et al., 2016; Lai et al., 2019). Signs of asymmetrical load transmission are apparent in the R1 trabecular structure and could be related to other skeletal abnormalities found in this specimen such as scoliotic signs in the sternum and presacral vertebrae (Gómez-Olivencia et al., 2012, 2013) and asymmetrical femoral shafts (Maureille et al., 2015a).

The pattern of morphological abnormalities in the R1 skeleton should be further examined. For our next purposes, we have shown that the asymmetry is substantially greater than that commonly observed in the modern population. This fact is important for the pelvic reconstruction, as the conformation of the sacrum affects articulation in the sacroiliac joints (SIJs). Since mirror-imaging techniques are often used in fossil reconstruction, we need to take this high degree of asymmetry into consideration. Virtual reconstruction of the R1 pelvis is described in detail in chapter 7.

Our secondary aims related to the adjustment of sex diagnosis methods on fragmentary material and to the comparability of 3D digitization protocols. In the study of **Rmoutilová et al. (2017)**, we focused on the analysis of sexual dimorphism in the iliac auricular surface and comparison of traditional and geometric morphometric techniques in sex estimation based on a partially preserved posterior ilium, as the sacroiliac region is generally better preserved than the ischio-pubic region in the archeological record (Waldron, 1987; Stojanowski et al., 2002). Sexual dimorphism of various traits has been suggested in the auricular region (Novotný, 1981; Valojerdy and Hogg, 1989; Ali and MacLaughlin, 1991; Brůžek et al., 1996; Novak et al., 2012; Anastasiou and Chamberlain, 2013; Wescott, 2015) that could be explained by differences in body size (Novotný, 1981; Ali and MacLaughlin, 1991), birth adaptations (Wescott, 2015), or weight transmission related to different positions in the center of gravity between males and females (Bellamy et al., 1983). However, shape dimorphism of the auricular outline could not be reliably assessed by traditional methods (Ali and MacLaughlin, 1991; Brůžek et al., 1996). Therefore, we used curve semilandmarks to analyze sexual differences in shape of the auricular surface on a sample of 121 photographed bones of individuals from three European populations. GM analysis identified subtle shape differences between males and females that are related

mainly to the width in the area of the auricular apex that is in agreement with previous studies (Anastasiou and Chamberlain, 2013). However, sex prediction using Support Vector Machine (SVM) algorithm based on shape was not successful; based on form we achieved accuracy of 81% with cross-validations. On the contrary, using visually evaluated traits (auricular surface elevation and postauricular sulcus) in combination with simple linear measurements suggested by Novak et al. (2012) and Wescott (2015), we achieved accuracy superior to 90% using SVM and linear discriminant analysis. We have provided a formula for the last method.

In this case, GM approach allowed us to objectively assess the degree of sexual dimorphism in the shape of the auricular surface. Based on our sample, there are very little differences between male and female auricular shapes that cannot be reliably assessed visually. However, the posterior ilium provides morphological traits that can be used for sex diagnosis.

In the publication of **Santos et al. (2019)**, we revised the visual sex estimation method originally proposed by Brůžek (2002). The original method evaluates five characters from the whole coxal bone and the final sex estimate is obtained on the basis of a majority rule. The method was tested on a larger sample by us and the result can now be evaluated with logistic regression slightly increasing the accuracy of the method. Furthermore, the method is fully adjusted to fragmentary remains via an online application that enables one to assess accuracy achieved only on a partial set of preserved characters.

In addition, we tested applicability of visual assessment on a sample of CT scanned material and we obtained comparable accuracy to that obtained on a sample of dry bones. These results are encouraging for future studies that use data from virtual material obtained from contemporary populations. However, subsequently published study of Colman et al. (2019) showed lower agreement in assessment of traits in the preauricular region of dry and scanned coxal bones. They did not compare differences in final sex estimates which could have been less marked, but their results may still indicate that the assessment of smaller morphological traits from the digitized material may be less reliable.

In the last publication of **Kotěrová et al. (2019)**, we analyzed differences between two widely used surface scanners (HP 3D SLS PRO 2 and NextEngine) and their potential impact on selected anthropological analyses. A sample of 29 coxal bones from the excavated Early Medieval site of Mikulčice was scanned by both scanners to evaluate their impact on sex estimation analysis based on linear coxal measurements (Murail et al., 2005;

Brůžek et al., 2017) and age-at-death estimation based on quantitative analysis of pubic surface topography (Stoyanova et al., 2015). A subsample of five pubic symphyses was also scanned by a high-precision industrial optical surface scanning device (Redlux profiler) that was taken as a reference in order to analyze scanners' outcomes of a highly structured surface of the pubic symphysis. While there were significant differences in some linear measurements between both scanners and also with regard to manual measurements of dry bones, there was no important effect on outcomes of the sex estimation method. It is difficult to assign this effect to differences in scanners' outcomes as the acquisition of linear measurements in virtual environment has not yet been standardized for the coxal bone; in fact, standardized measurement protocols have only been suggested for the cranium and some long bones (Guyomarc'h et al., 2014; Reynolds et al., 2017). Although the final sex estimate was not largely affected, one should be careful when combining virtual measurements with those on dry bones especially in univariate analyses.

While there are obvious differences between the devices in the capacity of capturing detail (especially on more rugose and irregular surfaces), different outcomes had negligible effects on the age-at-death estimates. However, more marked differences in surface deviation were detected in specific individuals with a higher degree of surface curvature, a pattern present in younger adults (Lovejoy et al., 1985; Villa et al., 2015a). We were able to assess this possible trend only visually as we did not know the exact age of the individuals. However, given that younger individuals are characterized by more billowed auricular and symphyseal surfaces (Lovejoy et al., 1985; Villa et al., 2015a), scanning devices unable to sufficiently capture detail could cause a directional bias in aging individuals by such quantitative methods of surface topography.

7 Preliminary reconstruction of the Regourdou 1 pelvis

Morphology of the human pelvis may be described in terms of three main factors: locomotion and posture, birth mechanism and thermoregulation (Gruss and Schmitt, 2015). Regarding the human pelvis, most obvious adaptations to bipedalism and upright posture can be found in the upper half of the pelvis (Lovejoy et al., 2009), but the lower half is also affected by the attachment of dorsal hip muscles. The upper part of the pelvis determines trunk width and is strongly related to climate (Ruff, 1991, 1993, 1994), but thermoregulatory demands are also reflected in transverse diameters of the true pelvis (Nuger, 2008; Betti, 2017), while the true pelvis mainly relates to the birth process (Ruff, 1995; Rosenberg and Trevathan, 2002).

Until the late 1980s, Neandertal pelvic remains were scarce and no complete pelvis was known (see Table 2 for a summary of Neandertal pelvic remains). Fragmentary remains allowed researchers to characterize Neandertal features (Gorjanović-Kramberger, 1906; Boule, 1911; McCown and Keith, 1939; Endo and Kimura, 1970; Heim, 1982; Trinkaus, 1983, 1996; Rak and Arensburg, 1987; Marchal, 1997). A large number of the features (e.g., well-developed and anteriorly positioned iliac pillar, supra-acetabular sulcus and fossa, robust anterior inferior iliac spine, insertions of hamstring muscles, intern obturator sulcus) were put in relation to Neandertal overall body robusticity and muscle insertions (Day, 1971; Frayer, 1987; Aiello and Dean, 1990; Trinkaus, 1996), and some of them were also shared with Middle Pleistocene specimens (Day, 1971; Stringer, 1986; Bonmatí and Arsuaga, 2007; Bonmatí et al., 2010).

Compared to modern humans, Neandertals had unusually long and slender superior pubic rami (Stewart, 1960; Trinkaus, 1976) which gave origin to several obstetrics-related hypotheses (Wolpoff, 1980; Trinkaus, 1984; Rosenberg, 1988; Friedlander and Jordan, 1994). However, discovery of the almost complete Kebara 2 pelvis in Israel showed that the long pubis does not substantially contribute to large pelvic inlet dimensions relative to body size because the sacrum is placed more anteriorly in relation to the dorsal end of the pelvis between the coxal bones that are everted laterally (Rak and Arensburg, 1987; Rak, 1991). Moreover, the outlet was even relatively more confined (Tague, 1992). Therefore, it was suggested that the long pubis rather relates to differences in locomotion and posture (Rak and Arensburg, 1987) which could be related to a relatively low lumbar lordosis (LL) implying postural differences (Been et al., 2014, 2017; but see Haeusler et al., 2019). The birth mechanism in Neandertals was further analyzed in two reconstructions of the Tabun

C1 female pelvis (Ponce De León et al., 2008; Weaver and Hublin, 2009). However, they provided two very different outcomes; both concur in platypelloid shape of the inlet, but they strongly disagree on the shape of the outlet resulting in contrasting opinions on the presence of rotational birth. Part of this disagreement is related to the fact that the Tabun C1 specimen lacks a sacrum and due to the taphonomic distortion present in this specimen.

Recent revisions of the faunal remains from the Regourdou site have allowed to identify new human remains belonging to the Regourdou 1 Neandertal skeleton (Madelaine et al., 2008; Gómez-Olivencia et al., 2013, 2019; Maureille et al., 2015a; Pablos et al., 2019). Among the new fossils, relatively complete portions of both coxal bones were found that allowed a first attempt of reconstruction of the R1 pelvis (Meyer et al., 2011). Since that study, additional fragments have further completed this pelvis. In this work we describe a preliminary reconstruction of the R1 pelvis using virtual reconstruction methods. Based on the reconstruction, we provide sex assessment of this individual and a morphometric analysis of newly available pelvic dimensions. Additionally, we compare our results to previous trials of reconstruction of the pelvis (Meyer, 2013; Plavcan et al., 2014).

7.1 Material

The site of Regourdou is located in Dordogne, southwest France. Two different Neandertal individuals are represented: the Regourdou 1 skeleton and a calcaneus of another individual Regourdou 2 (Vandermeersch and Trinkaus, 1995; Maureille et al., 2015a; Coutinho Nogueira et al., 2017). The Regourdou 1 skeleton was discovered in 1957 and systematic excavations followed during 1961–64 (Bonifay et al., 2007). The skeletal representation individual has substantially improved after a revision of collections since 2008 (Madelaine et al., 2008; Maureille et al., 2015a).

The individual has been determined as a young adult based on mandibular tooth wear and the closed medial clavicular epiphysis (Vandermeersch and Trinkaus, 1995; Volpato et al., 2012) who may not have exceeded 30 years (Volpato et al., 2012). The sex was rather considered indeterminate based on various metrics from postcranial bones (Vandermeersch and Trinkaus, 1995; Plavcan et al., 2014) although some scholars have proposed male sex (Vallois, 1965; Carretero, 1994; Gómez-Olivencia et al., 2007) and the preservation of the pelvic remains has not permitted sex diagnosis until now (Meyer et al., 2011).

Table 2. List of adult pelvic remains from the Neandertal lineage.

Specimen	Date (ky)	Location	Sex	Preservation	Ref.	Use in this study
Altamura	150	Europe	M	Right coxae, the rest is hidden by sediments	1	N
Amud 1	60	Near East	M	Left ilium, iliac crest and sup. pubic ramus, right iliac and ischial fragments	2	Y (obs.)
Arago 44	MP	Europe	F	Left coxae without pubis	3	N
Arago 121	MP	Europe	F	Left iliac ala	3	N
Arago sacrum	MP	Europe	-	Unknown	3	N
Feldhofer 1	40	Europe	M	Left coxae without pubis and majority of iliac crest	4, 5	Y (3D)
Feldhofer fragments	40	Europe	-	Ischial fragments and small sacral fragment (probably from Feldhofer 1)	5	N
Ferrassie 1	45	Europe	M	Left coxae without superior iliac ala, right ischium and pubis, sacral fragments, reconstructed in plaster	6	Y (3D)
Ferrassie 2	45	Europe	F	Fragments of both ilia	6	N
Grotte du Prince	MP	Europe	F	Fragment of right lower ilium	7	Y (lit.)
Chapelle-aux- Saints 1	50	Europe	M	Right coxae without iliac crest and pubis (lost, only cast), left coxae less preserved, right half of the sacrum	8	Y (3D)
Kebara 2	60	Near East	M	Right coxae complete, left coxae distorted, sacrum complete and slightly distorted	9	Y (3D)
Krapina 207	130	Europe	M	Right ilium with anterior portion of iliac crest and ischium	10	Y (3D)
Krapina 208	130	Europe	M	Right ischium, complete acetabulum, sup. pubic ramus	10	Y (3D)

Specimen	Date (ky)	Location	Sex	Preservation	Ref.	Use in this study
Krapina 209	130	Europe	F	Right lower ilium, complete acetabulum and sup. pubic ramus (together with fragment 212)	10	Y (3D)
Krapina fragments	130	Europe	-	Various smaller fragments	10	N
Palomas 92	55	Europe	F?	Crushed piece of ilium and sacrum in matrix	11	N
Palomas 96	55	Europe	F	Complete pelvis (not yet published)	11	N
Regourdou 1	MIS 5	Europe	?	Both ilia with posterior portion of the left iliac crest, right ischium and sup. pubic ramus, upper portion of the sacrum	12	Y (3D)
SH Pelvis 1	430	Europe	M	Complete pelvis	13	Y (lit.)
SH Pelvis 2	430	Europe	M	Right coxae and first sacral vertebra	13	Y (lit.)
SH Coxal 1, 3, 5	430	Europe	M	Well preserved coxae	13	N
SH fragments	430	Europe	F	Various fragments	13	N
Shanidar 1	50	Near East	M	Both pubic bones, right and left iliac and ischial fragments, sacrum largely complete but distorted	14	N
Shanidar 3	50	Near East	M	Right sup. pubic ramus and incomplete iliac ala, left fragments, sacrum largely complete (reconstructed with plaster)	14	Y (lit.)
Shanidar 4	70	Near East	M	Left iliac crest and sup. pubic ramus, right fragments, lower portion of sacrum	14, 15	N
Shanidar 5	50	Near East	M	Left sup. pubic ramus and symphysis, iliac fragments	14, 16	N

Specimen	Date (ky)	Location	Sex	Preservation	Ref.	Use in this study
Shanidar 6	70	Near East	F	Indeterminate fragments	14	N
Spy 2	35	Europe	M	Incomplete first sacral vertebra	17	N
Subalyuk 1	MIS 5	Europe	F?	Upper portion of sacrum	18	N
Tabun C1	130	Near East	F	Left iliac fragments, acetabulum and pubis, right pubic fragments, ischium, acetabulum and iliac body, taphonomical distortion	19	Y (3D)
Zafarraya	35	Europe	M?	Pubic fragment	20	N

MP = Middle Pleistocene, MIS = Marine Isotope Stage, F = female, M = male, ? = not reliable, 3D = digitized model available for this study, lit. = data from the literature, obs. = personal observation of the original, SH = Sima de los Huesos.

1 = Pesce Delfino and Vacca, 1994; Lari et al., 2015, 2 = Endo and Kimura, 1970; Valladas et al., 1999, 3 = de Lumley, 2015, 4 = Schaaffhausen, 1888; Skoglund et al., 2013, 5 = Schmitz et al., 2002, 6 = Heim, 1982; Guérin et al., 2015, 7 = de Lumley-Woodyear, 1973, 8 = Boule, 1911; Stringer and Grün, 1991; Trinkaus, 2011, 9 = Rak and Arensburg, 1987; Bar-Yosef and Vandermeersch, 1991; Tague, 1992, 10 = Gorjanović-Kramberger, 1906; Rink et al., 1995; Bonmatí and Arsuaga, 2007; Trinkaus, 2016, 11 = Walker et al., 2011; Trinkaus and Walker, 2017, 12 = Bonifay, 1964b; Meyer et al., 2011; Maureille et al., 2015b, 13 = Arsuaga et al., 1999, 2014; Bonmatí et al., 2010, 14 = Solecki, 1971; Trinkaus, 1983, 15 = Pomeroy et al., in press, 16 = Pomeroy et al., 2017, 17 = Fraipont, 1927; Genovés, 1954; Semal et al., 2009, 18 = Bartucz and Szabó, 1940; Pap et al., 1996, 19 = McCown and Keith, 1939; Grün and Stringer, 2000, 20 = Hublin et al., 1995.

Stratigraphic position of the skeleton allowed relative dating. Layers 8 to 3 defined by Bonifay are characterized by temperate fauna and the following layer 2 has a cold character which suggests that the stratigraphy of the Regourdou site covers periods of the warmer interglacial Marine isotope stage (MIS) 5 and glacial MIS 4. Regarding that the skeleton was found in layer 4, it probably comes from the end of MIS 5 (Bonifay, 1964b; Bonifay et al., 2007; Pelletier et al., 2017).

Human remains from the Regourdou site were variously relocated among institutions and researchers, but they were finally deposited in the Musée d'Art et d'Archéologie in Périgueux, while faunal remains were sent to the Musée national de la Préhistoire in Les Eyzies-de-Tayac (Bonifay et al., 2007; Madelaine et al., 2008). Until 2008, only the sacrum, the right ischium and the right superior pubic ramus had been known from the R1 pelvis (Figure 6; Piveteau, 1959). However, during revisions of faunal collections in the Musée national de la Préhistoire, new pelvic fragments were identified showing signs of fresh fractures indicating potential presence of other fragments (Madelaine et al., 2008; Maureille et al., 2015a). Among those fragments, there were six fragments of the right coxal bone that were glued together forming a large portion of the ilium, and a left iliac wing composed from two fragments, and separate fragments of the acetabulum and the ischial tuberosity from the left side (Madelaine et al., 2008; Meyer et al., 2011). Attribution of the new remains to the R1 individual was based on a good fit of both ilia to the sacrum in the sacroiliac articulation and similarity of the left ischial tuberosity to its right counterpart (Madelaine et al., 2008). The labels written on the bones indicated that the pelvic remains were uncovered during the salvage operation in 1957, and thus they were not integrated into the coordinate system used in the systematic excavations from 1961 (Maureille et al., 2015b). However, using unpublished drawings and field notes from 1957 a spatial distribution of these objects was reconstructed, with the pelvic remains probably on the border between squares G2 and G3, where most of the skeletal remains were concentrated (Maureille et al., 2015b).

The R1 pelvis is fragmentary (Figure 6). The right coxal bone preserves partial ilium, most of the ischium and a portion of the superior pubic ramus. The left coxal bone consists of the iliac ala with preserved posterior part of the iliac crest and two fragments of the ischium. The sacrum preserves the first sacral vertebra and a portion of the second and third vertebrae. The right auricular surface is complete, but the lower portion of the inferior arm is missing on the left side.

Micro-CT scans of R1 pelvic remains were acquired at platform AST-RX of the Musée de l'Homme in Paris and at the PLACAMAT department of the University of Bordeaux (microCT scanners V|tome|x L 240 and V|tome|x S, GE Sensing & Inspection Technologies Phoenix X|ray). Voxel size varied between 0.065 and 0.096 mm. To facilitate the manipulation, microCT scans were reduced before the segmentation in ImageJ (Rueden et al., 2017) using a macro created by Renaud Lebrun (www.morphomuseum.com) to a resolution still sufficient for macroscopic analyses. Surface models were semi-automatically segmented in Avizo 9.1 Lite (Visualization Sciences Group, SAS); inner trabecular bone must have been removed during segmentation in order not to have large surface files, but exposed trabecular bone was kept in the resulting models since it can provide important information in virtual reconstruction, especially during the reassembly of fragments.

3D models of pelvic remains of seven Neandertal specimens were used as a reference or for comparative purposes. The models are from CT or micro-CT scans that were either segmented by us or already segmented by the providing institution. Data on other Neandertal specimens were searched in the literature. Details on the Neandertal sample are in Table 2. Digitized models of several Upper Paleolithic (including one Mesolithic) specimens from Italy kindly provided by Vitale Sparacello were also used for comparative purposes (Sparacello et al., 2018). Coxal bones of these specimens and of La Chapelle 1 were reassembled with the sacra in order to measure comparative data. The virtual assembly was in all cases guided by well-preserved sacroiliac joints or pubic regions leading to a reliable reconstruction. Although the pubis was reconstructed by Boule (1911) in La Chapelle 1, it can be used to indicate a proper inclination of the coxal bone (Trinkaus, 2011). Other comparative data were searched in the literature and appropriate references are in Table 3.

Pelvic data for modern humans from identified collections from Coimbra (Rocha, 1995) and Spitalfields (Molleson and Cox, 1993) were kindly provided by the supervisor Jaroslav Brůžek. There were 36 males and 42 females from the Coimbra collection and 25 males and 27 females from the Spitalfields collection. Complete summary of comparative metrical data is in Table 3.

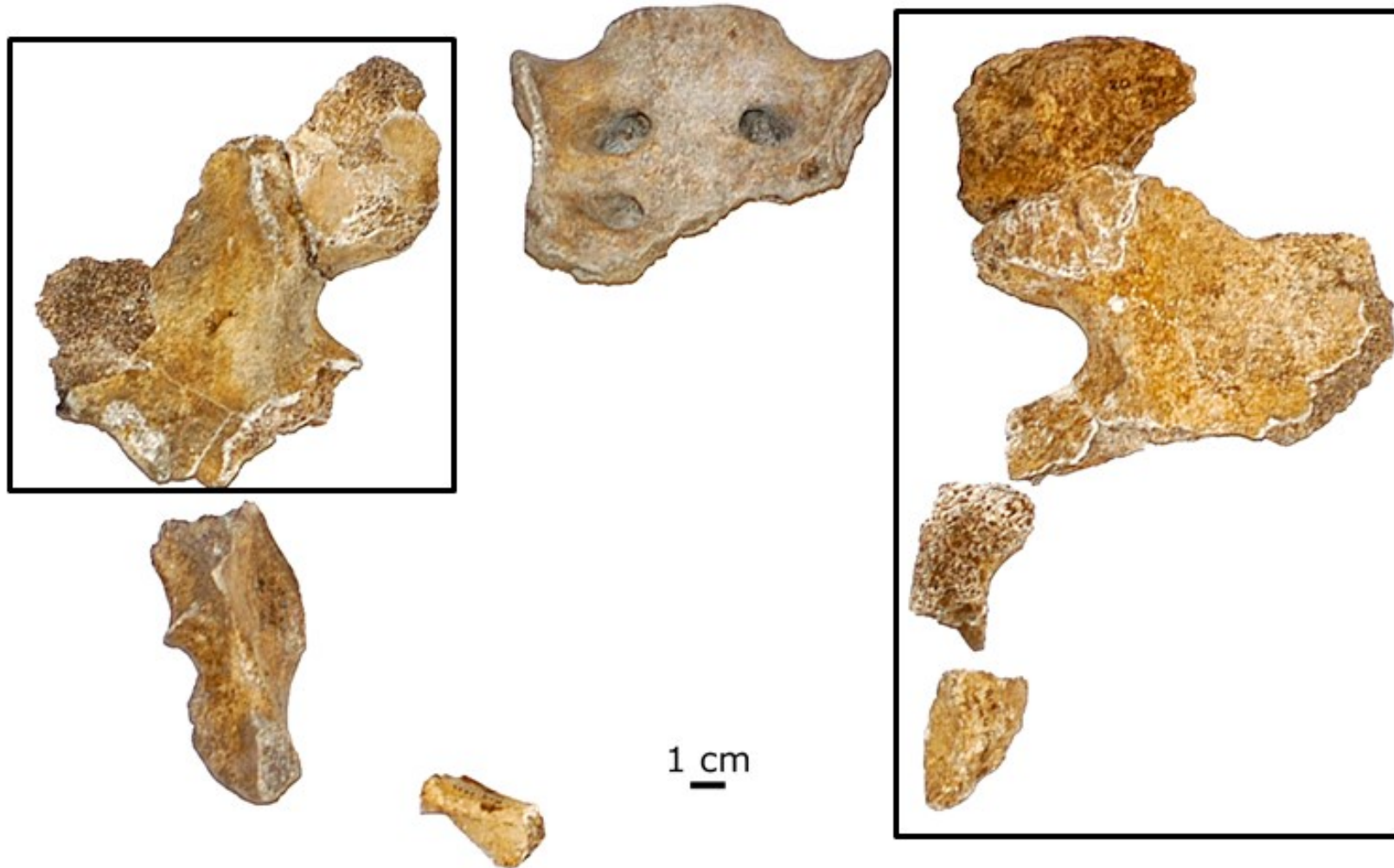


Figure 6. Regourdou 1 pelvic remains. Fragments in rectangles have been discovered since 2008; the others were identified during the field operation (Photo B. Maureille).

Table 3. Comparative specimens.

Group	Specimens	Data references
Recent modern humans	<u>Males</u> 36 from Coimbra 25 from Spitalfields <u>Females</u> 42 from Coimbra 27 from Spitalfields	(Molleson and Cox, 1993; Rocha, 1995)
Mesolithic and Upper Paleolithic modern humans	<u>Males</u> Arene Candide (AC) 2, 3 Dolní Věstonice (DV) 13, 14, 15 Mondeval (M) Předmostí (P) 3, 4, 14 Tagliente 2 (T2) <u>Females</u> Oberkassel 2 (O2) San Teodoro 1 (ST1)	(Bonnet, 1919; Matiegka, 1938; Sládek et al., 2000; Alciati et al., 2005; Tarsi et al., 2006; Trinkaus and Svoboda, 2006; Velemínská and Brůžek, 2008; Villotte, 2009; Sparacello et al., 2018)
Neandertals	<u>Males</u> Chapelle-aux-Saints 1 (CAS1) Kebara 2 (K2) Regourdou 1 (R1) <u>Females</u> Tabun C1 (TC1)	(Boule, 1911; McCown and Keith, 1939; Rak, 1991; Ponce De León et al., 2008; Weaver and Hublin, 2009; Trinkaus, 2011)
Middle Pleistocene males	SH Pelvis 1 (SH1)	(Bonmatí et al., 2010)
Early Pleistocene females	BSN49	(Simpson et al., 2008)

AC2, AC3, M, ST1, T2 and CAS1 were measured on digitized 3D models. Other data for Upper Paleolithic specimens are from the literature.

7.2 Methods

7.2.1 Reconstruction

Regourdou 1 has almost intact, undistorted sacroiliac joints, and so both ilia can be aligned to the sacrum. However, the reassembly is not as straightforward in virtual environment as using physical objects, so we tried several ways of alignment: 1) Landmarks were identified on corresponding structures of the complementary auricular surfaces and the coxal bones were aligned to the sacrum and manually shifted to prevent the overlap (based on Berge and Goularas, 2010; Claxton et al., 2016). 2) Auricular surfaces were cut and the ICP algorithm (Besl and McKay, 1992) was used to obtain a perfect fit between them. 3) The digitized coxal bones were aligned manually based on the articular topography and continuity of the *linea terminalis*. 4) The alignment was performed with printed 3D models using a box of rice and adhesive bands without correcting for articular cartilage. The printing was performed using plaster powder with ProJet x60 at the Department of Teaching and Didactics of Chemistry (Faculty of Science, Charles University). The assembled bones were scanned with a 3D scanner HP 3D SLS PRO 2. The outcomes of different types of alignment were evaluated using intermesh distances between the sacral auricular surfaces and the matching aligned ilia.

A compensation for sacroiliac joint thickness is often disregarded in other fossil pelvis reconstructions (Berge and Goularas, 2010; Milella et al., 2015; Claxton et al., 2016). With regard to the small deviation between fresh and reassembled pelvis (Bonneau et al., 2012), both ilia of R1 were positioned at the least distance from the sacrum and no correction of linear dimensions was used as it could introduce an unexpected error.

The right coxal bone was first reassembled from preserved fragments and then completed using the left counterpart. Direct connection was found between the ilium and the ischium so the ischium was manually aligned to the iliac fragment. The alignment was guided by a small area of direct connection in the region of the anterior arm of the greater sciatic notch and by the continuity of the lunate surface (Figure 7). In the second step, mirror imaging was used to add missing parts on the right iliac ala (postauricular area and inner and outer walls of the superior iliac ala). The right and the mirrored left ilium were superimposed using ICP algorithm in Meshlab software (www.meshlab.net). However, neither ilium is an exact reflected copy of its counterpart, due to the presence of some asymmetries in these bones. This incongruence is caused especially by different bone

thickness in the auricular area (Figure 8). To ensure a better fit between the meshes, areas of the mirrored left ilium missing on the right side were cut with sufficient areas of overlap with the preserved right ilium. These pieces were again superimposed onto the right ilium and merged with Geomagic Studio.

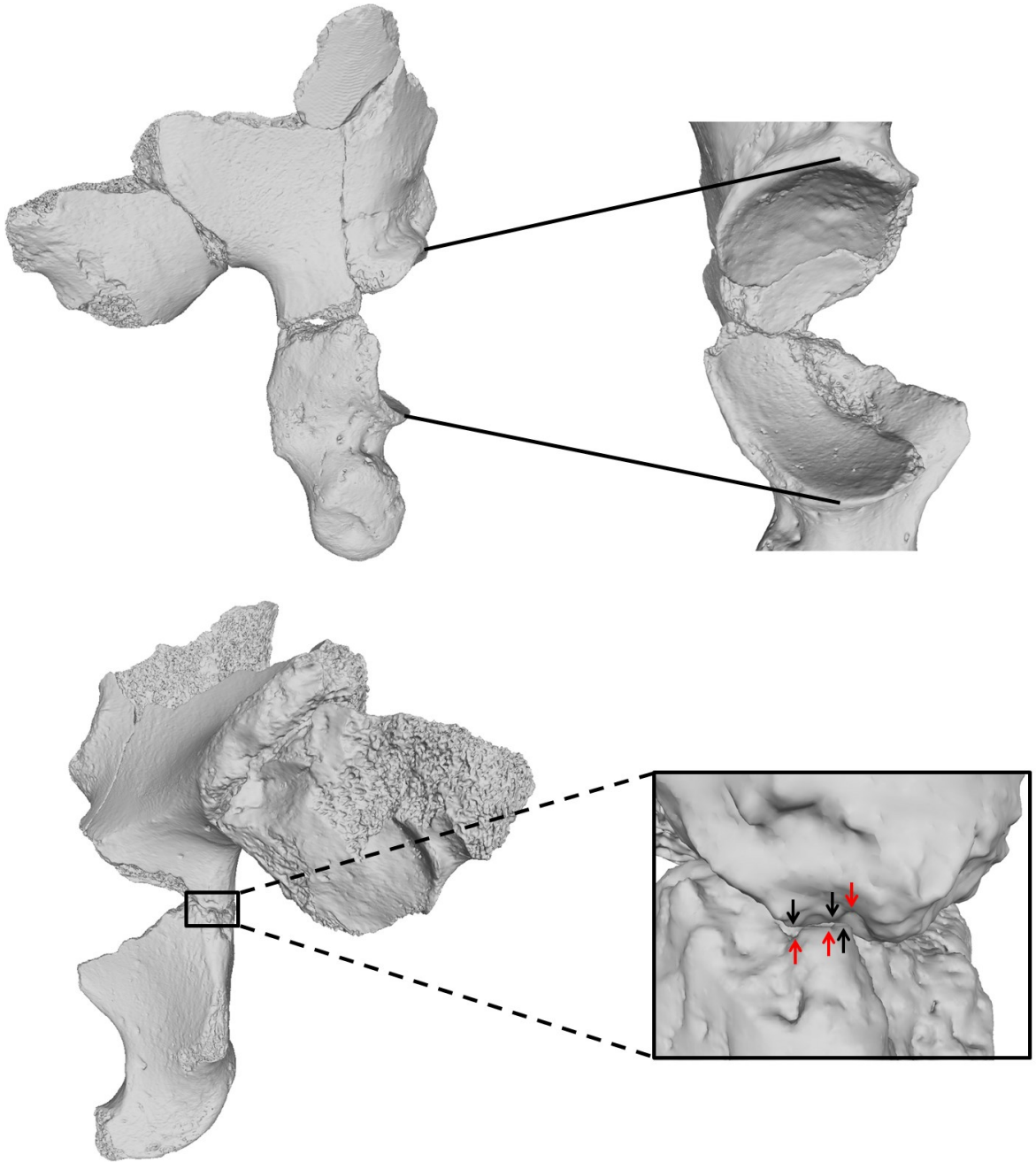


Figure 7. Alignment of the R1 right ischial fragment to the ilium. Red and black arrows indicate complementary pits and tubercles.

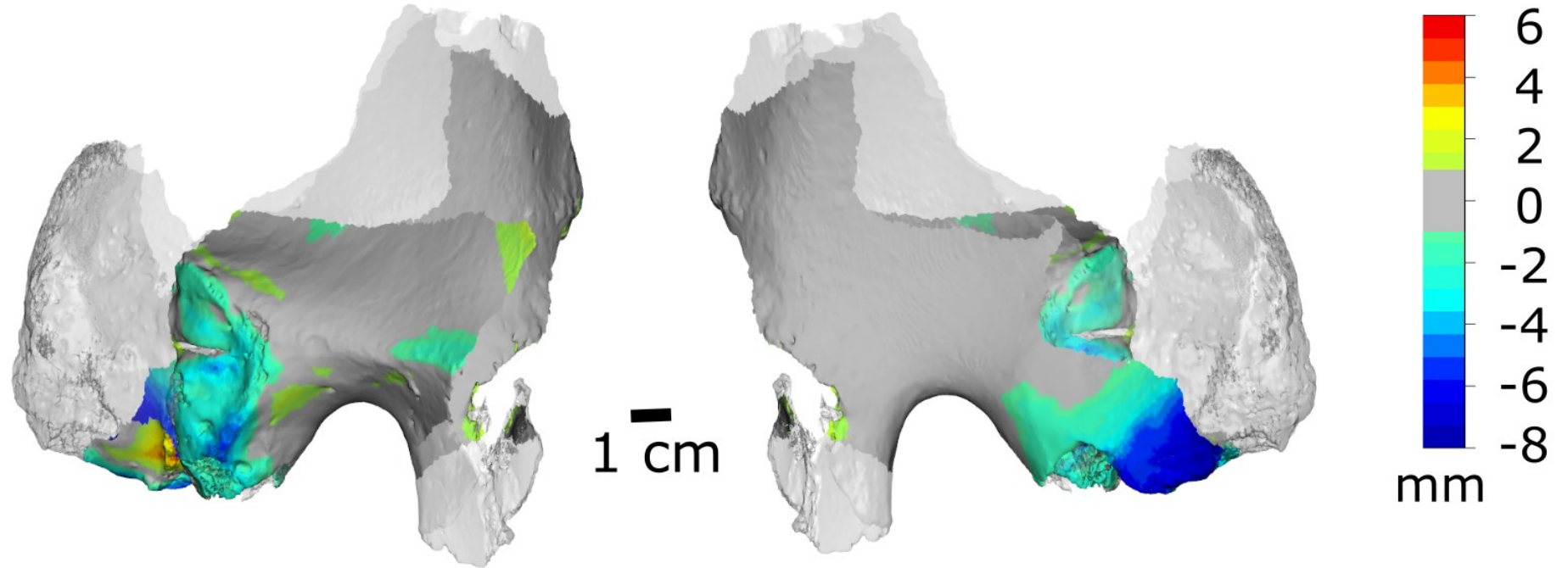


Figure 8. Colormap of distances between preserved complementary parts of the superimposed ilia of R1 (projected on the left coxae). The distance was computed from the left to the mirrored right coxae. Negative (blue) distance means that the left coxal bone is larger (or thicker).

After the alignment of the preserved fragments having direct connection, and mirror-image-based reconstruction, the right coxal bone consists of almost complete ilium and ischium with missing iliac crest and incomplete acetabulum. The acetabular cavity lacks the superior horn of the lunate surface. To complete the acetabulum, reference-based reconstruction was performed. A sample of three Neandertal coxal bones with complete acetabula (Kebara 2, Krapina 208 and 209) was used as a reference. The estimation procedure was as follows:

1. A template (Kebara 2) covering the missing acetabular area in R1 (Figure 9) was created from 12 anatomical landmarks and 154 semilandmarks in Viewbox 4 (www.dhal.com). From the total number of semilandmarks, 46 were localized on three curves (the arcuate line, the external and internal borders of lunate surface) and 108 were surface semilandmarks (localized on the lunate surface, acetabular notch, superior acetabular roof and the medial surface caudal to the arcuate line).

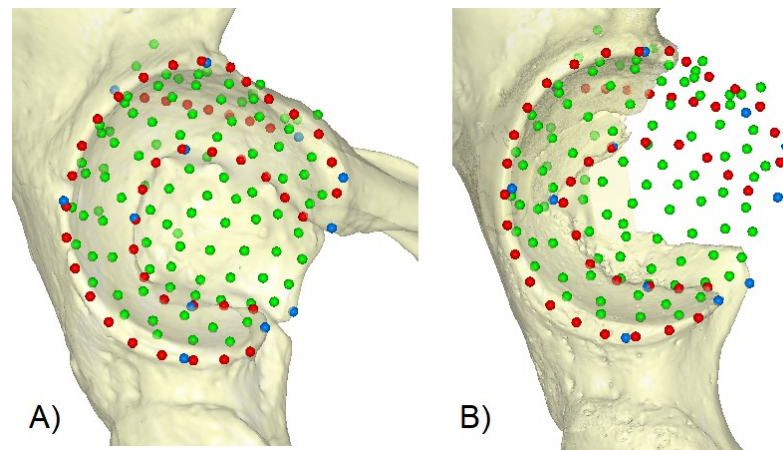


Figure 9. Estimation of the incomplete right acetabulum of R1. A) Kebara 2 as a template. B) Regourdou 1 with estimated missing landmarks. Blue = anatomical landmarks, red = curve semilandmarks, green = surface semilandmarks (pictures are tentatively in the same scale).

2. The template was applied to other reference specimens with semilandmarks sliding in order to locate these points in geometrically homologous positions with regard to the template.
3. The template was applied to the incomplete R1 right coxal bone. Preserved landmarks were located on the surface while missing landmarks were estimated using reference sample average (the estimations did not markedly differ based on

individual reference specimens). The TPS-based approach was used for the estimation using R package *geomorph* (Adams and Otárola-Castillo, 2013).

4. Kebara 2 surface mesh was first warped onto the average reference sample configuration and then onto the estimated configuration of R1. Warping was performed in R package *Morpho* (Schlager, 2016). The region of the superior acetabulum was cut and merged with the right coxal bone using Geomagic.

Fractures between physically glued or virtually aligned fragments were continuously being removed during the reconstruction process. For this purpose, surface inside the fractures was removed and gaps were filled with regard to the surrounding surface in Geomagic. An illustration of fracture removal is in Figure 10.

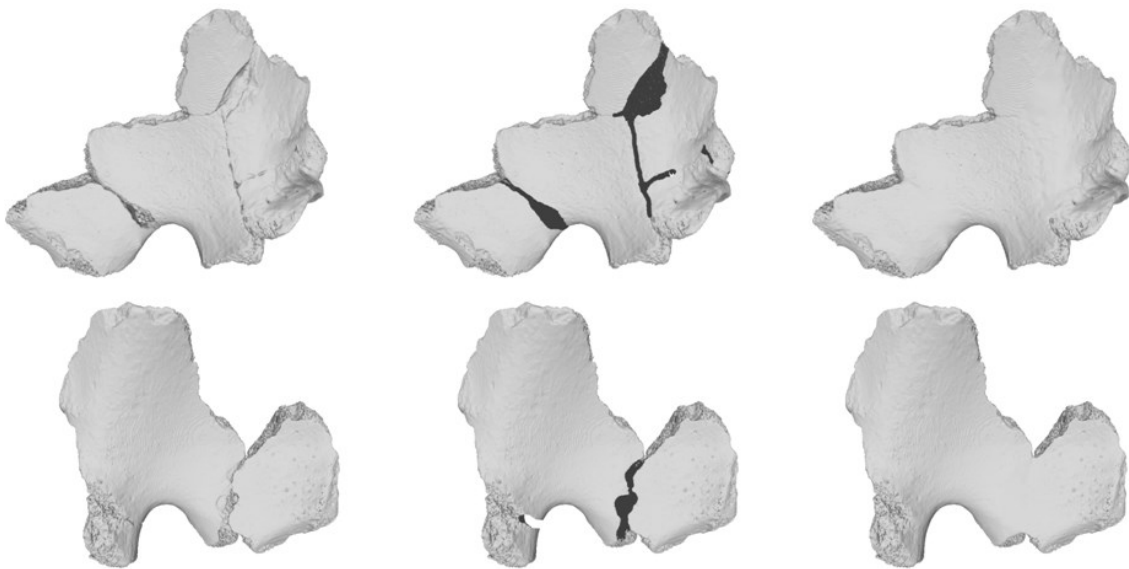


Figure 10. Removal of fractures and gaps in the right (up) and left (down) ilia. Left: original bone; middle: fractures removed; right: gaps filled (pictures are in the same scale).

Despite the asymmetry observed in the ilia, left ischial fragments closely match homologous regions of the mirrored right ischium (Figure 11). Therefore, the mirrored right ischium was aligned with the left ilium based on small overlapping regions in the lunate surface and the anterior arm of the greater sciatic notch. Anterior portion of the ilium as well as the acetabulum were reconstructed on the basis of the right counterpart. Reconstruction summary for the coxal bones is in Figure 11.

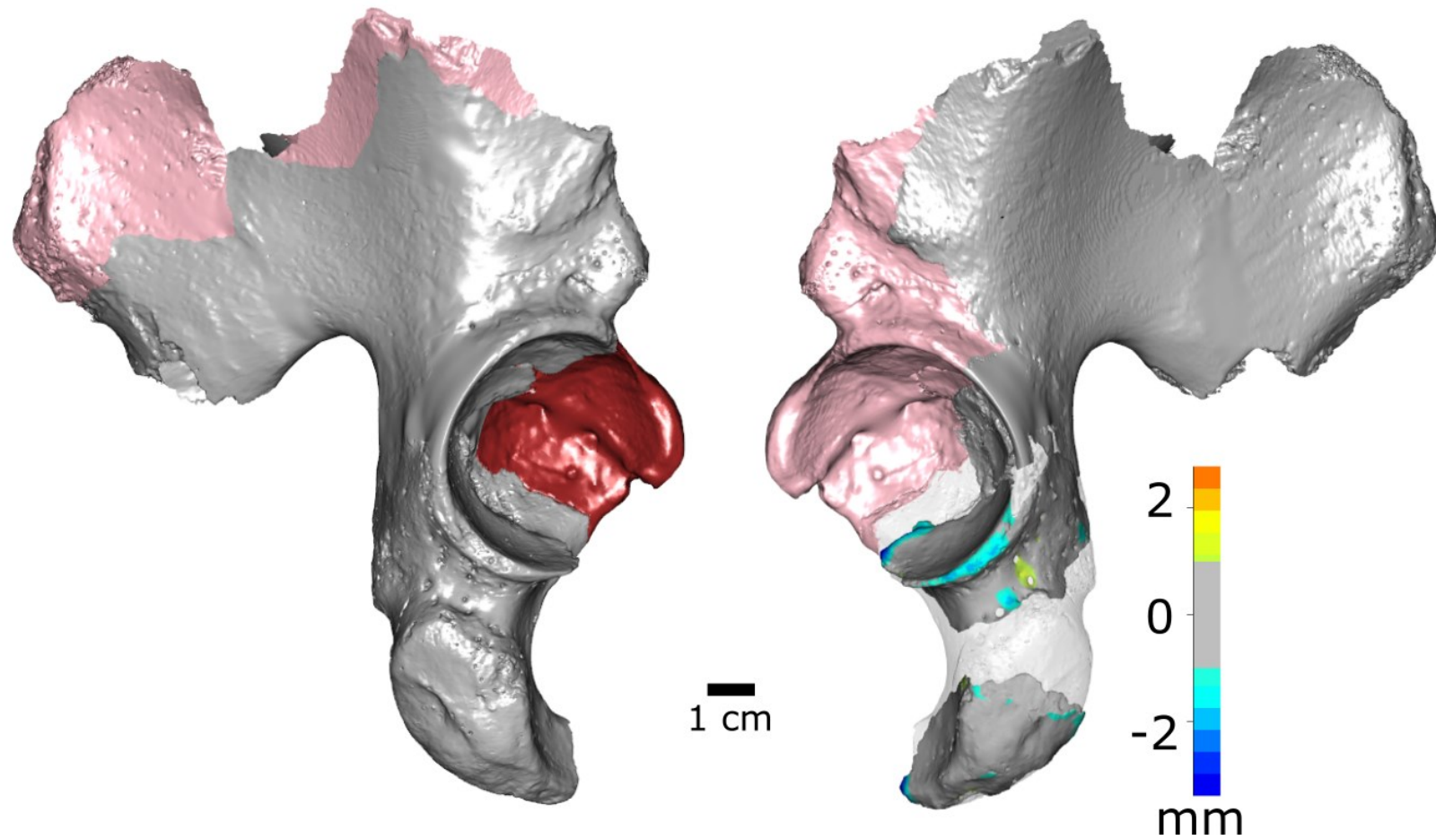


Figure 11. Summary of the reconstruction of both coxal bones of R1. Gray = original surface with filled fractures and gaps, pink = mirror-image-based warping, brown = reference-based reconstruction, transparent = mirrored right ischium. Mesh distance between both ischia is projected on the left ischial fragments.

7.2.2 Analysis

The new reconstruction of the R1 right coxal bone allowed us to try sex assessment of this individual, as the sexual traits and dimensions, previously unavailable, were completed. With regard to the preservation of pelvic remains, two methods were chosen for sex assessment: visual method proposed by Brůžek (2002) and morphometric method DSP (*Diagnose sexuelle probabiliste*) by Murail et al. (2005). Both are standard methods used in forensic, bioarcheological, and paleoanthropological context (Henry-Gambier et al., 2002; Gambier et al., 2006; Chapman et al., 2014; Mestekova et al., 2015; Quatrehomme et al., 2017) and both were recently revised and validated (Brůžek et al., 2017; Santos et al., 2019). Especially the visual method was further developed by adding statistical processing of data based on logistic regression. Therefore, both employed methods provide posterior probability of estimate.

As no standard method has ever been used to sex Neandertal pelvic remains, the methods were cross-validated on other Neandertal specimens, and results were compared to the most frequently assigned sex to these individuals in the literature. Only traits that do not show particularly different morphology in Neandertals compared to modern humans were selected, i.e. pubic region was completely excluded from the analysis, as it would bias the results towards the female sex due to long pubic rami in Neandertals. In the visual method (Brůžek, 2002), three morphological traits from the sacroiliac region were used (Figure 12): greater sciatic notch (GrSN), composed arc (CArc) and preauricular sulcus (PrSu). GrSN and PrSu are further divided into three sub-traits (GrSN 1–3 and PrSu 1–3). Following Figure 12, GrSN is evaluated with regard to the asymmetry in length of the notch arms AC to CB (GrSN1), the asymmetry in the overall notch shape (GrSN2), and intersection of a parallel line to CD passing through A with the notch outline (GrSN3; Figure 12a). CArc is evaluated as one continuous arc or a double arc (Figure 12b). PrSu is evaluated with regard to the presence of a negative relief (PrSu1), character of the relief (PrSu2), and the presence of a positive relief (PrSu3; Figure 12c). To assess the traits, one can choose from three categories: male, female or indeterminate. For detailed definitions please see Brůžek (2002) or Santos et al. (2019). In DSP, pubic length was excluded even if preserved in a specimen due to specific Neandertal morphology. All other dimensions could be measured and were included in the analysis (Figure 13). For detailed definitions please see Brůžek et al. (2017).

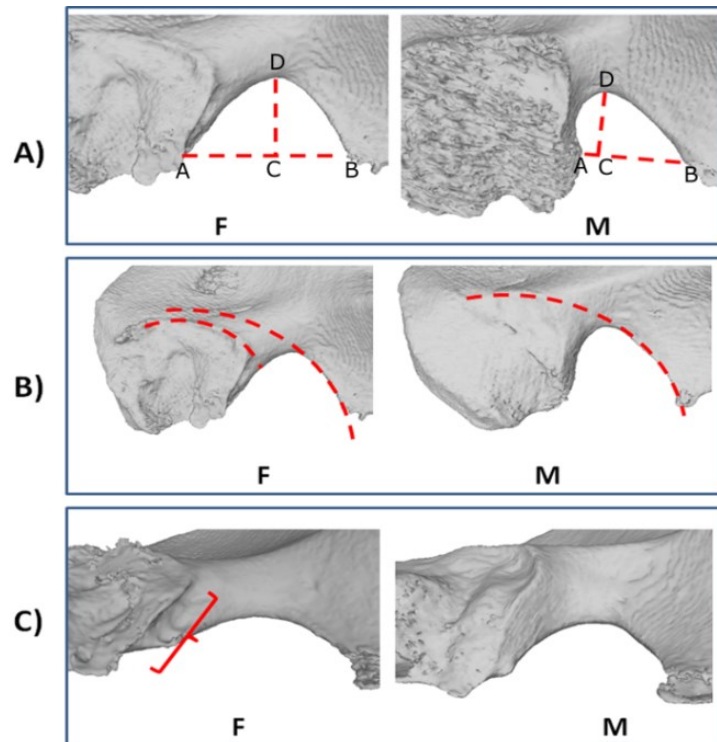


Figure 12. Male (M) and female (F) forms of visual traits from the method of Brůžek (2002) preserved in Neandertal specimens. A) Greater sciatic notch (GrSN), B) composed arc (CArc), C) preauricular sulcus (PrSu). Based on Santos et al. (2019).

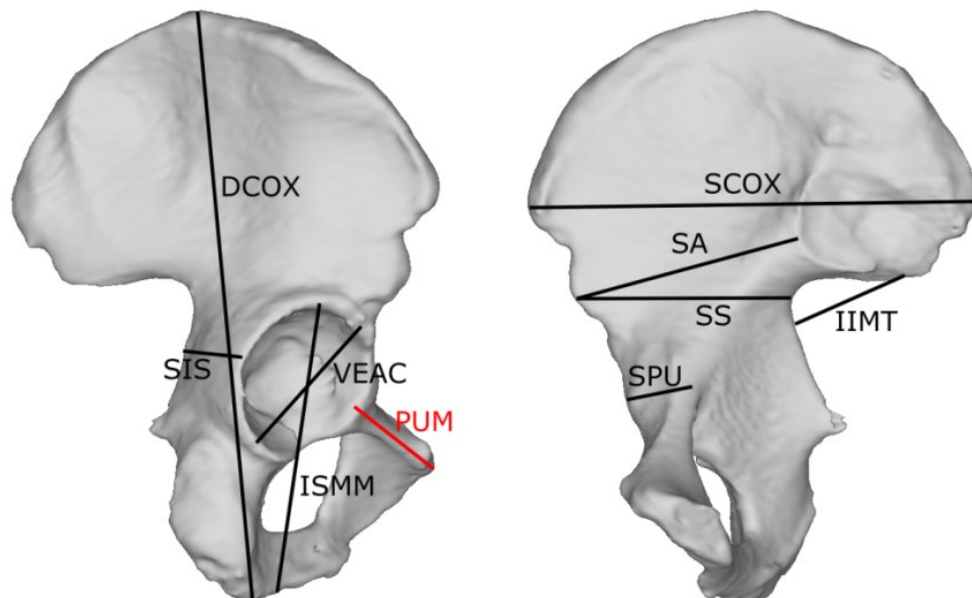


Figure 13. Linear dimensions from DSP (Brůžek et al., 2017). The pubic length (in red) was not included due to specific morphology of the Neandertal pubic region.

Several pelvic measurements were acquired on the reconstructed R1 pelvis and some other virtually reassembled pelves (Italian Upper Paleolithic specimens and La Chapelle 1). Pelvic measurements followed definitions of Martin (1928) and are indicated by “M” and an appropriate number. Pelvic incidence (PI) was also measured which is the orientation of the sacral superior surface in relation to the hip joint, and it is defined as the angle between a line perpendicular to the superior surface of the first sacral vertebra at its midpoint and the line connecting this point to an axis that connects the center of the acetabula (Figure 14; Peleg et al., 2007). This angle was originally measured on x-ray images; measuring this angle followed an adjustment to digitized 3D pelves using landmark coordinates (Bonmatí et al., 2010; Been et al., 2019). This angle was used in order to compute lumbar lordosis (LL) angle that is illustrated in Figure 14. Landmark coordinates were acquired and derived pelvic dimensions were computed in Viewbox 4.

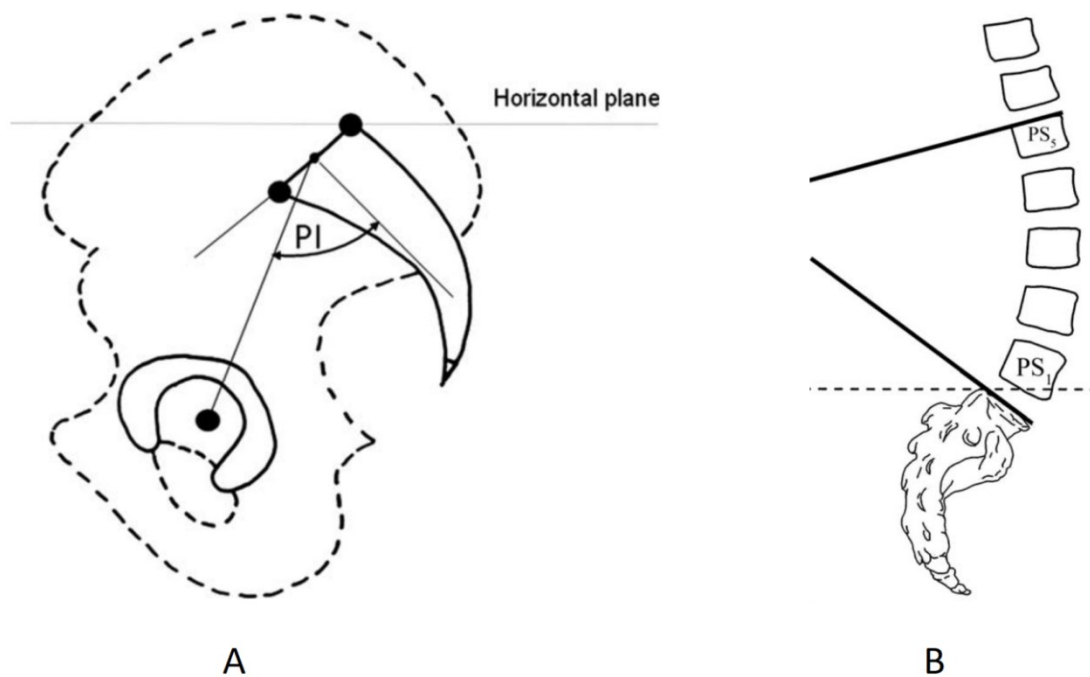


Figure 14. Definition of pelvic incidence angle (PI) in A) and lumbar lordosis angle in B). PS indicates presacral vertebrae (from Been et al., 2012 and 2014).

7.3 Results

7.3.1 Sacroiliac joint assembly

Although both sacroiliac joints are quite well preserved, the surfaces are slightly eroded so the margins are not well recognizable. Furthermore, missing pubic region makes the alignment more difficult because in a completely preserved coxal bone, it indicates the midsagittal plane and helps in finding appropriate orientation relative to the sacrum. For this reason, we tried several procedures; three of them used digitized models and the last one used 3D printed models. All the procedures were based on different criteria and led to different results which were evaluated using intermesh distances between the sacral auricular surfaces and the matching aligned ilia. The outcomes are summarized in Table 4 and illustrated in Figure 15 where the intermesh distances are projected on the sacral surfaces.

At first, we tried two automatic alignments. However in virtual environment, the models may overlap, so some manual refinement was always necessary. First, we examined articular pairs and identified complementary areas (such as matching depressions and tubercles) where landmarks were placed. The ilia were aligned based on landmark configurations and the positions were manually refined to prevent overlap of models. The ilia were also slightly translated along the sagittal plane, but the inclination in the sagittal plane was not much modified. This procedure resulted in a very asymmetrical alignment, but quite low and consistent distances between articular surfaces (Figure 15).

The second alignment was also more automatic and used the ICP algorithm. The auricular surfaces were cut from the wholes meshes, manually superimposed and their normals were oriented to the same side. The algorithm iteratively computed transformation to align the iliac surface to the sacral surface while minimizing distances between their vertices. This transformation was subsequently applied to the whole ilia. This procedure provided very variable outcomes when repeating the process pointing to the fact that the surfaces are not exact negatives. Therefore, we discarded this procedure.

The third option was a manual alignment of ilia guided by three anatomical criteria: articular congruence, continuity of the *linea terminalis* and bilateral symmetry. This obviously resulted in a more symmetrical pelvis than by the first procedure; both arcuate buttresses are at the same level with the right coxal bone inclined more caudally while the left one inclined more cranially compared to the first result (Figure 15). However, this

assembly produced relatively high intermesh distance with irregular distribution which means that the ilia were aligned less well with regard to the articular congruency.

Table 4. Summary of different assemblies of sacroiliac joint.

Method	Criterion	Result	Intermesh distance
Landmark-based alignment with manual refinement	Landmarks No overlap	Very asymmetrical inclination of both coxae in the sagittal plane	Rather low and consistent distances with high values in areas of depressions on the sacral surface.
ICP algorithm	No overlap	Very variable results	-
Manual alignment of digitized models	Articular congruence Continuity of the <i>linea terminalis</i> Symmetry No overlap	Rather symmetrical pelvis	Rather high and inconsistent distances with very high values in some areas.
Manual alignment of printed 3D models	Articular congruence Slight overlap allowed	Slightly asymmetrical	Very low and consistent distances with only slightly higher values in areas of sacral depressions.

ICP = Iterative Closest Point algorithm.

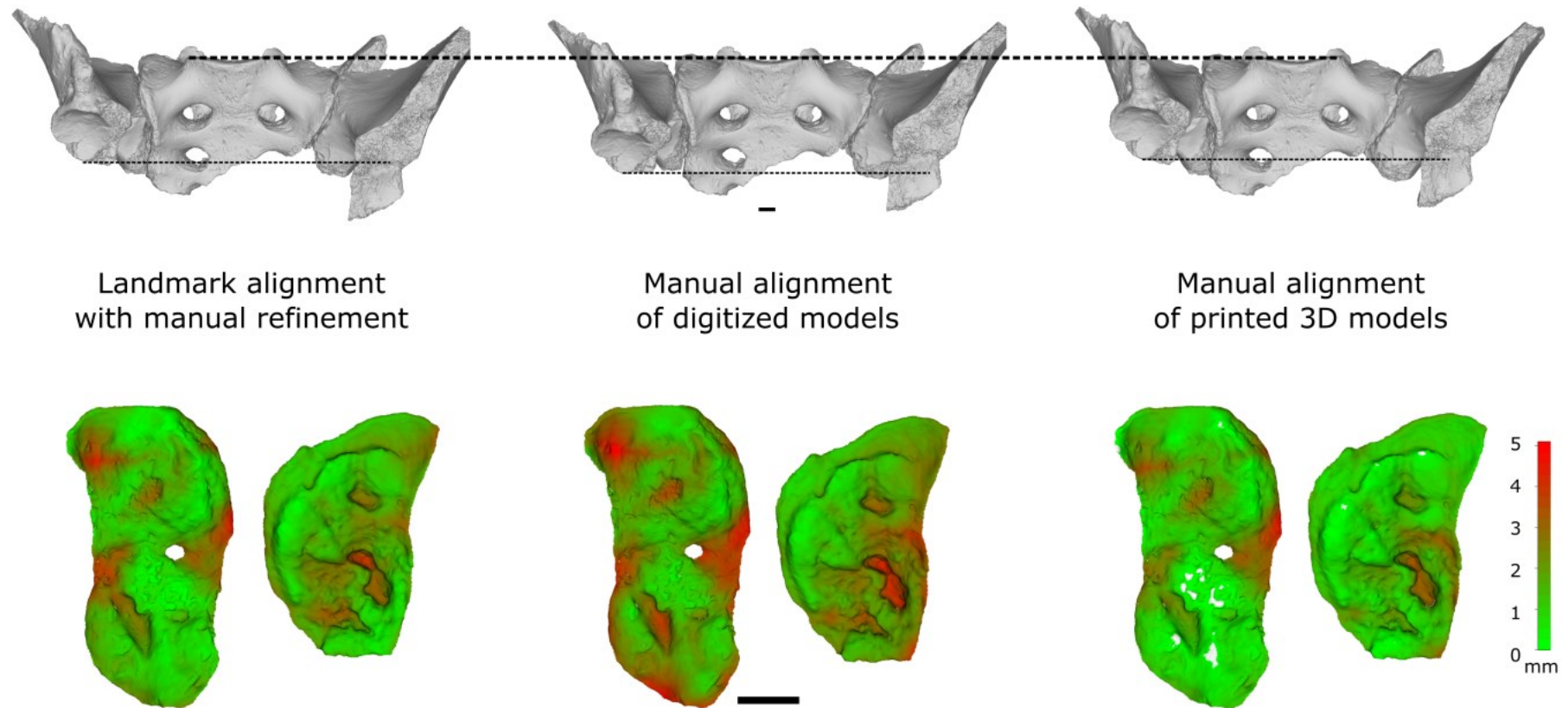


Figure 15. Comparison of outcomes of different SIJ assemblies in R1 (left, middle, right). Upper row: the assembled pelvises with the thicker line passing through the sacral base. The thinner line is parallel and shows differences in relative acetabular heights of both coxal bones (in the middle assembly it roughly connects complementary areas of the lunate surfaces). Lower row: intermesh distance between the right and left sacral auricular surfaces and matching aligned coxal bones. The last assembly shows the most consistent intermesh distance over the surface (white spots in this alignment are areas of negative distance where the ilia slightly overlapped with the sacrum). The scales are 1 cm.

With respect to the high degree of asymmetry in the R1 sacrum, the asymmetrical ilia, the fact that the sacroiliac surfaces do not possess marked complementary structures, and that the virtual alignment allows the models to overlap, it was not possible to determine which assembly more corresponds to the real state *in vivo* and we decided to print the digitized models and assemble them manually. We did not perform it on the original bones in order to prevent their damage and also because of their availability (deposition in two different institutions as explained in the Material section). Having the physical replicas, we were able to find optimal positions based on the articular congruency which restricted possible movements. The ilia were fixed and the assembled pelvis was scanned (Figure 16) providing a rough digitized model. The scan further served for the ICP alignment of the more detailed models segmented from micro-CT scans leading to the virtual replica of the manually assembled printed models. This process of physical assembly and scanning was repeated three times for each ilium. For the right ilium, the outcomes differed in the rotation along the vertical axis passing through the SIJ, but two results were almost identical, so one of them was selected. For the left ilium, the outcomes differed only very slightly in the sagittal orientation, and the one leading to a lower degree of asymmetry in the sagittal inclination of the coxal bones was selected for further analysis. This procedure resulted in a more cranially oriented right ilium (as in the landmark-based alignment) and an intermediate position of the left ilium with regard to the two previous reassembly methods leading to an intermediate degree of asymmetry. The intermesh distance was the lowest from all trials and was very consistently distributed over the articular surfaces. Therefore, we decided to take this assembly as the one that is the closest to the *in vivo* state and we work with it further.

After having selected the appropriate SI assembly, we followed the reconstruction process described in the Methods section and obtained the reconstructed pelvis lacking the anterior region (the pubic fragment does not have a direct connection), superior iliac alae and the lower sacrum. Final state of the reconstruction is in Figure 17.



Figure 16. 3D printed models of the R1 sacrum and right coxal bone assembled together.

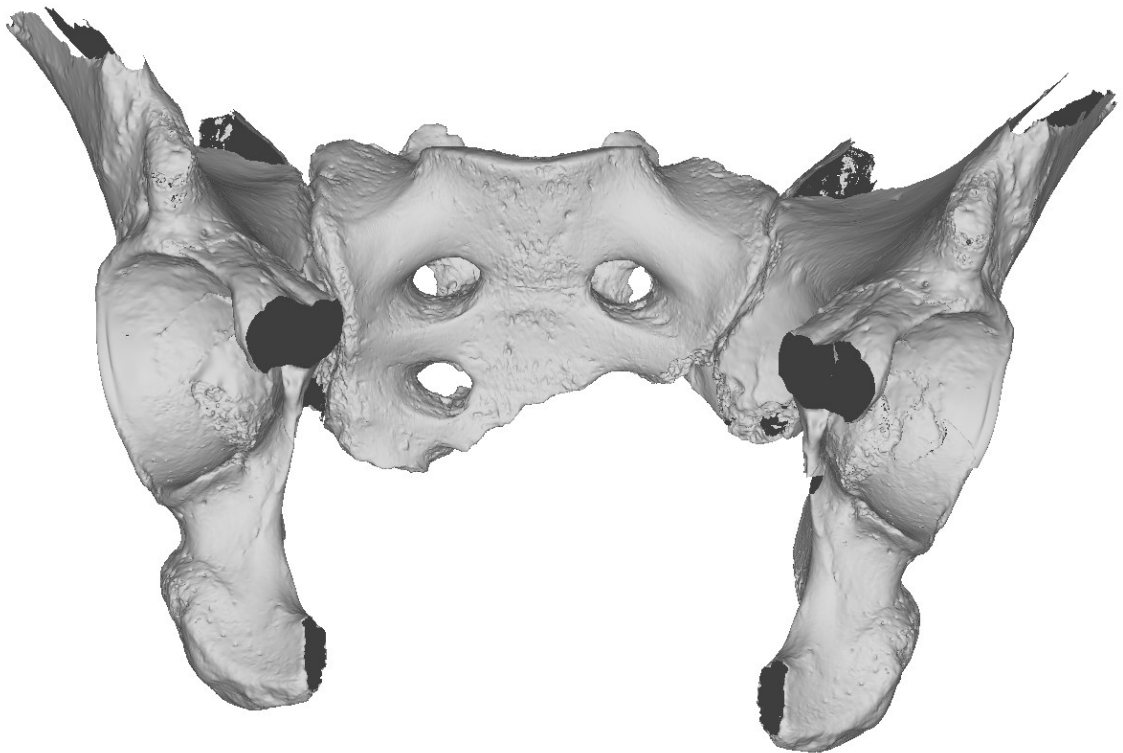


Figure 17. Final state of the R1 pelvic reconstruction (trabecular bone removed).

7.3.2 Validation of the reconstruction

Several measurements of the current reconstruction were compared to the previous reconstructions of the pelvis (Meyer, 2013) and of the right acetabulum (Plavcan et al., 2014). In the paper by Plavcan et al. (2014), the femoral head diameter was estimated from the acetabular lunate portion of the right ischium in order to estimate R1's body size. The most probable interval of the femoral head diameter ranged from 43.5 to 48.5 mm. Using the reconstructed R1 right coxae, we were able to directly measure the acetabular diameter ($M22 = 55.6$ mm) which tightly correlates with the femoral head diameter. Based on the equation published by Ruff (2010):

$$FHD = 0.945 \times M22 - 6.1 \ (r = 0.97)$$

we obtained a value of 46.4 mm for femoral head diameter which is slightly higher than the mean estimate (45.9 mm) given by Plavcan et al., but well inside their range. This partly validates the reconstruction of the right coxae.

Previously, a virtual reconstruction of the R1 pelvis had already been made by Meyer (2013) using a different protocol. Therefore, we can compare these reconstructions and their protocols in order to provide recommendations for pelvic reconstructions in general. As the previous work was focused on obstetrics, we were able to compare four diameters of the pelvic canal (Table 5). There are marked differences between the two reconstructions; in general, the new reconstruction is considerably wider in the inlet and outlet, approaching the mean values of a comparative modern sample used by Meyer (2013) (Table 5). The transverse diameters of the previous reconstruction of R1 were very small, at the lower end of the modern variation. There is one exception: the left diagonal inlet diameter is shorter in our reconstruction and values from both sides are more asymmetrical. With regard to the reconstruction protocols discussed later in section 7.4.1, we have further analyzed only the new reconstruction.

Table 5. Linear dimensions (in mm) of the reconstructed Regourdou 1 pelvis in comparison with the previous reconstruction (Meyer, 2013).

Var.	Definition	R1 (our)	R1 (2013)	Males ^c	Females ^c
M24	Inlet transverse diameter (Martin, 1928)	126.0	108.1	124.1±8.0	131.9±6.7
M25	Inlet diagonal diameter (Martin, 1928)	118.8/ 127.1 ^a	127.4/ 123.5 ^a	137.8±6.7	140.6±5.9
BIP	Bi-ischiatic diameter posterior between the most posterior points on the ischial tuberosities (Meyer, 2013)	135.8	98.6	127.7±10.1	142.6±9.2
BIA	Bi-ischiatic diameter anterior between the most anterior points on the ischial tuberosities (Meyer, 2013)	~100 ^b	66.9	74.4±9.3	94.4±9.9

^a left/right

^b The anterior tip of the ischial tuberosity is not preserved. This is an estimate.

^c For comparison data on a modern French population (73 males, 78 females) from Meyer (2013).

7.3.3 Sex diagnosis

The reconstruction of the right coxal bone completed the greater sciatic notch and allowed us to assess new features for sexual diagnosis that are not well preserved on the left side. For this purpose, we used sex estimation methods that provide posterior probability of the estimate (Brůžek et al., 2017; Santos et al., 2019), but they are based on modern human population samples. In order to examine performance of these methods in Neandertals, we first applied those methods on the available Neandertal coxae (n=12) and compared results with the sex assigned to them in the published literature. Visual scoring of Neandertal specimens is in Table 6, raw linear measurements are in Table 7, and results of both methods are summarized in Table 8.

All specimens for whom the visual method provided sex estimate (posterior probability >0.95) were sexed congruently to the literature data. There were four specimens that were indeterminate; three of them had posterior probability >0.90 and the more probable sex was congruent with the literature. However, for Amud 1 the probability was 0.88 for female sex which does not correspond to the most frequent sex in the literature.

Table 6. Scoring of Neandertal sexual traits based on the method of Brůžek (2002) and Santos et al. (2019).

Specimen	GrSN1	GrSN2	GrSN3	GrSN	CArc	PrSu1	PrSu2	PrSu3	PrSu
R1 (right coxae)	m	m	f	M	M	m	m	i	M
R1 (left coxae)	-	m	-	I	F	m	m	-	I
Amud 1 ^a	-	i	-	I	F	-	-	-	-
Feldhofer 1	m	m	m	M	M	m	i	m	M
Ferrassie 1	m	m	m	M	M	m	m	m	M
Grotte du Prince	f	f	f	F	F	-	-	-	-
Kebara 2	m	m	m	M	M	m	m	m	M
Krap. 207	m	m	m	M	F	m	m	i	M
Krap. 209	f	f	f	F	F	m	m	i	M
Chapelle 1	m	m	f	M	M	m	m	f	M
Palomas 96	f	f	f	F	F	-	-	-	-
Tabun C1	f	f	f	F	F	-	-	-	-

Sub-traits are classified with lower-case letters while main traits are classified with capital letter. The hyphen is used when a trait is not preserved or available (e.g., the case of Palomas 96).

^a The greater sciatic notch in Amud 1 has preserved the anterior arm and a cranial half of the posterior arm. Despite previous statements about the asymmetrical greater sciatic notch (Endo and Kimura, 1970; Trinkaus, 2016), we did not come to the same conclusion based on our observation and we think that the posterior arm could even continue in a symmetrical way.

The metrical method provided sex estimate for 8 of 10 individuals. Two individuals were considered indeterminate, but the more probable sexes were similar to the visual method and corresponded to the literature. From those with assigned sex (probability >0.95), two were classified incongruently with the literature (Amud 1 and Grotte du Prince).

Table 7. Linear dimensions (in mm) of the Neandertal specimens for sex diagnosis using the metrical (DSP) method (Murail et al., 2005; Brůžek et al., 2017).

Specimen	SPU	DCOX	IIMT	ISMM	SCOX	SS	SA	SIS	VEAC
R1 (right coxae)	-	-	<i>30.0–33.0^a</i>	<i>109.6^a</i>	-	67.4	77.1	34.3	55.6
Amud 1	24	-	-	-	-	74.2	90.6	38.7	57.1
Feldhofer 1	-	228	34.4	<i>123</i>	<i>160</i>	68.9	83.3	39.2	61.8
Ferrassie 1	30.7	-	28.4	<i>119</i>	-	-	-	36.2	59.9
Grotte du Prince	28	-	36	-	-	68	79	26	59
Kebara 2	31	227.5	31.8	111.9	157.9	63.9	76	31.9	58.9
Krapina 207	-	<i>205</i>	32	-	-	68	78	31.3	53.2
Krapina 208	30.7	-	-	<i>120</i>	-	-	-	36	56.1
Krapina 209	25.3	-	36.3	-	-	63.9	78.8	31	54.8
Chapelle 1	-	-	<i>30.4</i>	<i>123</i>	-	64	68.4	40	61
Tabun C1	26	<i>200</i>	-	<i>90.2</i>	-	60.5	73.1	29.9	48 ^b

Measurement of linear dimensions is illustrated in Figure 13 and detailed definitions are in Brůžek et al. (2017). Values in italics must have been slightly estimated; usually the missing delimiting point was very close to the preserved morphology.

^a For the IIMT, the delimiting point close to the auricular surface was not clear in R1. Therefore, minimum and maximum values were used. For the ISMM, the anterior tip of the ischial tuberosity is not preserved but borders of the tuberosity converge and they would meet soon. Therefore, the ISMM was measured to the most anterior preserved point on the ischial tuberosity which does not much affect the final value.

^b This value was estimated by McCown and Keith (1939) as the acetabulum is crushed.

Table 8. Sex estimates of Neandertal specimens based on the visual and metrical methods with a summary of congruency with literature data.

Specimen	Visual method (Santos et al., 2019)		Metrical method (Brůžek et al., 2017)		Literature	
	P(M)	Sex	P(M)	Sex	Sex	Ref.
R1 (right)	0.992	M	0.955–0.98	M	I	section 7.1
R1 (left)	0.846	I (M)	-	-	I	
Amud 1	0.123	I (F)	0.017	F	M	1, 2
Feldhofer 1 ^a	0.939	I (M)	1.0	M	M	2, 3
Ferrassie 1	0.995	M	1.0	M	M	2, 4
Grotte du Prince	0.014	F	0.969	M	F	5
Kebara 2	0.995	M	1.0	M	M	6
Krapina 207	0.909	I (M)	0.719	I (M)	M	7, 8
Krapina 208	-	-	0.992	M	M	7
Krapina 209	0.063	I (F)	0.291	I (F)	F	7, 8
Chapelle 1	0.995	M	1.0	M	M	2, 9
Palomas 96	0.014	F	-	-	F	10
Tabun C1	0.014	F	0.002	F	F	2, 11
Congruent results ^b		6 (60%)		6 (60%)		
Incongruent results		0		2 (20%)		
Indeterminate results		4 (40%)		2 (20%)		

P(M) is a posterior probability of male sex. Posterior probability of female sex, P(F), can be computed as 100 – P(M). Values in bold reach the 0.95 probability threshold allowing a reliable sex diagnosis. Results not reaching this threshold should be considered indeterminate (I), but we also give the sex that is more probable in brackets.

1 = Endo and Kimura (1970), 2 = Trinkaus (1980), 3 = Skoglund et al. (2013), 4 = Heim (1982), 5 = de Lumley-Woodyear (1973), 6 = Rak and Arensburg (1987), 7 = Bonmatí and Arsuaga (2007), 8 = Trinkaus (2016), 9 = Boule (1911), 10 = Walker et al. (2011), 11 = McCown and Keith (1939).

^a The only specimen that is sexed genetically (Skoglund et al., 2013).

^b Congruency with the literature data is computed from specimens that could be estimated by a given method and leaving out Regourdou 1, as its sex is considered indeterminate (n=10 for both methods).

The reconstructed R1 right coxae enabled us to use both methods. Visual traits are illustrated in Figure 18 a scored in Table 6. The greater sciatic notch is asymmetrical

resulting in the overall masculine morphology. Preauricular area does not show signs of the preauricular sulcus, found more often in females. Lastly, the anterior arm makes a contiguous arc with the superior border of the auricular surface. This set of traits leads to male sex with a posterior probability of 0.99.

For the DSP, six linear dimensions could be measured in R1. As the posterior inferior iliac spine is slightly eroded, IIMT (see Figure 13) was measured several times, minimum and maximum values were rounded to the respective lower or upper limits, and sex diagnosis was performed twice with these values. This method resulted in male sex estimation with posterior probability of 0.96–0.98.

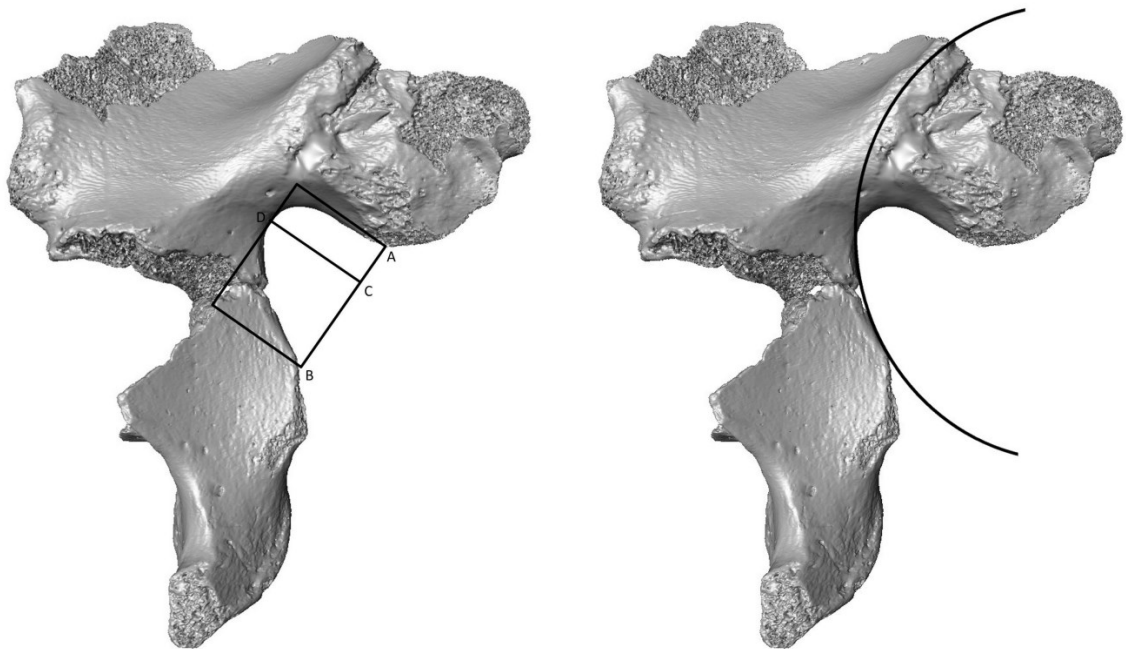


Figure 18. Visual sex traits in Regourdou 1 following Brůžek (2002). Left: scoring of the greater sciatic notch shape, right: composite arc.

However, the left coxae shows slightly different traits, but it is necessary to mention that the sacroiliac area is not sufficiently preserved. As was already described by Meyer (2013), the left greater sciatic notch is rather asymmetrical, but there is the composite arc. The preauricular region shows mild shallow depression which has indistinct margins, so this corresponds to the male morphology. The visual method still leads to male sex based on this set of traits although the probability is lower (0.846).

In summary, our assessment of the sex of R1 suggests that this skeleton probably belonged to a male individual.

7.3.4 Comparative analysis

Current state of the reconstruction enabled us to reliably measure transverse dimensions of the R1's pelvic inlet and outlet and pelvic incidence. To explore variation in our comparative samples, we have first analyzed shape in different pelvic planes. We have focused on the inlet and outlet as the midplane transverse diameter is not well preserved in the fossil record. Pelvic dimensions are summarized in Table 9.

Figure 19 shows shape in the pelvic inlet and outlet. Values of the inlet index (sagittal/transverse dimensions) are lower than 1 indicating transversally oval inlet while values for the outlet are distributed around $y = 1$ or are slightly higher which indicates rather round or slightly sagittally oval outlet. The position of the modern samples relative to the line $x = y$ indicates a difference between the inlet and outlet shapes. The inlet and outlet are shaped similarly in both modern males and females, but there is a slight difference in the variation of both modern samples with the Spitalfields collection limited to lower values of the inlet index suggesting a relatively more oval inlet.

The Upper Paleolithic individuals are inside the modern human variation for pelvic inlet and outlet shapes. Additionally, there are multiple values for the most complete Neandertal male (Kebara 2) and female (Tabun C1) pelvises: for Tabun C1 there are two different reconstructions varying mainly in the outlet shape (Ponce De León et al., 2008; Weaver and Hublin, 2009); for Kebara 2 there are two values measured by different researchers varying in the outlet transverse diameter (Rak, 1991; Tague, 1992). Both values for Kebara 2 are at the edge of the modern variation having transversally oval both inlet and outlet. The reconstruction by Weaver and Hublin (2009) is close to Kebara 2, while the one by Ponce de León et al. (2008) is in the middle of the modern human variation having differently shaped inlet and outlet. The last fossil specimen, the Middle Pleistocene SH Pelvis 1, is also close to the modern variation having oval inlet and rather round outlet.

Table 9. Summary of pelvic linear dimensions (in mm).

		M23	M24	M26	M27	M22
Recent (Coimbra)	Males	103.9±8.5	121.5±6.5	105.2±8.8	94.2±9.4	55.2±2.8
	Females	109.7±9.6	130.7±9.0	113.1±8.6	107.9±11.9	50.1±2.7
Recent (Spitalfields)	Males	100.4±7.4	126.0±7.0	106.4±7.5	95.0±8.6	57.5±2.9
	Females	105.9±10.1	135.3±7.6	117.7±9.9	112.7±13.3	50.8±2.7
Upper Paleolithic	Males	102.4±10.0	120.4 ±7.5	104.4 ±10.9	101.2 ±11.5	54.9±2.3
	Females	130.5	136.7	141.0	129.6	53.0
Neandertals	K2	117	141	88	104–114 ^a	58.9
	CAS1	-	131	-	114.5	61.5
	TC1 ^b	104	131	93	132	48
	TC1 ^c	109–121	143–145	123–134	116–126	48
	R1	-	126	-	120.7	55.6
Middle Pleistocene	SH1	108.3	139.3	127.5	133.6	58.8
Early Pleistocene	BSN49	98	124.5	-	133.3	41

M23 = inlet sagittal diameter, M24 = inlet transverse diam., M26 = outlet sagittal diam., M27 = outlet transverse diam., M22 = acetabular diameter (definitions according to Martin (1928)). Individual acronyms are in Table 3.

^a The lower value is from Rak (1991), the upper value is from Tague (1992).

^b Weaver and Hublin (2009).

^c Ponce de León et al. (2008).

Figure 20 shows analysis of inlet and outlet transverse diameters including the reconstructed R1. The transverse diameters are size-adjusted by the acetabular diameter. There are clear differences between modern male and female samples in the relative widths of the pelvic inlet and outlet. Upper Paleolithic humans fit well with these sex differences. For Neandertal males, the La Chapelle 1 individual tends to be closer to the modern male mean, while Kebara 2 and R1 are in the zone of overlap between males and females. R1 has almost similar inlet and outlet widths in contrast to Kebara 2. Both reconstructions of Tabun C1 are at the extreme of the modern female variation. With regard to size, SH Pelvis

1 is close to R1 having slightly wider pelvic planes. Completely outside modern human variation in the direction of modern females, there is the female pelvis assigned to *H. erectus* (Simpson et al., 2008) from the late Early Pleistocene which has very wide both inlet and outlet probably representing the ancestral pelvic conformation.

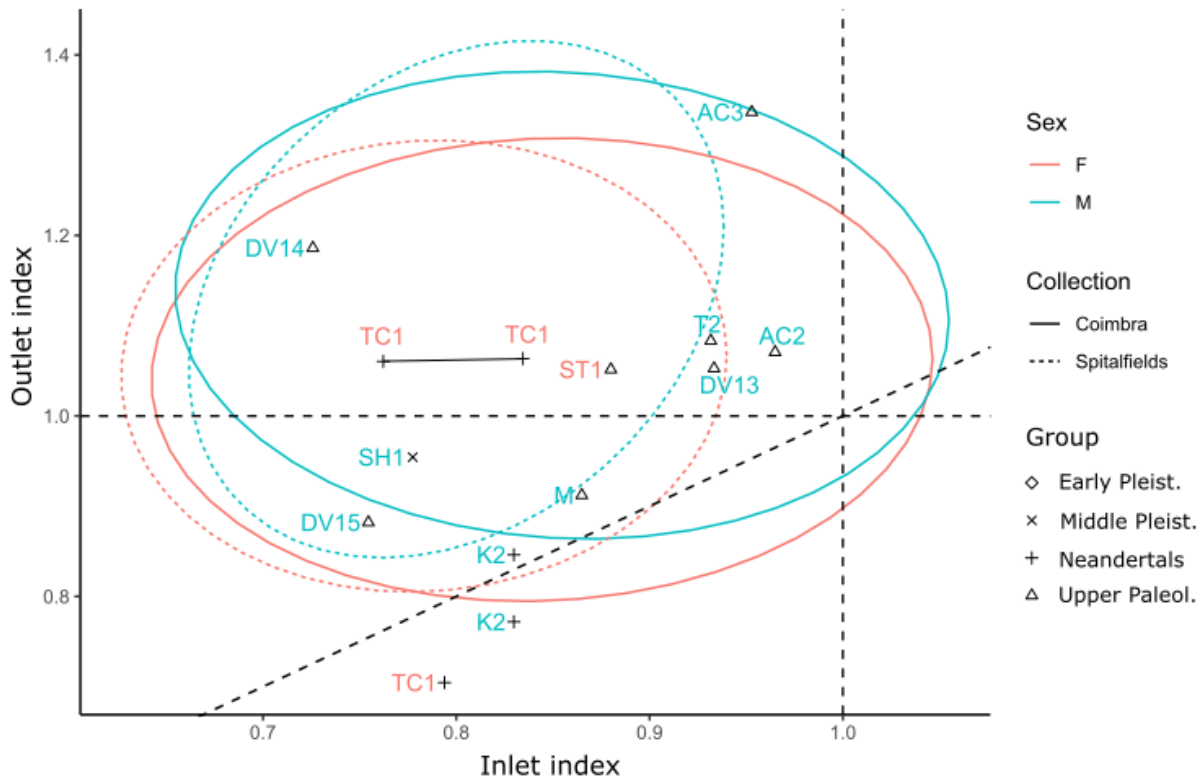


Figure 19. Analysis of shape in pelvic inlet and outlet. Inlet index (sagittal diam./transverse diam.) is on x-axis, outlet index is on y-axis. 95% confidence ellipses for males and females from modern collections. Individual points indicate fossil specimens (for their acronyms see Table 3). Black dashed lines indicate inlet and outlet shape ($x = 1$, $y = 1$) and relative differences between them ($x = y$). Two connected estimates for TC1 are from Ponce de Léon et al.'s (2008), the other is from Weaver and Hublin (2009).

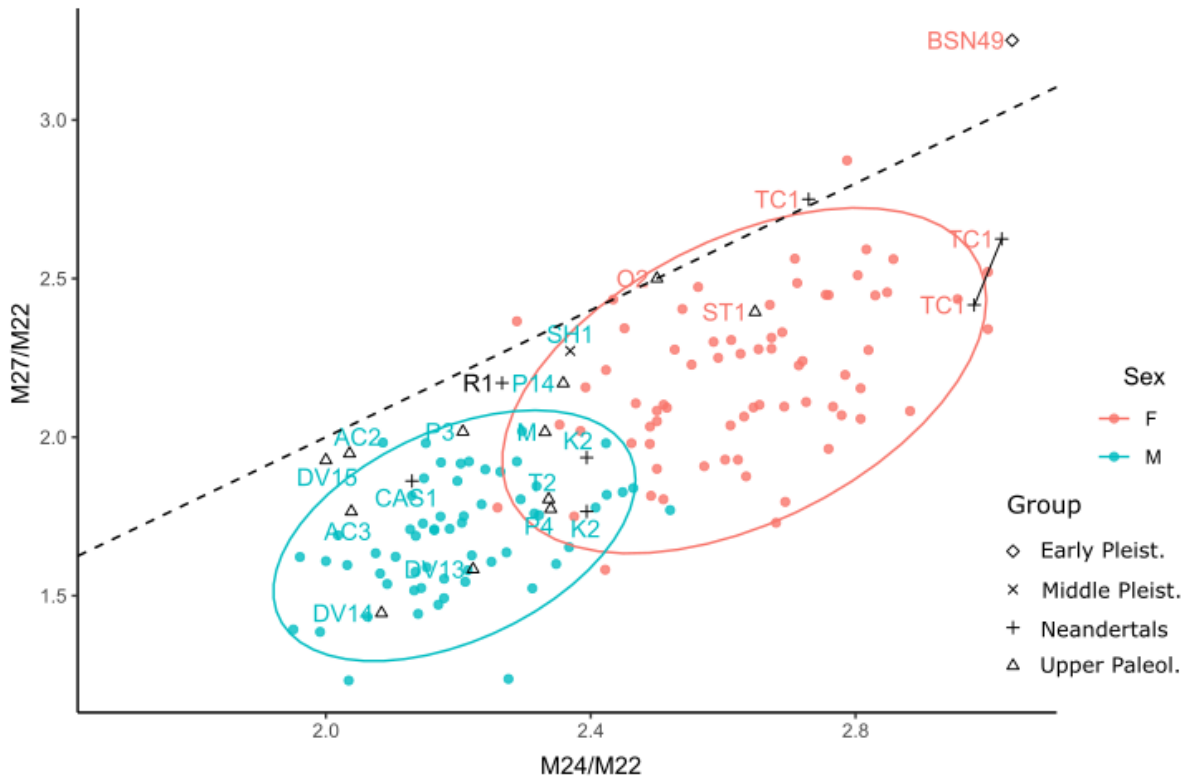


Figure 20. Inlet (M24) and outlet (M27) transverse diameters scaled to acetabular diameter (M22). 95% confidence ellipses are for modern males and females. Individual points indicate fossil specimens (for their acronyms see Table 3). Dashed line ($x = y$) indicates isometric changes. Two connected estimates for TC1 are from Ponce de Léon et al.'s (2008), the other is from Weaver and Hublin (2009).

Secondly, pelvic incidence was measured in the R1 reconstructed pelvis and compared to data from the literature (Table 10). Modern humans show a great variation of PI ranging from 20 to 90°. R1's PI falls close to modern human mean. Furthermore, it is substantially higher than previously proposed angles for Kebara 2 and SH Pelvis 1 and 2 (Bonmatí et al., 2010), but very close to the recently published value for La Chapelle 1 (Table 10).

Using following equations based on primate groups means and human data (Been et al., 2014), respectively,

$$LL = 0.999 \times PI - 5.16 \quad (r = 0.93),$$

$$LL = 0.718 \times PI + 11.724 \quad (r = 0.65)$$

we have calculated lumbar lordosis angle from the PI of R1. These models provided mean values of 45.7° and 48.3° that are close to the modern human mean, but there are again apparent differences between other Neandertal specimens for whom the LL was estimated by different methods (Table 11).

Table 10. Variation of pelvic incidence angle (in °).

Population or specimen	PI (mean)	Min	Max	Method of measurement	Ref.
Recent modern humans					
USA, Hamann-Todd collection (n=424)	54.1±12.6	18	89	Landmarks (assembled dry bones)	(Peleg et al., 2007)
France (n=145)	50.2±10.6	-	-	X-ray	(Legaye, 2007)
France, Olivier collection (n=51)	54.4±11.7	~27	~84	Landmarks (assembled dry bones)	(Legaye et al., 2011)
Israel (n=49)	54.9±10.0	39	84	X-ray	(Been et al., 2014)
Netherlands (n=310)	48.0±11.0	20	77	Landmarks (CT)	(Schlösser et al., 2014)
Hamann-Todd Collection (n=880)	46.0±11.0	~19	~81	Photographs	(Weinberg et al., 2016)
Sweden, healthy sample (n=44)	41.3±11.4	~18	~75	Landmarks (CT)	(Brink et al., 2019)
Sweden, scoliotic sample (n=37)	46.8±12.4	~28	~78	Landmarks (CT)	(Brink et al., 2019)
Neandertal lineage					
CAS1	56			Landmarks (3D)	(Haeusler et al., 2019)
K2	34			Landmarks (cast)	(Been et al., 2013)
R1	50.9			Landmarks (3D)	This study
SH1	27.6			Landmarks (3D)	(Bonmatí et al., 2010)
SH2	32.9			Landmarks (3D)	(Bonmatí et al., 2010)

Individual acronyms are in Table 3.

Table 11. Estimated lumbar lordosis angle (in °).

Specimen	LL^a	Method	Ref.
Modern humans	51.2±11.1 (30–80) ^b	X-ray	(Been et al., 2012)
(n=106 and 131)	55.6±11.2 (25–84) ^b	X-ray	(Tardieu et al., 2017)
Neandertal lineage			
CAS1	33	IAP	(Been et al., 2012)
	52	PI	(Haeusler et al., 2019)
K2	25.5	IAP	(Been et al., 2012)
	29–36	PI	(Been et al., 2014)
R1	47	PI	This study
Shanidar 3	31–40	IAP	(Been et al., 2012)
SH1	23–32	PI	(Been et al., 2014)
SH2	28–35	PI	(Been et al., 2014)
Late Pleistocene modern humans			
Skhul IV	58	PI	(Been et al., 2017)
Upper Paleolithic			
Cro-Magnon 1	45	IAP	(Been et al., 2012)
Cro-Magnon 3	65.5	IAP	(Been et al., 2012)
Ohalo 2	48	PI	(Been et al., 2014)

Individual acronyms are in Table 3.

IAP = method based on inferior articular processes orientation of lumbar vertebrae. Two major models were created based on different combinations of lumbar vertebrae using primate groups means ($r > 0.95$, error $< 5^\circ$) and human data ($r = 0.61$ – 0.79 , error $< 9^\circ$) (Been et al., 2012). PI = method based on pelvic incidence using primate groups means ($r = 0.93$, error = 6.7°) and human data ($r = 0.65$, error = 8.5°) (Been et al., 2014). X-ray = method of direct angle measurement (Been et al., 2012).

^a If estimates based on different equations using the same method differs $< 3^\circ$, a mean value is provided.

^b Range of minimum and maximum values in brackets.

7.4 Discussion and conclusions

In this study, we present a new reconstruction of the Regourdou 1 pelvis based on the virtual reconstruction methodology, and we provide new sex diagnosis and a preliminary analysis of certain newly available pelvic measurements. As virtual reconstruction methodology was mainly developed based on skull reconstructions (Zollikofer and Ponce de León, 2005; Gunz et al., 2009) and, in most of cases, applied to the same anatomical region (e.g., Ponce De León and Zollikofer, 1999; Benazzi et al., 2011; Amano et al., 2015; Haile-Selassie et al., 2019), we will first discuss unique issues in pelvic reconstructions. After that we provide some thoughts on the current research of the Neandertal pelvic morphology.

7.4.1 Pelvic reconstruction

Every reconstruction is nothing else than an approximation of the *in vivo* state. Although recent years provided more standardized procedures for fossil reconstruction than had been previously possible, virtual methods can still lead to variable outcomes depending on different variables such as the methodology employed, the completeness of the fossil to be reconstructed, the presence or lack of pathologies or asymmetries, as well as the degree, if any, of the taphonomic distortion. Some of these factors were apparent when our new reconstruction of the R1 pelvis was compared to the previous one (Meyer, 2013). Here, we discuss differences between both reconstructions.

In contrast to the state of preservation during the Meyer's reconstruction, we worked with a more complete left ilium that has been supplemented with a fragment of the retroauricular surface glued to the rest of the ilium. This portion will have a considerable influence on the reconstruction of missing superior iliac alae, but did not substantially influence our preliminary reconstruction. More importantly, we profited from the rare occasion when all the R1 remains were together in Musée national de la Préhistoire in November 2016. This enabled us to realize that the right ilium has a direct connection with the right ischium, which is, however, too restricted for gluing fragments together.

Therefore, most of the metrical differences between the reconstructions (Table 5) can be related to differences in reconstruction protocols. Primarily, the previous reconstruction (Meyer, 2013) did not use the right ischium, and the lower pelvis was estimated based on Kebara 2 using TPS function. The distant position of the estimated region implies

convergence towards reference morphology which is effectively apparent in this case as the original reconstruction of the Kebara 2 pelvis has a “funnel-shaped” pelvic canal with a very narrow outlet relative to the inlet (Rak and Arensburg, 1987; Tague, 1992). Differences in the inlet transverse diameter can only be associated to differences in the SIJ assembly. Meyer (2013) also described difficulties with a virtual assembly and finally decided for a manual assembly of original bones. However, she used adhesive matter between the ilia and the sacrum to compensate for SIJ cartilage, and the assembled pelvis was CT scanned using a medical scanner. We hypothesize that the different SIJ assembly could be a consequence of two potential problems: the adhesive matter between the bones prevented finding an optimum alignment of the ilia, and the attached bones could have moved before the scanning process. However, the latter issue would not probably cause a difference of such a magnitude without notice.

Apart from the SIJ assembly methods, the difference in the diagonal diameters of the inlet can also relate to the method of missing parts estimation, as the anterior limits of the diameters are not preserved although they are very close to the preserved morphology. Unlike Meyer (2013) who used only relatively sparsely spaced anatomical landmarks, we also used semilandmarks for the estimation. Dense cover by semilandmarks is crucial for the TPS estimation (Gunz et al., 2009). Most importantly, the semilandmarks provided information on the arcuate line curvature which makes estimation of the missing part more reliable. However, the asymmetry of the diagonal diameters should be assessed with caution, as the posterior limits are determined by auricular surfaces which have slightly eroded margins, especially on the right side.

Variation between different pelvic reconstructions is not uncommon. The female pelvis Tabun C1 was reconstructed independently by two teams (Ponce De León et al., 2008; Weaver and Hublin, 2009), which provided contrasting results regarding the inlet and outlet shapes and the inferred birth mechanism. The most problematic issue in this case was the estimation of the missing sacrum and a relative position of the reconstructed coxal that is, in addition, substantially distorted.

However, even if the sacroiliac joint is preserved, the reconstruction can be problematic. When the pubic region is missing, there is less information on the orientation of the coxal bones relative to the pelvic midsagittal plane. This can lead to inaccurate alignments of digitized models. To overcome this problem, we have tried several approaches and compared colormaps of the sacroiliac intermesh distances which were used as a criterion

for assessing the optimal surface match. Based on our own experience, we recommend using physical models of bones especially for cases where no sharp complementary features are present and the pubic bones are missing. This option led to the most consistent distribution of distances between the aligned meshes. It is important not to use adhesive matter between the matching surfaces as it may hinder efforts from finding the optimum position. In addition, to allow for the SIJ thickness, it is possible to subsequently translate the ilia in lateral direction or use a correction of transversal pelvic dimensions (Bonneau et al., 2012), but the SIJ thickness is very variable (Walker, 1992) and for large-scale dimensions, such as bi-iliac breadth, it would only constitute a small percentage of the value, and thus this correction would be negligible. Therefore, SIJ thickness is usually neglected in fossil pelvis reconstructions (e.g., Rak, 1991; Claxton et al., 2016).

7.4.2 Sex diagnosis in Neandertals

Sex attribution of Neandertal individuals has relied on traditional morphometric assessments, and more recent cross-methodologies have never been applied. Sex has usually been assigned based on the pelvic sexual dimorphism, body size or overall robusticity (Trinkaus, 1980). With respect to better preservation and unusual Neandertal morphology in the pubic region, the greater sciatic notch has been used preferentially (Boule, 1911; McCown and Keith, 1939; Trinkaus, 1980; Heim, 1982; Walker et al., 2011). However, visual assessment is subjective and may also depend on the angle of view (e.g., assessment of the composite arc; Brůžek, pers. comm.). Moreover, morphological traits can occur in a combination of male and female forms forcing one to decide which trait is more important; in a favorable situation the decision can be supported by body size inclined to one end of the Neandertal range of variation (Trinkaus, 2016).

To sex Regourdou 1, we used two methods based on visual traits and linear dimensions of the coxal bone. The right coxal bone indicates male sex by both methods. The left counterpart has a more ambiguous combination of visual traits as the auricular surfaces are asymmetrically positioned relative to the greater sciatic notches. This could be related to the asymmetry in the sacrum (having abnormally short right lateral ala and orientated right articular facet) and which could have led to an uneven dissipation of load on the lower legs via sacroiliac joints (Rmoutilová et al., in press). In fact, the ilia have different thickness at

the auricular regions (Figure 8) and the whole pelvis also shows considerable asymmetry (Figure 17).

Cross-validation of the employed methods on the sample of Neandertal coxal bones showed concordant results with the literature in most cases. This was expected for the visual method as the Neandertal coxae were previously sexed on the basis of description of morphological characters. Therefore, results of the metrical method are more relevant. Although there was a study comparing linear dimensions from the DSP of some Neandertal specimens to modern humans (Tillier et al., 2008), final sex diagnosis results were only considered for Kebara 2 (Chapman, 2017).

Two specimens were incongruently classified with one or the other method. The individual from Grotte du Prince has not been thoroughly published yet and we could only use published measurements, photographs and morphological descriptions (de Lumley-Woodyear, 1973). Therefore, these results should certainly be considered with caution. On the other hand, Amud 1 was classified as a female by both methods. The preservation allowed us to visually assess only two morphological traits which is insufficient and even more if the asymmetrical traits of R1 are taken into account. However, the metrical method also provided female sex. Obviously, there were fewer measurements than in other specimens and the unpreserved dimensions could greatly change the outcome, but regarding the fact that Amud 1 is considered very robust and having large body size and the highest stature of all Neandertals (Trinkaus, 1980; Carretero et al., 2012), this subset of pelvic measurements does not support this expectation. A complete review of the postcranial skeleton of this individual could help to clarify this issue. Furthermore, exceptional cases of probable robust females have been described in Middle and Late Pleistocene fossil record (Rosenberg et al., 2006; de Lumley, 2016).

In general, sex estimation in extinct hominins is problematic as we assume sexing criteria derived from living populations. Such criteria when used for fossil specimens of anatomically modern humans can be considered reliable; and genetic studies can provide a cross-validation (Fu et al., 2016; Mitnik et al., 2016). However, sexing individuals of an extinct species must obligatorily rely on assumptions. Regarding Neandertals we assume shape sexual dimorphism in the pelvis based on their large cranial capacities (Stanyon et al., 1993; Rosenberg and Trevathan, 2002). However, some scholars have proposed that the birth mechanism was not probably the same (Franciscus, 2009; Weaver and Hublin, 2009) and with regard to differences in their body shape (Holliday, 1997; Gómez-

Olivencia et al., 2018), pelvic sexual dimorphism may have differed correspondingly. In fact, it was suggested that the pubic region did not follow the same pattern of sexual dimorphism in Neandertals (Rosenberg, 1988). For this reason, the sacroiliac area is preferred. However, despite the absence of obvious differences in this region, it is also unclear whether this area did not compensate somehow for the special morphology in the anterior pelvis (Brůžek and Tillier, 1996). Furthermore, it was suggested that sexual differences in pelvis could have been less pronounced between Neandertal males and females than in today humans (Bonmatí et al., 2010; VanSickle, 2014).

7.4.3 Pelvic canal dimensions

In comparison with modern humans and other fossil specimens, R1 has medium-sized transverse inlet and outlet diameters relative to size which are in the overlap between modern male and females. With regard to other Neandertal males (La Chapelle 1 and Kebara 2), the outlet is relatively wider, close to the conformation observed in SH Pelvis 1 and Weaver and Hublin's Tabun C1, although Tabun C1 has, obviously, much greater absolute values.

Pelvic canal dimensions provide information on shape of the pelvic planes and thus on the mechanism of birth (Rosenberg and Trevathan, 2002). Differently shaped pelvic planes in modern humans are related to rotational movements of a voluminous newborn head during birth. First, the head enters the inlet mediolaterally and then it rotates to exit the pelvic outlet anteroposteriorly. Therefore, the inlet is transversally oval, while the midplane is sagittally oval, and the outlet is slightly rounder than the midplane (Bonmatí et al., 2010). The narrowest part is the midplane which is also the most sexually dimorphic in modern humans (Bonmatí et al., 2010).

It has been suggested that the transverse pelvic dimensions were constrained by thermoregulatory and biomechanical demands and that the rotational birth has originated in the Middle Pleistocene with increased cranial capacity (Ruff, 1995). This has been tentatively supported by the SH Pelvis 1 which has sagittally oriented midplane (Arsuaga et al., 1999) indicating that the rotational birth may have evolved in the last common ancestor of Neandertals and modern humans. Despite having transversally oriented pelvic planes, the Kebara 2 pelvis was also interpreted in terms of a difficult birth due to its very confined outlet, even relative to modern males (Tague, 1992). Nevertheless, inference of birth

mechanism from male individuals is problematic (Weaver and Hublin, 2009). Even though modern males and females have similarly shaped pelvic canal planes and females have just more spacious birth canals, we cannot be sure whether extinct hominins had similar pattern of sexual dimorphism. In fact, it has been suggested that the pelvic sexual dimorphism may have differed from modern humans (Bonmatí et al., 2010; VanSickle, 2014), with the pubis differentially oriented in Neandertal males and females in contrast to the sexual dimorphism in pubic length in modern humans (Weaver and Hublin, 2009). Furthermore, the Kebara 2 pelvis has a distorted sacral auricular surface preventing unambiguous ilium alignment (Trinkaus, 2011), and thus a new reconstruction of this important specimen could modify current image of the Neandertal male pelvis (Adegboyega et al., 2018).

The most complete Neandertal female pelvis provided contrasting outcomes from the two independent reconstructions (Ponce De León et al., 2008; Weaver and Hublin, 2009). However, the reconstruction by Ponce de León et al. (2008) is criticized as the authors assumed that a Neandertal newborn head moved through the pelvic canal in a modern way resulting in twisted shapes of the pelvic planes (Franciscus, 2009). Contrastingly, the reconstruction by Weaver and Hublin (2008), which is considered more reliable (Franciscus, 2009), obtained transversally oval both inlet and outlet, but they did not provide information on the midplane. However, the extremely platypelloid outlet indicates that Neandertals probably retained the primitive condition of a non-rotational birth. Nevertheless, this still should be taken with caution as Tabun C1 is very fragmentary and distorted, and the sacrum was completely estimated. Furthermore, a congruent result provided by extrapolation of the Kebara 2 pelvis (Weaver and Hublin, 2009) may also be misleading as the sacrum of Kebara 2 is taphonomically distorted and flattened (Bar-Yosef and Vandermeersch, 1991) having potential effects on the orientation of the coxal bones and outlet dimensions.

Pelvic dimensions of R1 indicate a transversally wide pelvic canal, but to explore shape in its pelvic planes, it will be necessary to estimate missing anterior region of the pelvis and the lower sacrum. Despite the facts that R1 is most probably a male and that the extrapolation of birth mechanism is uncertain from male specimens, further analyses of R1 can be focused on testing hypotheses that have been suggested with regard to sexual dimorphism in Neandertals. This may help in future attempts at interpreting male conformation relative to birth.

7.4.4 Spinopelvic alignment

The pelvic incidence angle in the reconstructed R1 pelvis is close to the modern mean resulting in a slightly higher lumbar lordosis angle than in majority of Neandertal individuals (Been et al., 2017). Lower lumbar lordosis would have important consequences on Neandertal posture. However, a recent study of the La Chapelle 1 specimen has challenged this issue (Haeusler et al., 2019).

Lumbar lordosis is an important adaptation that maintains the upright posture. During ontogeny, LL originates with the onset of upright posture (Scheuer and Black, 2000). In human evolution it evolved together with shortening the iliac alae (Lovejoy, 2005; Tardieu et al., 2013) and more acute ilio-ischial angle (Schlösser et al., 2014). These adaptations resulted in the center of gravity positioned directly above the hips (Tardieu et al., 2017). First evidence of higher levels of LL is seen in australopithecines and *H. erectus* (Tardieu et al., 2013; Been et al., 2017).

As vertebral bodies contribute more to the total lumbar lordosis than intervertebral discs (Been et al., 2010b), several methods have been proposed to estimate LL from skeletal material based on: lumbar vertebrae wedging (Been et al., 2007), inferior articular process orientation (Been et al., 2010a), and pelvic incidence (Been et al., 2014). The last two methods provide more accurate results (Been et al., 2007, 2014), while the latter enables estimation of LL based on the pelvis.

Pelvic incidence is a fixed anatomical angle that is not position- or posture-dependent and no sex-, age- or height-related changes were found in adult individuals (Weinberg et al., 2016; Tardieu et al., 2017). The angle increases with gait acquisition during growth and stabilizes around 10 years of age (Mangione et al., 1997; Tardieu et al., 2013) while the anterior iliac ala bends medially and the iliac pillar shifts more posteriorly (Tardieu et al., 2013).

However, measurement of this angle may be technique-dependent. Originally, the angle was defined on lateral radiographic images and studies measuring assembled dry pelvises or CT scans of living patients showed consistently lower values (see Table 10 to compare different methods) (Schlösser et al., 2014; Weinberg et al., 2016). Using CT scans controls for rotation of a patient and image distortion that can occur in lateral radiographic images (Schlösser et al., 2014). However, if a distortion occurred, the bias would be bi-directional increasing the variation but not changing the mean value (Tardieu et al., 2017). Therefore, it seems that differences are not related to different techniques but may be caused by other

factors such as sample composition. In addition, it has been proposed that activity levels and different types of loading behavior could affect LL among present populations (Castillo and Lieberman, 2018) and that the PI angle could also be sample specific (Weinberg et al., 2016).

The PI and LL angles were estimated to be low in Neandertals with different independent techniques (for summary see Table 11) (Been et al., 2017), and it has been suggested that this would be a derived feature in the genus *Homo* (Arsuaga et al., 2015; Gómez-Olivencia et al., 2017). However, La Chapelle 1 (Haeusler et al., 2019) and newly also R1 show higher values for these angles. The low LL in Kebara 2 and SH Pelvis 1 has been criticized, as both individuals show signs of either developmental or degenerative spinal pathologies and the Kebara 2 pelvis has additional taphonomical problems (Bar-Yosef and Vandermeersch, 1991; Bonmatí et al., 2010; Haeusler et al., 2019). Nevertheless, La Chapelle 1 exhibits spinal pathology too (Trinkaus, 1985), the results for Kebara 2 were obtained by two independent methods, and there are still other individuals (Shanidar 3 and SH Pelvis 2) that exhibit similarly low LL without any marked sign of pathology (Trinkaus, 1982; Bonmatí et al., 2010). Although the La Chapelle 1 and R1 pelvises show highest values of PI and LL in the Neandertal sample, they are close to the mean of modern populations. Therefore, this does not rule out the possibility that, on average, Neandertals could have had lower PI and LL.

Lumbar lordosis enables shock attenuation during running, but there is no greater association during walking (Castillo and Lieberman, 2018). Regarding the trade-off that curved LL allows for greater shock attenuation at a cost of increased risk of injury due to higher strain (Been et al., 2017; Castillo and Lieberman, 2018), the less curved lumbar spine of Neandertals could have been better adapted for stability at the expense of a reduced capacity for shock attenuation during dynamic activities (Castillo and Lieberman, 2018). With regard to pelvic and trunk morphology (Rak and Arensburg, 1987; Gómez-Olivencia et al., 2018), it has been suggested that Neandertals could have also had a more anterior center of gravity (Been et al., 2017). If this is true, it could have interesting implications for dealing with fetal load during pregnancy (Whitcome et al., 2007).

Furthermore, several morphological traits in the Neandertal pelvis have been suggested to be posture-related: long pubis, more anterior position of the iliac pillar, and more anterior position of the sacrum (Rak and Arensburg, 1987). It has also been suggested that the PI and LL angles are negatively correlated with a horizontal distance between the

sacral plate and the acetabula (Legaye, 2011) and positively correlated with a direct distance between these structures (Tardieu et al., 2013). Moreover, there are certain indices that the above mentioned traits could be developmentally interconnected (Tardieu et al., 2013) possibly reflecting changes in the center of gravity. Suggested relationships between those pelvic traits should certainly be more deeply examined in modern humans, in order to provide background for testing posture-related hypotheses in Neandertals. If these relationships exist and are significant, posture-related hypotheses could even be tested on fragmentary Neandertal pelvic remains which would substantially expand the number of tested specimens.

8 Conclusion

In this work we used virtual methods to revise paleoanthropological specimens. After virtual reconstruction of the Zlatý kůň cranium, we addressed questions about its sex attribution and morphological affinity. Female sex of this individual was confirmed with high probability based on reliably sexed Upper Paleolithic specimens. ZK cranium exhibits strong affinity to the pre-LGM Upper Paleolithic population despite its radiocarbon dating.

Prior to the reconstruction of Regourdou 1 pelvis, we analyzed the asymmetry of its sacrum in comparison with a healthy modern sample. The R1 sacrum shows considerable degree of asymmetry in sacral alae length and facets orientation. This pattern can have important implications for dissipation of load onto the lower legs and should be further analyzed together with other morphological abnormalities found in the skeleton. It must have also been considered in the subsequent pelvic reconstruction. The preliminary pelvic reconstruction provided new material for sex diagnosis, as well as transverse diameters of the pelvic canal and the pelvic incidence angle. Following modern criteria, the individual was probably a male. Transverse diameters of the inlet and outlet are slightly wider relative to modern males, but they do not provide sufficient information about shapes of these pelvic planes. Pelvic incidence angle allowed us to estimate lumbar lordosis angle which is close to the mean value for modern humans and slightly higher than in most of other Neandertals. This supports the idea that the lumbar lordosis interval was larger in Neandertals than previously thought, but it does not rule out that Neandertals had, on average, smaller lumbar lordosis than modern humans.

Regarding other aims of the thesis, we provided methods that are adjusted to fragmentary preservation. First, the revision of sexual dimorphism in the auricular surface showed that there are not pronounced sex-related differences in shape, but other traits from the posterior ilium could be used for sexual diagnosis from fragmentary remains. Second, the original method of Brůžek (2002) was adjusted to incomplete preservation of pelvic remains by providing an application that gives estimation accuracy and posterior probability for each combination of preserved traits. Finally, we analyzed compatibility of differently acquired 3D data by comparing two widely used surface scanners. Different outcomes did not have significant effect on selected anthropological analyses using linear measurements and surface topography. However, the scanners apparently differed in their

capacity to capture detail which should be taken into account when combining 3D data from different sources.

9 Perspectives

This thesis tried to answer several questions, but much more have remained open. Concerning Neandertal pelves, there is still a little known about the peculiar morphology which can also be partly blurred by previous reconstructions (Kebara 2, La Chapelle 1, La Ferrassie 1) that did not consider taphonomic distortion and whose shortcomings have already been described elsewhere (e.g., Trinkaus, 2011). Therefore, future studies should focus on revision of those reconstructions using virtual methods to provide outcomes that do not overly rely on personal experience.

Specifically for the Regourdou 1 pelvis, we plan to accomplish the reconstruction of missing parts using multiple estimations. This will allow us to address questions related to body form, posture, and pelvic sexual dimorphism. Relationship between the special pelvic morphology and posture in Neandertals has been suggested a long time ago (Rak and Arensburg, 1987) and since that time, not many studies got back to this question. Nevertheless, evidence for postural differences has been provided by thorough revisions of Neandertal vertebrae (Gómez-Olivencia, 2013a; b; Gómez-Olivencia et al., 2013, 2017) providing insight into the differences in spinopelvic alignment between Neandertals and modern humans (Been et al., 2017). To re-address the question of postural adaptations in the Neandertal pelvis, it is, first, necessary to study functional relationships in the human pelvis (e.g., Tardieu et al., 2013). Only after we understand how different morphological features are related in modern humans, we will have sufficient background for the interpretation of morphological features in the Neandertal pelvis.

SHRNUTÍ (Czech Summary)

Zachovalost kosterního materiálu ovlivněná tafonomickými procesy je hlavní problém paleoantropologických studií. Fragmentární nebo nekompletní nálezy jsou často vynechávány z analýz, čímž se zmenšuje studovaný soubor a snižuje se jeho reprezentativnost. Rozvoj moderních zobrazovacích metod a geometrické morfometrie pomáhá překonávat tento problém (Bookstein, 1991; Recheis et al., 1999; Weber a Bookstein, 2011). Díky zobrazovacím metodám jako výpočetní tomografie je možné analyzovat dříve nedostupné struktury, zatímco geometrická morfometrie umožňuje analyzovat tvar a tvarové souvislosti analyzovaného objektu (Weber et al., 2001; Braga et al., 2019).

Další možností, jak překonat překážku rozdílné zachovalosti, je rekonstrukce fragmentárních nálezů. Tradičně byla rekonstrukce fosilních nálezů prováděna zkušeným anatomem, a to často přímo na původním nálezu (White a Folkens, 2005). Tento přístup nejednou vedl k dalšímu poškození fosilie (Thompson a Illerhaus, 1998; Ponce de León a Zollikofer, 1999), ale především byl výsledek značně ovlivněn osobními zkušenostmi badatele, což vedlo k těžko zopakovatelným výstupům. V souvislosti s rozvojem virtuálních metod byl proto v poslední době kladen důraz i na zvýšení spolehlivosti rekonstrukce fosilního materiálu (Gunz et al., 2009). Výstupem je metodologický rámec kombinující digitalizovaná 3D data a počítačové metody, který umožňuje konzistentní přístup k otázce rekonstrukce (Zollikofer a Ponce de León, 2005). Virtuální rekonstrukce tak nezávisí pouze na anatomických pravidlech, ale i na matematických a geometrických principech, které umožňují lépe dokumentovat rekonstrukční protokol a reprodukovat výstupy nezávislými badateli (Weber, 2001). Virtuální metody tedy přispívají k paleoantropologickému výzkumu a pomáhají překonávat problém zachovalosti dvěma hlavními strategiemi: za prvé, umožňují extrahovat více informace z fragmentárního materiálu; za druhé, umožňují objektivnější rekonstrukci fragmentárních a nekompletních nálezů.

Hlavním cílem této práce byla rekonstrukce dvou fosilních nálezů: svrchně paleolitické lebky ze Zlatého koně v Českém krasu, Česká republika (Vlček, 1956; Svoboda et al., 2002), a neandertálské pánve Regourdou 1 z Francie (Piveteau, 1959; Meyer et al., 2011; Maureille et al., 2015a). Navzdory odlišné chronologii a taxonomické příslušnosti mají tyto dva nálezy společný stav zachovalosti. Vedlejší cíle souvisely s dalšími projekty dizertace,

kteře se týkaly pohlavní diagnózy z fragmentárního materiálu a analýzy kompatibility 3D dat pořizených různými způsoby. Tato dizertace je složena z pěti publikovaných článků, kteře jsou doplněny kapitolou o rekonstrukci pánve Regourdou 1.

Problematicku virtuální rekonstrukce jsme započali rekonstrukcí lebky ze Zlatého koně (Rmoutilová et al., 2018), což bylo výhodné, protože metody virtuální rekonstrukce byly původně navrženy při aplikaci na lebkách. Nález fosilní lebky Zlatý kůň byl objeven v 50. letech minulého století v Koněpruských jeskyních a oproti většině ostatních soudobých nálezů nepochází z Moravy ale z Čech. Přímé radiokarbonové datování (~15.4 ky cal BP; Svoboda et al., 2002) posunulo tuto fosilii z období raného svrchního paleolitu do období po posledním ledovcovém maximu (LGM z anglického *Last Glacial Maximum*), které trvalo před 23 až 19 tisíci lety (Clark et al., 2009). Ovšem datování Zlatého koně neodpovídalo všem kritériím spolehlivosti navrženým v publikaci Housley et al. (1997). Vzhledem k historii tohoto nálezů jsme vytvořili virtuální rekonstrukci této lebky se záměrem revidovat pohlavní diagnózu tohoto jedince a analyzovat morfologickou afinitu v porovnání se svrchně paleolitickými populacemi.

Proces rekonstrukce sestával z kroků, které využívaly zachovalou morfologii (složení fragmentů, zrcadlení a tzv. warping zrcadlového templátu), a z rekonstrukce založené na kompletní referenci (odhad bilaterálně chybějících oblastí), přičemž jsme se snažili využít maximum informace ze zachovalých fragmentů. Na rekonstruované lebce byly změřeny hlavní kraniální rozměry, které byly následně použity pro řešení výše zmíněných otázek. Jelikož pohlavní dimorfismus na lebce je populačně specifický a měnil se v průběhu času (Freyer, 1980; Cieri et al., 2014; Musilová et al., 2019), vytvořili jsme speciální model založený na svrchně paleolitických jedincích se spolehlivou pohlavní diagnózou (n=32, pohlaví odhadnuto geneticky nebo podle pánve či sekundární pohlavní diagnózy), který úspěšně odhadl pohlaví s křížovou validací (*cross-validation*) u 94 % referenčního souboru. Podle tohoto modelu byl jedinec ze Zlatého koně žena s 98% pravděpodobností.

Morfologická afinita lebky byla analyzována pomocí standardizovaných proměnných s odfiltrovanými velikostními rozdíly (Mosimann, 1970). V kontrastu s předchozím radiokarbonovým datováním (Svoboda et al., 2002) má lebka Zlatý kůň velkou morfologickou afinitu k populaci, která žila v Evropě před obdobím LGM. Poslední ledovcového maximum byla dramatická klimatická změna, která donutila populace ze severnějších oblastí k ústupu na jih a jejich následnému opětovnému rozšíření na sever (Housley et al., 1997; Verpoorte, 2004). Změny klimatu vedly ke mikroevołučním změnám

v tělesné morfologii (Straus, 1995; Churchill et al., 1999; Holt a Formicola, 2008). Avšak populační složení se změnilo i v souvislosti s genetickým driftem spolu s procesy tzv. zúžení hrdla láhve a efektem zakladatele. Změna v populačním složení byla detekována geneticky (Pala et al., 2012; Fu et al., 2016; Posth et al., 2016) ale také na kranio-metrické variabilitě pre-LGM a post-LGM populací (Brewster et al., 2014). Vzhledem k tomu, že přímé datování Zlatého koně nesplňuje navržená kritéria spolehlivosti (Housley et al., 1997) a nález neobsahuje zřetelné diagnostické kulturní artefakty, nemůžeme v současné době vyloučit, že morfologická afinita Zlatého koně může vyjadřovat skutečnou biologickou blízkost k pre-LGM populacím. Disproporce mezi přímým datováním a archaickou morfologií by vyžadovala datování opakovat.

Regourdou 1 je jedním z nejlépe zachovalých koster evropských neandertálců. Byla objevena v roce 1957 blízko vesnice Montignac-sur-Vézère v oblasti Dordogne ve Francii (Piveteau, 1959; Bonifay et al., 2007). Od roku 2008 byly během revize muzejních sbírek objeveny další kosterní pozůstatky (Madelaine et al., 2008; Maureille et al., 2015a), mezi kterými byly i fragmenty pánve. Na základě předběžného studia byla zmíněna značná asymetrie křížové kosti (Meyer et al., 2011). Proto jsme nejprve analyzovali míru této asymetrie ve srovnání s moderním souborem zdravých jedinců ($n=41$) a ostatními neandertálskými křížovými kostmi ($n=6$) (Rmoutilová et al., v tisku). Na základě landmarků a lineárních rozměrů jsme zjistili významnou asymetrii v délce křídel křížové kosti a v orientaci jejích artikulačních plošek. Dále jsme poskytli první kvantitativní analýzu neandertálských křížových kostí, která potvrdila některé dříve uvedené anatomické rozdíly jako relativně široký první křížový obratel a objemný vstup do křížového kanálu. Vzhledem k dostupné literatuře (Scheuer a Black, 2000; Pitre and Lovell, 2010; Pfeiffer, 2011) mohla výrazná asymetrie křídel křížové kosti vzniknout jako vývojová odchylka během raného ontogenetického vývoje. Asymetrie křížové kosti by zároveň mohla souviset s asymetrií v přenosu tíže trupu na dolní končetiny. Orientace artikulačních ploch je navíc důležitá pro udržení stability páteře proti smykovým silám (Noren et al., 1991), a asymetrie těchto plošek je asociovaná s degenerativními změnami obratlů (Dai, 2001; Kim et al., 2013; Schleich et al., 2016; Lai et al., 2019). Asymetrický přenos tíže by mohl souviset i s dalšími morfologickými abnormalitami na této kostře jako skoliotické známky na hrudní kosti a dalších obratlích (Gómez-Olivencia et al., 2012, 2013) a asymetrická těla stehenních kostí (Maureille et al., 2015a).

Posouzení míry asymetrie křížové kosti bylo důležité pro následnou rekonstrukci pánve Regourdou 1. Klíčovým krokem dosavadní rekonstrukce bylo připojení kyčelních kostí ke kosti křížové. K optimálnímu připojení jsme došli porovnáním několika přístupů. Jelikož virtuální připojení není spolehlivé při výskytu takto vysoké asymetrie, rozhodli jsme se pro připojení pomocí 3D výtisků kostí. Při další rekonstrukci jsme se omezili především na rekonstrukci na základě zachovalé morfologie. Nově dostupné morfologické znaky umožnily novou pohlavní diagnózu, která se přiklání k mužskému pohlaví pro tohoto jedince. Dosavadní stav rekonstrukce nám umožnil analyzovat transversální rozměry pánevního vchodu a východu. Východ se zdá být mírně širší vzhledem ke vchodu než u moderních mužů, což je v souladu s jinými nálezy pozdějších zástupců rodu *Homo* (Bonmatí et al., 2010). Podle transversálních rozměrů však nelze usuzovat na celkový tvar pánevních rovin. Analýza sklonu křížové kosti ukazuje na mírně větší lumbální lordózu, než bylo navrženo pro většinu neandertálských jedinců (Been et al., 2017; ale Haeusler et al., 2019). Hodnota se však pohybuje kolem průměru anatomicky moderních lidí, což stále nevyvrací možnost, že lumbální lordóza mohla být u neandertálců menší než u moderních lidí.

Rovněž jsme se zabývali odhadem pohlaví z fragmentárního materiálu. K tomuto účelu jsme se zaměřili na sakro-iliakální modul pánevní kosti (Rmoutilová et al., 2017), který je většinou lépe zachován než kost stydká modulu ischio-pubického (Waldron, 1987; Stojanowski et al., 2002). Metodami geometrické morfometrie jsme analyzovali pohlavní dimorfismus ve tvaru aurikulární plochy křížokyčelního skloubení, který byl navržen v řadě studií (Novotný, 1981; Valojerdy a Hogg, 1989; Ali a MacLaughlin, 1991; Brůžek et al., 1996; Novak et al., 2012; Anastasiou a Chamberlain, 2013; Wescott, 2015). K tomu jsme použili křivkové semilandmarky, které detailně definovaly obvod plochy vyfotografovaných kostí (n=121). Predikce pohlaví podle této struktury dosáhla úspěšnosti 81 %. Tradiční přístup kombinující vizuální hodnocení morfologických znaků a lineární rozměry z této anatomické oblasti byl úspěšnější a dosáhl úspěšnosti vyšší než 90 %.

V souvislosti s odhadem pohlaví jsme adaptovali široce užívanou vizuální metodu Brůžka (2002) pro užití na fragmentární materiál (Santos et al., 2019). Původní metoda byla testována na novém souboru a byla doplněna o hodnocení pomocí logistické regrese, které umožňuje kvantifikovat posteriorní pravděpodobnost odhadu podle jakékoli kombinace zachovaných znaků. Navíc bylo hodnocení vizuálních znaků testováno na

digitalizovaných 3D modelech kostí, které dosáhlo obdobné velmi vysoké úspěšnosti jako na souboru suchých kostí.

Poslední publikace se týkala srovnání výstupů dvou povrchových skenerů (HP 3D SLS PRO 2 and NextEngine) používaných pro digitalizaci kostí (Kotěrová et al., 2019). Možný vliv různých zařízení jsme analyzovali vzhledem k základním antropologickým analýzám odhadu pohlaví a věku. Výrazný vliv různých skenerů nebyl prokázán, ale zařízení se lišila ve schopnosti zachytit detail především ve více strukturovaných oblastech jako např. pubická symfýza.

Vzhledem k cílům práce nám virtuální rekonstrukce umožnila analyzovat dva fosilní nálezy a diskutovat problémy týkající se fosilií samotných, ale i jejich širšího evolučního kontextu. Pro další studium plánujeme dokončit rekonstrukci celé pánve Regourdou 1, která by mohla umožnit testování hypotéz navržených pro vysvětlení morfologie neandertálské pánve. Dále jsme poskytli nové metody odhadu pohlaví, které jsou přizpůsobené pro aplikaci na fragmentární materiál, a otestovali jsme kompatibilitu dvou skenerů, které se používají k digitalizaci kosterního materiálu.

RÉSUMÉ (French Summary)

La préservation taphonomique du matériel squelettique est un problème majeur dans les études paléanthropologiques. Des fossiles fragmentaires ou incomplets sont souvent omis des analyses, réduisant ainsi l'échantillon étudié et sa représentativité. Le développement des méthodes d'imagerie et de morphométrie géométrique aident à surmonter ces difficultés (par exemple, Bookstein, 1991 ; Recheis et al., 1999 ; Weber et Bookstein, 2011). Les méthodes d'imagerie telles que la tomodensitométrie permettent d'analyser des structures auparavant inaccessibles, tandis que la morphométrie géométrique permet d'analyser la forme de l'objet (par exemple, Weber et al., 2001 ; Braga et al., 2019).

Une autre possibilité pour surmonter l'obstacle de la préservation différentielle était et est parfois toujours la reconstruction d'un fossile. Traditionnellement, elle était effectuée par un anatomiste expérimenté, souvent directement sur le spécimen original (par exemple White et Folkens, 2005). Cette stratégie a parfois conduit à des dommages supplémentaires sur le fossile original (par exemple voir les cas discutés dans Thompson et Illerhaus, 1998 ; Ponce de Leon et Zollikofer, 1999). Mais la reconstitution finale était surtout influencée par l'expérience personnelle du chercheur, conduisant à des résultats difficilement reproductibles. Dans le cadre du développement des méthodes virtuelles, l'accent a récemment été mis sur l'amélioration de la fiabilité de la reconstruction (Gunz et al., 2009). Un nouveau cadre méthodologique a donc été créé, combinant des données 3D numérisées et des méthodes informatiques. Il permet une approche « cohérente » de la reconstruction (par exemple Zollikofer et Ponce de León, 2005). Les reconstitutions virtuelles dépendent donc non seulement de règles anatomiques, mais également de principes mathématiques et géométriques. Ils permettent théoriquement une meilleure documentation du protocole de reconstruction et donc autorisent la potentielle reproduction des résultats par d'autres chercheurs (Weber, 2001). Ainsi, les méthodes virtuelles contribuent de façon très novatrice à la recherche paléanthropologique et aident parfois à surmonter le problème de la préservation selon deux stratégies principales. Premièrement, extraire davantage d'informations à partir de matériel fragmentaire et deuxièmement, ils permettent une reconstruction réversible (donc potentiellement plus objective) de fossiles fragmentaires et/ou incomplets.

L'objectif principal de ce travail était de reconstituer deux spécimens fossiles : le crâne du Paléolithique supérieur de Zlatý kůň (République tchèque ; Vlcek, 1956 ; Svoboda et

al., 2002) et le bassin néandertalien de Regourdou 1 (France ; Piveteau, 1959; Meyer et al., 2011 ; Maureille et al., 2015). Malgré la chronologie et l'appartenance taxinomique différentes, ces deux spécimens partagent un état commun de préservation taphonomique. Les objectifs secondaires de notre travail concernaient le diagnostic sexuel à partir de matériel fragmentaire et l'analyse de la compatibilité des données 3D acquises de différentes manières. Cette thèse comprend cinq articles publiés, complétés par un chapitre sur la reconstruction du bassin de Regourdou 1.

Nous sommes entrés dans la problématique de la reconstruction virtuelle avec la celle du crâne de Zlatý kůň (Rmoutilová et al., 2018). Cela a été plus aisé car les méthodes de reconstruction virtuelle ont été expérimentées à l'origine principalement sur des crânes. Zlatý kůň a été découvert dans les années 1950 et, contrairement à la plupart des mises au jour de fossiles contemporaines de la République Tchèque, il ne vient pas de Moravie mais de Bohême. La datation directe au radiocarbone (~ 15,4 kcal BP; Svoboda et al., 2002) a déplacé ce fossile du début à la fin de la période du Paléolithique supérieur, après le dernier maximum glaciaire (LGM ; en anglais *Last Glacial Maximum*) datant de 23 à 19 000 ans (Clark et al., 2009), mais la datation de Zlatý kůň ne répondait pas à tous les critères de fiabilité proposés par Housley et al. (1997). Compte tenu de l'historique de cette découverte, nous avons réalisé une reconstruction virtuelle de ce crâne dans le but de tenter de réviser la diagnose sexuelle de l'individu et d'analyser son affinité morphologique relativement aux populations du Paléolithique supérieur.

Le processus de reconstruction comprenait des étapes qui utilisaient une morphologie bien préservée (composition des fragments, symétrisation et déformation du gabarit miroir) et une reconstruction à partir d'une référence complète (estimation des zones manquantes bilatéralement) dans le but de tirer le meilleur parti des informations des fragments préservés. Les principales dimensions du crâne ont été mesurées sur le crâne reconstruit. Elles ont été utilisées pour discuter les questions rappelées ci-dessus. Le dimorphisme sexuel sur le crâne étant spécifique à la population et évoluant avec le temps (Fruyer, 1980 ; Cieri et al., 2014 ; Musil et al., 2019), nous avons créé un modèle spécial basé sur des individus paléolithiques ayant un diagnostic sexuel fiable (n=32, sexe estimé suite à un diagnostic sexuel génétique ou pelvien ou secondaire). Il a permis d'identifier le sexe chez 94% du groupe de référence validé par croisement. Selon ce modèle, l'individu de Zlatý kůň était une femme avec une probabilité de 98%.

L'affinité morphologique du crâne a été analysée à l'aide des variables ajustées en fonction de la taille (Mosimann, 1970). Contrairement à la datation précédente au radiocarbone (Svoboda et al., 2002), Zlatý kůň présente une grande affinité morphologique avec la population européenne qui vivait avant la période du LGM. Ce LGM correspond à un changement climatique spectaculaire qui a forcé les populations des régions du nord à se retirer au sud, puis, après, à recoloniser le nord (Housley et al., 1997; Verpoorte, 2004). Ces contraintes environnementales ont probablement favorisé des phénomènes microévolutifs (Straus, 1995 ; Churchill et al., 1999 ; Holt et Formicola, 2008). Ainsi, les populations ont changé en relation avec la dérive génétique (processus dits de «goulot d'étranglement» et d'«effet fondateur»). Un tel changement dans la composition de la population a été détecté génétiquement (Pala et al., 2012 ; Fu et al., 2016 ; Posth et al., 2016) et sur la variabilité crânométrique des populations pré-LGM et post-LGM (Brewster et al., 2014). Étant donné que la datation directe de Zlatý kůň ne répond pas aux critères de fiabilité proposés (Housley et al., 1997) et que sa découverte ne s'accompagnait pas de celle d'artéfacts culturels diagnostics, nous ne pouvons pas exclure que l'affinité morphologique de Zlatý kůň reflète sa proximité biologique avec des populations antérieures au LGM. La disproportion entre la datation directe et la morphologie archaïque nécessiterait de répéter la datation.

Regourdou 1 est l'un des squelettes néandertaliens les plus complets d'Europe. Il a été découvert en 1957 près du village de Montignac-sur-Vézère en Dordogne (Piveteau, 1959 ; Bonifay et al., 2007). Depuis 2008, d'autres ossements du squelette ont été découverts lors de la révision des collections du Musée national de la Préhistoire (Madelaine et al., 2008; Maureille et al., 2015), notamment des fragments de bassin. Or, une étude préliminaire avait mentionné une asymétrie considérable du sacrum (Meyer et al., 2011). Par conséquent, nous avons d'abord analysé le degré de cette asymétrie par rapport à un échantillon moderne d'individus sains (n=41) et à d'autres sacra néandertaliens (n=6) (Rmoutilová et al., sous presse). Sur la base des dimensions linéaires et des repères, nous avons constaté une asymétrie importante dans la longueur des ailes du sacrum et dans l'orientation des apophyses articulaires. De plus, nous avons fourni la première analyse quantitative des sacra néandertaliens, confirmant certaines différences anatomiques telles que la première vertèbre sacrée relativement large et l'entrée volumineuse dans le canal sacré. Compte tenu de la littérature disponible (Scheuer et Black, 2000 ; Pitre et Lovell, 2010 ; Pfeiffer, 2011), une asymétrie aussi importante des ailes du sacrum pourrait être la conséquence d'un

dérèglement développemental précoce. L'asymétrie du sacrum pourrait être liée à une transmission déséquilibrée du poids du tronc aux membres inférieurs. De plus, l'orientation des apophyses articulaires est importante pour maintenir la stabilité de la colonne vertébrale contre les forces de glissement (Noren et al., 1991) et l'asymétrie dans leur orientation a été associée à des modifications dégénératives des vertèbres (Dai, 2001 ; Kim et al., 2013 ; Schleich et al., 2016 ; Lai et al., 2016, 2019). Un transfert asymétrique du poids pourrait également être associé à d'autres anomalies morphologiques de Regourdou 1 telles que des marques scoliotiques sur le sternum et les vertèbres (Gómez-Olivencia et al., 2012, 2013) ou la dissymétrie de ses diaphyses fémorales (Maureille et al., 2015).

L'évaluation du degré d'asymétrie du sacrum était importante pour la reconstruction ultérieure du bassin de Regourdou 1. Une étape clé consistait à articuler les os iliaques au sacrum. La connexion optimale a été obtenue en comparant plusieurs approches. La connexion virtuelle n'étant pas fiable en cas d'asymétrie aussi élevée, nous avons décidé de nous aider d'impressions 3D. Pour la reconstruction finale, nous nous sommes limité surtout à celle basée sur les pièces originales préservées. Les caractéristiques morphologiques nouvellement disponibles ont permis un nouveau diagnostic sexuel qui penche vers le sexe masculin de cet individu. L'état actuel de reconstruction nous a aussi permis d'analyser les dimensions transversales de l'entrée et de la sortie pelvienne. Cette dernière semble être légèrement plus large relativement à celle des hommes modernes. Ce résultat est conforme à ceux obtenus avec d'autres découvertes de bassins de fossiles archaïques (Bonmatí et al., 2010). Cependant, la forme globale des plans pelviens ne peut pas être déduite des dimensions transversales. L'analyse de l'orientation du sacrum de Regourdou 1 révèle une lordose lombaire légèrement supérieure à celle des Néandertaliens (Been et al., 2017; mais Haeusler et al., 2019). Cependant, la valeur de Regourdou 1 est proche de la valeur moyenne des hommes modernes. Même si cela favorise un interval plus large qu'auparavant chez les Néandertaliens, cela ne rejette pas la lordose lombaire plus basse chez les Néandertaliens en comparaison avec les hommes modernes.

Nous avons également examiné l'estimation du sexe à partir de matériel fragmentaire. À cette fin, nous nous sommes concentrés sur la partie postérieure de l'os coxal (Rmoutilová et al., 2017), qui est généralement mieux préservée que l'os pubien (Waldron, 1987 ; Stojanowski et al., 2002). Nous avons analysé le dimorphisme sexuel de la surface auriculaire de l'articulation sacroiliaque tel que proposé dans plusieurs études (Novotný, 1981; Valojerdy et Hogg, 1989 ; Ali et MacLaughlin, 1991 ; Brůžek et al., 1991 ;

Anastasio et Chamberlain, 2013 ; Wescott, 2015). Pour cela, nous avons utilisé des méthodes de morphométrie géométrique avec des semilandmarks, qui définissent en détail le périmètre de la surface auriculaire d'os photographiés (n=121). La prédiction du sexe a atteint un taux de réussite de 81%. L'approche traditionnelle combinant une évaluation visuelle des caractéristiques morphologiques et des dimensions linéaires de cette zone anatomique a été plus efficace et a atteint un taux de réussite de plus de 90%.

En relation avec l'estimation du sexe, nous avons adapté la méthode visuelle largement utilisée selon Brůžek (2002) pour l'utiliser sur un matériel fragmentaire (Santos et al., 2019). La méthode originale a été testée sur un nouvel échantillon. En plus, nous avons fourni une régression logistique pour évaluer le sexe permettant de quantifier la probabilité postérieure en fonction de toute combinaison de caractères préservés. En outre, l'évaluation des caractères visuels a été testée sur des modèles osseux 3D numérisés qui ont permis d'obtenir un taux de succès similaire à celui obtenu sur un échantillon d'ossements secs.

La dernière publication portait sur la comparaison des résultats de deux scanners surfaciques (HP 3D SLS PRO 2 et NextEngine) utilisés pour la numérisation d'ossements (Kotěrová et al., 2019). Nous avons analysé l'impact possible des différents scanners pour des analyses anthropologiques de base de l'estimation du sexe et de l'âge. Cet impact n'a pas été démontré. Mais la capacité à saisir les détails différait entre les appareils, en particulier dans des parties telles que la symphyse pubienne.

Compte tenu des objectifs du travail, la reconstruction virtuelle nous a permis d'analyser deux fossiles et de discuter des questions relatives aux fossiles eux-mêmes et de les considérer dans un contexte évolutif plus large. Pour Regourdou 1, nous prévoyons d'achever la reconstruction de l'ensemble du bassin, ce qui nous permettra de tester les hypothèses proposées pour expliquer la morphologie du pelvis néandertalien. En outre, nous avons fourni de nouvelles méthodes d'estimation du sexe adaptées à l'application de matériel fragmentaire et testé la compatibilité de deux scanners utilisés pour numériser du matériel squelettique.

BIBLIOGRAPHY

- Adams DC, Otárola-Castillo E. 2013. geomorph: An R package for the collection and analysis of geometric morphometric shape data. *Methods in Ecology and Evolution* 4:393–399.
- Adegboyega MT, Hublin J-J, Weaver TD. 2018. Virtual reconstruction of the Kebara 2 Neanderthal pelvis. *American Journal of Physical Anthropology* 6:6.
- Aiello L, Dean C. 1990. *An Introduction to Human Evolutionary Anatomy*. San Diego: Academic Press.
- Alciati G, Pesce Delfino V, Vacca E. 2005. Catalogue of Italian Fossil Human Remains from the Palaeolithic to the Mesolithic. *Journal of Anthropological Sciences* 84:1–184.
- Algee-Hewitt BFB, Wheat AD. 2016. The reality of virtual anthropology: Comparing digitizer and laser scan data collection methods for the quantitative assessment of the cranium. *American Journal of Physical Anthropology* 160:148–155.
- Ali RS, MacLaughlin SM. 1991. Sex identification from the auricular surface of the adult human ilium. *International Journal of Osteoarchaeology* 1:57–61.
- Amano H, Kikuchi T, Morita Y, Kondo O, Suzuki H, Ponce de León MS, Zollikofer CPE, Bastir M, Stringer C, Ogihara N. 2015. Virtual reconstruction of the Neanderthal Amud 1 cranium. *American Journal of Physical Anthropology* 158:185–197.
- Anastasiou E, Chamberlain AT. 2013. The sexual dimorphism of the sacro-iliac joint: an investigation using geometric morphometric techniques. *Journal of Forensic Sciences* 58:126–134.
- Angielczyk KD, Sheets HD. 2007. Investigation of simulated tectonic deformation in fossils using geometric morphometrics. *Paleobiology* 33:125–148.
- Arbour JH, Brown CM. 2014. Incomplete specimens in geometric morphometric analyses. *Methods in Ecology and Evolution* 5:16–26.
- Arbour VM, Currie PJ. 2012. Analyzing taphonomic deformation of ankylosaur skulls using retrodeformation and finite element analysis. *PLOS ONE* 7:1–13.
- Arsuaga J, Lorenzo C, Gracia A, Martí I. 1999. A complete human pelvis from the Middle Pleistocene of Spain. *Nature* 399:255–258.
- Arsuaga JL, Carretero JM, Lorenzo C, Gómez-Olivencia A, Pablos A, Rodríguez L, García-González R, Bonmatí A, Qua RM, Pantoja-Pérez A, Martínez I, Aranburu A, Gracia-Téllez A, Poza-Rey E, Sala N, García N, De Velasco AA, Cuenca-Bescós G, De Castro JMB, Carbonell E. 2015. Postcranial morphology of the middle Pleistocene humans from Sima de los Huesos, Spain. *PNAS* 112:11524–11529.
- Arsuaga JL, Martínez I, Arnold LJ, Aranburu A, Gracia-Téllez A, Sharp WD, Quam RM, Falguères C, Pantoja-Pérez A, Bischoff J, Poza-Rey E, Parés JM, Carretero JM, Demuro M, Lorenzo C, Sala N, Martínón-Torres M, García N, Alcázar De Velasco A, Cuenca-Bescós G, Gómez-Olivencia A, Moreno D, Pablos A, Shen CC, Rodríguez L, Ortega AI, García R, Bonmatí A, Bermúdez De Castro JM, Carbonell E. 2014. Neandertal roots: Cranial and chronological evidence from Sima de los Huesos. *Science* 344:1358–1363.
- Baab KL, McNulty KP, Rohlf FJ. 2012. The shape of human evolution: A geometric morphometrics perspective. *Evolutionary Anthropology* 21:151–165.
- Bar-Yosef O, Vandermeersch B. 1991. *Le Squelette Moustérien de Kébara 2*. Paris: Editions du CNRS.
- Bartucz L, Szabó J. 1940. Die Mussolini-Höhle (Subalyuk) bei Cserépfalu. *Geologica*

Hungarica Series Palaeontologica 14:49–105.

- Bastir M, Garcia-Martinez D, Torres-Tamayo N, Palancar CA, Fernandez-Perez FJ, Riesco-Lopez A, Osborne-Marquez P, Avila M, Lopez-Gallo P. 2019. Workflows in a Virtual Morphology Lab: 3D scanning, measuring, and printing. *Journal of Anthropological Sciences* 97:1–28.
- Been E, Barash A, Marom A, Aizenberg I, Kramer PA. 2010a. A new model for calculating the lumbar lordosis angle in early hominids and in the spine of the Neanderthal from Kebara. *The Anatomical Record* 293:1140–1145.
- Been E, Barash A, Marom A, Kramer PA. 2010b. Vertebral bodies or discs: Which contributes more to human-like lumbar lordosis? *Clinical Orthopaedics and Related Research* 468:1822–1829.
- Been E, Gómez-Olivencia A, Kramer PA. 2012. Lumbar lordosis of extinct hominins. *American Journal of Physical Anthropology* 147:64–77.
- Been E, Gómez-Olivencia A, Kramer PA. 2014. Brief Communication: Lumbar lordosis in extinct hominins: Implications of the pelvic incidence. *American Journal of Physical Anthropology* 154:307–314.
- Been E, Gómez-Olivencia A, Shefi S, Soudack M, Bastir M, Barash A. 2017. Evolution of spinopelvic alignment in hominins. *The Anatomical Record* 300:900–911.
- Been E, Pessah H, Been L, Tawil A, Peleg S. 2007. New method for predicting the lumbar lordosis angle in skeletal material. *The Anatomical Record* 290:1568–1573.
- Been E, Pessah H, Peleg S, Kramer P a. 2013. Sacral orientation in hominin evolution. *Advances in Anthropology* 3:133–141.
- Been E, Waintraub T, Gómez-Olivencia A, Kalichman L, Kramer PA, Shefi S, Soudack M, Barash A. 2019. How to build a 3D model of a fossil hominin vertebral spine based on osseous material. In: Been E, Gómez-Olivencia A, Kramer PA, editors. *Spinal Evolution*. Cham (Switzerland): Springer. p 341–359.
- Bellamy N, Park W, Rooney PJ. 1983. What do we know about the sacroiliac joint? *Seminars in Arthritis and Rheumatism* 12:282–313.
- Benazzi S, Bookstein FL, Strait DS, Weber GW. 2011a. A new OH5 reconstruction with an assessment of its uncertainty. *Journal of Human Evolution* 61:75–88.
- Benazzi S, Fiorenza L, Kozakowski S, Kullmer O. 2011b. Comparing 3D virtual methods for hemimandibular body reconstruction. *The Anatomical Record* 294:1116–1125.
- Benazzi S, Gruppioni G, Strait DS, Hublin JJ. 2014. Technical Note: Virtual reconstruction of KNM-ER 1813 *Homo habilis* cranium. *American Journal of Physical Anthropology* 153:154–160.
- Benazzi S, Senck S. 2011. Comparing 3-dimensional virtual methods for reconstruction in craniomaxillofacial surgery. *Journal of Oral and Maxillofacial Surgery* 69:1184–1194.
- Benazzi S, Stansfield E, Kullmer O, Fiorenza L, Gruppioni G. 2009a. Geometric morphometric methods for bone reconstruction: the mandibular condylar process of Pico della Mirandola. *The Anatomical Record* 292:1088–1097.
- Benazzi S, Stansfield E, Milani C, Gruppioni G. 2009b. Geometric morphometric methods for three-dimensional virtual reconstruction of a fragmented cranium: The case of Angelo Poliziano. *International Journal of Legal Medicine* 123:333–344.
- Berge C, Goularas D. 2010. A new reconstruction of Sts 14 pelvis (*Australopithecus africanus*) from computed tomography and three-dimensional modeling techniques. *Journal of Human Evolution* 58:262–272.
- Besl PJ, McKay ND. 1992. A method for registration of 3-D shapes. *IEEE Transactions on Pattern Analysis and Machine Intelligence* 14:239–256.

- Betti LIA. 2017. Human variation in pelvic shape and the effects of climate and past population history. *The Anatomical Record* 697:687–697.
- Biwasaka H, Sato K, Aoki Y, Kato H, Maeno Y, Tanijiri T, Fujita S, Dewa K. 2013. Three dimensional surface analyses of pubic symphyseal faces of contemporary Japanese reconstructed with 3D digitized scanner. *Legal Medicine* 15:264–268.
- Bonifay E. 1964a. La grotte de Régourdou (Montignac, Dordogne). Stratigraphie et industrie lithique moustérienne. *L'Anthropologie* 68:49–64.
- Bonifay E. 1964b. La grotte du Regourdou (Montignac, Dordogne). Stratigraphie et industrie lithique moustérienne. *L'Anthropologie* 68:49–64.
- Bonifay E, Vandermeersch B, Coutures C, Panattoni R. 2007. *La Sépulture Néandertalienne du Régourdou (Montignac-sur-Vézère, Dordogne)*. Mercuès: Documents du C.E.R.L.A.T.
- Bonmatí A, Arsuaga JL. 2007. The innominate bone sample from Krapina. *Periodicum Biologorum* 109:335–361.
- Bonmatí A, Gómez-Olivencia A, Arsuaga J, Carretero JM, Gracia A, Martínez I, Lorenzo C, Bermúdez de Castro JM, Carbonell E. 2010. Middle Pleistocene lower back and pelvis from an aged human individual from the Sima de los Huesos site, Spain. *PNAS* 107:1–31.
- Bonneau N, Bouhallier J, Simonis C, Baylac M, Gagey O, Tardieu C. 2012. Technical note: Shape variability induced by reassembly of human pelvic bones. *American Journal of Physical Anthropology* 148:139–147.
- Bonnet R. 1919. Die Skelet. In: Verworn M, Bonnet R, Steinmann G, editors. *Der diluviale Menschenfund von Oberkassel bei Bonn*. Weisbaden: Verlag von JF Bergmann. p 11–185.
- Bookstein F. 1991. *Morphometric Tools For Landmark Data: Geometry and Biology*. First edit. Cambridge: Cambridge University Press.
- Bookstein FL. 1989. Principal warps: Thin-plate splines and the decomposition of deformations. *IEEE Transactions on Pattern Analysis and Machine Intelligence* 11:567–585.
- Bookstein FL. 1997. Landmark methods for forms without landmarks: morphometrics of group differences in outline shape. *Medical Image Analysis* 1:225–243.
- Boule M. 1911. L'homme fossile de La Chapelle-aux-Saints. *Annales de Paléontologie* 6:111-172; 7:21–56, 85–192; 8: 1-70.
- Boyd AA, Motani R. 2008. Three-dimensional re-evaluation of the deformation removal technique based on “jigsaw puzzling.” *Palaeontologia Electronica* 11:7A.
- Boyde SK. 2009. Micro-computed tomography. In: Sensen CW, Hallgrímsson B, editors. *Advanced Imaging in Biology and Medicine: Technology, Software Environments, Applications*. Berlin, Heidelberg: Springer-Verlag. p 3–25.
- Braga J, Samir C, Risser L, Dumoncel J, Descouens D, Thackeray JF, Balaesque P, Oettlé A, Loubes J-M, Fradi A. 2019. Cochlear shape reveals that the human organ of hearing is sex-typed from birth. *Scientific Reports* 9:1–9.
- Bräuer G. 1988. Ostéométrie. In: Knussmann R, editor. *Anthropologie. Handbuch der vergleichenden Biologie des Menschen. Begründet von Rudolf Martin*. Stuttgart: G. Fischer Verlag. p 160–231.
- Bräuer G, Groden C, Gröning F, Kroll A, Kupczik K, Mbua E, Pommert A, Schiemann T. 2004. Virtual study of the endocranial morphology of the matrix-filled cranium from Eliye Springs, Kenya. *The Anatomical Record* 276A:113–133.
- Brewster C, Meiklejohn C, von Cramon-Taubadel N, Pinhasi R. 2014. Craniometric analysis of European Upper Palaeolithic and Mesolithic samples supports

- discontinuity at the Last Glacial Maximum. *Nature Communications* 5:4094.
- Brink RC, Vavrouch L, Schlösser TPC, Abul-Kasim K, Ohlin A, Tropp H, Castelein RM, Vrtovec T. 2019. Three-dimensional pelvic incidence is much higher in (thoraco)lumbar scoliosis than in controls. *European Spine Journal* 28:544–550.
- Bruner E. 2019. Human paleoneurology: Shaping cortical evolution in fossil hominids. *Journal of Comparative Neurology* 527:1753–1765.
- Brůžek J. 2002. A method for visual determination of sex, using the human hip bone. *American Journal of Physical Anthropology* 117:157–68.
- Brůžek J, Castex D, Majó T. 1996. Évaluation des caractères morphologiques de la face sacro-pelvienne de l'os coxal. Proposition d'une nouvelle méthode de diagnose sexuelle. *BMSAP* 8:491–502.
- Brůžek J, Murail P. 2006. Methodology and reliability of sex determination from the skeleton. In: Schmitt A, Cunha E, Pinheiro J, editors. *Forensic Anthropology and Medicine: Complementary Sciences from Recovery to Cause of Death*. Totowa (New Jersey): Humana Press. p 225–242.
- Brůžek J, Santos F, Dutailly B, Murail P, Cunha E. 2017. Validation and reliability of the sex estimation of the human os coxae using freely available DSP2 software for bioarchaeology and forensic anthropology. *American Journal of Physical Anthropology* 164:440–449.
- Brůžek J, Tillier A-M. 1996. A reconsideration of the Předmostí pelvis (Gravettian, Czech Republic). *Anthropologie* 34:231–238.
- Carretero JM. 1994. *Estudio del esqueleto de las dos cinturas y el miembro superior de los homínidos de la Sima de los Huesos, Sierra de Atapuerca, Burgos* (Unpublished doctoral dissertation). Universidad Complutense de Madrid.
- Carretero JM, Rodríguez L, García-González R, Arsuaga JL, Gómez-Olivencia A, Lorenzo C, Bonmatí A, Gracia A, Martínez I, Quam R. 2012. Stature estimation from complete long bones in the Middle Pleistocene humans from the Sima de los Huesos, Sierra de Atapuerca (Spain). *Journal of Human Evolution* 62:242–255.
- Castillo ER, Lieberman DE. 2018. Shock attenuation in the human lumbar spine during walking and running. *Journal of Experimental Biology* 221:jeb177949.
- Chapman T. 2017. *Morphometric, Functional and Biomechanical Analysis of a Virtual Neandertal in Comparison with Anatomically Modern Humans* (Unpublished doctoral dissertation). Université Libre de Bruxelles.
- Chapman T, Lefevre P, Semal P, Moiseev F, Sholukha V, Louryan S, Rooze M, Van Sint Jan S. 2014. Sex determination using the probabilistic sex diagnosis (DSP: Diagnose sexuelle probabiliste) tool in a virtual environment. *Forensic Science International* 234:189.e1-189.e8.
- Churchill SE, Formicola V, Holliday TW, Holt B, Schumann B. 1999. The Upper Palaeolithic population of Europe in an evolutionary perspective. In: Roebroeks W, Mussi M, Svoboda JA, Fennema K, editors. *Hunters of the Golden Age: The Mid Upper Palaeolithic of Eurasia 30,000-20,000 BP*. Leiden: University of Leiden. p 31–58.
- Cieri RL, Churchill SE, Franciscus RG, Tan J, Hare B. 2014. Craniofacial feminization, social tolerance, and the origins of behavioral modernity. *Current Anthropology* 55:419–443.
- Clark PU, Dyke AS, Shakun JD, Carlson AE, Clark J, Wohlfarth B, Mitrovica JX, Hostetler SW, McCabe AM. 2009. The Last Glacial Maximum. *Science* 325:710–714.
- Claxton AG, Hammond AS, Romano J, Oleinik E, DeSilva JM. 2016. Virtual reconstruction of the *Australopithecus africanus* pelvis Sts 65 with implications for

- obstetrics and locomotion. *Journal of Human Evolution* 99:10–24.
- Colman KL, van der Merwe AE, Stull KE, Dobbe JGG, Streekstra GJ, van Rijn RR, Oostra R-J, de Boer HH. 2019. The accuracy of 3D virtual bone models of the pelvis for morphological sex estimation. *International Journal of Legal Medicine* 133:1853–1860.
- Coutinho Nogueira D, Dutailly B, Comte F, Vasil'iev A, Khokhlov A, Shvedchikova T, Berezina N, Buzhilova A, Dutour O, Coqueugniot H. 2019. “Gueule cassée” (facial injuries): a 3D paleotraumatology study and facial approximation of a Napoleonic soldier who died in 1812 at Königsberg during the Russian Campaign. *International Journal of Osteoarchaeology* 29:191–197.
- Coutinho Nogueira D, Santos F, Courtaud P, Couture-Veschambre C. 2017. Le calcanéus « Regourdou 2 » : étude morphométrique comparative et discussion autour de sa place dans la variabilité des Néandertaliens. *PALEO* 28:71–89.
- Cuff AR, Rayfield EJ. 2015. Retrodeformation and muscular reconstruction of ornithomimosaurian dinosaur crania. *PeerJ* 3:e1093.
- Dai LY. 2001. Orientation and tropism of lumbar facet joints in degenerative spondylolisthesis. *International Orthopaedics* 25:40–42.
- Day MH. 1971. Postcranial remains of *Homo erectus* from Bed IV, Olduvai Gorge, Tanzania. *Nature* 232:383–387.
- Dupej J, Krajíček V, Velemínská J, Pelikán J. 2014. Statistical mesh shape analysis with nonlandmark nonrigid registration. In: *12th Eurographics Symposium on Geometry Processing*. Cardiff, UK.
- Durrleman S, Prastawa M, Charon N, Korenberg JR, Joshi S, Gerig G, Trounev A. 2014. Morphometry of anatomical shape complexes with dense deformations and sparse parameters. *NeuroImage* 101:35–49.
- Eder M, Brockmann G, Zimmermann A, Papadopoulos MA, Schwenzer-Zimmerer K, Zeilhofer HF, Sader R, Papadopoulos NA, Kovacs L. 2013. Evaluation of precision and accuracy assessment of different 3 d surface imaging systems for biomedical purposes. *Journal of Digital Imaging* 26:163–172.
- Endo B, Kimura T. 1970. Postcranial skeleton of the Amud Man. In: Suzuki H, Takai F, editors. *The Amud Man and His Cave Site*. Tokyo: University of Tokyo Academic Press of Japan. p 231–406.
- Estalrich A, Rosas A. 2015. Division of labor by sex and age in Neandertals: An approach through the study of activity-related dental wear. *Journal of Human Evolution* 80:51–63.
- Falkingham PL. 2012. Acquisition of high resolution three-dimensional models using free, open-source, photogrammetric software. *Palaeontologia Electronica* 15:1–15.
- Fernandez-Jalvo Y, Andrews P. 2016. *Atlas of Taphonomic Identifications: 1001+ Images of Fossil and Recent Mammal Bone Modification*. Dordrecht, Netherlands: Springer.
- Fischer B, Mitteroecker P. 2017. Allometry and Sexual Dimorphism in the Human Pelvis. *The Anatomical Record* 300:698–705.
- Formicola V. 1995. X-linked hypophosphatemic rickets: A probable upper paleolithic case. *American Journal of Physical Anthropology* 98:403–409.
- Fourie Z, Damstra J, Gerrits PO, Ren Y. 2011. Evaluation of anthropometric accuracy and reliability using different three-dimensional scanning systems. *Forensic Science International* 207:127–134.
- Frapont C. 1927. Sur l'omoplate et le sacrum de l'homme de Spy. *Revue Anthropologique* 37:189–195.
- Franciscus RG. 2009. When did the modern human pattern of childbirth arise? New

- insights from an old Neandertal pelvis. *PNAS* 106:9125–9126.
- Freyer DW. 1980. Sexual dimorphism and cultural evolution in the Late Pleistocene and Holocene of Europe. *Journal of Human Evolution* 9:399–415.
- Freyer DW. 1987. The supra-acetabular fossa and groove : a skeletal marker for northwest European Mesolithic populations. *Human Evolution* 3:163–176.
- Friedlander NJ, Jordan DK. 1994. Obstetric implications of Neanderthal robusticity and bone density. *Human Evolution* 9:331–342.
- Friess M. 2012. Scratching the surface? The use of surface scanning in physical and paleoanthropology. *Journal of Anthropological Sciences* 90:7–31.
- Fu Q, Posth C, Hajdinjak M, Petr M, Mallick S, Fernandes D, Furtwängler A, Haak W, Meyer M, Mittnik A, Nickel B, Peltzer A, Rohland N, Slon V, Talamo S, Lazaridis I, Lipson M, Mathieson I, Schiffels S, Skoglund P, Derevianko AP, Drozdov N, Slavinsky V, Tsybankov A, Cremonesi RG, Mallegni F, Gély B, Vacca E, Morales MRG, Straus LG, Neugebauer-Maresch C, Teschler-Nicola M, Constantin S, Moldovan OT, Benazzi S, Peresani M, Coppola D, Lari M, Ricci S, Ronchitelli A, Valentin F, Thevenet C, Wehrberger K, Grigorescu D, Rougier H, Crevecoeur I, Flas D, Semal P, Mannino MA, Cupillard C, Bocherens H, Conard NJ, Harvati K, Moiseyev V, Drucker DG, Svoboda J, Richards MP, Caramelli D, Pinhasi R, Kelso J, Patterson N, Krause J, Pääbo S, Reich D. 2016. The genetic history of Ice Age Europe. *Nature* 534:200–205.
- Gambier D, Brůžek J, Schmitt A, Houët F, Murail P. 2006. Révision du sexe et de l'âge au décès des fossiles de Cro-Magnon (Dordogne, France) à partir de l'os coxal. *Comptes Rendus Palevol* 5:735–741.
- Garas M, Vaccarezza M, Newland G, McVay-Doornbusch K, Hasani J. 2018. 3D-Printed specimens as a valuable tool in anatomy education: A pilot study. *Annals of Anatomy* 219:57–64.
- Genovés S. 1954. The problem of the sex of certain fossil hominids, with special reference to the Neandertal skeletons from Spy. *The Journal of the Royal Anthropological Institute of Great Britain and Ireland* 84:131–144.
- Gómez-Olivencia A. 2013a. Back to the old man's back: reassessment of the anatomical determination of the vertebrae of the Neandertal individual of la Chapelle-aux-Saints. *Annales de Paléontologie* 99:43–65.
- Gómez-Olivencia A. 2013b. The presacral spine of the La Ferrassie 1 Neandertal: a revised inventory. *BMSAP* 25:19–38.
- Gómez-Olivencia A, Arlegi M, Barash A, Stock JT, Been E. 2017. The Neandertal vertebral column 2: The lumbar spine. *Journal of Human Evolution* 106:84–101.
- Gómez-Olivencia A, Barash A, García-Martínez D, Arlegi M, Kramer P, Bastir M, Been E. 2018. 3D virtual reconstruction of the Kebara 2 Neandertal thorax. *Nature Communications* 9:4387.
- Gómez-Olivencia A, Carretero JM, Arsuaga JL, Rodríguez-García L, García-González R, Martínez I. 2007. Metric and morphological study of the upper cervical spine from the Sima de los Huesos site (Sierra de Atapuerca, Burgos, Spain). *Journal of Human Evolution* 53:6–25.
- Gómez-Olivencia A, Couture-Veschambre C, Madelaine S, Maureille B. 2013. The vertebral column of the Regourdou 1 Neandertal. *Journal of Human Evolution* 64:582–607.
- Gómez-Olivencia A, Franciscus RG, Couture-Veschambre C, Maureille B, Arsuaga JL. 2012. The mesosternum of the Regourdou 1 Neandertal revisited. *Journal of Human Evolution* 62:511–519.

- Gómez-Olivencia A, Holliday T, Madelaine S, Couture-Veschambre C, Maureille B. 2019. The costal skeleton of the Regourdou 1 Neandertal. *Journal of Human Evolution* 130:151–171.
- González PN, Bernal V, Ivan Perez S, Barrientos G. 2007. Analysis of dimorphic structures of the human pelvis: its implications for sex estimation in samples without reference collections. *Journal of Archaeological Science* 34:1720–1730.
- Gorjanović-Kramberger D. 1906. *Der diluviale Mensch von Krapina in Kroatien: ein Beitrag zur Paläoanthropologie*. Wiesbaden: C. W. Kreidel's Verlag.
- Grine FE, Gunz P, Betti-Nash L, Neubauer S, Morris AG. 2010. Reconstruction of the late Pleistocene human skull from Hofmeyr, South Africa. *Journal of Human Evolution* 59:1–15.
- Grün R, Stringer C. 2000. Tabun revisited: Revised ESR chronology and new ESR and U-series analyses of dental material from Tabun C1. *Journal of Human Evolution* 39:601–612.
- Gruss LT, Schmitt D. 2015. The evolution of the human pelvis: changing adaptations to bipedalism, obstetrics and thermoregulation. *Philosophical Transactions of the Royal Society B: Biological Sciences* 370:20140063–20140063.
- Guérin G, Frouin M, Talamo S. 2015. A multi-method luminescence dating of the Palaeolithic sequence of La Ferrassie based on new excavations adjacent to the La Ferrassie 1 and 2 skeletons. *Journal of Archaeological Science* 58:147–166.
- Guidi G, Remondino F, Morlando G, Del Mastio A, Uccheddu F, Pelagotti A. 2007. Performances evaluation of a low-cost active sensor for cultural heritage documentation. *Proceeding of VIII Conference on Optical 3D Measurement Techniques* 2:59–69.
- Gunz P, Mitteroecker P. 2013. Semilandmarks: A method for quantifying curves and surfaces. *Hystrix* 24:103–109.
- Gunz P, Mitteroecker P, Bookstein F. 2005. Semilandmarks in three dimensions. In: Slice DE, editor. *Modern Morphometrics in Physical Anthropology*. New York: Kluwer Academic. p 73–98.
- Gunz P, Mitteroecker P, Bookstein FL, Weber GW. 2004. Computer aided reconstruction of human crania using statistical and geometrical estimation methods. In: *Enter the Past: Computer Applications and Quantitative Methods in Archaeology*. Oxford: BAR International Series. p 92–95.
- Gunz P, Mitteroecker P, Neubauer S, Weber GW, Bookstein FL. 2009. Principles for the virtual reconstruction of hominin crania. *Journal of Human Evolution* 57:48–62.
- Guyomarc'h P, Dutailly B, Charton J, Santos F, Desbarats P, Coqueugniot H. 2014. Anthropological facial approximation in three dimensions (AFA3D): computer-assisted estimation of the facial morphology using geometric morphometrics. *Journal of Forensic Sciences* 59:1502–1516.
- Haeusler M, Trinkaus E, Fornai C, Müller J, Bonneau N, Boeni T, Frater N. 2019. Morphology, pathology, and the vertebral posture of the la Chapelle-aux-Saints Neandertal. *PNAS* 116:4923–4927.
- Haile-Selassie Y, Melillo SM, Vazzana A, Benazzi S, Ryan TM. 2019. A 3.8-million-year-old hominin cranium from Woranso-Mille, Ethiopia. *Nature* 573:214–219.
- Hedrick BP, Dodson P. 2013. Lujiatun Psittacosaurids: understanding individual and taphonomic variation using 3D geometric morphometrics. *PLOS ONE* 8:e69265.
- Heim J. 1982. *Les Hommes Fossiles de La Ferrassie. Tome II. Les Squelettes Adultes (Squelette de Membres)*. Mémoire 38. Paris: Masson, Archives de l'Institut de Paléontologie Humaine.

- Henderson P, Marlow CA, Molleson TI, Williams CT. 1983. Patterns of chemical change during bone fossilization. *Nature* 306:358–360.
- Henry-Gambier D, Brůžek J, Murail P, Houët F. 2002. Révision du sexe du squelette magdalénien de Saint-Germain-la-Rivière (Gironde, France). *PALEO* 14:205–212.
- Holliday TW. 1997. Postcranial evidence of cold adaptation in European Neandertals. *American Journal of Physical Anthropology* 104:245–258.
- Holt BM, Formicola V. 2008. Hunters of the Ice Age: The biology of Upper Paleolithic people. *Yearbook of Physical Anthropology* 51:70–99.
- Hora M, Sladek V. 2014. Influence of lower limb configuration on walking cost in Late Pleistocene humans. *Journal of Human Evolution* 67:19–32.
- Housley RA, Gamble C, Street M, Pettitt P. 1997. Radiocarbon evidence for the late glacial recolonisation of northern Europe. *Proceedings of the Prehistoric Society* 63:25–54.
- Hublin J-J. 2015. Prospects and pitfalls. In: Henke W, Tattersall I, editors. *Handbook of Paleoanthropology*. 3rd ed. Heidelberg: Springer. p 1035–1050.
- Hublin J-J, Barroso C, Medina P, Fontugne M, Reyss J-L. 1995. The Mousterian site of Zafarraya (Andalucia, Spain): Dating and implications on the Paleolithic peopling processes of Western Europe. *Comptes-Rendus de l'Académie des Sciences de Paris* 321:931–937.
- Immel A, Le Cabec A, Bonazzi M, Herbig A, Temming H, Schuenemann VJ, Bos KI, Langbein F, Harvati K, Bridault A, Pion G, Julien M-A, Krotova O, Conard NJ, Münzel SC, Drucker DG, Viola B, Hublin J-J, Tafforeau P, Krause J. 2016. Effect of X-ray irradiation on ancient DNA in sub-fossil bones – Guidelines for safe X-ray imaging. *Scientific Reports* 6:32969.
- Irish JD, Bratlund B, Schild R, Kolstrup E, Królik H, Mańka D, Boroń T. 2008. A late Magdalenian perinatal human skeleton from Wilczyce, Poland. *Journal of Human Evolution* 55:736–740.
- Jurda M, Urbanová P, Chmelík J. 2019. Digital restoration of fragmentary human skeletal remains: Testing the feasibility of virtual reality. *Journal of Forensic and Legal Medicine* 66:50–57.
- Jurda M, Urbanová P, Králík M. 2015. The post-mortem pressure distortion of human crania uncovered in an early medieval pohansko (Czech Republic) graveyard. *International Journal of Osteoarchaeology* 25:539–549.
- Kalvin AD, Dean D, Hublin J-J. 1995. Reconstruction of human fossils. *IEEE Computer Graphics and Applications* 15:12–15.
- Kalvin AD, Dean D, Hublin J-J, Braun M. 1992. Visualization in anthropology: reconstruction of human fossils from multiple pieces. *Proceedings of the 3rd Conference on Visualization '92 IEEE Computer Society Press*:404–410.
- Katz D, Friess M. 2014. Technical Note: 3D from standard digital photography of human crania — A preliminary assessment. *American Journal of Physical Anthropology* 154:152–158.
- Kikuchi T, Ogihara N. 2013. Computerized assembly of neurocranial fragments based on surface extrapolation. *Anthropological Science* 121:115–122.
- Kim H, Chun H, Lee H-M, Kang K, Lee C, Chang B, Yeom JS. 2013. The biomechanical influence of the facet joint orientation and the facet tropism in the lumbar spine. *The Spine Journal* 13:1301–1308.
- Klaas E, Kropp J, Mongon B. 2011. The impact of different alignment strategies on the overall performance of a white light scanner according to sphere spacing error specified in VDI 2634. *Three-Dimensional Imaging, Interaction, and Measurement*

7864:78640B.

- Klingenberg CP. 2014. Studying morphological integration and modularity at multiple levels: concepts and analysis. *Philosophical Transactions of the Royal Society of London Series B, Biological sciences* 369:2010249.
- Kotěrová A, Králík V, Rmoutilová R, Friedl L, Růžicka P, Velemínská J, Marchal F, Brůžek J. 2019. Impact of 3D surface scanning protocols on the Os coxae digital data: Implications for sex and age-at-death assessment. *Journal of Forensic and Legal Medicine* 68:101866.
- Kozłowski SK, Połtowicz-Bobak M, Bobak D, Terberger T. 2012. New information from Maszycka Cave and the Late Glacial recolonisation of Central Europe. *Quaternary International* 272–273:288–296.
- Kranioti EF, Holloway R, Senck S, Ciprut T, Grigorescu D, Harvati K. 2011. Virtual assessment of the endocranial morphology of the early modern European fossil calvaria from Cioclovina, Romania. *The Anatomical Record* 294:1083–1092.
- Kuhn SL, Stiner MC. 2006. What's a Mother to Do? The Division of Labor among Neandertals and Modern Humans in Eurasia. *Current Anthropology* 47:953–981.
- Lai Q, Dai M, Liu Y, Zhang B, Guo R, Lv X, Wang Q, Zhu J. 2019. A study of lumbar disc herniation and facet joint asymmetry. *International Surgery* 103:87–94.
- Lari M, Di Vincenzo F, Borsato A, Ghirotto S, Micheli M, Balsamo C, Collina C, De Bellis G, Frisia S, Giacobini G, Gigli E, Hellstrom JC, Lannino A, Modi A, Pietrelli A, Pilli E, Profico A, Ramirez O, Rizzi E, Vai S, Venturo D, Piperno M, Lalueza-Fox C, Barbujani G, Caramelli D, Manzi G. 2015. The Neanderthal in the karst: First dating, morphometric, and paleogenetic data on the fossil skeleton from Altamura (Italy). *Journal of Human Evolution* 82:88–94.
- Lautenschlager S. 2016. Reconstructing the past: methods and techniques for the digital restoration of fossils. *Royal Society Open Science* 3:160342.
- Legaye J. 2007. The femoro-sacral posterior angle: An anatomical sagittal pelvic parameter usable with dome-shaped sacrum. *European Spine Journal* 16:219–225.
- Legaye J. 2011. Analysis of the dynamic sagittal balance of the lumbo-pelvi-femoral complex. In: Klika V, editor. *Biomechanics in Applications*. Rijeka (Croatia): InTech. p 221–246.
- Legaye J, Duval-Beaupere G, Barrau A, Boulay C, Hecquet J, Montigny JP, Tardieu C. 2011. Relationship between sacral pelvic incidence and acetabular orientation. *HIP International* 21:87–97.
- Lestrel PE, Wolfe CA, Bodt A. 2013. Mandibular shape analysis in fossil hominins: Fourier descriptors in norma lateralis. *Homo* 64:247–272.
- Li X, Yin Z, Wei L, Wan S, Yu W, Li M. 2011. Symmetry and template guided completion of damaged skulls. *Computers and Graphics* 35:885–893.
- Lovejoy CO. 2005. The natural history of human gait and posture. Part 1. Spine and pelvis. *Gait and Posture* 21:95–112.
- Lovejoy CO, Meindl RS, Pryzbeck TR, Mensforth RP. 1985. Chronological metamorphosis of the auricular surface of the ilium: a new method for the determination of adult skeletal age at death. *American Journal of Physical Anthropology* 68:15–28.
- Lovejoy CO, Suwa G, Spurlock L, Asfaw B, White TD. 2009. The pelvis and femur of *Ardipithecus ramidus*: the emergence of upright walking. *Science* 326:71e1–e6.
- de Lumley-Woodyear MA. 1973. *Anténéandertaliens et Néandertaliens du Bassin Méditerranéen Occidental Européen*. Provence: Éditions du Laboratoire de paléontologie humaine et de préhistoire, Université de Provence.

- de Lumley H. 2016. *La Grotte du Cavillon Sous la falaise des Baousse Rousse, Grimaldi, Vintimille, Italie*. Paris: CNRS éditions.
- de Lumley MA. 2015. Tautavel man. One European evolved Homo erectus. Homo erectus tautavelensis. *L'Anthropologie* 119:303–348.
- Lyman RL. 1994. *Vertebrate Taphonomy*. Cambridge: Cambridge University Press.
- Lynch JJ. 2018. An automated two-dimensional pairwise form registration method for pair-matching of fragmented skeletal remains. *Journal of Forensic Sciences* 63:1790–1795.
- Madelaine S, Maureille B, Cavanhié N, Couture C, Bonifay E, Armand D, Bonifay M-F, Duday H, Fosse P, Vandermeersch B. 2008. Nouveaux restes humains moustériens rapportés au squelette néandertalien de Regourdou 1 (Regourdou, commune de Montignac, Dordogne, France). *PALEO* 20:101–113.
- Mahfouz MR, Mustafa A, Fatah EEA, Herrmann NP, Langley NR. 2017. Computerized reconstruction of fragmentary skeletal remains. *Forensic Science International* 275:212–223.
- Maier A. 2015. *The Central European Magdalenian*. Dordrecht: Springer Netherlands.
- Mangione P, Gomez D, Senegas J. 1997. Study of the course of the incidence angle during growth. *European Spine Journal* 6:163–167.
- Marchal F. 1997. *L'os coxal des hominidés fossiles* (Unpublished doctoral dissertation). Université de la Méditerranée Aix-Marseille II.
- Marcy AE, Fruciano C, Phillips MJ, Mardon K, Weisbecker V. 2018. Low resolution scans can provide a sufficiently accurate, cost- and time-effective alternative to high resolution scans for 3D shape analyses. *PeerJ* 6:e5032.
- Martin R. 1928. *Lehrbuch der Anthropologie in systematischer Darstellung*. 2nd ed. Jena: Gustav Fischer.
- Mathys A, Brecko J, Semal P. 2013. Comparing 3D digitizing technologies: What are the differences? In: *Ist Digital Heritage International Congress*. Strassbourg. p 201–204.
- Matiegka J. 1938. *Homo Předmostensis, Fossilný Člověk z Předmostí na Moravě II. Ostatní části kostrové*. Prague: Česká Akademie Věd a Umění.
- Maureille B, Gómez-Olivencia A, Couture-Veschambre C, Madelaine S, Holliday T. 2015a. Nouveaux restes humains provenant du gisement de Regourdou (Montignac-sur-Vézère, Dordogne, France). *PALEO* 26:117–138.
- Maureille B, Holliday T, Royer A, Pelletier M, Madelaine S, Lacrampe-Cuyaubère F, Muth X, Le Gueut E, Couture-Veschambre C, Gómez-Olivencia A, Discamps E, Texier J, Turq A, Lahaye C. 2015b. Importance des données de terrain pour la compréhension d'un potentiel dépôt funéraire moustérien: le cas du squelette de Regourdou 1 (Montignac-sur-Vézère, Dordogne, France). *PALEO* 26:139–159.
- McCown TD, Keith A. 1939. *The Stone Age of Mount Carmel. The Fossil Human Remains from the Levalloiso-Mousterian*. Oxford: Clarendon Press.
- Mestekova S, Brůžek J, Velemínska J, Chaumoitre K. 2015. A test of the DSP sexing method on CT images from a modern French sample. *Journal of Forensic Sciences* 60:1295–1299.
- Meyer V. 2013. *Apport de la Reconstruction Virtuelle du Bassin Regourdou 1 (Dordogne, France) à la Connaissance de l'Obstétrique Néandertalienne* (Unpublished doctoral dissertation). Bordeaux: Université Bordeaux I, France.
- Meyer V, Brůžek J, Couture C, Madelaine S, Maureille B. 2011. Un nouveau bassin néandertalien: Description morphologique des restes pelviens de Regourdou 1 (Montignac, Dordogne, France). *PALEO* 22:207–222.
- Milella M, Zollikofer CPEE, Ponce de León MS. 2015. Virtual reconstruction and

- geometric morphometrics as tools for paleopathology: a new approach to study rare developmental disorders of the skeleton. *The Anatomical Record* 298:335–345.
- Mitteroecker P, Gunz P. 2009. Advances in geometric morphometrics. *Evolutionary Biology* 36:235–247.
- Mittnik A, Wang C-C, Svoboda J, Krause J. 2016. A molecular approach to the sexing of the triple burial at the Upper Paleolithic site of Dolní Věstonice. *PLOS ONE* 11:e0163019.
- Molleson T, Cox M. 1993. *The Spitalfields Project, Volume 2: The Anthropology*. York: Council for British Archeology.
- Mosimann JE. 1970. Size allometry: size and shape variables with characterizations of the lognormal and generalized Gamma distributions. *Journal of the American Statistical Association* 65:930–945.
- Mullins RA, Albanese J. 2018. Estimating biological characteristics with virtual laser data. *Journal of Forensic Sciences* 63:815–823.
- Murail P, Brůžek J, Braga J. 1999. A new approach to sexual diagnosis in past populations. Practical adjustments from Van Vark's procedure. *International Journal of Osteoarchaeology* 9:39–53.
- Murail P, Brůžek J, Houët F, Cunha E. 2005. DSP: a tool for probabilistic sex diagnosis using worldwide variability in hip-bone measurements. *BMSAP* 17:167–176.
- Musilová B, Dupej J, Brůžek J, Bejdová Š, Velemínská J. 2019. Sex and ancestry related differences between two Central European populations determined using exocranial meshes. *Forensic Science International* 297:364–369.
- Neeser R, Ackermann RR, Gain J. 2009. Comparing the accuracy and precision of three techniques used for estimating missing landmarks when reconstructing fossil hominin crania. *American Journal of Physical Anthropology* 140:1–18.
- Nerudová Z, Vaníčková E, Tvrđý Z, Ramba J, Bílek O, Kostrhun P. 2019. The woman from the Dolní Věstonice 3 burial: a new view of the face using modern technologies. *Archaeological and Anthropological Sciences* 11:2527–2538.
- Noren R, Trafimow J, Andersson GBJ, Huckman MS. 1991. The role of facet joint tropism and facet angle in disc degeneration. *Spine* 16:530–532.
- Novak L, Schultz JJ, McIntyre M. 2012. Determining sex of the posterior ilium from the Robert J. Terry and William M. Bass collections. *Journal of Forensic Sciences* 57:1155–60.
- Novotný V. 1981. *Pohlavní rozdíly a identifikace pohlaví pánevní kosti* (Unpublished doctoral dissertation). Brno: Jan Evangelista Purkyně University.
- Nuger R. 2008. *The Influence of Climate on the Obstetrical Dimensions of the Human Bony Pelvis* (Unpublished doctoral dissertation). City University of New York.
- Ogihara N, Amano H, Kikuchi T, Morita Y, Hasegawa K, Kochiyama T, Tanabe HC. 2015. Towards digital reconstruction of fossil crania and brain morphology. *Anthropological Science* 123:57–68.
- Ogihara N, Nakatsukasa M, Nakano Y, Ishida H. 2006. Computerized restoration of nonhomogeneous deformation of a fossil cranium based on bilateral symmetry. *American Journal of Physical Anthropology* 130:1–9.
- Pablos A, Gómez-Olivencia A, Maureille B, Holliday TW, Madelaine S, Trinkaus E, Couture-Veschambre C. 2019. Neandertal foot remains from Regourdou 1 (Montignac-sur-Vézère, Dordogne, France). *Journal of Human Evolution* 128:17–44.
- Pal GP. 1989. Weight transmission through the sacrum in man. *Journal of Anatomy* 162:9–17.
- Pala M, Olivieri A, Achilli A, Accetturo M, Metspalu E, Reidla M, Tamm E, Karmin M,

- Reisberg T, Kashani BH, Perego UA, Carossa V, Gandini F, Pereira JB, Soares P, Angerhofer N, Rychkov S, Al-Zahery N, Carelli V, Sanati MH, Houshmand M, Hatina J, Macaulay V, Pereira L, Woodward SR, Davies W, Gamble C, Baird D, Semino O, Vilems R, Torroni A, Richards MB. 2012. Mitochondrial DNA signals of Late Glacial recolonization of Europe from Near Eastern refugia. *The American Journal of Human Genetics* 90:915–924.
- Pampush JD, Winchester JM, Morse PE, Vining AQ, Boyer DM, Kay RF. 2016. Introducing molaR: a new R package for quantitative topographic analysis of teeth (and other topographic surfaces). *Journal of Mammalian Evolution* 23:397–412.
- Pap I, Tillier A-M, Arensburg B, Chech M. 1996. The Subalyuk Neanderthal remains (Hungary): a re-examination. *Annales Historico-Naturales Musei Nationalis Hungarici* 88:233–270.
- Papaioannou G, Karabassi EA, Theoharis T. 2002. Reconstruction of three-dimensional objects through matching of their parts. *IEEE Transactions on Pattern Analysis and Machine Intelligence* 24:114–124.
- Peleg S, Dar G, Medlej B, Steinberg N, Masharawi Y, Latimer B, Jellema L, Peled N, Arensburg B, Hershkovitz I. 2007. Orientation of the human sacrum: anthropological perspectives and methodological approaches. *American Journal of Physical Anthropology* 133:967–977.
- Pelletier M, Royer A, Holliday TW, Discamps E, Madelaine S, Maureille B. 2017. Rabbits in the grave! Consequences of bioturbation on the Neandertal “burial” at Regourdou (Montignac-sur-Vézère, Dordogne). *Journal of Human Evolution* 110:1–17.
- Perez SI, Bernal V, Gonzalez PN. 2006. Differences between sliding semi-landmark methods in geometric morphometrics, with an application to human craniofacial and dental variation. *Journal of Anatomy* 208:769–784.
- Perrone RV, Williams JL. 2019. Dimensional accuracy and repeatability of the NextEngine laser scanner for use in osteology and forensic anthropology. *Journal of Archaeological Science: Reports* 25:308–319.
- Pesce Delfino V, Vacca E. 1994. Report of an archaic human skeleton discovered at altamura (Bari), in the “Lamalunga” district. *Human Evolution* 9:1–9.
- Pfeiffer S. 2011. Pelvic stress injuries in a small-bodied forager. *International Journal of Osteoarchaeology* 21:694–703.
- Pitre MC, Lovell NC. 2010. A sacral anomaly from the quaker cemetery, Kingston-upon-Thames, England. *International Journal of Osteoarchaeology* 20:351–357.
- Piveteau J. 1959. Les restes humains de la grotte de Regourdou (Dordogne). *Comptes Rendus de l'Académie des Sciences de Paris série D*:40–44.
- Plavcan JM, Meyer V, Hammond AS, Couture C, Madelaine S, Holliday TW, Maureille B, Ward C V., Trinkaus E. 2014. The Regourdou 1 Neandertal body size. *Comptes Rendus Palevol* 13:747–754.
- Pomeroy E, Bennett P, Hunt C, Reynolds T, Farr L, Frouin M, Holman J, Lane R, French C, Barker G. in press. New Neanderthal remains associated with the ‘Flower Burial’ at Shanidar Cave, Iraqi Kurdistan. *Antiquity: A Review of World Archaeology*:246–249.
- Pomeroy E, Mirazón Lahr M, Crivellaro F, Farr L, Reynolds T, Hunt CO, Barker G. 2017. Newly discovered Neanderthal remains from Shanidar Cave, Iraqi Kurdistan, and their attribution to Shanidar 5. *Journal of Human Evolution* 111:102–118.
- Ponce De León MS, Golovanova L, Doronichev V, Romanova G, Akazawa T, Kondo O, Ishida H, Zollikofer CPE. 2008. Neanderthal brain size at birth provides insights into the evolution of human life history. *PNAS* 105:13764–12768.

- Ponce de León MS, Zollikofer CPE. 1999. New evidence from Le Moustier 1: computer-assisted reconstruction and morphometry of the skull. *The Anatomical Record* 254:474–489.
- Posth C, Renaud G, Mittnik A, Drucker DG, Rougier H, Cupillard C, Valentin F, Thevenet C, Furtwängler A, Wißing C, Francken M, Malina M, Bolus M, Lari M, Gigli E, Capecchi G, Crevecoeur I, Beauval C, Flas D, Germonpré M, Van Der Plicht J, Cottiaux R, Gély B, Ronchitelli A, Wehrberger K, Grigorescu D, Svoboda J, Semal P, Caramelli D, Bocherens H, Harvati K, Conard NJ, Haak W, Powell A, Krause J. 2016. Pleistocene mitochondrial genomes suggest a single major dispersal of non-africans and a late glacial population turnover in Europe. *Current Biology* 26:827–833.
- Profico A, Bellucci L, Buzi C, Di Vincenzo F, Micarelli I, Strani F, Tafuri MA, Manzi G. 2019a. Virtual anthropology and its application in cultural heritage studies. *Studies in Conservation* 64:323–336.
- Profico A, Buzi C, Davis C, Melchionna M, Veneziano A, Raia P, Manzi G. 2019b. A new tool for digital alignment in virtual anthropology. *The Anatomical Record* 302:1104–1115.
- Quatrehomme G, Radoman I, Nogueira L, du Jardin P, Alunni V. 2017. Sex determination using the DSP (probabilistic sex diagnosis) method on the coxal bone: Efficiency of method according to number of available variables. *Forensic Science International* 272:190–193.
- Rahman IA, Adcock K, Garwood RJ. 2012. Virtual fossils: A new resource for science communication in paleontology. *Evolution: Education and Outreach* 5:635–641.
- Rak Y. 1991. The pelvis. In: Bar-Yosef O, Vandermeersch B, editors. *Le Squelette Moustérien de Kebara 2*. Paris: Editions du CNRS. p 147–182.
- Rak Y, Arensburg B. 1987. Kebara 2 Neanderthal pelvis: first look at a complete inlet. *American Journal of Physical Anthropology* 73:227–231.
- Recheis W, Weber GW, Schäfer K, Knapp R, Seidler H, zur Nedden D. 1999. Virtual reality and anthropology. *European Journal of Radiology* 31:88–96.
- Reynolds MS, MacGregor DM, Barry MD, Lottering N, Schmutz B, Wilson LJ, Meredith M, Gregory LS. 2017. Standardized anthropological measurement of postcranial bones using three-dimensional models in CAD software. *Forensic Science International* 278:381–387.
- Rink W, Schwarcz H, Smith F, Radović J. 1995. ESR ages for Krapina hominids. *Nature* 378:24.
- Rmoutilová R, Dupej J, Velemínská J, Brůžek J. 2017. Geometric morphometric and traditional methods for sex assessment using the posterior ilium. *Legal Medicine* 26:52–61.
- Rmoutilová R, Gómez-Olivencia A, Brůžek J, Holliday T, Ledevin R, Couture-Veschambre C, Madelaine S, Džupa V, Velemínská J, Maureille B. in press. A case of marked bilateral asymmetry in the sacral alae of the Neandertal specimen Regourdou 1 (Périgord, France). *American Journal of Physical Anthropology*.
- Rmoutilová R, Guyomarc'h P, Velemínský P, Šefčáková A, Samsel M, Santos F, Maureille B, Brůžek J. 2018. Virtual reconstruction of the Upper Palaeolithic skull from Zlatý Kůň, Czech Republic: Sex assessment and morphological affinity. *PLOS ONE* 13:e0201431.
- Rocha MA. 1995. Les collections ostéologiques humaines identifiées du Musée Anthropologique de l'Université de Coimbra. *Antropologia Portuguesa* 13:7–38.
- Rosenberg K, Trevathan W. 2002. Birth, obstetrics and human evolution. *BJOG: an*

- international journal of obstetrics and gynaecology* 109:1199–1206.
- Rosenberg KR. 1988. The functional significance of pubic Neandertal length. *Current Anthropology* 29:595–617.
- Rosenberg KR, Zúñe L, Ruff CB. 2006. Body size, body proportions, and encephalization in a Middle Pleistocene archaic human from northern China. *PNAS* 103:3552–3556.
- Rueden CT, Schindelin J, Hiner MC, DeZonia BE, Walter AE, Arena ET, Eliceiri KW. 2017. ImageJ2: ImageJ for the next generation of scientific image data. *BMC Bioinformatics* 18:529.
- Ruff C. 1991. Climate and body shape in hominid evolution. *Journal of Human Evolution* 21:81–105.
- Ruff C. 2010. Body size and body shape in early hominins - implications of the Gona Pelvis. *Journal of Human Evolution* 58:166–178.
- Ruff CB. 1993. Climatic adaptation and hominid evolution: The thermoregulatory imperative. *Evolutionary Anthropology: Issues, News, and Reviews* 2:53–60.
- Ruff CB. 1994. Morphological adaptation to climate in modern and fossil hominids. *American Journal of Physical Anthropology* 107:65–107.
- Ruff CB. 1995. Biomechanics of the hip and birth in early Homo. *American Journal of Physical Anthropology* 98:527–574.
- Santos F, Guyomarc'h P, Rmoutilova R, Brůžek J. 2019. A method of sexing the human os coxae based on logistic regressions and Bruzek's nonmetric traits. *American Journal of Physical Anthropology* 169:435–447.
- Schaaffhausen H. 1888. *Der Neanderthaler Fund*. Bonn (Germany): Marcus.
- Scheuer L, Black S. 2000. *Developmental Juvenile Osteology*. San Diego: Elsevier Academic Press.
- Schlager S. 2016. Morpho: Calculations and Visualisations Related to Geometric Morphometrics. Available from: <https://cran.r-project.org/web/packages/Morpho/index.html>
- Schlager S, Profico A, Di Vincenzo F, Manzi G. 2018. Retrodeformation of fossil specimens based on 3D bilateral semi-landmarks: Implementation in the R package "Morpho." *PLOS ONE* 13:e0194073.
- Schlager S, Wittwer-Backofen U. 2015. Images in paleoanthropology: Facing our ancestors. In: Henke W, Tattersall I, editors. *Handbook of Paleoanthropology*. Berlin, Heidelberg: Springer Berlin Heidelberg. p 1007–1034.
- Schleich C, Müller-Lutz A, Blum K, Boos J, Bittersohl B, Schmitt B, Gerß J, Matuschke F, Witsack H, Antoch G, Miese F. 2016. Facet tropism and facet joint orientation: risk factors for the development of early biochemical alterations of lumbar intervertebral discs. *Osteoarthritis and Cartilage* 24:1761–1768.
- Schlösser TPC, Janssen MMA, Vrtovec T, Pernuš F, Öner FC, Viergever MA, Vincken KL, Castelein RM. 2014. Evolution of the ischio-iliac lordosis during natural growth and its relation with the pelvic incidence. *European Spine Journal* 23:1433–1441.
- Schmitz RW, Serre D, Bonani G, Feine S, Hillgruber F, Krainitzki H, Pääbo S, Smith FH. 2002. The Neandertal type site revisited: interdisciplinary investigations of skeletal remains from the Neander Valley, Germany. *PNAS* 99:13342–13347.
- Šefčáková A, Katina S, Mizera I, Halouzka R, Barta P, Thurzo M. 2011. A Late Upper Palaeolithic skull from Moča (The Slovak Republic) in the context of Central Europe. *Acta Musei Nationalis Pragae* 67:3–24.
- Semal P, Rougier H, Crevecoeur I, Jungels C, Flas D, Hauzeur A, Maureille B, Germonpré M, Bocherens H, Pirson S, Cammaert L, De Clerck N, Hambucken A, Higham T, Toussaint M, Van Plicht J Der. 2009. New data on the late Neandertals: direct dating

- of the Belgian Spy fossils. *American Journal of Physical Anthropology* 138:421–428.
- Senck S, Bookstein FL, Benazzi S, Kastner J, Weber GW. 2015. Virtual reconstruction of modern and fossil hominoid crania: consequences of reference sample choice. *The Anatomical Record* 298:827–841.
- Senck S, Coquerelle M, Weber GW, Benazzi S. 2013. Virtual reconstruction of very large skull defects featuring partly and completely missing midsagittal planes. *The Anatomical Record* 296:745–758.
- Sholts SB, Flores L, Walker PL, Wärmländer SKTS. 2011. Comparison of coordinate measurement precision of different landmark types on human crania using a 3D laser scanner and a 3D digitiser: Implications for applications of digital morphometrics. *International Journal of Osteoarchaeology* 21:535–543.
- Sholts SB, Wärmländer SKTS, Flores LM, Miller KWP, Walker PL. 2010. Variation in the measurement of cranial volume and surface area using 3D laser scanning technology. *Journal of Forensic Sciences* 55:871–876.
- Simpson SW, Quade J, Levin NE, Butler R, Dupont-Nivet G, Everett M, Semaw S. 2008. A female *Homo erectus* pelvis from Gona, Ethiopia. *Science* 322:1089–1092.
- Skoglund P, Storå J, Götherström A, Jakobsson M. 2013. Accurate sex identification of ancient human remains using DNA shotgun sequencing. *Journal of Archaeological Science* 40:4477–4482.
- Sládek V, Ruff CB, Berner M, Holt B, Niskanen M, Schuplerová E, Hora M. 2016. The impact of subsistence changes on humeral bilateral asymmetry in Terminal Pleistocene and Holocene Europe. *Journal of Human Evolution* 92:37–49.
- Sládek V, Trinkaus E, Hillson S, Holliday T. 2000. *The People of the Pavlovian. Skeletal Catalogue and Osteometrics of the Gravettian Fossil Hominids from Dolni-Vestonice and Pavlov*. Brno: Academy of Sciences of the Czech Republic, Institute of Archaeology.
- Sládek V, Trinkaus E, Šefčáková A, Halouzka R. 2002. Morphological affinities of the Šal'a 1 frontal bone. *Journal of Human Evolution* 43:787–815.
- Slizewski A, Friess M, Semal P. 2010. Surface scanning of anthropological specimens: nominal-actual comparison with low cost laser scanner and high end fringe light projection surface scanning systems. *Quartär* 57:179–187.
- Smith FH, Allsworth-Jones P, Boaz NT, Brace CL, Harrold FB, Howells WW, Luchterhand K, Musil R, Stringer CB, Trinkaus E, Valoch K, Walker MJ, Wolpoff MH. 1982. Upper Pleistocene hominid evolution in South-Central Europe: a review of the evidence and analysis of trends (and comments and reply). *Current Anthropology* 23:667–703.
- Smith FH, Ranyard GC. 1980. Evolution of the supraorbital region in Upper Pleistocene fossil hominids from South-Central Europe. *American Journal of Physical Anthropology* 53:589–610.
- Solecki RS. 1971. *Shanidar, the First Flower People*. New York: Knopf.
- Sparacello VS, Rossi S, Pettitt P, Roberts C, Riel-Salvatore J, Formicola V. 2018. New insights on Final Epigravettian funerary behavior at Arene Candide Cave (Western Liguria, Italy). *Journal of Anthropological Sciences* 96:1–24.
- Sparacello VS, Villotte S, Shackelford LL, Trinkaus E. 2017. Patterns of humeral asymmetry among Late Pleistocene humans. *Comptes Rendus Palevol* 16:680–689.
- Spoor F, Jeffery N, Zonneveld F. 2000a. Using diagnostic radiology in human evolutionary studies. *Journal of Anatomy* 197:61–76.
- Spoor F, Jeffery NS, Zonneveld F. 2000b. Imaging skeletal growth and evolution. In: O'Higgins P, Cohn M, editors. *Development, Growth and Evolution: Implications for*

- the Study of Hominid Skeletal Evolution*. Vol. 20. London: Academic Press. p 123–162.
- Stanyon R, Consigliere S, Morescalchi MA. 1993. Cranial capacity in hominid evolution. *Human Evolution* 8:205–216.
- Stewart DB. 1984. The pelvis as a passageway. I. Evolution and adaptations. *British Journal of Obstetrics and Gynaecology* 91:611–617.
- Stewart TD. 1960. Form of the pubic bone in Neanderthal man. *Science* 131:1437–1438.
- Stojanowski CM, Seidemann RM, Doran GH. 2002. Differential skeletal preservation at Windover Pond: causes and consequences. *American Journal of Physical Anthropology* 119:15–26.
- Stoyanova D, Algee-Hewitt BFB, Slice DE. 2015. An enhanced computational method for age-at-death estimation based on the pubic symphysis using 3D laser scans and thin plate splines. *American Journal of Physical Anthropology* 158:431–440.
- Straus LG. 1995. The Upper Paleolithic of Europe: an overview. *Evolutionary Anthropology* 4:4–16.
- Street M, Terberger T, Orschiedt J. 2006. A critical review of the German Paleolithic hominin record. *Journal of Human Evolution* 51:551–579.
- Stringer CB. 1986. An archaic character in the Broken Hill innominate E. 719. *American Journal of Physical Anthropology* 71:115–120.
- Stringer CB, Grün R. 1991. Time for the last Neanderthals. *Nature* 351:701–702.
- Sutton M, Rahman I, Garwood R. 2016. Virtual paleontology — an overview. *The Paleontological Society Papers* 22:1–20.
- Svoboda JA, van der Plicht J, Kuželka V. 2002. Upper Paleolithic and Mesolithic human fossils from Moravia and Bohemia (Czech Republic): some new 14C dates. *Antiquity* 76:957–962.
- Tague RG. 1989. Variation in pelvic size between males and females. *American Journal of Physical Anthropology* 80:59–71.
- Tague RG. 1992. Sexual dimorphism in the human bony pelvis, with a consideration of the Neandertal pelvis from Kebara Cave, Israel. *American Journal of Physical Anthropology* 88:1–21.
- Tallman M, Amenta N, Delson E, Frost SR, Ghosh D, Klukkert ZS, Morrow A, Sawyer GJ. 2014. Evaluation of a new method of fossil retrodeformation by algorithmic symmetrization: crania of papionins (primates, cercopithecidae) as a test case. *PLOS ONE* 9:e100833.
- Tardieu C, Bonneau N, Hecquet J, Boulay C, Marty C, Legaye J, Duval-Beaupère G. 2013. How is sagittal balance acquired during bipedal gait acquisition? Comparison of neonatal and adult pelves in three dimensions. Evolutionary implications. *Journal of Human Evolution* 65:209–22.
- Tardieu C, Hasegawa K, Haeusler M. 2017. How did the pelvis and vertebral column become a functional unit during the transition from occasional to permanent bipedalism? *The Anatomical Record* 300:912–931.
- Tarsi T, Noto F, Martínez-Labarga C, Giampaolo R, Babalini C, Scano G, Contini I, Lorente JA, Lorente M, Pacciani E, Silvestrini M, Del Lucchese A, Maggi R, Lattanzi E, Formicola V, Mallegni F, Martini F, Rickards O. 2006. Ricostruzione della storia genetica per via materna delle comunità paleolitiche dei Balzi Rossi, delle Arene Candide e del Romito, e di quelle neolitiche ed eneolitiche di Samari e di Fontenoce di Recanati. In: Martini AF, editor. *La Cultura del Morire nelle Società Preistoriche e Protostoriche Italiane dal Paleolitico all'età del Rame, Origines, Progetti, III*. Firenze: Istituto Italiano di Preistoria e Proistoria. p 315–346.

- Teshima T, Patel V, Mainprize JG, Edwards G, Antonyshyn OM. 2015. A three-dimensional statistical average skull: Application of biometric morphing in generating missing anatomy. *Journal of Craniofacial Surgery* 26:1634–1638.
- Thompson JL, Illerhaus B. 1998. A new reconstruction of the Le Moustier 1 skull and investigation of internal structures using 3-D- μ CT data. *Journal of Human Evolution* 35:647–665.
- Tillier A-M, Arensburg B, Brůžek J. 2008. Identité biologique des artisans moustériens de Kebara (Mont Carmel, Israël). Réflexions sur le concept de néanderthalien au Levant méditerranéen. *BMSAP* 20:33–58.
- Tocheri MW. 2009. Laser scanning: 3D analysis of biological surfaces. In: Sensen CW, Hallgrímsson B, editors. *Advanced Imaging in Biology and Medicine: Technology, Software Environments, Applications*. Berlin (Heidelberg): Springer-Verlag. p 85–101.
- Trinkaus E. 1976. The morphology of European and Southwest Asian Neandertal pubic bones. *American Journal of Physical Anthropology* 44:95–103.
- Trinkaus E. 1980. Sexual differences in Neanderthal limb bones. *Journal of Human Evolution* 9:377–397.
- Trinkaus E. 1982. The Shanidar 3 Neandertal. *American Journal of Physical Anthropology* 57:37–60.
- Trinkaus E. 1983. *The Shanidar Neandertals*. New York: Academic Press.
- Trinkaus E. 1984. Neandertal pubic morphology and gestation length. *Current Anthropology* 25:509–514.
- Trinkaus E. 1985. Pathology and the posture of the La Chapelle-aux-Saints Neandertal. *American Journal of Physical Anthropology* 67:19–41.
- Trinkaus E. 1996. The M. Obturator Internus sulcus on Middle and Late Pleistocene human ischia. *American Journal of Physical Anthropology* 101:503–513.
- Trinkaus E. 2011. The postcranial dimensions of the La Chapelle-aux-Saints 1 Neandertal. *American Journal of Physical Anthropology* 145:461–468.
- Trinkaus E. 2016. *The Krapina Human Postcranial Remains: Morphology, Morphometrics and Paleopathology*. Zagreb: FF Press.
- Trinkaus E, Svoboda J. 2006. *Early Modern Human Evolution in Central Europe: the People of Dolní Věstonice and Pavlov*. New York: Oxford University Press.
- Trinkaus E, Walker MJ. 2017. *The People of Palomas. Neandertals from the Sima de las Palomas del Cabezo Gordo, Southeastern Spain*. Texas: Texas A&M University Press.
- Uldin T. 2017. Virtual anthropology – a brief review of the literature and history of computed tomography. *Forensic Sciences Research* 1790:1–9.
- Valladas H, Mercier N, Froget L, Hovers E, Joron JL, Kimbel WH, Rak Y. 1999. TL dates for the Neanderthal site of the Amud Cave, Israel. *Journal of Archaeological Science* 26:259–268.
- Vallois H V. 1965. Le sternum néandertalien du Regourdou. *Anthropologischer Anzeiger* 29:273–289.
- Valojerdy M, Hogg D. 1989. Sex differences in the morphology of the auricular surfaces of the human sacroiliac joint. *Clinical Anatomy* 2:63–67.
- Vandermeersch B, Trinkaus E. 1995. The postcranial remains of the Régourdou 1 Neandertal: the shoulder and arm remains. *Journal of Human Evolution* 28:439–476.
- VanSickle C. 2014. *A New Examination of Childbirth-related Pelvic Anatomy in Neandertal Females* (Unpublished doctoral dissertation). University of Michigan.
- Velemínská J, Brůžek J. 2008. *Early Modern Humans from Předmostí near Přerov, Czech*

- Republic: A New Reading of Old Documentation*. Prague: Academia.
- Velemínská J, Krajíček V, Dupej J, Gómez-Valdés J a., Velemínský P, Šefčáková A, Pelikán J, Sánchez-Mejorada G, Brůžek J. 2013. Technical Note: Geometric morphometrics and sexual dimorphism of the greater sciatic notch in adults from two skeletal collections: The accuracy and reliability of sex classification. *American Journal of Physical Anthropology* 152:558–565.
- Veneziano A, Landi F, Profico A. 2018. Surface smoothing, decimation, and their effects on 3D biological specimens. *American Journal of Physical Anthropology* 166:473–480.
- Verpoorte A. 2004. Eastern Central Europe during the Pleniglacial. *Antiquity* 78:257–266.
- Villa C, Buckberry J, Cattaneo C, Frohlich B, Lynnerup N. 2015a. Quantitative analysis of the morphological changes of the pubic symphyseal face and the auricular surface and implications for age at death estimation. *Journal of Forensic Sciences* 60:556–565.
- Villa C, Gaudio D, Cattaneo C, Buckberry J, Wilson AS, Lynnerup N. 2015b. Surface curvature of pelvic joints from three laser scanners: separating anatomy from measurement error. *Journal of Forensic Sciences* 60:374–381.
- Villotte S. 2009. *Enthésopathies et Activités des Hommes Préhistoriques - Recherche Méthodologique et Application aux Fossiles Européens du Paléolithique Supérieur et du Mésolithique*. Oxford: Archaeopress.
- Villotte S, Churchill SE, Dutour OJ, Henry-Gambier D. 2010. Subsistence activities and the sexual division of labor in the European Upper Paleolithic and Mesolithic: evidence from upper limb enthesopathies. *Journal of Human Evolution* 59:35–43.
- Vlček E. 1956. Pleistocenní člověk z jeskyně na Zlatém koni u Koněprus. *Anthropozoikum* 6:283–311.
- Vlček E. 1991. L'homme fossile en Europe Centrale. *L'Anthropologie* 95:409–472.
- Volpato V, Macchiarelli R, Guatelli-Steinberg D, Fiore I, Bondioli L, Frayer DW. 2012. Hand to mouth in a Neandertal: right-handedness in Regourdou 1. *PLOS ONE* 7:3–8.
- Waldron T. 1987. The relative survival of the human skeleton: implications for palaeopathology. In: Boddington A, Garland A, editors. *Death, Decay and Reconstruction: Approaches to Archaeology and Forensic Science*. Manchester: Manchester University Press. p 55–64.
- Walker JM. 1992. The sacroiliac joint: a critical review. *Physical Therapy* 72:903–16.
- Walker MJ, Ortega J, Parmova K, Lopez M V., Trinkaus E. 2011. Morphology, body proportions, and postcranial hypertrophy of a female Neandertal from the Sima de las Palomas, southeastern Spain. *PNAS* 108:10087–10091.
- Warrener AG, Lewton KL, Pontzer H, Lieberman DE. 2015. A wider pelvis does not increase locomotor cost in humans, with implications for the evolution of childbirth. *PLOS ONE* 10:e0118903.
- Weaver TD, Hublin J-J. 2009. Neandertal birth canal shape and the evolution of human childbirth. *PNAS* 106:8151–8156.
- Weber G, Bookstein F. 2011. *Virtual Anthropology: A Guide to a New Interdisciplinary Field*. Vienna: Springer-Verlag Wien.
- Weber GW. 2001. Virtual anthropology (VA): A call for glasnost in paleoanthropology. *The Anatomical Record* 265:193–201.
- Weber GW. 2015. Virtual anthropology. *American Journal of Physical Anthropology* 156:22–42.
- Weber GW, Schäfer K, Prossinger H, Gunz P, Mitteröcker P, Seidler H. 2001. Virtual anthropology: the digital evolution in anthropological sciences. *Journal of Physiological Anthropology and Applied Human Science* 20:69–80.

- Weinberg DS, Morris WZ, Gebhart JJ, Liu RW. 2016. Pelvic incidence: an anatomic investigation of 880 cadaveric specimens. *European Spine Journal* 25:3589–3595.
- Wescott DJ. 2015. Sexual dimorphism in auricular surface projection and postauricular sulcus morphology. *Journal of Forensic Sciences* 60:679–685.
- Whitcome KK, Shapiro LJ, Lieberman DE. 2007. Fetal load and the evolution of lumbar lordosis in bipedal hominins. *Nature* 450:1075–1078.
- White T. 2003. Early hominids: diversity or distortion? *Science* 299:1994–1997.
- White TD, Folkens PA. 2005. *The Human Bone Manual*. San Diego (California): Elsevier Academic Press.
- Winchester JM. 2016. MorphoTester: an open source application for morphological topographic analysis. *PLOS ONE* 11:1–18.
- Wolpoff MH. 1980. *Paleoanthropology*. New York: Knopf.
- Wolpoff MH, Frayer DW, Jelinek J. 2006. Aurignacian female crania and teeth from the Mladeč caves, Moravia, Czech Republic. In: Teschler-Nicola M, editor. *Early Modern Humans at the Moravian Gate: The Mladeč Caves and their Remains*. Vienna: Springer Vienna. p 273–340.
- Woźniak K, Rzepecka-Woźniak E, Moskała A, Pohl J, Latacz K, Dybała B. 2012. Weapon identification using antemortem computed tomography with virtual 3D and rapid prototype modeling-A report in a case of blunt force head injury. *Forensic Science International* 222:29–32.
- Yin Z, Wei L, Li X, Manhein M. 2011. An automatic assembly and completion framework for fragmented skulls. *Proceedings of the IEEE International Conference on Computer Vision*:2532–2539.
- Zelditch M, Swiderski D, Sheets H, Fink W. 2004. *Geometric Morphometrics for Biologists: A Primer*. New York: Elsevier Academic Press.
- Zhang Z. 1994. Iterative point matching for registration of free-form curves and surfaces. *International Journal of Computer Vision* 13:119–152.
- Zheng G, Lösch S. 2013. Volumetric morphometrics (VMM) for physical anthropology: Preliminary results. *Bulletin de la Société Suisse d'Anthropologie* 19:25–31.
- Zollikofer C, Ponce de León MS, Martin RD. 1998. Computer-assisted paleoanthropology. *Evolutionary Anthropology* 6:41–54.
- Zollikofer CP, Ponce de León M. 2005. *Virtual Reconstruction: A Primer in Computer-Assisted Paleontology and Biomedicine*. New York: Wiley.
- Zollikofer CPE. 2002. A Computational Approach to Paleoanthropology. *Evolutionary Anthropology* 11:64–67.
- Zollikofer CPE, Ponce de León MS, Martin RD, Stucki P. 1995. Neanderthal computer skulls. *Nature* 375:283–285.

APPENDICES

A. List of presented publications

- Rmoutilová R, Guyomarc'h P, Velemínský P, Šefčáková A, Samsel M, Santos F, Maureille B, Brůžek J. 2018. Virtual reconstruction of the Upper Palaeolithic skull from Zlatý Kůň, Czech Republic: Sex assessment and morphological affinity. *PLOS ONE* 13:e0201431.
- Rmoutilová R, Gómez-Olivencia A, Brůžek J, Holliday T, Ledevin R, Couture-Veschambre C, Madelaine S, Džupa V, Velemínská J, Maureille B. in press. A case of marked bilateral asymmetry in the sacral alae of the Neandertal specimen Regourdou 1 (Périgord, France). *American Journal of Physical Anthropology*.
- Rmoutilová R, Dupej J, Velemínská J, Brůžek J. 2017. Geometric morphometric and traditional methods for sex assessment using the posterior ilium. *Legal Medicine* 26:52–61.
- Kotěrová A, Králík V, Rmoutilová R, Friedl L, Růžička P, Velemínská J, Marchal F, Brůžek J. 2019. Impact of 3D surface scanning protocols on the *Os coxae* digital data: Implications for sex and age-at-death assessment. *Journal of Forensic and Legal Medicine* 68:101866.
- Santos F, Guyomarc'h P, Rmoutilova R, Brůžek J. 2019. A method of sexing the human os coxae based on logistic regressions and Brůžek's nonmetric traits. *American Journal of Physical Anthropology* 169:435–447.

B. List of other published work

Conference abstracts

- Brůžek J, Dupej J, Kotěrová A, Rmoutilová R, Velemínská J. 2017. Use of the structured light scanner David SLS-2 for recording auricular surface in 3D and implications for age at death assessment. *American Journal of Physical Anthropology* 162:131.
- Kotěrová A, Rmoutilová R, Králík V, Růžicka P, Brůžek J. 2019. Evaluation of an impact of different 3D surface scanning protocols on sex and age-at-death assessment from Os Coxae in Bioarchaeolog. In: *84th Annual Meeting of the Society of American Archaeology*. p 429.
- Rmoutilová R, Brůžek J, Ledevin R, Gómez-Olivencia A, Couture-Veschambre C, Holliday T, Madelaine S, Velemínská J, Maureille B. 2019. New insight on the Neandertal pelvis: Virtual reconstruction of the pelvis of Regourdou 1 specimen. *American Journal of Physical Anthropology* 168:205.
- Rmoutilová R, Brůžek J, Maureille B. 2019. Revision of sex in Neandertals using visual and morphometric methods. In: *Paleoanthropology Society 2019 Annual Meeting*.
- Rmoutilová R, Gómez-Olivencia A, Brůžek J, Ledevin R, Couture-Veschambre C, Holliday TW, Madelaine S, Velemínská J, Maureille B. 2018. Extreme asymmetry of sacral alae in the Neandertal Regourdou 1 (Montignac-sur-Vézère, Dordogne, France). In: *Proceedings of the European Society for the study of Human Evolution* 8. p 164.
- Rmoutilová R, Guyomarc'h, Pierre Velemínský P, Brůžek J. 2017. Reconstruction virtuelle du crâne Magdalénien de Zlatý kůň (République tchèque). *BMSAP* 29:S30.

Publications in other periodicals and monographies

- Maureille B, Rmoutilova R, Brůžek J. Les données anthropologiques (et paléogénomiques). in press. In: Bellier C, Cattelain P, Gillard M, Smolderen A, editors. *La Femme dans la Préhistoire*. Treignes: Éd. du Cédarc.
- Rmoutilová R, Maureille B, Meyer V, Couture-Veschambre C, Gómez-Olivencia A, Holliday TW, Velemínská J, Brůžek J. 2017. First glimpse at the asymmetry of Neandertal sacrum Regourdou 1 (Dordogne, France). *Slovenská antropológia* 20:70–75 (in Czech).

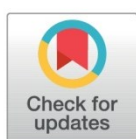
RESEARCH ARTICLE

Virtual reconstruction of the Upper Palaeolithic skull from Zlatý Kůň, Czech Republic: Sex assessment and morphological affinity

Rebeka Rmoutilová^{1,2*}, Pierre Guyomarc'h², Petr Velemínský³, Alena Šefčáková⁴, Mathilde Samsel², Frédéric Santos², Bruno Maureille², Jaroslav Brůžek¹

1 Department of Anthropology and Human Genetics, Faculty of Science, Charles University, Prague, Czech Republic, **2** UMR 5199 PACEA, University of Bordeaux, CNRS, MCC, Pessac, France, **3** Department of Anthropology, National Museum, Prague, Czech Republic, **4** Department of Anthropology, Slovak National Museum-Natural History Museum, Bratislava, Slovak Republic

* vejnaror@natur.cuni.cz



OPEN ACCESS

Citation: Rmoutilová R, Guyomarc'h P, Velemínský P, Šefčáková A, Samsel M, Santos F, et al. (2018) Virtual reconstruction of the Upper Palaeolithic skull from Zlatý Kůň, Czech Republic: Sex assessment and morphological affinity. PLoS ONE 13(8): e0201431. <https://doi.org/10.1371/journal.pone.0201431>

Editor: Karen Rosenberg, University of Delaware, UNITED STATES

Received: February 16, 2018

Accepted: July 16, 2018

Published: August 30, 2018

Copyright: © 2018 Rmoutilová et al. This is an open access article distributed under the terms of the [Creative Commons Attribution License](https://creativecommons.org/licenses/by/4.0/), which permits unrestricted use, distribution, and reproduction in any medium, provided the original author and source are credited.

Data Availability Statement: All relevant data are within the paper and its Supporting Information files.

Funding: RR was supported by the Charles University Grant Agency, research grant GAUK No. 1088217. National Museum (00023272) obtained funding from the Ministry of Culture of the Czech Republic (DKRVO 2018/17) (PV).

Competing interests: The authors have declared that no competing interests exist.

Abstract

The incomplete cranium discovered at the Zlatý kůň site in the Bohemian Karst is a rare piece of skeletal evidence of human presence in Central Europe during the Late Glacial period. The relative position of cranial fragments was restored and missing parts of the cranium were virtually reconstructed using mirroring and the Thin-plate splines algorithm. The reconstruction allowed us to collect principal cranial measurements, revise a previous unfounded sex assignment and explore the specimen's morphological affinity. Visual assessment could not reliably provide a sexual diagnosis, as such methods have been developed on modern populations. Using a population-specific approach developed on cranial measurements collected from the literature on reliably sexed European Upper Palaeolithic specimens, linear discriminant analysis confirmed previous assignment to the female sex. However, caution is necessary with regard to the fact that it was assessed from the skull. The Zlatý kůň specimen clearly falls within the range of Upper Palaeolithic cranio-metric variation. Despite the shift in cranial variation that accompanied the Last Glacial Maximum (LGM), the Zlatý kůň skull exhibits a morphological affinity with the pre-LGM population. Several interpretations are proposed with regard to the complex population processes that occurred after the LGM in Europe.

1 Introduction

The Late Glacial period, characterized by a retreat of the continental ice sheet after the Last Glacial Maximum (LGM; ca 23 to 19 ky cal BP) [1] and abrupt climatic changes [2], provided a rich human skeletal record in Southern and Western Europe. However, there is a paucity of human remains dated to the Late Glacial period in Central Europe [3,4]: an adult skeleton from Bichon in Switzerland (11,760 ± 110 BP) [5], one adult individual from Mittlere Klause

in Bavaria ($18,590 \pm 260$ BP) [6], an adult and a newborn from Irlich ($11,910 \pm 70$ BP and $12,110 \pm 90$ BP) [7], two adult skeletons from Oberkassel in Central Rhineland ($11,875 \pm 100$ BP) [8], the Moča cranium from Slovakia ($11,255 \pm 80$ BP) [9] and a perinatal skeleton from Wilczyce, Poland ($12,870 \pm 60$ BP) [10]. Other localities provided only very fragmentary human remains whose preservation state prevents wider morphological analyses [11–13]. Radiocarbon dating also revealed a more recent age of some specimens previously assigned to the Late Glacial period [11,14]. By contrast, Southwestern Europe excluding Italy had yielded six Middle Magdalenian skeletons and almost 30 specimens dated to the Final Upper Palaeolithic (for a review, see [15–17]).

Here we report on the partially preserved human skull of Zlatý kůň (ZK), one of the rare pieces of skeletal evidence of human habitation in Central Europe during the post-glacial period. Human remains, considered to be from the Early Upper Palaeolithic (EUP) period (see section 2.1.3), were discovered in 1950–53 in a karstic system near the village of Koněprusy in the Czech Republic [18]. During the subsequent fifty years, the Zlatý kůň fossil underwent three major modifications: a reassessment of the number of individuals, a sexual diagnosis and a dating. At first, the remains were considered to belong to more than one individual, one of them being a male [18]. Subsequently, the cranial fragments were assembled together, the number of individuals was reduced to one [19] and the sex of the individual was reevaluated to female [20]. Finally, in 2002, direct radiocarbon dating shifted the fossil from the pre-LGM phase to the post-LGM chrono-cultural period of the Magdalenian [21].

The LGM was a crucial stage in the Late Pleistocene history of the human population. It corresponds to a marked climatic event in the Northern hemisphere [1], characterized by a decrease in temperature and increasing aridity of the environment, leading hunter-gatherers to abandon northern latitudes and to retreat to a southern refuge [22,23]. The LGM also strongly affected the behaviour, morphological features and population genetic structure of European Upper Palaeolithic human groups: Pre- and post-LGM individuals tend to show differences in stature, body proportions and robusticity of the postcranial skeleton as well as differences in cranial morphology [24–28]. In addition, molecular data highlighted a turnover in the composition of European populations correlating with the LGM event and further late-glacial resettlement of Europe [24,25,29,30].

Given the potential significance of the Zlatý kůň skull in the Central European human record, we have undertaken its virtual reconstruction using geometric morphometric techniques. We provide here a brief history of the Zlatý kůň remains, together with photographs and measurements. Considering the new chrono-cultural attribution of the Zlatý kůň specimen and the context of a genetic and morphological shift attributed to the LGM, we addressed two questions concerning the history of the specimen: (1) What is the morphological affinity of the Zlatý kůň skull when compared with extant and UP European populations? and (2) Is it possible to determine the sex of the Zlatý kůň individual based on its cranial morphology? We addressed these questions using linear data extracted from a virtually reconstructed model which we compared with available cranial data obtained from recent and UP specimens. Prospective research directions are proposed which could provide interesting information about population processes in the European Upper Palaeolithic.

2 Material

Permission to study the fossil remains of Zlatý kůň (inventory numbers AP2, AP3, AP9, AP10, AP12, AP15, AP17, AP18, AP21) was granted by the Department of Anthropology of the National Museum (Prague, Czech Republic) where the specimen is deposited. The specimen belongs to a publicly accessible collection and was examined with the explicit permission of

the appropriate curator (see Acknowledgement). The study was non-invasive and therefore no special permission was necessary. We followed all Czech regulations for fossil studies.

2.1 History and preservation of Zlatý kůň

The first skeletal fragments of the Zlatý kůň specimen were discovered in November 1950 in the karstic massif of the Zlatý kůň hill; other skeletal pieces continued to be found until 1953 [18]. The first discovery followed a controlled explosion in a limestone quarry which had made new areas on the second floor of the cave accessible [31]. Many bones of Pleistocene fauna were discovered in the largest part of the cave called Prošek's Hall, including several fragments of a human posterior calvarium and a right zygomatic bone. These elements were deposited on the surface of a debris cone accumulated through a vertical chimney [32]. The bones were donated to the Geological-Palaeontological Institute of the National Museum in Prague, where they were cleaned and dried [32]. In the spring of 1951, the National Archaeological Institute commenced systematic research on the locality and found more human remains (a left zygomatic bone, a mandible, cervical and thoracic vertebrae and rib fragments), which were accompanied by cultural artefacts [33,34]. The research was methodologically advanced; the team consisted of archaeologists, geologists, palaeontologists and climatologists [35]. The archaeological situation and depositional context are better documented compared to earlier Palaeolithic findings [36]. During the second season in 1952, several vertebral and rib fragments were discovered together with an anterior portion of the calvarium; in 1953 the last piece, a right maxillary fragment, was discovered [18].

Human and other vertebral skeletal remains were found either on the surface of or inside the debris cone. Bones lying on the surface were of a light ochre colour whereas those from inside the debris cone were very dark due to the concentration of manganese in the soil. The latter ones were also reported to be very wet and required a special drying procedure, after which they tended to shrink significantly [32]. The colour difference in particular caused the excavators to believe that two adult individuals were present, designated ZK1 and ZK2 [36,37]. The posterior calvarium, the right zygomatic and the maxilla were assigned to the ZK1 individual; the anterior calvarium together with the left zygomatic and the mandible were assigned to the male specimen ZK2 [18]. However, three decades after its discovery, all fragments were assembled and reinterpreted as only one older adult individual referred to as Zlatý kůň (ZK) [19].

The ZK skull is represented by a partial neurocranium and several bones from the facial skeleton. The neurocranial bones were reassembled into two portions of the skull: a posterior and an anterior portion (Fig 1). The posterior portion consisted of fragmentary parietal bones (each assembled from several fragments) and a largely complete occipital bone preserved in one piece with a right temporal bone. After the reassembly, the parietal bones are almost complete, the right one being better preserved than the left. The occipital bone has a very well preserved squama but lacks its basilar part. The temporal bone comprises part of the squama, the zygomatic process, the petrous portion of the temporal bone and the mastoid process. A hole at the intersection of the sagittal and lambdoid sutures indicates an inserted intrasutural bone [34]. The anterior cranial portion consisted of a large frontal fragment with a small parietal portion just posterior to the coronal suture. The left side of the frontal part shows traces of gnawing by a carnivore [38].

The facial skeleton provided incomplete zygomatic bones, the intact mandible and the right maxillary fragment. In contrast to the right one, the left zygomatic bone has a preserved lower orbital margin and a zygomatico-facial foramen. Both zygomatics have clearly visible zygomatico-temporal foramina on the temporal surfaces. The right maxilla is preserved from the level

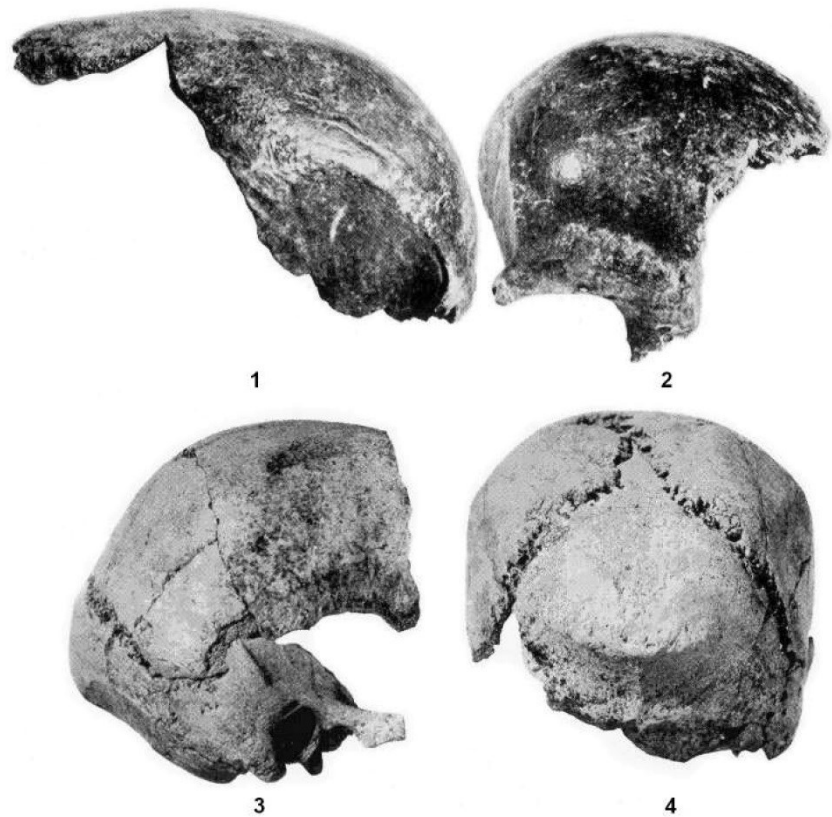


Fig 1. Anterior and posterior (3, 4) cranial portions in the post-recovery state recorded in 1956 (from the Archive of the Department of Anthropology of the National Museum, Prague). Lateral view (1, 3), anterior view (2) and posterior view (4). Not in comparable scale.

<https://doi.org/10.1371/journal.pone.0201431.g001>

of the second molar to the incomplete alveolar cavity of the first incisor. The frontal process is preserved with the piriform border but the orbital surface and the body are missing. The mandible shows there was an erupted third molar on the left but an unerupted one on the right. All maxillary and mandibular teeth are heavily worn. As documented by Vlček [18], all the teeth were extracted from their dental alveoli and glued back.

The original parts of the Zlatý kůň skull except the left zygomatic bone were manually assembled based on fracture lines and articulations. The re-assembly of fragments also entailed a reconstruction of the missing right zygomatic arch (Fig 2; [20]). However, the absence of the left cranial portion resulted in an anatomically incorrect position of the mandible. The adhesive material did not persist and the formerly attached fragments (the maxilla and the right zygomatic bone) got separated again. Fortunately, the manual modification did not cause any irreversible damage to the fossil. In its present state (Fig 3), only the calvarium and the mandible are still glued together, supported by two wooden sticks; the first from the nasal root to the mandibular alveolus after the right central incisor and the second from the lower edge of the left parietal bone to the left inner mandibular angle.



Fig 2. The Zlatý kůň skull with the reconstructed zygomatic arch marked by red curve and attached maxillary fragment (recorded in 1991; from the Archive of the Department of Anthropology of the National Museum, Prague).

<https://doi.org/10.1371/journal.pone.0201431.g002>



Fig 3. Actual state of the Zlatý kůň skull with separate fragments—Zygomatic bones and maxilla (recorded in 2018; photo Marek Jantač).

<https://doi.org/10.1371/journal.pone.0201431.g003>

2.2 Previous dating and sex assessment of Zlatý kůň

The first descriptions of the Zlatý kůň specimen indicated that all preserved cranial bones are relatively robust and thick [18,32,33]. Further studies pointed out features similar to Czech EUP (pre-LGM) specimens, namely the occipital bun [19,39], the frontal bone [40] and supra-orbital areas, the latter being within the metric variability of specimens from Mladeč, Brno, Dolní Věstonice and Pavlov [41,42]. The cranium's morphological resemblance to pre-LGM specimens was also emphasized by the statement that “while the geological age and cultural associations of the Zlatý kůň hominid are not entirely certain, the morphological affinities of this specimen are quite clear” [43]. Support for the EUP age was also seen in the depositional context analogous to the Mladeč site, the faunal remains and the assemblage of five artifacts consisting of three lithic tools, a naturally perforated mollusk and a bone point [35,38,44]. However, subsequent direct radiocarbon dating revealed a much younger age close to the end of the Late Pleistocene ($12,870 \pm 70$ uncal BP [21,45]; $15,138\text{--}15,635$ cal BP, Calib Rev 7.0.4 [46]). Further dating based on a human rib fragment failed to confirm the previous result because of a low amount of ^{14}C in the sample [45]. The first dating thus remains the primary evidence concerning the age of the Zlatý kůň cranium.

Many other fossils of presumed EUP age were dated to different periods of the Holocene (Vogelherd [47], Svitávka [21], Svatý Prokop [45], Velika Pečina [48]) and the Zlatý kůň cranium is the only re-dated specimen whose age falls within the Upper Palaeolithic. Chrono-culturally, the specimen is classified to the Magdalenian period of human occupation, archaeologically documented at the nearby sites of Hostim ($12,420 \pm 470$ uncal BP) [49] and Děrává jeskyně [50] but not widely established in Bohemia [51]. This period was characterized by a resettlement of Central and Northern Europe as a consequence of climatic amelioration after the LGM [24]. Nevertheless, Central Europe was still relatively sparsely inhabited in this phase [3].

The two portions of the Zlatý kůň calvarium were thought for a long time to belong to two different individuals (ZK1 and ZK2). The ZK2 individual was considered a male specimen mainly on the basis of sexually dimorphic features in the frontal area—the glabella, supra-orbital arch, upper orbital margin and temporal line [18,37,52]. However, further analyses showed that all the cranial fragments match together, representing a single individual [19,20,53]. Since then, the Zlatý kůň skull has been consistently regarded as a female, though without extensive justifications [20,36] and contrary to the previous conclusion [18,19]. The statement was retrospectively supported by Wolpoff et al. [41] based on a morphological comparison with Mladeč 1 and 5 and Pavlov 1 crania; however, sex has been reliably determined only in the case of the last specimen [54]. The poorly preserved postcranial remains of the Zlatý kůň thorax [55] do not provide useful information for the sex diagnosis. As the assessment of sex is also dependent on population variation, we will expand on this topic based upon a comparison of the cranial morphology of the Zlatý kůň individual with that of extant and comparative UP individuals.

3 Methods

The virtual reconstruction and subsequent analyses are explained in detail in the following sections. The computer programmes used in each step are listed in section 3.4.

3.1 Virtual reconstruction

To virtually reconstruct the skull of Zlatý kůň, the skeletal elements were scanned at the Radiology department of the Hospital Na Homolce in Prague by computed tomography (CT), using a Somatom Sensation 16 scanner (Siemens, Erlangen, Germany). Acquisition

parameters were optimally set with a voxel dimension of 0.49 mm, a thickness of 0.6 mm, and a space between slices of 0.3 mm. The wooden sticks were removed from the virtual 3D model and the mandible was separated from the calvarium, as it was misaligned in relation to the midsagittal plane. As a result, we obtained five independent surface models of the calvarium, the right and left zygomatic bones, the right maxilla and the mandible.

Following the definition of fossil distortions [56], the Zlatý kůň cranium exhibits two types of distortion: fragmentation and missing parts. The main steps of the reconstruction are illustrated in Fig 4, and a list of landmarks and semilandmarks used in each reconstruction step is provided in S1 and S2 Tables. We can divide the reconstruction into two phases: (a) a preserved morphology-based reconstruction and (b) a reference-based reconstruction. In the first phase, we exploited the preserved morphology to reconstruct unilaterally missing parts (steps 1, 2 and 4). In the second phase, we used a reference sample to estimate missing regions (steps 3 and 5). Based on different subsamples derived from the reference sample, we created seven versions of the reconstruction. The reference sample consisted of recent skulls segmented from CT scans acquired at the *CHU de Bordeaux* (15 males, 15 females) and the geochronologically closest specimen, the Magdalenian cranium from Moča (Slovakia, ca 13,100 cal BP). The modern crania were used with ethical consent of the *Université de Bordeaux* Institutional Review Board and the *Comité de Protection des Personnes Sud-Ouest et Outre Mer III* (DC 2015/172). The Moča cranium was also CT scanned at the Hospital Na Homolce in Prague, with similar acquisition parameters as those used in the study of the Zlatý kůň specimen.

Step 1: Calvarium reconstruction. The calvarium lacks a large portion of its left side, but there is still a large portion preserved posteriorly. Instead of using a simple mirror imaging of the complete right side, we used an approach based on the Thin-Plate Spline (TPS) algorithm to estimate the missing parts of the left side, preserving the natural asymmetry of the cranium [57–59]. As there were not enough anatomical landmarks preserved on the left portion of the calvarium, curve and surface semilandmarks were used. Missing landmarks on the left side were interpolated based on a subset of landmarks available on both sides and the mirror template was then warped to fit the original calvarium.

To obtain a better estimation of the missing contralateral regions, the mandible was attached to the calvarium based on the right temporomandibular articulation and cranial and mandibular midplanes. The midplanes were estimated using Principal component analysis (PCA) of sagittal landmarks [57]. While attached to the calvarium, three translational and two rotational degrees of freedom of the mandible were eliminated (only the rotation along the transversal axis remained), which allowed us to place landmarks on the left mandibular condyle. This procedure was useful in that it preserved the natural asymmetry of the cranium.

Step 2: Rearticulation of zygomatic bones. The left zygomatic bone is slightly better preserved than the right one. A mirror image of the left one was therefore used as a template for the completion of the right one in the same way as in the reconstruction of the calvarium. A small portion of the lower orbital margin was thus added to the right zygomatic. Both zygomatic bones were subsequently manually attached to the calvarium based on the direct anatomical connection with the frontal bone and the continuity with the zygomatic process of the temporal bone. This yielded a model of the rearticulated incomplete cranium.

Step 3 and 4: Right maxilla rearticulation and mirroring. The fragment of the right maxilla could not be directly attached to the cranium, so its position was estimated on the basis of the reference sample of complete crania. The set of landmarks and semilandmarks employed in the reconstruction was digitized on the reference crania and the Zlatý kůň cranium using a predefined template (Fig 5, S1 Table). Maxillary landmarks were estimated relative to the Zlatý kůň cranium based on the different reference subsamples and the maxillary

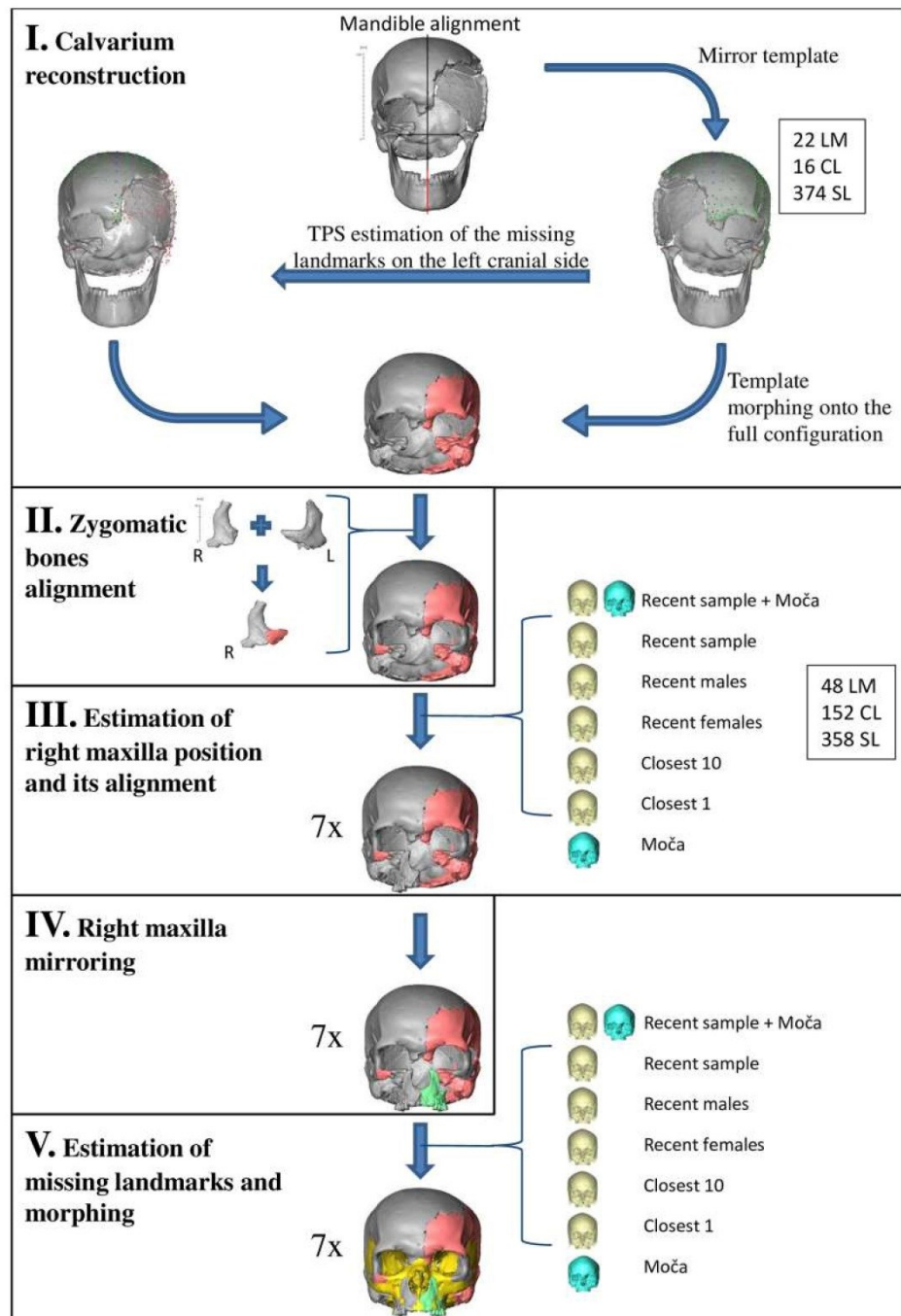


Fig 4. Reconstruction schema. Original bones in grey, preserved-morphology-based reconstruction in orange, mirror-imaging in green, reference-based reconstruction in yellow. Information on number of anatomical landmarks (LM), curve semilandmarks (CL) and surface semilandmarks (SL).

<https://doi.org/10.1371/journal.pone.0201431.g004>

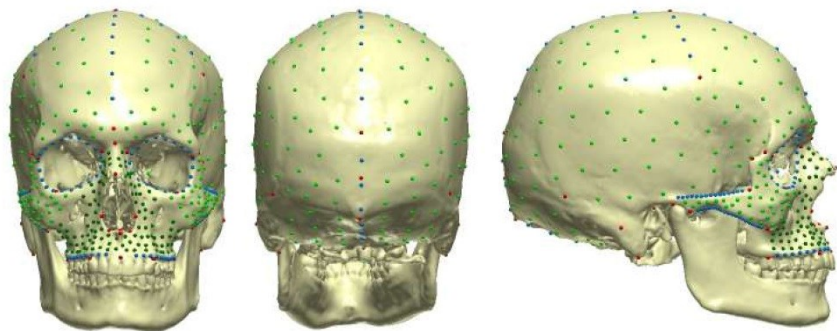


Fig 5. Illustration of landmarks used for the reconstruction. Red (anatomical landmarks), blue (curve semilandmarks), green (surface semilandmarks).

<https://doi.org/10.1371/journal.pone.0201431.g005>

fragment was subsequently aligned into its estimated anatomical position. The estimation was done seven times based on a different selection of reference specimens (Table 1). This resulted in seven models of the cranium with the maxilla attached. In all seven models of the Zlatý kůň skull, the right maxilla was mirrored across the cranial midplane.

Step 5: Estimation of missing landmarks and warping. Having all the cranial fragments (excluding the mandible) articulated in their anatomical positions, the remaining missing landmarks were estimated in each of the seven models of the cranium using the same reference sample as in step 3. Finally, the closest complete specimen (according to Procrustes distance) was selected to be warped onto the completed configurations. Areas missing from the Zlatý kůň skull were filled using this warped specimen.

Validation. To validate the reconstruction process, a PCA was performed on the full landmark configurations of all the reconstructions and the individuals from the reference sample. The distribution of the reconstructions across the sample allowed us to assess the reliability of the reconstruction process [56]. A Procrustes ANOVA further quantified the variations of the reconstruction procedures compared to the general cranial morphology of the reference sample [60]. Several cranial measurements were also compared to estimated values given by Vlček [18].

3.2 Visual sex attribution

As morphometric methods of sex assessment are highly population-specific, a morphoscopic assessment was carried out on the original specimen. Four methods were used to estimate the

Table 1. Reference samples for the cranial reconstruction.

Subsample	Description	Number of specimens
1	All specimens (recent crania and Moča)	31
2	Recent specimens	30
3	Recent males	15
4	Recent females	15
5	Closest 10 recent specimens*	10
6	Closest 1 recent specimen*	1
7	Moča	1

*Closest specimens to the incomplete landmark configuration of Zlatý kůň based on Procrustes distance.

<https://doi.org/10.1371/journal.pone.0201431.t001>

sex from the cranium and mandible: (a) the traditional method following the recommendations made by the Workshop of European anthropologists evaluating cranial and mandibular characters [61,62]; (b) the method of Walker [63] involving discriminant function analysis (DFA) on five cranial and mandibular features; (c) modified Walker's method supplemented with scoring of zygomatic extension using decision trees [64]; and (d) a method evaluating the shape of the mandibular ramus [65,66].

3.3 Morphometric analysis of affinity and sex attribution

Classical cranial measurements defined by Martin [67] or Bräuer [68] were acquired on the Zlatý kůň reconstructed cranium and analysed in comparison with recent and Upper Palaeolithic European specimens. Three European populations (Austrian, Hungarian and Norse) from the Howells craniometric database (<https://web.utk.edu/~auerbach/HOWL.htm>) [69,70] were used to represent recent variability of modern humans. Cranial metric data were collected from the published literature on 68 reliably dated UP specimens (for references see S3 Table). Because fossils were often sexed by assessing the skull or the overall robusticity of the skeleton, attention was paid to how their sex was assessed. Information on the sex of individuals was used if it was determined by primary diagnosis from the pelvis [71,72], secondary diagnosis following reliable criteria (see [15,73]) or genetic analysis. Otherwise, the sex was considered unknown.

In total, 20 cranial measurements were inspected (see Results for definitions). From the set of cranial variables, 13 were comparable with variables in the Howells database. Because of the differential taphonomic preservation of the comparative specimens, missing data were imputed using the PCA algorithm, which takes into account similarity between individuals and relationships between variables [74]. On the basis of multiple imputations, we removed specimens for which the presence of missing values caused too much uncertainty about their position along the first two principal axes. This treatment is consistent with the study of Arbour and Brown [75], which concludes that the estimation of missing data provides a better image of reality when only the most uncertain specimens are excluded.

To analyse morphological affinity without the confounding effect of size sexual dimorphism [27], linear measurements were transformed to size-adjusted shape variables via division by the geometric mean and logarithmization [76,77]. UP individuals were divided into two groups, one from before and the other from after the LGM (see [27]). Linear discriminant analysis (LDA) was performed to assess the cranial shape of Zlatý kůň in relation to the different population samples.

To analyse the sex attribution of the Zlatý kůň specimen, raw cranial measurements were used, as size is an important factor in human sexual dimorphism. First, the random forest classification method [78] was applied to the UP sample of known sex. This method usually does not provide high posterior probabilities but allows us to select the most important variables related to sex classification. Subsequently, this set of variables was used in LDA to assign the sex of Zlatý kůň.

3.4 Software

The software TIVMI (<http://projets.pacea.u-bordeaux.fr/TIVMI>) [79] was used to segment surface models from CT scans and to measure linear dimensions on the Zlatý kůň cranium. Surface models were reconstructed from CT scans using the HMM algorithm implemented in TIVMI [80,81]. Landmarks and curve and surface semilandmarks were digitized in Viewbox 4 (dHAL software, Athens, Greece). Semilandmarks were placed semi-automatically using a pre-defined cranial template. Homologous position of semilandmarks was ensured by a sliding

procedure. For more details about sliding semilandmarks in three dimensions see [82]. Missing point estimation, warping and mesh alignment were done using the R package *Morpho* [83]. Surface model processing was done in Meshlab (Visual Computing Lab, Italian National Research Council) and Avizo 7.1 (Visualization Sciences Group, SAS). Data processing and statistical analyses were performed in R 3.3.3 (R Foundation for Statistical Computing, Vienna, Austria, 2015). Missing measurements in the comparative sample were estimated using PCA implemented in the R package *missMDA* [84]. Classification was carried out using the packages *randomForest* [78] and *MASS* [85].

4 Results

4.1 Reconstruction

The reconstruction of the calvarium resulted in a perfect fit between the reconstructed and preserved morphology that would not be possible with simple mirror imaging because of the presence of natural asymmetry. The smooth transition between the preserved and reconstructed morphology provides confidence that the original morphology of the calvarium is closely approximated.

In total, seven independent reconstructions of the Zlatý kůň cranium were created based on different reference subsamples used to estimate the position of the right maxilla and the unpreserved regions of the Zlatý kůň cranium. Plotted with other individuals from the reference sample following a PCA on residuals of the Procrustes analysis, the different versions of the reconstructed Zlatý kůň cranium form a cluster with small variation relative to the inter-individual variability (Fig 6), which indicates that there is low uncertainty in the reconstruction. The most different reconstructions of the Zlatý kůň cranium were those based on Moča and the closest specimen (Fig 6). The main difference resided in the position of the maxilla manifesting in maxillary prognathism and maxillary breadth. Both were greater in the Moča-based reconstruction than in the reconstruction based on the closest specimen. The latter was at the same time slightly more distant from all other reconstructions (Fig 6). After the alignment of the mandible (rotation along the axis at the temporomandibular joints), the maxillae did not fit very well in the occlusal plane in both distant reconstructions. On the other hand, in the reconstruction based on the entire reference sample, the maxilla was similarly situated as

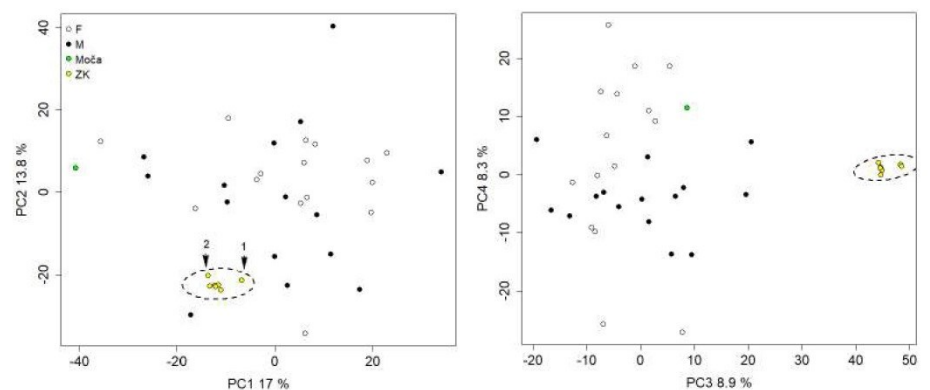


Fig 6. Principal component analysis performed on coordinates of the Zlatý kůň cranial reconstructions and the reference cranial sample. Variability of reconstructions is indicated by 95% confidence ellipses. The most distant reconstructions: 1) based on the closest one specimen, 2) based on the Moča cranium.

<https://doi.org/10.1371/journal.pone.0201431.g006>

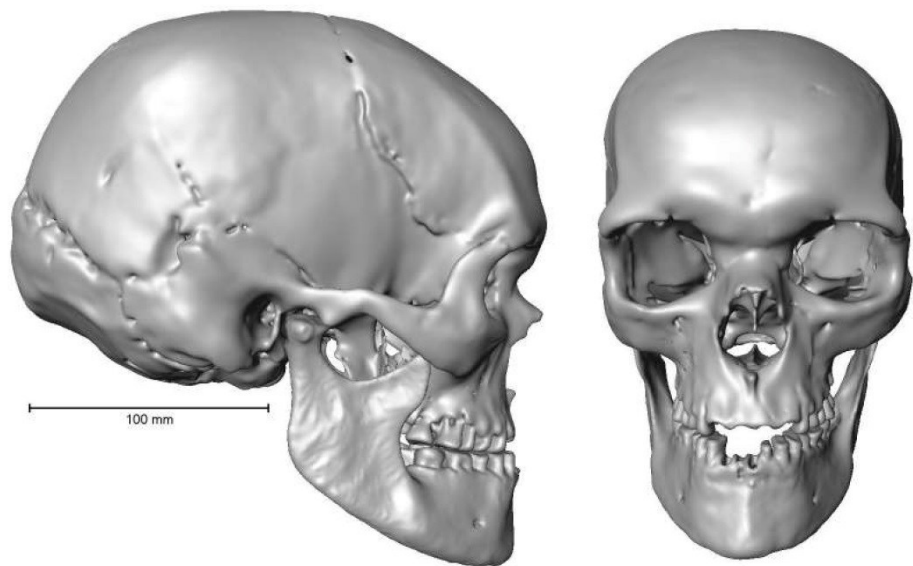


Fig 7. The reconstructed cranium with attached mandible (based on all reference specimens).

<https://doi.org/10.1371/journal.pone.0201431.g007>

in Moča but slightly dorso-superiorly rotated, which resulted in better fit with the mandible (Fig 7).

Furthermore, the variation of different reconstructions was quantified using Procrustes ANOVA and accounted for only 2.6% of the total shape variation of the sample and 0.3% in terms of centroid size. Given the small differences between the reconstructions, the one based on all reference specimens was chosen for further morphometric analyses (Fig 7, S1 File).

Several measurements were also taken for comparison with the previous estimates [18]. Depending on the type of reconstruction, they were taken only once (mirroring and preserved morphology-based reconstruction) or from every reconstruction (reference-based reconstruction). Greater differences were noticed in minimum and maximum frontal breadth, spinoalveolar height and nasal breadth, while minimal differences were in palatal breadths (Table 2).

Table 2. Comparison of measurements recorded for the Zlatý kůň cranium.

Measurement	M	Vlček [18]	Virtual reconstruction	
Minimum frontal breadth	9	109*	97.2	[Rm]
Maximum frontal breadth	10	116*	122.9	[Rm]
Spinoalveolar height	48(1)	21.5	18.7 ± 0.1	[Rr]
Nasal breadth	54	32*	25.1 ± 0.6	[Rr]
Palatal breadth at C	**	28*	27.6 ± 1.2	[Rr]
Palatal breadth at P4	**	38*	38.6 ± 1.3	[Rr]

M = measurement number and definition by Martin [67] or Bräuer [68]; [Rr] = measurement taken from multiple reference-based virtual reconstruction; [Rm] = measurement taken from virtual reconstruction based on preserved morphology. Measurements are in mm.

* Measurement estimated by Vlček as unilateral half of the current measurement, therefore, multiplied by two for the comparison purpose.

** Defined by Vlček [18].

<https://doi.org/10.1371/journal.pone.0201431.t002>

Table 3. Raw measurements for the Zlatý kůň cranium.

M	Variable	Zlatý Kůň
1	Maximum cranial length	197.7
5	Length of the skull base	99.2
8	Maximum cranial breadth	137.2
9	Minimum frontal breadth	97.2
10	Maximum frontal breadth	122.9
17	Basibregmatic height	128.5
20	Auriculo-bregmatic height	109.5
23	Horizontal circumference	566.3
26	Frontal sagittal arc	140.0
27	Parietal sagittal arc	124.8
28	Occipital sagittal arc	125.9
40	Basion-prosthion length	96.3
45	Bi-zygomatic breadth	125.1
48	Naso-alveolar height	61.8
51	Orbital breadth	43.1
52	Orbital height	30.0
54	Nasal breadth	25.1
55	Nasal height	43.5
61	Maxillo-alveolar breadth	62.0
63	Internal palate breadth	39.2

M = measurement number and definition by Martin [67] or Bräuer [68].

<https://doi.org/10.1371/journal.pone.0201431.t003>

4.2 Analysis of morphological affinity

Cranial measurements were taken on the reconstruction of the Zlatý kůň cranium to analyse the morphological affinity of the skull (Table 3, S4 Table). To filter out the effect of general size, morphological variation was inspected using LDA on log-shape ratios derived from 13 cranial measurements (see Table 4) corresponding to measurements in the Howells database.

Four discriminant functions were obtained, but only the first two were important for our study. The first discriminant axis separated past UP populations from the recent European populations (Fig 8). The second discriminant axis separated the pre-LGM and post-LGM samples. The coefficients of the discriminant functions revealed that the first function differentiated maximum cranial length, maximum cranial breadth, orbital breadth, bi-zygomatic breadth and orbital height. The second discriminant function differentiated maximum frontal breadth, basibregmatic height and maximum cranial breadth (Table 4 and Fig 8). Zlatý kůň was located in the centre of the pre-LGM variation and at the edge of the post-LGM sample variation (Fig 8).

Using cross-validations, 60–70% of individuals were classified into correct population samples whereas the majority of misclassifications occurred either within the variation range of recent populations or of UP ones (Table 5). The Zlatý kůň cranium was classified as belonging to the pre-LGM sample with the probability of 0.96 (Table 5).

4.3 Visual sex assessment

The Zlatý kůň skull was evaluated by a method based on European recommendations [61] as follows: glabella (0), mastoid process (−2), nuchal crest (+1), zygomatic process (0),

Table 4. Function loadings of population DFA for size-adjusted craniometric variables.

Measurement		Function 1	Function 2
Martin [67]	Howells [69]		
M1	GOL	16.96	-1.84
M5	BNL	-5.11	2.46
M8	XCB	-14.63	-10.82
M10	XFB	-1.36	18.95
M17	BBH	6.68	-14.34
M40	BPL	4.45	1.58
M45	ZYB	11.88	-5.02
M48	NPH	-0.01	-0.83
M51	OBH	13.13	4.83
M52	OBH	-10.54	-6.09
M54	NLB	-1.04	4.97
M55	NLH	4.78	3.49
M61	MAB	-4.01	-3.73

<https://doi.org/10.1371/journal.pone.0201431.t004>

superciliary arch (+1), frontal eminence (-2), external occipital protuberance (+1), zygomatic bone (-1), frontal inclination (+1). The mandible did not possess a marked level of sexualization and all three characters were neutral (0).

Based on Walker [63], the character scoring was as follows: glabella (3), mastoid process (1), nuchal crest (4), supraorbital margin (2) and mental eminence (3). In addition to Walker's five features, zygomatic extension was evaluated (3) by the method of Langley et al. [64]. Mandibular flexure was evaluated as slightly flexed, which corresponds to the female sex.

The results of sex assessment based on visual traits are summarized in Table 6. Most of the methods used lean towards the female sex, but methods providing posterior probability show low reliability. In addition, the greatest posterior probability results (over 80%) point towards the male sex.

4.4 Morphometric sex assessment

Raw cranial measurements were used in the sex classification of Zlatý kůň based on an UP sample of reliably sexed specimens. The random forest algorithm was used to order variables according to their importance in the sex classification and only the most important variables were used to create a classification model with LDA. In order not to overfit the model with too many variables, a subset of variables with the greatest cross-validation success rate was chosen. As a result, four variables (bi-zygomatic breadth, naso-alveolar height, horizontal circumference and orbital breadth, in decreasing order; Table 7) were included in the classification model, which correctly classified 94% of individuals with the posterior probability threshold of 0.5 (Table 8). In 50% of individuals, all of which were classified correctly, the posterior probability was greater than 0.95. When this model was applied to Zlatý kůň, the cranium was classified as belonging to a female with a probability of 0.98 (Table 8).

To visually present the classification results, PCA was performed on this subset of variables. Clear clusters of males and females were obtained, separated along the first principal component axis, which accounted for 60% of the total variation (Fig 9). This shows that the combination of the four variables is important for sex classification based on skulls of UP specimens. However, the Zlatý kůň cranium is plotted very close to the transition between males and females (Fig 9).

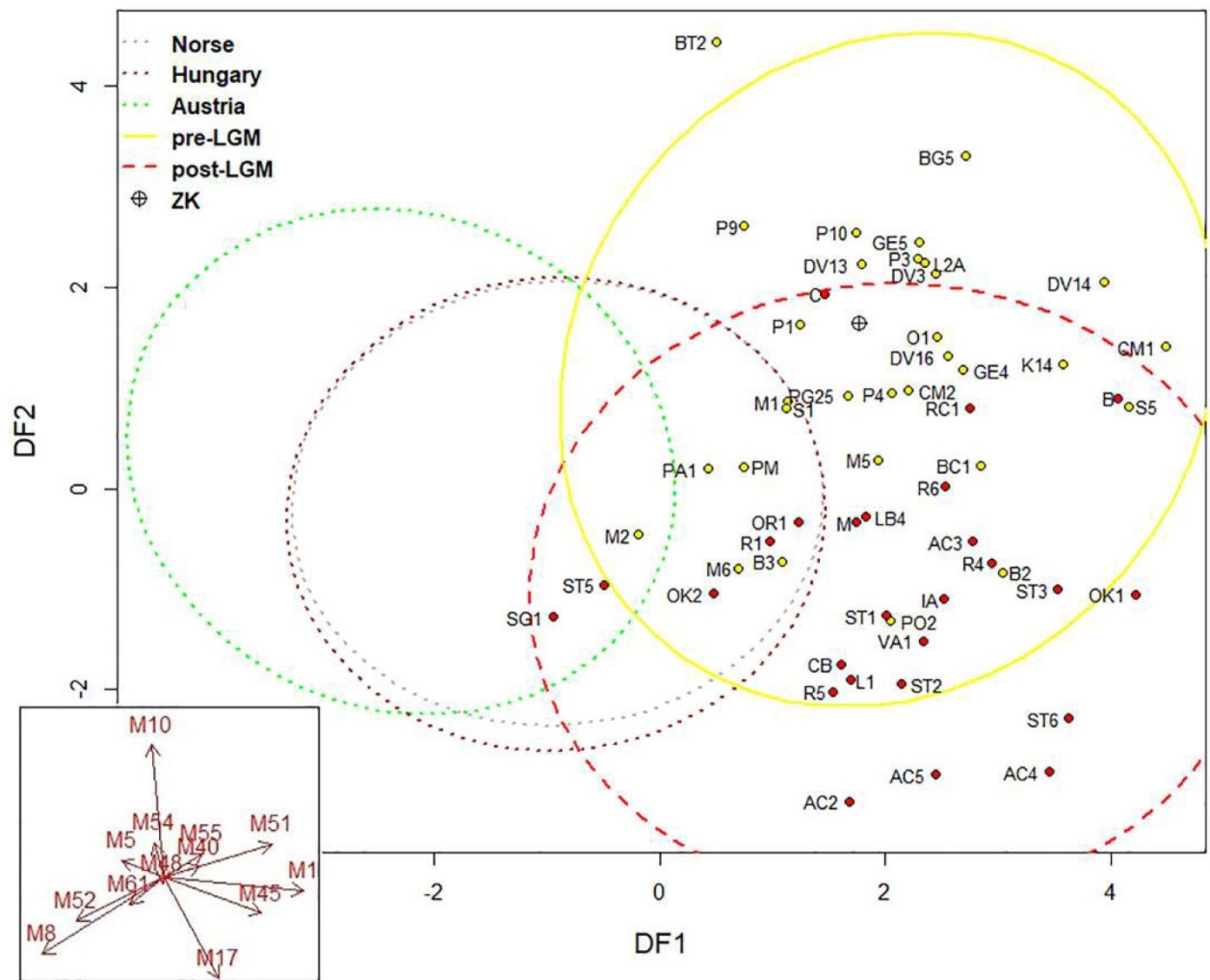


Fig 8. Linear discriminant analysis of recent and fossil samples. Variability of individual samples is indicated by 95% confidence ellipses. Norse, Hungary, Austria = recent samples (individual points not shown for better legibility); ZK = Zlatý kůň. Specimen acronyms are in S3 Table. Red arrows indicate loadings of log-shape variables on the discriminant axes.

<https://doi.org/10.1371/journal.pone.0201431.g008>

Table 5. Cross-validation probabilities of classification into population samples from LDA (with absolute numbers) and classification results for Zlatý kůň.

	Austria	Norse	Hungary	pre-LGM	post-LGM
Austria	0.72 (79)	0.17 (19)	0.09 (10)	0.01 (1)	0.00 (0)
Norse	0.05 (5)	0.65 (72)	0.25 (28)	0.03 (3)	0.02 (2)
Hungary	0.12 (12)	0.20 (20)	0.60 (59)	0.05 (5)	0.02 (2)
pre-LGM	0.00 (0)	0.03 (1)	0.10 (3)	0.71 (22)	0.16 (5)
post-LGM	0.00 (0)	0.04 (1)	0.08 (2)	0.19 (5)	0.69 (18)
ZK posterior probability	0.00	0.02	0.00	0.96	0.02

<https://doi.org/10.1371/journal.pone.0201431.t005>

Table 6. Summary of visual methods of sex assessment.

Method	Anatomical region	Number of variables	Posterior probability	Sex assessment
Ferembach et al. (1980)	Cranium	9	-	F
Ferembach et al. (1980)	Mandible	4	-	?
Ferembach et al. (1980)	Skull	13	-	F
Loth and Henneberg (1996)	Mandible	1	-	F
Walker (2008)	Skull	3	0.59	F
Walker (2008)	Skull	2	0.78	F
Walker (2008)	Skull	2	0.84	M
Walker (2008)	Skull	2	0.75	F
Walker (2008)	Skull	2	0.82	M
Walker (2008)	Skull	3	0.73	F
Langley et al. (2017)	Skull	3	0.73	F

<https://doi.org/10.1371/journal.pone.0201431.t006>

5 Discussion

Preservation is a limiting factor in palaeoanthropological studies, as fossils are often found in a fragmentary and incomplete state. Similarly, the Zlatý kůň individual is represented mainly by fragmentary cranial remains with large missing regions. Until now the Zlatý kůň skull has been included almost exclusively in studies analysing the expression of single cranial or mandibular traits in Late Pleistocene hominins [19,28,39,41,42,86]. More widely focused analyses considered only the well preserved mandible [87] or a restricted part of the frontal bone [40]. The reconstruction of the Zlatý kůň cranium facilitates its inclusion into a wider range of morphometric analyses.

Table 7. Importance for first 10 variables in random forest for sex.

Variable	Importance
M45	1.883
M48	1.262
M23	1.075
M51	0.906
M8	0.680
M1	0.499
M26	0.454
M20	0.411
M55	0.318
M5	0.286

<https://doi.org/10.1371/journal.pone.0201431.t007>

Table 8. Cross-validation probabilities of classification into sex groups from LDA (with absolute values between parentheses) and classification results for Zlatý kůň.

	0.5 threshold		0.95 threshold		
	F	M	F	M	I
F	1.0 (13)	0.0 (0)	0.54 (7)	0.0 (0)	0.46 (6)
M	0.1 (2)	0.9 (17)	0.0 (0)	0.53 (10)	0.47 (9)
ZK posterior probability	0.98	0.02	-	-	-

F (females), M (males), I (indeterminate = posterior probability lower than 0.95).

<https://doi.org/10.1371/journal.pone.0201431.t008>

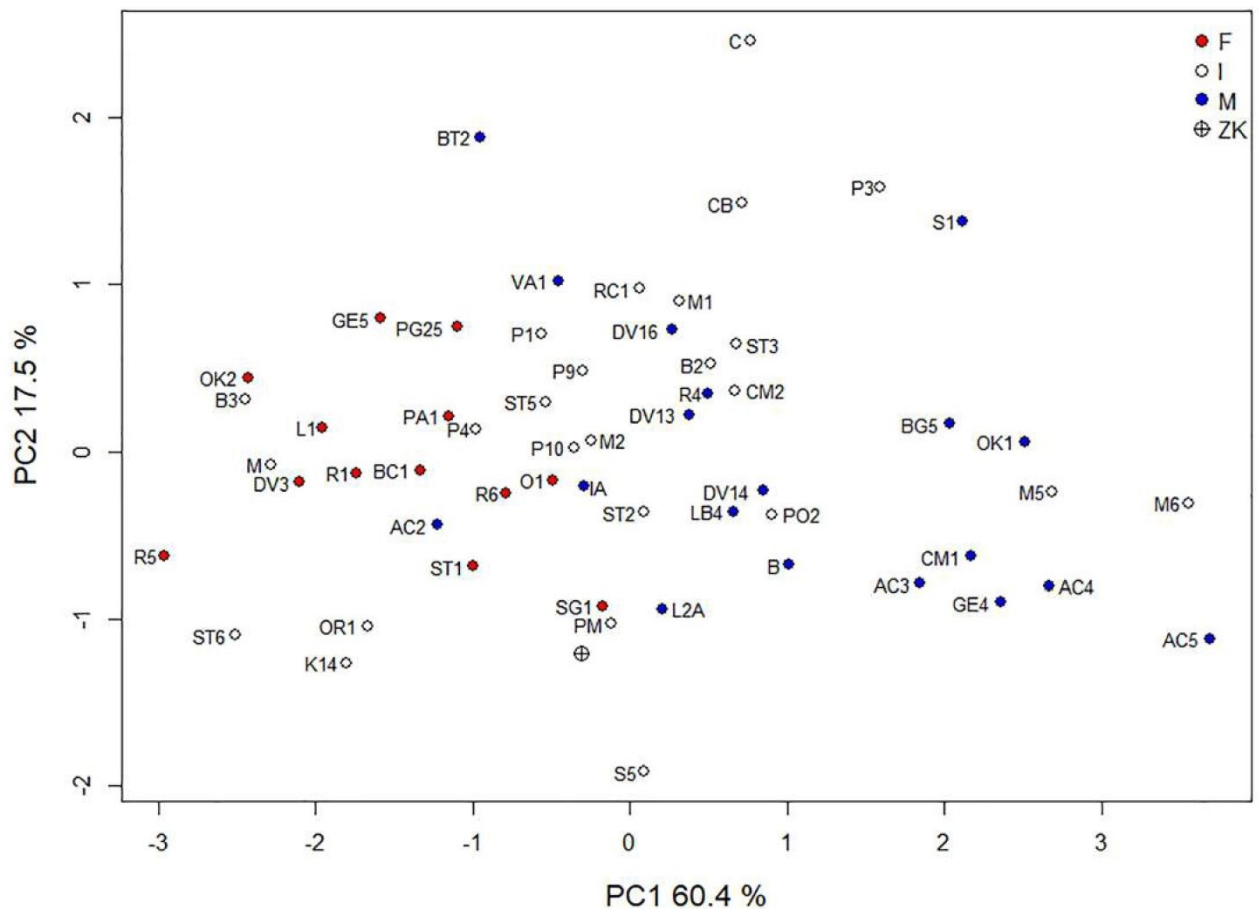


Fig 9. Principal component analysis performed on the four most important cranial variables for sex classification. Specimen acronyms are in S3 Table.

<https://doi.org/10.1371/journal.pone.0201431.g009>

5.1 Reconstruction

The present reconstruction is based on virtual computer techniques which offer more objective tools than manual methods based on the anatomical knowledge of an experienced anthropologist. Using virtual tools, the mandible was safely separated from the rest of the cranium and all fragments, except for the maxilla, were re-assembled following anatomical rules. Although an approach employing dental occlusion could also be taken into consideration [88], it would not be appropriate in this situation for the two following reasons: (a) the heavy attrition of the teeth and (b) the extraction of the teeth and their subsequent placement back in their alveoli. Both circumstances prevent a reliable occlusal match between the maxilla and the mandible.

Every reconstruction depends on prior assumptions [57] and the method used to estimate missing parts. Both effects should be considered before and during subsequent analyses. The main assumption in the reconstruction of the Zlatý kůň cranium was the use of a recent sample of modern human crania to estimate missing parts. However, keeping in mind our further aim to analyse morphological affinity and sex of the Zlatý kůň individual, the contemporaneous

cranium of Moča [9] was included and the reference sample was divided into several subsamples, which potentially could have affected the reconstruction. The use of either the recent reference sample or the contemporaneous reference specimen resulted in a negligible effect on the final reconstruction, as did the use of either the male or the female subsample.

Missing regions of the Zlatý kůň cranium were located mainly in the middle face, the temporal fossa and the cranial base. The preserved and missing areas influence the efficacy of the TPS estimation. The TPS algorithm is known to work well on smooth surfaces such as the cranial vault [82], but fortunately, the missing regions in the area of the face of Zlatý kůň were not large and were well surrounded by structures with preserved morphology. Also, a large number of semilandmarks ensured an adequate warping of the reference morphology. However, it must be noted that some areas with high variability and low integration, such as the cranial base, may be predicted with very low accuracy [89].

5.2 Sex attribution

Reconstructions of the biology and behaviour of past populations rely on the accurate assessment of the sex of fossil specimens [90–92]. For many years, skull robusticity had been commonly used as an indicator of sex [62,93]. However, sexing of fossil individuals requires specific methods because the degree of cranial sexual dimorphism changed over time [90].

The sex assessment based on visual cranial traits, using the methods of Ferembach et al. [61] and Loth and Henneberg [65], identified the Zlatý kůň individual as a female. Discriminant functions designed by Walker [63], combining scores of visually rated characters, did not provide a clear conclusion; DFA combining the glabellar area and mental eminence and another DFA involving the orbital margin and mental eminence indicated male sex because the scores of both characters were equal to 3. Such a score value was earlier found only in 1.9% of females for the orbital margin, 31% of males and females for the glabella and in 17% of females for the mental eminence in the Euro-American population [63]. Therefore it is not surprising that these two DFAs indicated that the Zlatý kůň individual was a male. According to the hyperfeminine value for the mastoid process (1), the last four DFAs indicated female sex. Mental eminence, included in the DFAs indicating the male sex of the Zlatý kůň individual, exhibits a particularly high scoring error [94]. Despite only slight intra- and inter-observer disagreement in Walker's other visual traits, subjectivity in trait scoring leads to differences in sex classification [94].

Simultaneously, a new classification technique called decision tree was used for assessing sex on the basis of three non-metric features [64]. The posterior probability of 0.73 indicated female sex of the Zlatý kůň skull. As emphasized by Garvin and Kales [95], the decision tree model produces a strong sex bias, with females correctly classified in 94% and males only in 49% of the test sample.

Results obtained by visual sexing techniques cannot be considered reliable because classification methods of sex estimation from the skull are population-specific. It should be remembered that the equations used here were devised from a recent human population sample, which may not be an appropriate model for sexing an Upper Palaeolithic individual. What is known about the extent and character of sex-related variation within the UP population is based on only a small sample [90]; it is generally accepted that fossil specimens showed higher robustness than today's human population. This fact is described as an evolutionary trend of skeletal gracilization which goes hand in hand with craniofacial feminization, manifested particularly in males but not excluding females [90,96]. It is therefore necessary to anticipate a certain degree of shifts in the outcomes of sex estimations: A fossil skull classified as an uncertain

female by a method derived from a contemporary reference sample might more likely turn out to be a female in the UP context.

One of the most daunting situations in sex assessment is when conflicting results are obtained from the same skeleton [97]. Therefore, the risk of misclassification must be reduced as much as possible, which is why we applied a more objective method based on cranial measurements. However, population specificity of cranial measurements [98] affects sex estimation methods [99]. To overcome this problem, we used an Upper Palaeolithic sample of individuals whose sex was estimated by reliable techniques. Most of the selected dimensions were from the facial skeleton and are traditionally used in methods of sex estimation from the skull [61]. Using the morphometric approach to sex estimation produced evidence that the Zlatý kůň individual was more likely a female, with a high posterior probability (0.98). Estimates with posterior probability over 95% can be considered reliable [100]. However, despite the good performance in the UP sample, we have to keep in mind the small size of the reference sample and the possibility of an error.

5.3 Cranial morphology in the UP context

The Zlatý kůň cranium exhibits a clear morphological affinity to specimens dated to the period prior the Last Glacial Maximum. This fact is in concordance with earlier descriptions of the archaic morphology of the Zlatý kůň specimen (see section 2.2) but contrasts with direct radiocarbon dating, which estimated the age of the specimen at ca 15.4 ky cal BP [21]. Chronologically, Zlatý kůň belongs to the period after the LGM (23 to 19 ky cal BP [1]) but before the onset of a sudden warming phase which started 14.7 ky cal BP (Bølling) and is related to the main reoccupation of Central Europe [2].

Craniometrics is one of the main tools of biological distance analysis [101] reflecting similarities between human groups [102]. Since the publication of comparative studies on the craniometrics and genetic variation of different human populations of the world, it is believed that cranial measurements reflect genetic variation and neutral evolution [103,104]. Craniometric variation is thus geographically structured [105] and it is widely used for population history [106] or population affinity analyses [107], even in palaeoanthropological studies [108,109]. Morphological similarity means closer relatedness, which may be caused by common ancestry, gene flow or a combination of factors [110]. However, biological affinity of a cranium separated temporally from the reference population is hard to interpret because, instead of a putative population continuity, it could be a result of selective pressure or genetic drift [103]. To explore possible interpretations of the position of the Zlatý kůň specimen, we need to consider palaeodemographic processes in the Late Glacial period and the sources of their evidence.

The LGM is known to have had a profound effect on the biogeography of many animal and plant species [111,112] as well as on human populations in the Upper Palaeolithic, which resulted in population movements across the continent [3]. Traditionally, the environmental deterioration during the LGM has been linked to an abandonment of Central and Northern Europe. The process of subsequent recolonization has been extensively studied mainly since the radiocarbon technique provided a chronological dating of the localities concerned [22]. Based on these data, a two-phase colonization model for Northern Europe was proposed, with an initial pioneer phase and a later residential phase of settlement, coinciding with the onset of Bølling 13 ky uncal BP [22]. However, this theory was questioned on the basis of data calibration which converts radiocarbon dates to calendar ages [113,114]. Calibrated dates showed that increased human occupation correlates with climatic amelioration but they did not permit the inference about two separate phases [2,113].

Further evidence of the recolonization process in the Late Glacial period is provided by genetic studies of present-day populations. The Franco-Cantabrian refuge was confirmed to be a major source of the European gene pool [115]. The process of recolonization from a refuge is documented by the distribution of mitochondrial haplogroups H and V, which spread throughout Europe during the expansion of humans from the southwest to the northeast in the Late Glacial period [115,116]. However, a contemporary population can only provide information conserved within it and cannot say anything about processes of abandonment or unsuccessful colonization. Such processes can be inferred only from archaeological material, which, however, always provides only partial knowledge and needs to be confronted with various sources of information.

Craniometric data obtained from UP specimens indicate a major shift in cranial variability corresponding to the LGM [27]. The results have been ascribed to neutral demographic processes even though they were mainly influenced by facial measurements (nasal height, nasal width, orbital height and least frontal breadth), which are also highly environmentally plastic [117], and it is therefore possible that a portion of the cranial variation was influenced by the changing climate. The analysis could not tell whether the change occurred already in the refuge or during the recolonization process [27]. Concordant results were obtained from palaeogenetic data [29,30]. The pre-LGM population most probably survived the LGM but was quickly replaced around 14.5 ky cal BP [29]. Finally, the disappearance of certain haplogroups from the European gene pool also points to possible local extinctions [29,30].

Processes of abandonment or unsuccessful colonization were given less attention in the context of Late Glacial biogeography, but they are equally important because they reflect limits and constraints on human adaptation [3]. A growing body of evidence shows that Central Europe was not completely abandoned during the LGM [6,13,118,119]. Human populations were certainly reduced, but they were still possibly present throughout the Pleniglacial [23,120]. New findings from eastern Central Europe point to a possible existence of at least seasonally occupied areas with a milder environment [118,121,122] where some vertebrate species survived, possibly attracting human hunters. This indicates the importance of local microclimatic conditions [118] and suggests that the processes taking place in eastern Central Europe were not necessarily the same as in the more extensively studied western part of Central Europe [3,123]. Following a large-scale synthesis of spatiotemporal processes documented by evidence of raw material gathering, production technologies and calibrated ^{14}C dates, it seems that the eastern and western populations were not completely separated by the LGM. Instead, they maintained contact through the LGM, as supported by similarities between the western Badegoulian and eastern early Epigravettian cultures [4]. The late-glacial recolonization of Central Europe was then realized from two source areas in the west (Franco-Cantabria) and in the east (Carpathian basin), which is described as the so-called bidirectional model [4,124].

Based on this knowledge of population processes, the biological affinity of the Zlatý kůň specimen can be interpreted in several different ways. Given the complexity of population processes and new evidence of a certain continuity of settlement in Central Europe, the biological affinity of the Zlatý kůň cranium may reflect actual population affinity to the pre-LGM population sample. This would be supported by the fact that the main variables separating the pre- and post-LGM samples are not located in the facial skeleton, which is more sensitive to selective pressure [117]. Secondly, migration from a refuge into a new region with a different kind of selective pressure could have led to this phenotype. The majority of Central European specimens from the pre-LGM period (Dolní Věstonice, Předmostí and Mladeč) are also very close to the Zlatý kůň skull, which supports both interpretations. However, other post-LGM specimens from Central Europe (of which there are very few) are located well within the post-LGM

population (Fig 8), which does not lend support to the idea of a selective pressure leading to the same phenotype. Although Brewster et al. [27] showed that the LGM had a disruptive effect on craniometric variation even in specimens from a common region, they did not test for geographic differences due to the dispersed nature of the data. Finally, the position of Zlatý kůň within the range of craniometric variation could be caused simply by genetic drift, which plays an important role especially in small populations. That is probably not far from the post-glacial reality.

We offer possible interpretations based on two assumptions: (1) Cranial variation reflects biological similarity; and (2) Zlatý kůň has been dated to ca 15.4 ky cal BP. Although the Zlatý kůň cranium is referred to as a Magdalenian specimen, the associated artefacts do not show any strong cultural diagnostic features. In addition, the radiocarbon dating was performed on a fragment 'most probably from the cranial base of the buried individual' [21]. The choice of the dated material is thus archaeologically suspect [22]. On the other hand, it is still the only evidence of the age of the Zlatý kůň specimen which is supported by the presence of reliably dated Magdalenian sites in the close proximity of the Zlatý kůň site and by the absence of any important Early Upper Palaeolithic site in the whole of the Bohemian Karst [21]. The results obtained by our craniometric analysis possibly reflect Late Glacial processes only discernible from archaeological material. However, in the case of Zlatý kůň, we cannot rule out the possibility that the results indicate a real population affinity.

5.4 Future research directions

Our virtual reconstruction of the Zlatý kůň cranium allowed us to scrutinize the previous sex attribution and to explore its biological affinity. The estimation of the sex of an individual from the skull is strongly population-specific. As we discuss in the previous section, the population affinity of the Zlatý kůň individual should be tested further using other methods. A repeated, reliable dating of the fossil, properly performed in all aspects of the radiocarbon technique, will be key [22]. Next, a genetic analysis could provide a reliable sex determination. And last but not least, genetic and isotopic analyses could contribute to the mosaic of information about population processes in the Upper Palaeolithic [125].

6 Conclusion

The present study reports on a virtual reconstruction of the incomplete cranium from the Zlatý kůň site in the Bohemian Karst, Czech Republic. The reconstruction allowed us to acquire important cranial measurements and explore the sex attribution and morphological affinity of the specimen. The sex of the individual could not be reliably assessed using visual methods, as those have been developed on a human recent population sample. A metric approach based on reliably sexed Upper Palaeolithic specimens confirmed the previously suggested female sex of the individual with high probability. However, the small size of the reference sample should be kept in mind.

Despite the shift in craniometric variation caused by the Last Glacial Maximum, Zlatý kůň exhibits morphological affinity with the pre-LGM population. This can be explained by various phenomena arising from the complex population history in the Late Glacial period. However, a new dating would allow us to verify the chronological attribution of the fossil. If the Zlatý kůň specimen is really from the Late Glacial period, further investigations and analyses of ancient DNA could contribute to the mosaic of information about population processes in Central Europe.

Supporting information

S1 Table. List of landmarks.

(PDF)

S2 Table. List of anatomical landmarks and semilandmarks used in different steps of reconstruction.

(PDF)

S3 Table. Upper Paleolithic comparative sample.

(PDF)

S4 Table. Descriptive statistics of cranial measurements for UP sample with values for Zlatý kůň.

(PDF)

S1 File. Video illustration of the skull reconstruction.

(AVI)

S2 File. Supplementary bibliography.

(PDF)

Acknowledgments

We thank the curator of the National Museum in Prague, Vítězslav Kuželka, for access to the Zlatý kůň fossil. We are grateful to the following institutions, curators and researchers that provided Mathilde Samsel access to their facilities and granted her permission to examine the palaeoanthropological material in their care: Institut de Paléontologie Humaine (H. de Lumley, A. Viallet), Musée d'Archéologie Nationale (C. Schwab), Musée d'art et d'archéologie du Périgord (V. Merlin-Anglade), Musée d'Histoire Naturelle Victor Brun à Montauban, Museo Geologico "G.G. Gemmellaro" di Palermo (C. di Patti), Musée Labenche de la Ville de Brive (L. Michelin), Musée National de Préhistoire (J.-J. Cleyet-Merle), SRA Rhône Alpes & Musat à Saint-Paul-Trois-Châteaux (M. Lert), LVR-LandesMuseum Bonn (R.W. Schmitz) and J.J. Hublin (Department of Human Evolution Max Planck Institute for Evolutionary Anthropology, Leipzig). Further, we thank Dr. Martin Horák from the Department of Radiology of the Na Homolce Hospital in Prague for CT scanning of the Zlatý kůň and Moča skulls, Yann Heuzé from PACEA for 3D reference material and for his help with the software, and Marek Jantač for photography documentation. We also thank Martin Rmoutil from the Faculty of Mathematics and Physics (Charles University) for his mathematical help with R scripting.

Author Contributions

Conceptualization: Rebeka Rmoutilová, Pierre Guyomarc'h, Jaroslav Brůžek.

Formal analysis: Rebeka Rmoutilová, Pierre Guyomarc'h, Frédéric Santos.

Funding acquisition: Rebeka Rmoutilová, Petr Velemínský.

Investigation: Rebeka Rmoutilová, Pierre Guyomarc'h, Mathilde Samsel, Jaroslav Brůžek.

Resources: Petr Velemínský, Alena Šefčáková.

Writing – original draft: Rebeka Rmoutilová, Pierre Guyomarc'h, Mathilde Samsel, Jaroslav Brůžek.

Writing – review & editing: Petr Velemínský, Alena Šefčáková, Frédéric Santos, Bruno Maureille.

References

1. Clark PU, Dyke AS, Shakun JD, Carlson AE, Clark J, Wohlfarth B, et al. The Last Glacial Maximum. *Science*. 2009; 325: 710–714. <https://doi.org/10.1126/science.1172873> PMID: 19661421
2. Blockley SPE, Blockley SM, Donahue RE, Lane CS, Lowe JJ, Pollard AM. The chronology of abrupt climate change and Late Upper Palaeolithic human adaptation in Europe. *Journal of Quaternary Science*. 2006; 21: 575–584. <https://doi.org/10.1002/jqs.1041>
3. Verpoorte A. Limiting factors on early modern human dispersals: The human biogeography of late Pleniglacial Europe. *Quaternary International*. 2009; 201: 77–85. <https://doi.org/10.1016/j.quaint.2008.05.021>
4. Maier A. The Central European Magdalenian. Dordrecht: Springer Netherlands; 2015. <https://doi.org/10.1007/978-94-017-7206-8>
5. Morel P. Une chasse à l'ours brun il y a 12000 ans: nouvelle découverte à la grotte du Bichon (La Chaux-de-Fonds). *Archäologie der Schweiz*. 1993; 16: 110–117.
6. Terberger T, Street M. Hiatus or continuity? New results for the question of pleniglacial settlement in Central Europe. *Antiquity*. 2002; 76: 691–698. <https://doi.org/10.1017/S0003598X00091134>
7. Bronk Ramsey C, Higham TFG, Brock F, Baker D, Ditchfield P. Radiocarbon dates from the Oxford AMS system: Archaeometry datelist 31. *Archaeometry*. 2002; 44: 1–149.
8. Street M. Ein wiedersehen mit dem hund von Bonn-Oberkassel. *Bonner Zoologische Beiträge*. 2002; 50: 269–290.
9. Šefčáková A, Katina S, Mížera I, Halouzka R, Barta P, Thurzo M. A Late Upper Palaeolithic skull from Moča (The Slovak Republic) in the context of Central Europe. *Acta Musei Nationalis Pragae*. 2011; 67: 3–24.
10. Irish JD, Bratlund B, Schild R, Kolstrup E, Królik H, Mańka D, et al. A late Magdalenian perinatal human skeleton from Wilczyce, Poland. *Journal of Human Evolution*. 2008; 55: 736–740. <https://doi.org/10.1016/j.jhevol.2008.03.007> PMID: 18639314
11. Street M, Terberger T, Orschiedt J. A critical review of the German Paleolithic hominin record. *Journal of Human Evolution*. 2006; 51: 551–579. <https://doi.org/10.1016/j.jhevol.2006.04.014> PMID: 17014890
12. Orschiedt J. Secondary burial in the Magdalenian: the Brillenhöhle (Blaubeuren, southwest Germany). *Paléo*. 2002; 14: 241–256.
13. Kozłowski SK, Poltowicz-Bobak M, Bobak D, Terberger T. New information from Maszycka Cave and the Late Glacial recolonisation of Central Europe. *Quaternary International*. 2012; 272–273: 288–296. <https://doi.org/10.1016/j.quaint.2012.02.052>
14. Meiklejohn C. A direct date from the Staré Město skeleton (Czech Republic) indicates that the find is medieval. *Mesolithic Miscellany*. 2015; 23: 12–13.
15. Villotte S. *Enthésopathies et activités des Hommes préhistoriques—Recherche méthodologique et application aux fossiles européens du Paléolithique supérieur et du Mésolithique*. Archaeopress: Oxford. 2009.
16. Samsel M, Knüsel CJ, Villotte S. Infracranial variability among the Magdalenian people of southwest-ern France. *American Journal of Physical Anthropology*. 2017; 162: 343.
17. Samsel M. Microévolution et bioarchéologie des groupes humains de la fin du Pléistocène et du début de l'Holocène en Europe occidentale: apports de l'anthropologie biologique aux connaissances sur le Paléolithique final et le Mésolithique. Université de Bordeaux. 2018.
18. Vlček E. Pleistocénní člověk z jeskyně na Zlatém koni u Koněprus. *Anthropozoikum*. 1956; 6: 283–311.
19. Smith FH, Allsworth-Jones P, Boaz NT, Brace CL, Harrold FB, Howells WW, et al. Upper Pleistocene hominid evolution in South-Central Europe: a review of the evidence and analysis of trends (and comments and reply). *Current Anthropology*. 1982; 23: 667–703. <https://doi.org/10.1086/202920>
20. Vlček E. L'homme fossile en Europe Centrale. *L'Anthropologie*. 1991; 95: 409–472.
21. Svoboda JA, van der Plicht J, Kuželka V. Upper Paleolithic and Mesolithic human fossils from Moravia and Bohemia (Czech Republic): some new 14C dates. *Antiquity*. 2002; 76: 957–962. <https://doi.org/10.1017/S0003598X00091754>

22. Housley RA, Gamble C, Street M, Pettitt P. Radiocarbon evidence for the late glacial recolonisation of northern Europe. *Proceedings of the Prehistoric Society*. 1997; 63: 25–54. <https://doi.org/10.1017/S0079497X0000236X>
23. Verpoorte A. Eastern Central Europe during the Pleniglacial. *Antiquity*. Cambridge University Press; 2004; 78: 257–266. <https://doi.org/10.1017/S0003598X0011292X>
24. Straus LG. The Upper Paleolithic of Europe: an overview. *Evolutionary Anthropology*. 1995; 4: 4–16. <https://doi.org/10.1002/evan.1360040103>
25. Holt BM, Formicola V. Hunters of the Ice Age: The biology of Upper Paleolithic people. *Yearbook of Physical Anthropology*. 2008; 51: 70–99. <https://doi.org/10.1002/ajpa.20950> PMID: 19003886
26. Pala M, Olivieri A, Achilli A, Accetturo M, Metspalu E, Reidla M, et al. Mitochondrial DNA signals of Late Glacial recolonization of Europe from Near Eastern refugia. *The American Journal of Human Genetics*. Cell Press; 2012; 90: 915–924. <https://doi.org/10.1016/j.ajhg.2012.04.003> PMID: 22560092
27. Brewster C, Meiklejohn C, von Cramon-Taubadel N, Pinhasi R. Craniometric analysis of European Upper Palaeolithic and Mesolithic samples supports discontinuity at the Last Glacial Maximum. *Nature communications*. Europe PMC Funders; 2014; 5: 4094. <https://doi.org/10.1038/ncomms5094> PMID: 24912847
28. Churchill SE, Formicola V, Holliday TW, Holt B, Schumann B. The Upper Palaeolithic population of Europe in an evolutionary perspective. In: Roebroeks W, Mussi M, Svoboda JA, Fennema K, editors. *Hunters of the Golden Age: The Mid Upper Palaeolithic of Eurasia 30,000–20,000 BP*. Leiden: Faculty of the Archaeology, University of Leiden; 1999. pp. 31–58.
29. Posth C, Renaud G, Mitnik A, Drucker DG, Rougier H, Cupillard C, et al. Pleistocene mitochondrial genomes suggest a single major dispersal of non-africans and a late glacial population turnover in Europe. *Current Biology*. 2016; 26: 827–833. <https://doi.org/10.1016/j.cub.2016.01.037> PMID: 26853362
30. Fu Q, Posth C, Hajdinjak M, Petr M, Mallick S, Fernandes D, et al. The genetic history of Ice Age Europe. *Nature*. Nature Research; 2016; 534: 200–205. <https://doi.org/10.1038/nature17993> PMID: 27135931
31. Kukla J. The report of the result of Zlatý kůň Cave explorations in 1951 made by the Carstive Section of Nature-Science Club in Prague. *Československý Kras*. 1952; 5: 49–68.
32. Zázvorka V. Preliminary report of the find of fossil bones at the Zlatý kůň near Koněprusy (Central Bohemia). *Československý Kras*. 1951; 4: 60–66.
33. Vlček E. Nález pleistocenního člověka v Čechách. *Časopis Českých Lékařů*. 1951; 49: 1457–1462.
34. Vlček E. The Pleistocene man (Zlatý Kůň). *Československý Kras*. 1952; V: 180–191.
35. Prošek F, Stárka V, Hrdlička L, Hokr Z, Ložek V, Dohnal Z. Výzkum jeskyně Zlatého koně u Koněprus: zpráva za I. výzkumné období r. 1951. *Československý Kras*. 1952; 1–2: 161–179.
36. Svoboda JA, Kuželka V, Vlček E. The Koněprusy Caves: depositional context of a human skeleton and the first radiocarbon dating. In: Hašek V, Nekuda R, Unger J, editors. *Ve službách archeologie 4*. Brno: Muzejní a vlastivědná společnost v Brně; 2003. pp. 278–284.
37. Vlček E. Další nálezy pozůstatků pleistocenního člověka na Zlatém koni u Koněprus. *Archeologické rozhledy*. 1957; IX: 305–310.
38. Svoboda JA. The depositional context of the Early Upper Paleolithic human fossils from the Koneprusy (Zlatý kůň) and Mladeč caves, Czech republic. *Journal of Human Evolution*. 2000; 38: 523–536. <https://doi.org/10.1006/jhev.1999.0361> PMID: 10715195
39. Trinkaus E, Lemay M. Occipital bunning among later pleistocene hominids. *American Journal of Physical Anthropology*. Wiley Subscription Services, Inc., A Wiley Company; 1982; 57: 27–35. <https://doi.org/10.1002/ajpa.1330570106> PMID: 6814258
40. Bräuer G, Broeg H, Stringer CB. Earliest Upper Paleolithic crania from Mladeč, Czech Republic, and the question of Neanderthal-modern continuity: metrical evidence from the fronto-facial region. In: Hublin J-J, Harvati K, Harrison T, editors. *Neanderthals Revisited: New Approaches and Perspectives*. Dordrecht: Springer Netherlands; 2006. pp. 269–279. https://doi.org/10.1007/978-1-4020-5121-0_15
41. Wolpoff MH, Frayer DW, Jelínek J. Aurignacian female crania and teeth from the Mladeč caves, Moravia, Czech Republic. In: Teschler-Nicola M, editor. *Early Modern Humans at the Moravian Gate: The Mladeč Caves and their Remains*. Vienna: Springer Vienna; 2006. pp. 273–340. https://doi.org/10.1007/978-3-211-49294-9_10
42. Smith FH, Ranyard GC. Evolution of the supraorbital region in Upper Pleistocene fossil hominids from South-Central Europe. *American Journal of Physical Anthropology*. 1980; 53: 589–610. <https://doi.org/10.1002/ajpa.1330530414>
43. Churchill SE, Smith FH. Makers of the early Aurignacian of Europe. *Yearbook of Physical Anthropology*. 2000; 43: 61–115.

44. Schwartz JH, Tattersall I. The Human Fossil Record, Volume 1: Terminology and Craniodental Morphology of Genus Homo (Europe). John Wiley & Sons; 2002.
45. Svoboda JA, van der Plicht J, Vlček E, Kuželka V. New radiocarbon datings of human fossils from caves and rockshelters in Bohemia (Czech Republic). *Anthropologie*. 2004; XLII: 161–166.
46. Stuiver M, Reimer PJ. Extended 14C data base and revised CALIB 3.0 14C age calibration program. *Radiocarbon*. Cambridge University Press; 1993; 35: 215–230. <https://doi.org/10.1017/S0033822200013904>
47. Conard NJ, Grootes PM, Smith FH. Unexpectedly recent dates for human remains from Vogelherd. *Nature*. 2004; 430: 198–201. <https://doi.org/10.1038/nature02690> PMID: 15241412
48. Smith FH, Trinkaus E, Pettitt PB, Karavanić I, Paunović M. Direct radiocarbon dates for Vindija G1 and Velika Pečina Late Pleistocene hominid remains. *Proceedings of the National Academy of Sciences*. 1999; 96: 12281–12286. <https://doi.org/10.1073/pnas.96.22.12281>
49. Vencl S. Radiocarbon date for Magdalenian from Hostim near Beroun (Bohemia). *Archeologické rozhledy*. 1976; 28: 424.
50. Šída P. Kamenná industrie získaná J. Petrbokem v Děravé jeskyni (K. Ú. Tmaň). *Archeologie ve Střední Čechách*. 2007; 11: 9–17.
51. Lázníčková-Gonyševová M. Art mobilier magdalénien en matières dures animales de Moravie (République tchèque). Aspects technologique et stylistique. *L'Anthropologie*. 2002; 106: 525–564. [https://doi.org/10.1016/S0003-5521\(02\)01125-1](https://doi.org/10.1016/S0003-5521(02)01125-1)
52. Vlček E. Czechoslovakia. In: Oakley K, Campbell BG, Molleson T, editors. *Catalogue of Fossil Hominids Part 2 Europe*. London: British Museum of Natural History; 1971. pp. 47–64.
53. Jelínek J, Orvanová E. Hominid Remains: Czech and Slovak Republics. Orban R, Sema P, editors. Brno: Anthropos Institute; 1999.
54. Brůžek J, Franciscus RG, Novotný V, Trinkaus E. The Assessment of sex. In: Trinkaus E, Svoboda JA, editors. *Early Modern Human Evolution in Central Europe: The People of Dolní Věstonice and Pavlov*. New York: Oxford University Press; 2006. pp. 46–62.
55. Kuželka V. The postcranial skeletal remains of Pleistocene man from Zlatý kůň near Koněprusy (Bohemia). *Anthropologie*. 1997; XXXV: 247–249.
56. Weber G, Bookstein F. *Virtual Anthropology: A Guide to a New Interdisciplinary Field*. Vienna: Springer-Verlag Wien; 2011.
57. Gunz P, Mitteroecker P, Neubauer S, Weber GW, Bookstein FL. Principles for the virtual reconstruction of hominin crania. *Journal of Human Evolution*. 2009; 57: 48–62. <https://doi.org/10.1016/j.jhevol.2009.04.004> PMID: 19482335
58. Benazzi S, Stansfield E, Kullmer O, Fiorenza L, Gruppioni G. Geometric morphometric methods for bone reconstruction: the mandibular condylar process of Pico della Mirandola. *The Anatomical Record*. 2009; 292: 1088–1097. <https://doi.org/10.1002/ar.20933> PMID: 19645014
59. Godinho RM, O'Higgins P. Virtual reconstruction of cranial remains: The H. Heidelbergensis, Kabwe 1 fossil. In: Erickson D, Thompson T, editors. *Human Remains: Another Dimension*. London: Academic Press; 2017. pp. 135–147. <https://doi.org/10.1016/B978-0-12-804602-9.00011-4>
60. Klingenberg CP, McIntyre GS. Geometric morphometric of developmental instability: analyzing patterns of fluctuating asymmetry with Procrustes methods. *Evolution*. 1998; 52: 1363–1375. <https://doi.org/10.1111/j.1558-5646.1998.tb02018.x> PMID: 28565401
61. Ferembach D, Schwidetzky I, Stloukal M. Recommendation for age and sex diagnoses of skeletons. *Journal of Human Evolution*. 1980; 9: 517–549.
62. Walrath DE, Turner P, Brůžek J. Reliability test of the visual assessment of cranial traits for sex determination. *American Journal of Physical Anthropology*. 2004; 125: 132–137. <https://doi.org/10.1002/ajpa.10373> PMID: 15365979
63. Walker PL. Sexing skulls using discriminant function analysis of visually assessed traits. *American Journal of Physical Anthropology*. 2008; 136: 39–50. <https://doi.org/10.1002/ajpa.20776> PMID: 18324631
64. Langley NR, Dudzik B, Cloutier A. A decision tree for nonmetric sex assessment from the skull. *Journal of Forensic Sciences*. 2017; <https://doi.org/10.1111/1556-4029.13534> PMID: 28508544
65. Loth SR, Henneberg M. Mandibular ramus flexure: a new morphologic indicator of sexual dimorphism in the human skeleton. *American Journal of Physical Anthropology*. 1996; 99: 473–485. [https://doi.org/10.1002/\(SICI\)1096-8644\(199603\)99:3<473::AID-AJPA8>3.0.CO;2-X](https://doi.org/10.1002/(SICI)1096-8644(199603)99:3<473::AID-AJPA8>3.0.CO;2-X) PMID: 8850186
66. Coqueugnot H, Tillier A-M, Bruzek J. Mandibular ramus posterior flexure: a sex indicator in Homo sapiens fossil hominids? *International Journal of Osteoarchaeology*. 2000; 10: 426–431.

67. Martin R. *Lehrbuch der Anthropologie in systematischer Darstellung*. Second. Jena: Gustav Fischer; 1928.
68. Bräuer G. Ostéométrie. In: Knussmann R, editor. *Anthropologie Handbuch der vergleichenden Biologie des Menschen Begründet von Rudolf Martin*. Stuttgart: G. Fischer Verlag; 1988. pp. 160–231.
69. Howells W. *Cranial Variation in Man. A Study by Multivariate Analysis of Patterns of Differences among Recent Human Populations*. Papers of the Peabody Museum of Archaeology and Ethnology. Cambridge: Harvard University Press; 1973.
70. Auerbach BM. Howells craniometric database [Internet]. [cited 10 Dec 2017]. <https://web.utk.edu/~auerbach/>
71. Brůžek J. A method for visual determination of sex, using the human hip bone. *American Journal of Physical Anthropology*. 2002; 117: 157–68. <https://doi.org/10.1002/ajpa.10012> PMID: 11815949
72. Brůžek J, Santos F, Dutailly B, Murail P, Cunha E. Validation and reliability of the sex estimation of the human os coxae using freely available DSP2 software for bioarchaeology and forensic anthropology. *American Journal of Physical Anthropology*. 2017; 164: 440–449. <https://doi.org/10.1002/ajpa.23282> PMID: 28714560
73. Villotte S, Henry-Gambier D, Murail P, Brůžek J. Population specific tools for sex diagnosis of Upper Palaeolithic and Mesolithic hominids from Europe. *Paleoanthropology Society Meeting*. Philadelphia; 2007.
74. Josse J, Husson F. missMDA: A package for handling missing values in multivariate data analysis. *Journal of Statistical Software*. 2016; 70: 1–31. <https://doi.org/10.18637/jss.v070.i01>
75. Arbour JH, Brown CM. Incomplete specimens in geometric morphometric analyses. *Methods in Ecology and Evolution*. 2014; 5: 16–26. <https://doi.org/10.1111/2041-210X.12128>
76. Mosimann JE. Size allometry: size and shape variables with characterizations of the lognormal and generalized Gamma distributions. *Journal of the American Statistical Association*. 1970; 65: 930–945. <https://doi.org/10.1080/01621459.1970.10481136>
77. Claude J. Log-shape ratios, Procrustes superimposition, Elliptic Fourier analysis: three worked examples in R. *Hystrix, the Italian Journal of Mammalogy*. 2013; 24: 94–102. <https://doi.org/10.4404/hystrix-24.1-6316>
78. Liaw A, Wiener M. Classification and regression by randomForest. *R News*. 2002; 2/3: 18–22.
79. Dutailly B. TIVMI [Internet]. [cited 10 Feb 2018]. <http://projets.pacea.u-bordeaux.fr/TIVMI/>
80. Dutailly B, Coqueugnot H, Desbarats P, Gueorguieva S, Synave R. 3D surface reconstruction using HMH algorithm. *Proceedings of the IEEE International Conference on Image Processing*. 2009. pp. 2505–2508.
81. Dutailly B. *Plongement de surfaces continues dans des surfaces discrètes épaisses*. Ph.D. Thesis. Université de Bordeaux. 2016.
82. Gunz P, Mitteroecker P, Bookstein F. Semilandmarks in three dimensions. In: Slice DE, editor. *Modern Morphometrics in Physical Anthropology*. New York: Kluwer Academic; 2005. pp. 73–98. https://doi.org/10.1007/0-387-27614-9_3
83. Schlager S. *Morpho: Calculations and Visualisations Related to Geometric Morphometrics*. 2016.
84. Josse J, Husson F. Handling missing values in exploratory multivariate data analysis methods. *Journal de la Société Française de Statistique*. 2012; 153: 79–99.
85. Venables WN, Ripley BD. *Modern applied statistics with S*. Fourth. New York: Springer-Verlag; 2002.
86. Sládek V, Trinkaus E, Šefčáková A, Halouzka R. Morphological affinities of the Šal'a 1 frontal bone. *Journal of Human Evolution*. 2002; 43: 787–815. <https://doi.org/10.1006/jhev.2002.0606> PMID: 12473484
87. Lestrel PE, Wolfe CA, Bodt A. Mandibular shape analysis in fossil hominins: Fourier descriptors in norma lateralis. *Homo*. 2013; 64: 247–272. <https://doi.org/10.1016/j.jchb.2013.05.001> PMID: 23769600
88. Amano H, Kikuchi T, Morita Y, Kondo O, Suzuki H, Ponce de León MS, et al. Virtual reconstruction of the Neanderthal Amud 1 cranium. *American Journal of Physical Anthropology*. 2015; 158: 185–197. <https://doi.org/10.1002/ajpa.22777> PMID: 26249757
89. Amano H, Morita Y, Nagano H, Kondo O, Suzuki H, Nakatsukasa M, et al. Statistical interpolation of missing parts in human crania using regularized multivariate linear regression analysis. In: Akazawa T, Ogiwara N, Tanabe HC, Terashima H, editors. *Dynamics of Learning in Neanderthals and Modern Humans Volume 2: Cognitive and Physical Perspectives*. Tokyo: Springer Japan; 2014. pp. 161–169. https://doi.org/10.1007/978-4-431-54553-8_18
90. Frayer DW. Sexual dimorphism and cultural evolution in the Late Pleistocene and Holocene of Europe. *Journal of Human Evolution*. 1980; 9: 399–415. [https://doi.org/10.1016/0047-2484\(80\)90050-0](https://doi.org/10.1016/0047-2484(80)90050-0)

91. Ruff C. Sexual dimorphism in human lower limb bone structure: relationship to subsistence strategy and sexual division of labor. *Journal of Human Evolution*. 1987; 16: 391–416.
92. Villotte S, Churchill SE, Dutour OJ, Henry-Gambier D. Subsistence activities and the sexual division of labor in the European Upper Paleolithic and Mesolithic: evidence from upper limb enthesopathies. *Journal of Human Evolution*. 2010; 59: 35–43. <https://doi.org/10.1016/j.jhevol.2010.02.001> PMID: 20602985
93. Hansen J, Petersen HC, Frei KM, Courtaud P, Tillier A, Fischer A, et al. The Maglemosian skeleton from Koelbjerg, Denmark revisited: identifying sex and provenance. *Danish Journal of Archaeology*. 2017; 6: 50–66. <https://doi.org/10.1080/21662282.2017.1381418>
94. Lewis CJ, Garvin HM. Reliability of the Walker cranial nonmetric method and implications for sex estimation. *Journal of Forensic Sciences*. 2016; 61: 743–751. <https://doi.org/10.1111/1556-4029.13013> PMID: 27122414
95. Garvin HM, Klaes AR. A validation study of the Langley et al. (2017) decision tree model for sex estimation. *Journal of Forensic Sciences*. 2017; <https://doi.org/10.1111/1556-4029.13688> PMID: 29148064
96. Cieri RL, Churchill SE, Franciscus RG, Tan J, Hare B. Craniofacial feminization, social tolerance, and the origins of behavioral modernity. *Current Anthropology*. 2014; 55: 419–443. <https://doi.org/10.1086/677209>
97. Berg GE. Sex estimation of unknown human skeletal remains. In: Langley NR, Tersigni-Tarrant MA, editors. *Forensic Anthropology: A Comprehensive Introduction*. Second. Boca Raton: CRC Press; 2017. pp. 143–161.
98. Santos F, Guyomarc'h P, Brůžek J. Statistical sex determination from craniometrics: comparison of linear discriminant analysis, logistic regression, and support vector machines. *Forensic Science International*. 2014; 245: 204.e1–204.e8. <https://doi.org/10.1016/j.forsciint.2014.10.010> PMID: 25459272
99. Ubelaker DH, DeGaglia CM. Population variation in skeletal sexual dimorphism. *Forensic Science International*. 2017; 278: 407.e1–407.e7. <https://doi.org/10.1016/J.FORSCIINT.2017.06.012> PMID: 28698063
100. Kranioti EK, García-Donas JG, Almeida Prado PS, Kyriakou XP, Langstaff HC. Sexual dimorphism of the tibia in contemporary Greek-Cypriots and Cretans: forensic applications. *Forensic Science International*. 2017; 271: 129.e1–129.e7. <https://doi.org/10.1016/J.FORSCIINT.2016.11.018> PMID: 27919515
101. Pilloud MA, Hefner JT. *Biological Distance Analysis: Forensic and Bioarchaeological Perspectives*. Amsterdam: Elsevier; 2016.
102. Pietrusewsky M. Biological distance in bioarchaeology and human osteology. In: Smith C, editor. *Encyclopedia of Global Archaeology*. Berlin: Springer-Verlag; 2012. pp. 244–249.
103. Roseman CC, Weaver TD. Multivariate apportionment of global human craniometric diversity. *American Journal of Physical Anthropology*. 2004; 125: 257–263. <https://doi.org/10.1002/ajpa.10424> PMID: 15386236
104. Relethford JH. Understanding human cranial variation in light of modern human origins. In: Smith FH, Ahern JCM, editors. *The Origins of Modern Humans: Biology Reconsidered*. Hoboken: John Wiley & Sons, Inc; 2013. pp. 321–337. <https://doi.org/10.1002/9781118659991.ch9>
105. Howells WW. *Skull Shapes and the Map: Craniometric Analyses in the Dispersion of Modern Homo*. Cambridge, Mass.: Peabody Museum; 1989.
106. von Cramon-Taubadel N. Population biodiversity in global perspective. In: Pilloud MA, Hefner JT, editors. *Biological Distance Analysis*. Amsterdam: Elsevier; 2016. pp. 425–445.
107. Ross AH, Ubelaker DH, Kimmerle EH. Implications of dimorphism, population variation, and secular change in estimating population affinity in the Iberian Peninsula. *Forensic Science International*. 2011; 206: 214.e1–214.e5. <https://doi.org/10.1016/j.forsciint.2011.01.003>
108. Grine FE, Bailey RM, Harvati K, Nathan RP, Morris AG, Henderson GM, et al. Late pleistocene human skull from Hofmeyr, South Africa, and modern human origins. *Science*. 2007; 315: 226–229. <https://doi.org/10.1126/science.1136294> PMID: 17218524
109. D'Amore G, Di Marco S, Tartarelli G, Bigazzi R, Sineo L. Late Pleistocene human evolution in Sicily: comparative morphometric analysis of Grotta di San Teodoro craniofacial remains. *Journal of Human Evolution*. 2009; 56: 537–550. <https://doi.org/10.1016/j.jhevol.2009.02.002> PMID: 19446307
110. Relethford JH. Biological distances and population genetics in bioarchaeology. In: Pilloud MA, Hefner JT, editors. *Biological Distance Analysis: Forensic and Bioarchaeological Perspectives*. Amsterdam: Elsevier; 2016. pp. 23–33. <https://doi.org/10.1016/B978-0-12-801966-5.00002-0>
111. Horáček I, Ložek V, Knitlová M, Juříčková L. Darkness under candlestick: glacial refugia on mountain glaciers. In: Sázelová S, Novák M, Mizerová A, editors. *Forgotten Times and Spaces*. New

- Perspectives in Paleoanthropological, Paleoetnological and Archeological Studies. Brno: Masaryk University; 2015. pp. 363–377.
112. García-Vázquez A, Pinto-Llona AC, Grandal-d'Anglade A. Brown bear (*Ursus arctos* L.) palaeoecology and diet in the Late Pleistocene and Holocene of the NW of the Iberian Peninsula: a study on stable isotopes. *Quaternary International*. Pergamon; in press. <https://doi.org/10.1016/J.QUAINT.2017.08.063>
113. Blockley SPE, Donahue RE, Pollard AM. Radiocarbon calibration and Late Glacial occupation in north-west Europe. *Antiquity*. 2000; 74: 112–121. <https://doi.org/10.1017/S0003598X00066199>
114. Blockley SPE, Housley RA. Calibration commentary. *Radiocarbon*. 2009; 51: 287–290. <https://doi.org/10.1017/S0033822200033828>
115. Achilli A, Rengo C, Magri C, Battaglia V, Olivieri A, Scozzari R, et al. The molecular dissection of mtDNA haplogroup H confirms that the Franco-Cantabrian glacial refuge was a major source for the European gene pool. *The American Journal of Human Genetics*. 2004; 75: 910–918. <https://doi.org/10.1086/425590> PMID: 15382008
116. Torroni A, Bandelt H-J, D'Urbano L, Lahermo P, Moral P, Sellitto D, et al. mtDNA analysis reveals a major Late Paleolithic population expansion from southwestern to northeastern Europe. *The American Journal of Human Genetics*. 1998; 62: 1137–1152. <https://doi.org/10.1086/301822> PMID: 9545392
117. Holló G, Szathmáry L, Marcsik A, Barta Z. Linear measurements of the neurocranium are better indicators of population differences than those of the facial skeleton: comparative study of 1,961 skulls. *Human Biology*. 2010; 82: 29–46. <https://doi.org/10.3378/027.082.0103> PMID: 20504170
118. Nerudová Z, Neruda P. Moravia between Gravettian and Magdalenian. In: Sázalová S, Novák M, Mizerová A, editors. *Forgotten Times and Spaces: New Perspectives in Paleoanthropological, Paleoetnological and Archeological Studies*. Brno: Masaryk University; 2015. pp. 378–394. <https://doi.org/10.5817/CZ.MUNI.M210-7781-2015-28>
119. Street M, Terberger T. The last Pleniglacial and the human settlement of Central Europe: new information from the Rhineland site of Wiesbaden-Igstadt. *Antiquity*. 1999; 73: 259–272. <https://doi.org/10.1017/S0003598X00088232>
120. Svoboda JA, Novák M. Eastern Central Europe after the Upper Pleniglacial: changing points of observation. *Archaisches Korrespondenzblatt*. 2004; 34: 463–477.
121. Musil R. Palaeoenvironment at Gravettian sites in central Europe with emphasis on Moravia (Czech Republic). *Quartär*. 2010; 57: 95–123.
122. Škrdl P, Nejman L, Bartík J, Rychtaříková T, Nikolajev P, Eigner J, et al. Terminal LGM dwelling structure from Mohelno in the Czech-Moravian Highlands. In: Sázalová S, Novák M, Mizerová A, editors. *Forgotten Times and Spaces: New Perspectives in Paleoanthropological, Paleoetnological and Archeological Studies*. Brno: Masaryk University; 2015. pp. 395–409. <https://doi.org/10.5817/CZ.MUNI.M210-7781-2015-29>
123. Wygal BT, Heidenreich SM. Deglaciation and Human Colonization of Northern Europe. *Journal of World Prehistory*. 2014; 27: 111–144. <https://doi.org/10.1007/s10963-014-9075-z>
124. Wiśniewski A, Połtowicz-Bobak M, Bobak D, Jary Z, Moska P. The Epigravettian and the Magdalenian in Poland: new chronological data and an old problem. *Geochronometria*. 2017; 44: 16–29. <https://doi.org/10.1515/geochr-2015-0052>
125. Günther T, Malmström H, Svensson EM, Omrak A, Sánchez-Quinto F, Kılınc GM, et al. Population genomics of Mesolithic Scandinavia: investigating early postglacial migration routes and high-latitude adaptation. *PLOS Biology*. 2018; 16: e2003703. <https://doi.org/10.1371/journal.pbio.2003703> PMID: 29315301

S1 Table
Landmarks used in the reconstruction of Zlatý kůň cranium

S1 Table: List of landmarks

Landmark name	Abbreviation	Definition
Cranium		
Akanthion	ak	Bräuer, 1988
Apertion	apt	Guyomarc'h et al., 2014
Articular eminence	ae	Guyomarc'h, Brůžek, 2010
Asterion	ast	Bräuer, 1988
Basion	ba	Bräuer, 1988
Bregma	br	Bräuer, 1988
Canine alveolare externus	cae	Guyomarc'h, 2011
Ectomolare	ecm	Bräuer, 1988
Frontomolare orbitale	fmo	Bräuer, 1988
Frontomolare temporale	fmt	Bräuer, 1988
Glabella	g	Bräuer, 1988
Glenoidale laterale	gll	The most lateral point of the glenoid fossa.
Inion	i	Bräuer, 1988
Jugale	ju	Bräuer, 1988
Lambda	la	Bräuer, 1988
Lateromastoideale	lm	Guyomarc'h, 2011
Mastoideale	ms	Bräuer, 1988
Nariale	nr	Guyomarc'h, Brůžek, 2010
Nasion	n	Bräuer, 1988
Nasomaxillofrontale	nmf	Guyomarc'h et al., 2014
Nasospinale superius	nss	Bräuer, 1988
Opisthion	o	Bräuer, 1988
Opisthocranion	op	Bräuer, 1988
Orbitale	or	Bräuer, 1988
Porion	po	Bräuer, 1988
Prosthion	pr	Bräuer, 1988
Rhinion	rhi	Bräuer, 1988
Stephanion	st	Bräuer, 1988
Tuber articulare	tua	Guyomarc'h, Brůžek, 2010
Zygomaticofaciale*	zf	The inferior point of the zygomaticofacial foramen.
Zygomaticotemporale*	zt	The inferior point of the zygomaticotemporal foramen.
Zygomaxillare	zm	Guyomarc'h et al., 2014
Zygoorbitale*	zo	Bräuer, 1988
Mandible*		
Genion	Mge	Bräuer, 1988
Gnathion	Mgn	Bräuer, 1988
Infradentale	Mid	Bräuer, 1988
Kondyilion anterius	Mkda	The most anterior point on the condylar process.
Kondyilion laterale	Mkdl	Bräuer, 1988
Kondyilion mediale	Mkdm	Bräuer, 1988
Linguale	Mlin	Bräuer, 1988
Pogonion	Mpg	Bräuer, 1988

* landmarks digitised only on Zlatý kůň (not on the reference sample crania)

S2 Table: List of anatomical landmarks and semilandmarks used in different steps of reconstruction.

Abbreviation	Midplane estimation	Calvarium reconstruction	Right zygomatic reconstruction	Maxilla alignment	Cranium reconstruction
Cranium					
ak					*m
aptL					*
aptR				*	*
aeL					*
aeR			*		*
astL		*m			*
astR					*
ba					*m
br	*	*			*
caeL					*
caeR				*	*
ecmL					*
ecmR				*	*
fmoL		*m			*
fmoR			*		*
fmtL		*m			*
fmtR			*		*
g	*	*			*
gllL		*m			*
gllR					*
i	*	*			*
juL					*
juR			*		*
la	*	*			*
lmL		*m			*
lmR					*
msL		*m			*
msR					*
nrL					*
nrR				*	*
n	*	*			*
nmfL		*m			*
nmfR					*
nss				*	*
o					*m
op	*	*			*
orL					*
orR			*m		*
poL		*m			*
poR					*
pr					*m
rhi					*m
stL		*m			*
stR					*
tuaL		*m			*
tuaR					*

Abbreviation	Midplane estimation	Calvarium reconstruction	Right zygomatic reconstruction	Maxilla alignment	Cranium reconstruction
zfR			*m		
ztR			*		
zmL					*m
zmR					*m
zoR			*m		
Mandible					
Mge	*				
Mgn	*				
Mid	*				
MkdaL		*			
MkdaR		*			
MkdIL		*			
MkdIR		*			
MkdmL		*			
MkdmR		*			
Mlin	*				
Mpg	*				
Total: Anatomical landmarks	cranium 6; mandible 5	22 (10)	8 (3)	5	48 (7)
Total: Curve semilandmarks	0	16 (0)	7 (2)	7	152 (54)
Total: Surface semilandmarks	0	374 (144)	20 (7)	30	358 (104)

Asterisk (*) marks that the landmark was used in the reconstruction step; (m) means that the landmark was missing.

S3 Table: Upper Paleolithic comparative sample

Individual	Abbr.	LGM	Country	Sex	Sex-based	Reference-sex	Reference-cranial measurements
Arene Candide 2	AC2	post	Italy	M	pelvis	Tarsi et al. 2006; Villotte 2009	Paoli et al. 1980; Sergi et al. 1974
Arene Candide 3	AC3	post	Italy	M	pelvis	Tarsi et al. 2006; Villotte 2009	Paoli et al. 1980; Sergi et al. 1974
Arene Candide 4	AC4	post	Italy	M	pelvis	Tarsi et al. 2006; Villotte 2009	Paoli et al. 1980; Sergi et al. 1974
Arene Candide 5	AC5	post	Italy	M	pelvis	Tarsi et al. 2006; Villotte 2009	Paoli et al. 1980; Sergi et al. 1974
Baoussou da Torre 2	BT2	pre	Italy	M	pelvis	Villotte et al. 2017	Villotte et al. 2017
Barma del Caviglione 1	BC1	pre	Italy	F	pelvis	de Lumley et al. 2016	de Lumley et al. 2016; Guipert et al. 2014
Barma Grande 1	BG1	pre	Italy	M	pelvis	de Lumley et al. 2016; Villotte et al. 2011	De Lumley et al. 2016; Graziosi 1942
Barma Grande 5	BG5	pre	Italy	M	pelvis	de Lumley et al. 2016; Villotte et al. 2011	De Lumley et al. 2016; Graziosi 1942
Brno 2	B2	pre	Czech	I	?	Matiegka 1934 (M)	Matiegka 1934; Coppola 2013
Brno 3	B3	pre	Czech	I	?	Matiegka 1934 (F)	Matiegka 1934; Coppola 2013
Cap Blanc	CB	post	France	I	skull/PC	von Bonin 1935 (F)/Villotte et al. 2015 (F)	von Bonin 1935
Cro-Magnon 1	CM1	pre	France	M	pelvis	Gambier et al. 2006	Vallois, Billy 1965
Cro-Magnon 2	CM2	pre	France	I	pelvis	Gambier et al. 2006 (I)	Vallois, Billy 1965
Cro-Magnon 3	CM3	pre	France	I	pelvis	Gambier et al. 2006 (I)	Vallois, Billy 1965
Cussac L2A	L2A	pre	France	M	pelvis,skull	Villotte et al. 2015; Guyomarc'h et al. 2017	Guyomarc'h et al. 2017
Dolní Věstonice 13	DV13	pre	Czech	M	pelvis, DNA	Trinkaus and Svoboda 2006; Fu et al. 2016; Mittnik et al. 2016	Sládek et al. 2000
Dolní Věstonice 14	DV14	pre	Czech	M	pelvis, DNA	Trinkaus and Svoboda 2006; Fu et al. 2016; Mittnik et al. 2016	Sládek et al. 2000
Dolní Věstonice 15	DV15	pre	Czech	M	pelvis, DNA	Trinkaus and Svoboda 2006; Fu et al. 2016; Mittnik et al. 2016	Sládek et al. 2000
Dolní Věstonice 16	DV16	pre	Czech	M	pelvis, DNA	Trinkaus and Svoboda 2006; Fu et al. 2016	Sládek et al. 2000
Dolní Věstonice 3	DV3	pre	Czech	F	pelvis	Trinkaus and Svoboda 2006	Sládek et al. 2000; Manolis et al. 1996; Jelínek 1964

Individual	Abbr.	LGM	Country	Sex	Sex-based	Reference-sex	Reference-cranial measurements
Grotte des Enfants 4	GE4	pre	Italy	M	pelvis, skull	Villotte 2009	Verneau 1902; Henke 1989
Grotte des Enfants 5	GE5	pre	Italy	F	pelvis	Villotte 2009	Verneau 1902; Coppola 2013
Chancelade	C	post	France	I	PC	Villotte 2009 (F)	pers.obs.
Iboussiere A	IA	post	France	M	pelvis	pers.obs.	pers.obs.
Kostenki 1	K1	post	Russia	I	-	-	Henke 1989
Kostenki Markina Gora 14	K14	pre	Russia	I	pelvis,skull	Rogachev 1957 (M); Howells 1973, https://web.utk.edu/~auerbach/ (F)	Jelínek 1964; Henke 1989; Howells, 1973, https://web.utk.edu/~auerbach/
Lafaye 1	L1	post	France	F	pelvis	Villotte 2009	pers.obs.
Laugerie-Basse 4	LB4	post	France	M	pelvis	Villotte 2009	pers.obs.
Le Bichon	B	post	Switzerland	M	pelvis	Villotte 2009	Chauviere 2008
Le Peyrat 5	LP5	post	France	M	pelvis	Samsel et al. 2016	Samsel et al. 2016
Maritza 2	MA	post	Italy	I	PC	Villotte 2009	Henke 1989; Borgognini-Tarli 1972
Mladec 1	M1	pre	Czech	I	skull	Szombathy 1925 (M); Wolpoff 2006 (F)	Wolpoff 2006; Matiegka 1934
Mladec 2	M2	pre	Czech	I	skull	Henke 1989 (F); Wolpoff 2006 (F)	Wolpoff 2006; Henke 1989; Mallegni et al. 1999
Mladec 5	M5	pre	Czech	I	skull	Frayet et al. 2006 (M)	Frayet et al. 2006
Mladec 6	M6	pre	Czech	I	skull	Frayet et al. 2006 (M)	Frayet et al. 2006
Moca	M	post	Slovakia	I	skull	Šefčáková et al. 2011 (F)	Šefčáková et al. 2011
Oberkassel 1	OK1	post	Germany	M	pelvis	Trinkaus 2015	pers.obs.; Bonnet 1919
Oberkassel 2	OK2	post	Germany	F	pelvis	Trinkaus 2015	pers.obs.; Bonnet 1919
Ortucchio1	OR1	post	Italy	I	-	-	Henke 1989; Parenti 1960
Ostuni 1	O1	pre	Italy	F	pelvis, DNA	Villotte 2009; Fu et al. 2016	Coppola 2013
Paglicci 25	PG25	pre	Italy	F	pelvis	Villotte 2009	Mallegni et al. 1999
Pataud 1	PA1	pre	France	F	pelvis	Villotte et al. 2015	Billy 1975
Pavlov 1	PV1	pre	Czech	M	pelvis, DNA	Trinkaus and Svoboda 2006; Fu et al. 2016	Sládek et al. 2000
Pestera cu Oase 2	PO2	pre	Romania	I	-	-	Crevecoeur et al. 2009; Trinkaus et al. 2003
Pestera Muierii 1	PM	pre	Romania	I	skull	Dobos et al. 2010 (I)	Dobos et al. 2010
Predmosti 1	P1	pre	Czech	I	skull	Matiegka 1934 (M)	Matiegka 1934
Predmosti 10	P10	pre	Czech	I	skull	Matiegka 1934 (F)	Matiegka 1934; Velemínská, Brůžek 2008

Individual	Abbr.	LGM	Country	Sex	Sex-based	Reference-sex	Reference-cranial measurements
Predmosti 3	P3	pre	Czech	I	skull	Matiegka 1934 (M)	Matiegka 1934; Manolis et al. 1996
Predmosti 4	P4	pre	Czech	I	skull	Matiegka 1934 (F)	Matiegka 1934; Velemínská, Brůžek 2008
Predmosti 9	P9	pre	Czech	I	skull	Matiegka 1934 (M)	Matiegka 1934; Manolis et al. 1996
Rochereil 1	RC1	post	France	I	skull	Ferembach 1974 (M)	pers.obs.
Romito 1	R1	post	Italy	F	second. diag.	Villotte 2009; Villotte et al. 2015	Mallegni,Fabbri 1995
Romito 3	R3	post	Italy	M	pelvis	Villotte 2009	Mallegni,Fabbri 1995
Romito 4	R4	post	Italy	M	second. diag.	Villotte 2009; Villotte et al. 2015	Mallegni,Fabbri 1995
Romito 5	R5	post	Italy	F	second. diag.	Villotte et al. 2015	Mallegni,Fabbri 1995
Romito 6	R6	post	Italy	F	pelvis	Villotte 2009	Mallegni,Fabbri 1995
San Teodoro 1	ST1	post	Italy	F	pelvis	Villotte 2009	pers.obs.
San Teodoro 2	ST2	post	Italy	I	skull	D'Amore et al. 2009 (M)	Henke 1989; Parenti 1960
San Teodoro 3	ST3	post	Italy	I	pelvis,second. diag./skull	Villotte 2009 (I)/D'Amore et al. 2009 (M)	Graziosi 1947
San Teodoro 5	ST5	post	Italy	I	pelvis,PC/ skull	Villotte 2009 (I)/D'Amore et al. 2009 (M)	Graziosi 1947; Henke 1989
San Teodoro 6	ST6	post	Italy	I	skull	D'Amore et al. 2009 (F)	Graziosi 1947
San Teodoro 7	ST7	post	Italy	I	skull	D'Amore et al. 2009 (M)	Graziosi 1947
St Germain la Riviere	SG1	post	France	F	pelvis	Henry-Gambier et al. 2002	pers.obs.
Sunghir 1	S1	pre	Russia	M	pelvis/DNA	Trinkaus et al. 2014; Villotte 2009/Poltoraus et al. 2000	Trinkaus et al. 2014
Sunghir 5	S5	pre	Russia	I	skull	Trinkaus et al. 2014 (I)	Trinkaus et al. 2014
Vado all Arancio 1	VA1	post	Italy	M	pelvis	Villotte 2009	Pardini et al. 1981
Villabruna 1	V1	post	Italy	M	pelvis, DNA	Vercellotti et al. 2008; Villotte 2009; Fu et al. 2016	Vercellotti et al. 2008
Zlatý kůň	ZK	post	Czech	I	skull	VIček 1991 (F)	pers.obs.

Abbr. = specimen acronym; LGM: chronology regarding the LGM; Sex (F = female, M = male, I = unknown); Sex-based: sexual diagnosis type.

S4 Table:
Descriptive statistics of cranial measurements following Martin (1928) and Bräuer (1988) for UP sample with values for Zlatý kůň

Variable	N (F)	N (M)	Mean (F)	SD (F)	Mean (M)	SD (M)	N (pre-LGM)	N (post-LGM)	Mean (pre-LGM)	SD (pre-LGM)	Mean (post-LGM)	SD (post-LGM)	Min	Max	Zlatý kůň
M1	13	24	187.0	7.2	193.5	6.5	35	29	193.0	7.6	189.1	6.9	177.0	205.6	197.7
M5	11	18	100.4	5.6	102.1	14.2	19	24	105.6	13.6	100.3	6.7	87.0	151.0	99.2
M8	13	24	136.0	4.1	140.6	4.7	35	29	140.0	8.1	138.8	4.5	127.0	166.5	137.2
M9	13	23	94.5	4.8	99.0	5.1	33	30	99.9	4.7	95.3	4.3	83.5	112.0	97.2
M10	13	21	115.2	5.2	119.5	6.1	34	27	120.8	5.9	115.0	5.0	104.0	136.9	122.9
M17	12	17	132.8	5.0	134.4	5.6	21	28	133.3	3.3	136.2	6.8	125.0	149.0	128.5
M20	12	19	114.4	4.0	116.6	7.2	27	24	116.3	7.3	114.4	6.6	100.0	136.0	109.5
M23	13	15	521.2	14.7	550.6	17.7	23	25	533.5	19.4	535.7	21.6	496.0	590.0	566.3
M26	10	22	129.8	3.4	135.8	6.8	34	20	133.6	7.9	132.2	8.3	116.0	154.0	140.0
M27	10	21	134.5	8.9	133.4	8.9	35	20	131.4	7.0	135.1	8.8	117.0	159.0	124.8
M28	8	16	121.3	10.6	121.3	7.3	25	19	121.4	6.6	118.5	10.5	105.0	143.0	125.9
M40	7	17	97.7	8.6	97.0	7.3	14	22	101.7	6.5	95.4	6.6	85.0	110.0	96.3
M45	12	17	129.6	5.2	141.9	8.2	22	24	135.2	8.4	137.9	8.4	119.2	155.0	125.1
M48	11	21	64.5	2.0	67.9	3.8	27	27	66.9	4.2	66.4	4.5	58.0	78.0	61.8
M51	11	22	39.7	1.6	43.0	3.2	28	26	41.9	2.4	41.6	3.4	37.0	49.0	43.1
M52	12	23	29.5	2.5	30.0	2.4	29	28	29.9	2.5	30.2	2.4	26.0	37.0	30.0
M54	12	20	24.5	2.0	25.4	2.6	29	26	26.3	1.8	23.9	2.0	20.0	30.0	25.1
M55	12	21	48.5	3.0	50.9	3.6	26	27	51.2	4.0	49.3	3.7	43.0	60.0	43.5
M61	11	18	61.7	4.7	63.8	3.4	25	20	63.5	4.9	62.5	4.5	50.0	72.2	62.0
M63	9	16	36.6	4.0	37.8	2.4	16	19	37.8	4.1	38.0	3.0	32.0	48.0	39.2

S1 File. Video illustration of the skull reconstruction. <https://doi.org/10.1371/journal.pone.0201431.s005>

S2 File. Supplementary bibliography.

- Auerbach BM. Howells database online. <https://web.utk.edu/~auerbach/> (F).
- Billy G. 1975. Etude anthropologique des restes humains de l'Abri Pataud. In: Movius HL, editor. Excavation of the Abri Pataud. Les Eyzies (Dordogne). Cambridge: Harvard University, Peabody Museum, American School of Prehistoric Research. p 201–261.
- Bonnet R. 1919. Der diluviale Menschenfund von Oberkassel bei Bonn. In: Verworn M, Bonnet R, Steinmann G, editors. Die Skelet. Weisbaden: Verlag von JF Bergmann. p 11–185.
- Borgognini-Tarli SM. 1972. Etude anthropologique d'un squelette mésolithique provenant de la grotte Maritza (Avezzano, Abruzzo). In: Etudes sur le quaternaire dans le monde : Union Internationale pour l'étude du Quaternaire, VIIIe Congrès INQUA, Paris. p 1005–1011.
- Bräuer G. 1988. Ostéométrie. In: Knussmann R, editor. Anthropologie. Handbuch der vergleichenden Biologie des Menschen. Begründet von Rudolf Martin. Stuttgart: G. Fischer Verlag. p 160–231.
- Coppola D. 2013. Il Riparo di Agnano nel Paleolitico superiore - La sepoltura Ostuni 1 ed i suoi simboli.
- Crevecoeur I, Rougier H, Grine F, Froment A. 2009. Modern human cranial diversity in the late pleistocene of Africa and Eurasia: Evidence from Nazlet Khater, Peștera cu Oase, and Hofmeyr. *Am J Phys Anthropol* 140:347–358.
- D'Amore G, Di Marco S, Tartarelli G, Bigazzi R, Sineo L. 2009. Late Pleistocene human evolution in Sicily: comparative morphometric analysis of Grotta di San Teodoro craniofacial remains. *J Hum Evol* 56:537–550.
- De Lumley H. 2016. La Grotte du Cavillon Sous la falaise des Baousse Rousse, Grimaldi, Vintimille, Italie. Paris: CNRS éditions.
- Dobos A, Soficaru A, Trinkaus E. 2010. The Prehistory and Paleontology of the Peștera Muierii (Romania). Liège: ERAUL 124.
- Ferembach D. 1974. Les hommes de l'Épipaléolithique et du Mésolithique de la France et du Nord-Ouest du Bassin méditerranéen. *Bull Mem Soc Anthropol Paris* 2:201–236.
- Freyer D, Jelínek J, Oliva M, Wolpoff M. 2006. Aurignacian male crania, jaws and teeth from the Mladeč caves, Moravia, Czech Republic. In: Teschler-Nicola M, editor. Early Modern Humans at the Moravian Gate: The Mladeč Caves and their Remains. Vienna: Springer. p 185–272.
- Fu Q, Posth C, Hajdinjak M, Petr M, Mallick S, Fernandes D, Furtwängler A, Haak W, Meyer M, Mittnik A, Nickel B, Peltzer A, Rohland N, Slon V, Talamo S, Lazaridis I, Lipson M, Mathieson I, Schiffels S, Skoglund P, Derevianko AP, Drozdov N, Slavinsky V, Tsybankov A, Cremonesi RG, Mallegni F, Gély B, Vacca E, Morales MRG, Straus LG, Neugebauer-Maresch C, Teschler-Nicola M, Constantin S, Moldovan OT, Benazzi S, Peresani M, Coppola D, Lari M, Ricci S, Ronchitelli A, Valentin F, Thevenet C,

- Wehrberger K, Grigorescu D, Rougier H, Crevecoeur I, Flas D, Semal P, Mannino MA, Cupillard C, Bocherens H, Conard NJ, Harvati K, Moiseyev V, Drucker DG, Svoboda J, Richards MP, Caramelli D, Pinhasi R, Kelso J, Patterson N, Krause J, Pääbo S, Reich D. 2016. The genetic history of Ice Age Europe. *Nature* 534:200–205.
- Gambier D, Bruzek J, Schmitt A, Houët F, Murail P. 2006. Révision du sexe et de l'âge au décès des fossiles de Cro-Magnon (Dordogne, France) à partir de l'os coxal. *Comptes Rendus Palevol* 5:735–741.
- Graziosi P. 1942. L'uomo fossile della Barma Grande ai Balzi Rossi nel Museo di Mentone. *Arch per l'Antropologia e l'Etnologia* 72:22–51.
- Graziosi P. 1947. Gli uomini paleolitici della Grotta di San Teodoro (Messina). *Riv di Sci Preist* 2:123–233.
- Guipert G, de Lumley H, de Lumley M-A. 2014. Reconstruction du crâne Barma del Cavaglione 1 (Dame du Cavillon), Baoussé-Roussé, Grottes de Grimaldi Gaspard. *Ann dell'Università di Ferrara* 10:239–244.
- Guyomarc'h P, Bruzek J. 2010. Dimorphisme sexuel du crâne de sujets identifiés (collection Olivier, MNHN, Paris): Évaluation par morphométrie géométrique. *Bull Mem Soc Anthropol Paris* 22:216–229.
- Guyomarc'h P. 2011. Reconstitution Faciale par Imagerie 3D : Variabilité morphométrique et mise en oeuvre informatique.
- Guyomarc'h P, Dutailly B, Charton J, Santos F, Desbarats P, Coqueugniot H. 2014. Anthropological facial approximation in three dimensions (AFA3D): computer-assisted estimation of the facial morphology using geometric morphometrics. *J Forensic Sci* 59:1502–1516.
- Guyomarc'h P, Samsel M, Courtaud P, Mora P, Dutailly B, Villotte S. 2017. New data on the paleobiology of the Gravettian individual L2A from Cussac cave (Dordogne, France) through a virtual approach. *J Archaeol Sci Reports* 14:365–373.
- Henke W. 1989. Jungpaläolithiker und mesolithiker Beiträge zur Anthropologie.
- Henry-Gambier D, Bruzek J, Murail P, Houët F. 2002. Révision du sexe du squelette magdalénien de Saint-Germain-la-Rivière (Gironde, France). *Paléo* 14:205–212.
- Howells W. 1973. *Cranial Variation in Man. A Study by Multivariate Analysis of Patterns of Differences among Recent Human Populations*. Cambridge: Harvard University Press.
- Chauvière F-X. 2008. La grotte du Bichon: un site préhistorique des montagnes neuchâteloises. Neuchâtel Off musée Cant d'archéologie Neuchâtel.
- Jelínek J. 1964. Betrachtungen über die Verwandtschaft der anthropologischen Funde Dolni Vestonice, Abri Pataud und Markina Gora.

- Mallegni F, Bertoldi F, Manolis SK. 1999. The Gravettian female human skeleton from Grotta Paglicci, south Italy. *Homo* 50:127–148.
- Mallegni F, Fabbri PF. 1995. The human skeletal remains from the upper palaeolithic burials found in Romito cave (Papasidero, Cosenza, Italy). *Bull Mem Soc Anthropol Paris* 7:99–137.
- Manolis SK, Mallegni F. 1996. The Gravettian fossil hominids of Italy. *Anthropologie* 34:99–108.
- Matiegka J. 1934. *Homo předměstensis*, fosilný člověk z Předmostí na Moravě.
- Mittnik A, Wang C-C, Svoboda J, Krause J. 2016. A molecular approach to the sexing of the triple burial at the Upper Paleolithic site of Dolní Věstonice. *PLoS One* 11:e0163019.
- Paoli G, Parenti R, Sergi S. 1980. Gli scheletri mesolitici della caverna delle Arene Candide (Liguria). *Mem dell'Istituto Ital di Paleontol Um Roma* 3:33–154.
- Pardini E, Lombardi Pardini EC. 1981. I Paleolitici di Vado all'Arancio (Grosseto). *Arch per l'Antropologia e la Etnol Firenze* 61:75–119.
- Parenti R. 1960. Calvario cromagnonoide trovato in un deposito mesolitico del bacino fucense (Abruzzo). *Arch per l'Antropologia e l'Etnologia* 90:5–92.
- Poltoraus AB, Kulikov EE, Lebedeva IA. 2000. The molecular analysis of DNA from the remains of three individuals from the Sunghir site (preliminary data). In: Alexeeva TI, Bader N., Munchaev RM, Buzhilova A., Kozlovskaya MV, Mednikova M., editors. *Homo Sungirensis, Upper Palaeolithic Man: Ecological and Evolutionary Aspects of the Investigation*. Moscow: Scientific World. p 302–314.
- Rogachev A. 1957. *Mnogoslounye stoyanki Kostenkovsko-Borshevskogo raiona na Donu i problema razvitiya kul'tury v epokhy verkhnego paleolita na Russkoi Ravnine*. *Mater I Issled Po Arkheologii, SSSR* 59:9–134.</p>
<div data-bbox="124 638 790 683" data-label="Text">
<p>Samsel M, Knüsel CJ, Villotte S. 2016. Réévaluation du sexe et de l'âge au décès du sujet azilien Le Peyrat 5, Saint-Rabier (Dordogne, France). *Bull Mem Soc Anthropol Paris* 28:213–220.</p>
</div>
<div data-bbox="124 697 794 728" data-label="Text">
<p>Sergi S, Parenti R, Paoli G. 1974. Il giovane paleolitico della caverna delle Arene Candide. *Mem dell'Istituto Ital di Paleontol Um* 2:13–38.</p>
</div>
<div data-bbox="124 742 820 788" data-label="Text">
<p>Sládek V, Trinkaus E, Hillson S, Holliday T. 2000. The People of the Pavlovian. *Skeletal Catalogue and Osteometrics of the Gravettian Fossil Hominids from Dolni Vestonice and Pavlov*. Brno: Academy of Sciences of the Czech Republic, Institute of Archaeology.</p>
</div>
<div data-bbox="124 802 820 832" data-label="Text">
<p>Szombathy J. 1925. Die diluvialen Menschenreste aus der Fürst-Johanns-Höhle bei Lautsch in Mähren. *Die Eiszeit* 2:1-34-95.</p>
</div>
</div>
<div data-bbox="467 921 503 938" data-label="Page-Footer">
<p>146</p>
</div>

- Šefčáková A, Katina S, Mizera I, Halouzka R, Barta P, Thurzo M. 2011. A Late Upper Palaeolithic skull from Moča (The Slovak Republic) in the context of Central Europe. *Acta Musei Natl Pragae* 67:3–24.
- Tarsi T, Noto F, Martínez-Labarga C, Giampaolo R, Babalini C, Scano G, Contini I, Lorente JA, Lorente M, Pacciani E, Silvestrini M, Del Lucchese A, Maggi R, Lattanzi E, Formicola V, Mallegni F, Martini F, Rickards O. 2006. Ricostruzione della storia genetica per via materna delle comunità paleolitiche dei Balzi Rossi, delle Arene Candide e del Romito, e di quelle neolitiche ed eneolitiche di Samari e di Fontenoce di Recanatì. In: Martini AF, editor. *La cultura del morire nelle società preistoriche e protostoriche italiane dal paleolitico all'età del rame, origines, progetti, III*. Firenze: Istituto Italiano di Preistoria e Proistoria. p 315–346.
- Trinkaus E, Svoboda J. 2006. Early Modern Human Evolution in Central Europe: the People of Dolní Věstonice and Pavlov.
- Trinkaus E. 2015. The appendicular skeletal remains of Oberkassel 1 and 2. In: Giemsch L, Schmitz RW, editors. *The Late Glacial Burial from Oberkassel Revisited*. Darmstadt: Verlag Philipp von Zabern. p 75–132.
- Trinkaus E, Milota Š, Rodrigo R, Mircea G, Moldovan O. 2003. Early modern human cranial remains from the Peștera cu Oase, Romania. *J Hum Evol* 45:245–253.
- Trinkaus ME, Buzhilova PA, Mednikova BM, Dobrovolskaya VM. 2014. *The People of Sunghir: Burials, Bodies and Behavior in the Earlier Upper Paleolithic*. New York: Oxford University Press.
- Vallois H, Billy G. 1965. Nouvelles recherches sur les hommes fossiles de l'abri de Cro-Magnon. *Anthropologie* 69:47–74.
- Velemínská J, Brůžek J, Velemínský P, Bigoni L, Šefčáková A, Katina S. 2008. Variability of the Upper Palaeolithic skulls from Předmostí near Přerov (Czech Republic): Craniometric comparison with recent human standards. *HOMO- J Comp Hum Biol* 59:1–26.
- Vercellotti G, Alclati G, Richards MP, Formicola V. 2008. The Late Upper Paleolithic skeleton Villabruna 1 (Italy): A source of data on biology and behavior of a 14.000 year-old hunter. *J Anthropol Sci* 86:143–163.
- Verneau R. 1902. Les fouilles du prince de Monaco aux Baoussé-Roussé. Un nouveau type humain. *Anthropologie* 13:561–585.
- Villotte S. 2009. *Enthésopathies et activités des Hommes préhistoriques - Recherche méthodologique et application aux fossiles européens du Paléolithique supérieur et du Mésolithique*.
- Villotte S, Brůžek J, Henry-Gambier D. 2011. Révision de l'âge au décès et du sexe des sujets adultes gravettiens. *Mémoire LII la Société préhistorique française*:209–216.

- Villotte S, Churchill SE, Dutour OJ, Henry-Gambier D. 2010. Subsistence activities and the sexual division of labor in the European Upper Paleolithic and Mesolithic: Evidence from upper limb enthesopathies. *J Hum Evol* 59:35–43.
- Villotte S, Samsel M, Sparacello V. 2017. The paleobiology of two adult skeletons from Baouso da Torre (Bausu da Ture) (Liguria, Italy): Implications for Gravettian lifestyle. *Comptes Rendus Palevol* 16:462–473.
- Villotte S, Santos F, Courtaud P. 2015. Brief communication: In situ study of the Gravettian individual from Cussac cave, locus 2 (Dordogne, France). *Am J Phys Anthropol* 158:759–768.
- Vlček E. 1991. L'homme fossile en Europe centrale. *Anthropologie* 95:409–472.
- von Bonin G. 1935. The Magdalenian skeleton from Cap-Blanc in the Field Museum of Natural History. Urbana: University of Illinois.
- Wolpoff MH, Frayer DW, Jelinek J. 2006. Aurignacian female crania and teeth from the Mladeč caves, Moravia, Czech Republic. In: Teschler-Nicola M, editor. *Early Modern Humans at the Moravian Gate: The Mladeč Caves and their Remains*. Vienna: Springer Vienna. p 273–340.

A case of marked bilateral asymmetry in the sacral alae of the Neandertal specimen Regourdou 1 (Périgord, France)

Rebeka Rmoutilová^{1,2} | Asier Gómez-Olivencia^{3,4,5} | Jaroslav Brůžek^{1,2} |
Trenton Holliday^{6,7} | Ronan Ledevin¹ | Christine Couture-Veschambre¹ |
Stéphane Madelaine^{8,1} | Valér Džupa⁹ | Jana Velemínská² | Bruno Maureille¹

¹CNRS, Université de Bordeaux, MCC, UMR5199 PACEA, Université de Bordeaux, Pessac Cedex, France

²Department of Anthropology and Human Genetics, Faculty of Science, Charles University, Prague, Czech Republic

³Departamento Estratigrafía y Paleontología, Facultad de Ciencia y Tecnología, Universidad del País Vasco/Euskal Herriko Unibertsitatea (UPV/EHU), Leioa, Spain

⁴IKERBASQUE. Basque Foundation for Science, Bilbao, Spain

⁵Centro UCM-ISCIII de Investigación sobre Evolución y Comportamiento Humanos, Madrid, Spain

⁶Department of Anthropology, Tulane University, New Orleans, Louisiana

⁷Evolutionary Studies Institute, University of the Witwatersrand, Johannesburg, Republic of South Africa

⁸Musée National de Préhistoire, Les Eyzies-de-Tayac, France

⁹Department of Orthopaedics and Traumatology, Third Faculty of Medicine, Charles University, and University Hospital Královské Vinohrady, Prague, Czech Republic

Correspondence

Rebeka Rmoutilová, Department of Anthropology and Human Genetics, Faculty of Science, Charles University, Viničná 7, 128 44 Prague, Czech Republic.
Email: vejnaror@natur.cuni.cz

Funding information

French National Research Agency, Grant/Award Number: ANR-10-LABX-52; Grant Agency of Charles University, Grant/Award Number: 1088217; Irene Levi Sala CARE Archaeological Foundation; Leakey Foundation; Louisiana Board of Regents, Grant/Award Number: LEQSF(2015-18)-RD-A-22; Ministerio de Ciencia, Innovación y Universidades, Grant/Award Number: PGC2018-093925-B-C33; Ministerio de Economía y Competitividad, Grant/Award Number: CGL2015-65387-C3-2-P; Région Nouvelle Aquitaine, Grant/Award Number: 2016-1R40240-00007349-00007350; Universidad del País Vasco/Euskal Herriko Unibertsitatea, Grant/Award Number: 1044-16; Eusko Jaurlaritza-Gobierno Vasco, Grant/Award Number: IT1418-19

Abstract

Objectives: A marked asymmetry was previously reported in the sacral alae and S1-L5 facets orientation of the Neandertal individual Regourdou 1. Here, we provide a detailed description and quantification of the morphology and degree of asymmetry of this sacrum.

Material and methods: Regourdou 1 was compared to a modern human sample composed of 24 females and 17 males, and to other Neandertal individuals. Both traditional and geometric morphometric analyses were used in order to quantify the degree of sacral asymmetry of Regourdou 1.

Results: The asymmetry of both sacral alae and facets orientation substantially exceeds directional and absolute asymmetry of the healthy modern sample. Regourdou 1 shows a considerably shorter right ala, which is absolutely and relatively outside of the modern and Neandertal variations.

Conclusion: Regourdou 1 shows marked sacral asymmetry that probably originated in early ontogenetic development. An asymmetric sacrum reflects asymmetric load dissipation and could relate to other morphological abnormalities observed in the skeleton, especially the mild scoliosis of the spine and the asymmetry of the femoral diaphyses. Further investigation is necessary to elucidate the relationship between those morphologies as well as a potential impact on the life of the individual.

KEYWORDS

facet orientation, geometric morphometrics, sacral asymmetry, sacral development

1 | INTRODUCTION

The sacrum is important in weight transmission and posture (Pal, 1989) as its orientation within the pelvic girdle influences the lumbar lordosis (Been, Gómez-Olivencia, & Kramer, 2014; Been, Pessah, Peleg, & Kramer, 2013; Peleg et al., 2007). In addition, it has an impact on the shape and dimensions of the birth canal (Tague, 2000, 2007). It is generally assumed that Neandertals had similar sacral morphology to anatomically modern humans despite the presence of specific morphological traits described in several specimens: a very voluminous sacral canal (Meyer, Brůžek, Couture, Madelaine, & Maureille, 2011; Pap, Tillier, Arensburg, & Chech, 1996; Trinkaus, 1983), a less marked promontory with relatively flat vertical curvature (Bartucz & Szabó, 1940; Boule, 1911; Rak, 1991), and a relatively narrow sacral breadth (Bartucz & Szabó, 1940; Boule, 1911; Fraipont, 1927; Fraipont & Lohest, 1887). Unfortunately, there are only a few well-preserved Neandertal sacra (Supplementary Table S1), and no recent study has investigated potential differences between Neandertal sacra and contemporary or extant ones. With regard to the recent attempts at Neandertal body reconstruction (Chapman, 2017; Gómez-Olivencia et al., 2018; Sawyer & Maley, 2005), the sacrum is even more important as it provides information on the spinopelvic alignment (Been et al., 2017).

Based on this knowledge, we provide an analysis of the sacrum of the Regourdou 1 (R1) Neandertal that has a relatively well-preserved pelvis and thorax, but whose sacrum shows a peculiar morphology that demands further exploration before any attempts at reconstruction of the body.

2 | THE REGOURDOU 1 NEANDERTAL

The Neandertal skeleton Regourdou 1 was discovered in September 1957 in Dordogne in the southwest of France (Piveteau, 1959) and the site was systematically excavated during 1961–1964. Some of the R1 skeletal pieces were recently found in faunal collections curated at the *Musée National de Préhistoire*, the *Musée d'Art et d'Archéologie du Périgord* and the Regourdou site Museum (Madelaine et al., 2008; Maureille, Gómez-Olivencia, Couture-Veschambre, Madelaine, & Holliday, 2015). Those new findings have nearly completed the trunk, lower limbs, feet, and pelvic girdle, and have thus allowed detailed analyses of certain anatomical regions, providing not only new data on Neandertal variation, but also on the paleobiology of this individual (Gómez-Olivencia, Couture-Veschambre, Madelaine, & Maureille, 2013; Gómez-Olivencia, Holliday, Madelaine, Couture-Veschambre, & Maureille, 2019; Meyer et al., 2011; Pablos et al., 2019). Despite not preserving the calvarium (i.e., skull without mandible following Martin, 1928), R1 is now one of the most complete adult Neandertal skeletons (Maureille et al., 2015). While direct dates have not yet been obtained, Layer 4 of the site, in which the skeleton was buried, is attributed to the latter part of MIS 5 (Bonifay, 1964; Pelletier et al., 2017; Turq, Jaubert, Maureille, & Laville, 2008).

Based on mandibular tooth wear and the closed medial clavicular epiphyses, R1 was a young adult (Vandermeersch & Trinkaus, 1995; Volpato et al., 2012) who may not have exceeded 30 years (Volpato et al., 2012). Some scholars have proposed that this skeleton belongs to a male individual based on either its overall morphology (Vallois, 1965), or specific features such as measurements of the axis (Gómez-Olivencia et al., 2007), canine breadth, or the proportion of the body and alae of the sacrum (Volpato et al., 2012). At present, the sex of the individual cannot be assessed from the pelvic remains, and metrics from other bones provides ambiguous information concerning sex assignment of the specimen (Meyer et al., 2011; Plavcan et al., 2014; Vandermeersch & Trinkaus, 1995).

The sacral base of R1 shows apparent asymmetry in the length of the alae, with the left more laterally pronounced than the right (Meyer et al., 2011). Additionally, the orientation of the facets that articulate with the fifth lumbar vertebra is also asymmetrical: the right shows a more dorsal orientation while the left shows a more dorsomedial orientation (Gómez-Olivencia et al., 2013). Asymmetry in size of the facets cannot be assessed due to slight erosion of the processes (Meyer et al., 2011). The sacrum is not the only region of the R1 skeleton showing a marked degree of asymmetry or morphological abnormality. High asymmetry was found in the upper limb bones (Vandermeersch & Trinkaus, 1995) and an unusual pattern of asymmetry was also noted for femora, tali, and thorax (Gómez-Olivencia et al., 2013; Maureille et al., 2015; Pablos et al., 2019). Particular periosteal abnormalities involving cortical bone were found on ribs and femoral diaphyses (Gómez-Olivencia et al., 2019; Maureille et al., 2016).

In this article, we explore the degree of asymmetry in the Regourdou 1 sacrum which is compared to healthy modern human individuals and all available Neandertal specimens using classical and geometric morphometric analysis enhanced with imaging techniques. Implications for the paleobiology of Regourdou 1 and further study of the specimen are proposed following the results.

3 | MATERIALS AND METHODS

3.1 | Regourdou 1 sacrum

The sacrum of R1 (Figure 1) is incomplete, preserving the upper part of the bone at the level of the first and second sacral vertebrae (S1, S2 respectively). The body of S1 is completely preserved and the sacral base is almost complete, missing only a small portion of the posterior left ala. The right auricular surface is complete, but the lower portion of the inferior arm is missing on the left side. The sacrum does not exhibit any sign of a trauma or healed fracture (Linstrom et al., 2009).

The R1 sacrum was micro-CT scanned (voxel size 0.065 mm) at the AST-RX platform of the *Musée de l'Homme* (Paris) using the micro-focus tube of the micro-CT scanner “v|tome|x L 240” (GE Sensing & Inspection Technologies Phoenix X-ray). A 3D model semi-automatically segmented in Avizo 9.1 Lite (Visualization Sciences

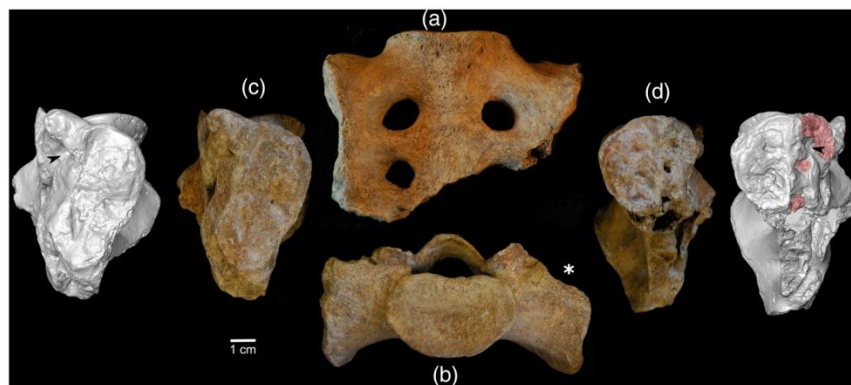


FIGURE 1 The sacrum of Regourdou 1. (a) Anterior, (b) superior, (c) right lateral, and (d) left lateral views. Lateral views are supplemented with surface models rendered from the micro-CT. An asterisk marks a missing portion of the left ala which is indicated in the lateral view by a large red area. Other red areas mark taphonomic defects that are also visible in the photograph. Arrowheads show fossae developed posterior to both auricular surfaces for the attachment of the sacroiliac ligament

Group, SAS) was used in this study. To facilitate the manipulation, the micro-CT scan was reduced before the segmentation in ImageJ (Rueden et al., 2017) using a macro created by Renaud Lebrun (www.morphomuseum.com) to a resolution still sufficient for macroscopic analyses.

3.2 | Comparative material

For this analysis, we used 3D models segmented from CT scans of Neandertal sacra of La Chapelle-aux-Saints 1 (LCAS; provided by Musée de l'Homme) and Kebara 2 (K2; provided by Tel Aviv University). Further data on later Neandertal specimens (LCAS, K2, Spy 2, Subalyuk 1, Shanidar 1, Shanidar 3) were culled from the literature (Supplementary Table S1).

For comparative purposes, we used 41 abdominal CT scans of 24 females and 17 males from the *Hôpital Nord* in Marseille (the data were collected with the approval of the ethics committee of the Faculty of Medicine in Marseille). Individuals between 20 and 40 years of age were used because of a high prevalence of sacroiliac degenerative defects in older patients. Patients with apparent vertebral or pelvic disorders (including scoliosis, sacralization, lumbarization, or sacroiliac joint fusion) were excluded from the study. 3D models of sacra were obtained by semi-automatic segmentation in Avizo. Five specimens (one male and four females) could not be digitized completely as the superior articular processes were not segmented properly on either one or both sides due to tight space between adjacent processes. These specimens were not included in the geometric morphometric analysis but were used in the analysis of linear measurements.

3.3 | Data acquisition

In order to analyze the Regourdou 1 sacral base morphology, landmarks, linear measurements, and indices were acquired and compared

with the ones of an extant modern human sample and Neandertal specimens. To collect data, each 3D model was positioned with the superior surface of the S1 body perpendicular to the z-axis of the virtual coordinate system and thus parallel to the screen (Figure 2) and from this view a set of 21 landmarks (Table 1) was digitized in the software Viewbox 4 (dHAL software, Athens, Greece). Landmark coordinates were subsequently projected onto a plane estimated from eight landmarks (Landmarks 1–5 in Table 1) lying on the border of the first sacral vertebra (Gunz, Mitteroecker, Neubauer, Weber, & Bookstein, 2009) (the plane estimation and projection of landmarks were performed following Gunz et al. (2009)). Ten linear dimensions were computed from projected coordinates (Table 2). For statistical testing of asymmetry, the modern comparative sample was digitized twice.

Seven indices were also computed from the measurements for a comparison of modern and fossil specimens (Table 3). Due to differential preservation of fossil remains and the availability of published data, a subset of these landmarks and linear variables were used to analyze the degree of R1 asymmetry and differences between Neandertals and modern humans. In order to include Kebara 2 and LCAS in the analysis, special treatment was necessary due to their taphonomic defects or deformation (Supplementary Figures S1 and S2).

3.4 | Data analysis

As asymmetry is common in limb bones (Auerbach & Ruff, 2006; Kujanová, Bigoni, Velemínská, & Velemínský, 2008) and several studies have proposed the existence of asymmetry in the sacrum (Akman, Karakas, & Bozkir, 2008; Plochocki, 2002), we first tested for the presence of asymmetry in the modern comparative sample. Asymmetry can be divided into two components: directional and fluctuating. Directional asymmetry (DA) is a tendency of a trait to be differently developed on the left or right side; that is, it is a mean asymmetry in

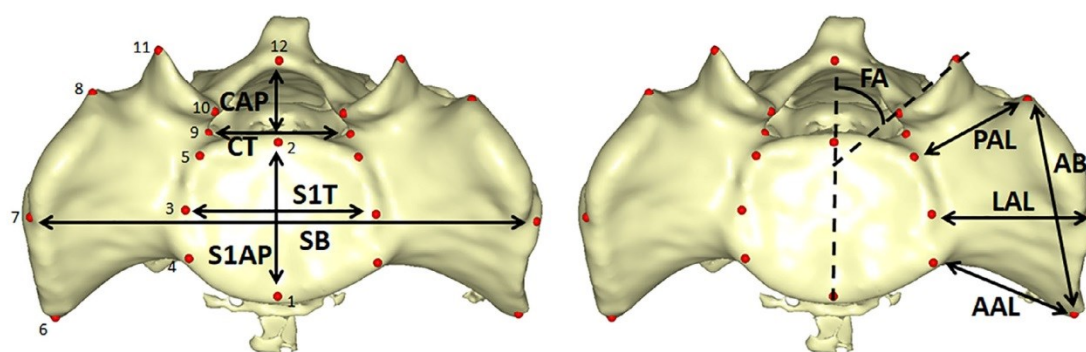


FIGURE 2 Sacral landmarks and measurements. Unilateral measurements are on the right, bilateral measurements on the left. Landmark numbers indicated on the left picture (bilateral landmarks labeled only on one side) correspond to those in Table 1. Measurements definitions are given in Table 2

TABLE 1 Description of sacral landmarks

Number	Abbr.	Name	Bilateral or medial	Definition	Reference
1	pr	Promontory	m	The most anterior point on S1 body on midsagittal plane	Rusk and Ousley (2016) and Schiess, Boeni, Rühli, and Haeusler (2014)
2	mp	Medial posterior	m	The most posterior point on S1 body on midsagittal plane	Rusk and Ousley (2016) and Schiess et al. (2014)
3	ls	Lateral S1	b	Lateral point on the border of S1 body in the half of the distance from pr to mp	Rusk and Ousley (2016)
4	oa	Oblique anterior	b	The closest point on the S1 outline from the aa	Based on the AAL measurement
5	op	Oblique posterior	b	The closest point on the S1 outline from the ap	Based on the PAL measurement
6	aa	Ala anterior	b	The most anterior point on the superior ala	Based on the AAL measurement
7	al	Ala lateral	b	The most lateral point on the sacral ala in the extension of transverse diameter of S1	Based on the LAL measurement
8	ap	Ala posterior	b	The most posterior point on the superior ala	Based on the PAL measurement
9	pb	Processus base	b	Base of the articular process	Schiess et al. (2014)
10	pm	Processus medial	b	Medial point on the articular process	Schiess et al. (2014)
11	pl	Processus lateral	b	Lateral point on the articular process	Schiess et al. (2014)
12	c	Canal	m	Medial point on the sacral canal wall	Schiess et al. (2014)

the sample and often originates in response to the same mechanical conditions. On the other hand, fluctuating asymmetry (FA) consists of non-directional deviations from symmetry that originate due to small imprecisions in developmental processes (Klingenberg, 2003). For bilateral linear measurements, percentage scores of directional (%DA) and absolute (%AA) asymmetry were computed following Auerbach and Ruff (2006). The %DA score for each individual was computed as a difference between right and left side multiplied by 100 and divided by the average of both sides. Positive results indicate right-dominant asymmetry. In contrast, %AA takes an absolute difference in the calculation. Both %DA and %AA are expressed as a mean value of

individual scores. The formulas for %DA and %AA scores according to Auerbach and Ruff (2006) are as follows:

$$\%DA \text{ score} = \frac{(\text{Right} - \text{Left}) \times 100}{\text{Average of left and right}} \text{ and}$$

$$\%AA \text{ score} = \frac{|(\text{Right} - \text{Left})| \times 100}{\text{Average of left and right}}$$

Mixed model analysis of variance (ANOVA) was used to statistically test DA in the linear measurements as it also considers the effect

TABLE 2 Sacral measurements and angles computed from projected landmarks

Number	Abbr.	Name	Bilateral or medial	Landmark boundaries	Reference
1	SB	Sacral breadth	m	al-al	Tague (2007)
2	S1AP	S1 A-P breadth	m	pr-mp	Tague (2007)
3	S1T	S1 transversal breadth	m	ls-ls	Tague (2007)
4	CAP	Canal A-P breadth	m	mp-c	Bräuer (1988)
5	CT	Canal transverse breadth	m	pb-pb	Bräuer (1988)
6	AB	Alar breadth	b	aa-ap	Plochocki (2002)
7	AAL	Anterior ala length	b	aa-oa	This study
8	LAL	Lateral ala length	b	al-ls	Tague (2007)
9	PAL	Posterior ala length	b	ap-op	Plochocki (2002)
10	FA	Facet angle	b	(pl-pm)-(pr-mp)	Noren, Trafimow, Andersson, and Huckman (1991)

TABLE 3 Indices computed from sacral measurements

Number	Abbr.	Name	Unilateral or bilateral	Computation
1	SBi	Sacral base index	u	S1T/SB
2	S1i	S1 index	u	S1AP/S1T
3	Ci	Canal index	u	CAP/CT
4	LALi	Lateral ala length asymmetry	u	LAL_R/LAL_L
5	FAi	Facet angle asymmetry	u	FA_R/FA_L
6	LALSBi	LAL to SB	b	LAL/SB
7	LALS1Ti	LAL to S1T	b	LAL/S1T

TABLE 4 Summary of bilateral measurements (in mm) and their asymmetry of the comparative sample and values from Regourdou 1 (R1)

Variable	Mean (right) ^a	Mean (left) ^a	Side difference	p-Value	Mean %DA	Mean %AA	R1%DA score ^a
AAL	33.6 ± 4.9	33.9 ± 5.3	-0.38 ± 2.5	.372	-1 ± 7.1	5.7 ± 4.3	-14.7
LAL	33.2 ± 4	32.9 ± 4.5	0.33 ± 1.6	.076	1.1 ± 5.0	4.1 ± 3.0	<u>-16.8</u>
PAL	31.7 ± 3.6	30.6 ± 3.8	1.11 ± 1.9	<.001	3.7 ± 6.4	6.4 ± 3.5	-
AB	45.7 ± 4.9	45.4 ± 4.5	0.29 ± 2.5	.524	0.5 ± 5.5	4.5 ± 3.3	-
FA	48.5 ± 11.1	52.1 ± 9.3	-4.24 ± 8.2	.001	-9.5 ± 16.3	14.5 ± 11.9	<u>31.8</u>

Note: Significant p-values are in bold.

Abbreviations: %DA, percentage directional asymmetry. %AA, percentage absolute asymmetry.

^aUnderlined values are beyond 2 SD from the modern human sample mean.

of measurement error (Palmer & Strobeck, 1986; Van Dongen, Molenberghs, & Matthysen, 1999). The model was fit with R package *lme4* (Bates et al., 2018). The index of asymmetry using the same equation as for %DA was also computed for R1 in order to know the amount of asymmetry compared to the healthy sample.

Traditional metric analysis only provides information about asymmetry in size, but geometric morphometrics also evaluates asymmetry in shape. To test asymmetry in shape, projected landmarks were superimposed using generalized Procrustes analysis (GPA) in order to filter out different positions, rotations, and size (Bookstein, 1991). Presence of DA and FA in shape was tested by Procrustes ANOVA (Klingenberg, 2015) and DA was visualized. As direction of FA in individuals is not of biological interest, the amount of FA can be

computed as individual deviations from the mean asymmetry in units of Procrustes distance (Klingenberg & Montero, 2005). The R1 configuration was corrected for the mean asymmetry of the modern comparative sample and a resulting FA score was compared to the amount of FA in the sample.

Differences between modern and Neandertal samples were tested for raw measurements and indices by nonparametric two-tailed Wilcoxon rank-sum test. For those variables that may be pathologically affected in R1, the test was repeated without this specimen.

Finally, to analyze the degree of asymmetry in R1, the raw measurements and indices were transformed into adjusted z-scores that were first used in Maureille, Rougier, Houet, and Vandermeersch (2001) (see also Sclan, Santos, Tillier, Maureille, & Quintard, 2012).

Effect	Sum of squares	Mean square ^a	Degrees of freedom	F
Individual	0.4260	0.420	1,015	10.39*
Side	0.0037	0.135	27	3.34*
Ind × side	0.0382	0.040	945	12.04*
Error	0.0068	0.003	2,016	

Note: Individual effect represents the variation between individuals in the symmetric component of shape. Side represents directional asymmetry. Ind × side quantifies fluctuating asymmetry. Error is the residual variation due to measurement error.

Abbreviation: ANOVA, analysis of variance.

^aMean square was multiplied by 1,000.

* $p < .0001$.

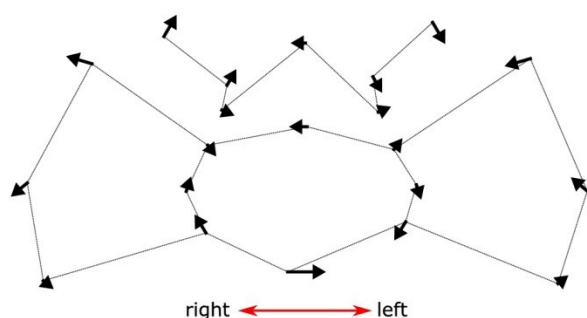


FIGURE 3 Mean asymmetry in the modern sample. Arrows indicate shape change from the mirrored to the original configuration. For better visibility, the observed difference is exaggerated 10 times

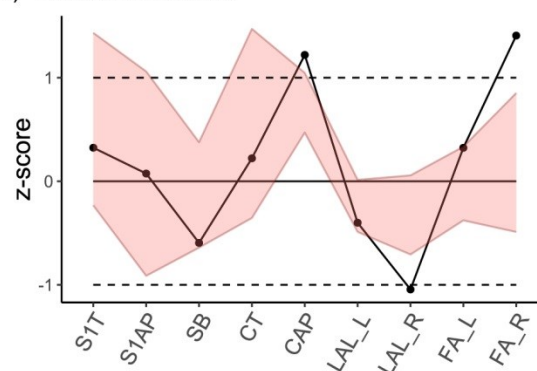
R1 variables were compared with 95% confidence intervals of the modern sample's variability and minimum and maximum values of Neandertal sample. Shape of the R1 sacrum was analyzed relative to the comparative sample by principal component analysis (PCA) performed on the covariance matrix of Procrustes coordinates. Special attention was given to the asymmetric component of landmark configurations that result after subtraction of symmetrized configuration from each specimen (Klingenberg, Barluenga, & Meyer, 2002).

Virtual imaging has proved to be a very useful tool in assessing abnormal morphological conditions in skeletal remains (Milella, Zollikofer, & Ponce de León, 2015; Zurmühle et al., 2017). Sacral asymmetry was visually inspected using mirror imaging, volume rendering, and cross sections in defined positions (see details in the Supplementary Information). Visualization using volume rendering allows us to explore the trabecular system of the sacrum. For this, only a sub-region of the sacrum demarcated by the S1-S2 transition was considered as it was not affected by post-mortem trabecular loss in the caudal portions.

Data processing, analyses, and visualizations were performed in RStudio IDE (RStudio Team, 2016) using a set of R packages *geomorph* (Adams & Otárola-Castillo, 2013), *Morpho* (Schlager, 2016), and *tidyverse* (Wickham, 2017). Visualizations of shape changes were created in MorphoJ (Klingenberg, 2011) and processed in Inkscape (www.inkscape.org).

TABLE 5 Procrustes ANOVA sacral shape based on projected landmarks

(a) Measurements



(b) Indices

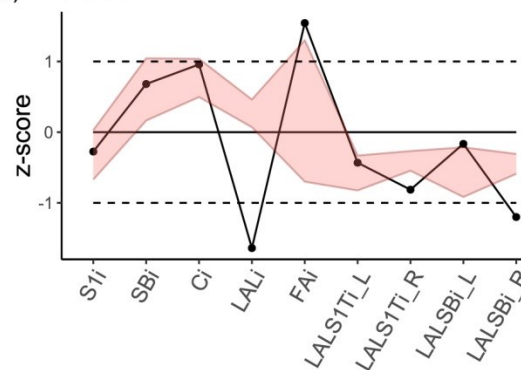


FIGURE 4 Adjusted z-scores of Regourdou 1 sacral measurements (a) and indices (b). Dashed line represents a 95% confidence interval of modern human sample. Red area represents interval between minimum and maximum values of other Neandertal specimens. Variable definitions are in Tables 2 and 3

3.5 | Error of measurement

The intraobserver error was computed for projected landmarks and linear dimensions. To evaluate the error related to projected landmarks acquisition, they were superimposed using GPA without scaling the landmarks configurations (von Cramon-Taubadel, Frazier, & Lahr, 2007). The measurement error of individual landmarks was then

TABLE 6 Variable statistics for modern human sample and values of raw measurements and indices for Neandertal specimens

Variable	N	Mean	SD	95% inferior	95% superior	R1 ^a	K2 ^a	LCAS ^a	Su1 ^b	Sh1 ^b	Sh3 ^b	Spy 2 ^b
Measurements												
SB	41	112.8	7.5	97.5	128	103.7 (107.9) ^c	118.5	103.3	107.8	104.0	117.0	103.0
S1AP	41	29.4	2.7	24.1	34.8	29.8	30.4	24.5	32.8	–	<u>35.1</u>	–
S1T	41	46.6	4.6	37.3	56.0	49.6	53.0	44.4	49.3	47.0	<u>60.0</u>	48.0
CAP	39	17.0	2.5	11.9	22.1	<u>23.2</u>	–	<u>22.3</u>	19.0	–	–	–
CT	41	31.9	2.4	27.0	36.7	32.9	30.1	31.1	31.2	<u>38.0</u>	<u>39.0</u>	–
LAL_R	41	33.2	4.0	25.1	41.4	<u>24.8</u>	33.7	28.8	30.25	–	–	27.5
LAL_L	41	32.9	4.5	23.9	42.0	29.3	33.0	–	28.55	28.5	28.5	–
AB_R	41	45.7	4.9	35.7	55.7	38.2	41.2	<u>34.9</u>	–	–	–	–
AB_L	41	45.4	4.5	36.3	54.5	–	<u>36.3</u> ^d	–	–	–	–	–
FA_R	38	48.5	11.1	25.9	71.0	<u>80.2</u>	58.8	67.7	37.4	–	–	–
FA_L	38	52.1	9.3	33.3	70.9	58.2	45.0	58.4	52.5	–	–	–
Indices												
SBi	41	0.41	0.05	0.32	0.51	0.48	0.45	0.43	0.46	0.45	<u>0.51</u>	0.47
S1i	41	0.63	0.06	0.51	0.76	0.60	0.57	0.55	0.67	–	0.59	–
Ci	39	0.54	0.09	0.36	0.71	<u>0.71</u>	–	<u>0.72</u>	0.61	–	–	–
LALi	41	1.01	0.05	0.91	1.12	<u>0.85</u>	1.02	–	1.06	–	–	–
FAi	37	0.92	0.15	0.62	1.22	<u>1.38</u>	<u>1.31</u>	1.16	0.71	–	–	–
LALSBi_R	41	0.29	0.02	0.25	0.34	<u>0.24</u>	0.29	–	0.28	–	–	0.27
LALSBi_L	41	0.29	0.03	0.24	0.34	0.28	0.28	–	0.27	0.27	<u>0.24</u>	–
LALS1Ti_R	41	0.72	0.14	0.45	1.00	0.50	0.64	0.65	0.61	–	–	0.57
LALS1Ti_L	41	0.72	0.15	0.42	1.01	0.59	0.62	–	0.58	0.61	0.48	–

Note: Variable definitions are in Table 2. Underlined values are at the limit or outside the 95% confidence interval of the modern human sample.

Abbreviations: K2, Kebara 2; LCAS, La Chapelle-aux-Saints 1; R1, Regourdou 1; Su1, Subalyuk 1; Sh1 and Sh3, Shanidar 1 and 3.

^aMeasured on the 3D model.

^bFrom the literature (Bartucz & Szabó, 1940; Chapman, 2017; Meyer, 2013; Pap et al., 1996; Trinkaus, 1983; Trinkaus, 2011). Values for Su1 calculated from z-scores for LAL (Meyer, 2013) and for FA they were measured on a photograph from superior view (Bartucz & Szabó, 1940) which does not show any marked distortion and moreover an angle does not rely on scale. LAL values for Sh1, Sh3, and Spy 2 calculated from SB and S1T.

^cThe value in parentheses is an estimation based on a reflection of the left side.

^dThis value is not reliable even after the slight correction of the taphonomic distortion which has most affected anteroposterior dimensions of the left ala.

represented by the median of Euclidian distances between pairs of homologous landmarks. It ranged between 0.27 mm for landmark *pbL* (the base of the left articular process) and 0.83 mm for landmark *alR* (lateral margin of the right sacral ala), with an overall error of 0.5 mm (Supplementary Table S2). The maximum deviation was 3.44 mm in landmark *pmL* (medial point on the articular process), but no other specimen exceeded 2.5 mm for other measurements (Supplementary Table S2).

Absolute and relative measurement errors were computed to evaluate the intraobserver error of linear measurements and angles (Supplementary Table S3). Concerning linear measurements, relative error ranged between 0.22% for sacral breadth and 2.33% for canal anteroposterior diameter. Facet angles had slightly higher intraobserver error (around 2.6%).

4 | RESULTS

4.1 | Asymmetry in the modern sample

DA was tested on four linear measurements and one angle in the reference sample by mixed model ANOVA considering the effect of

measurement error. Table 4 summarizes the results providing also the amount of %AA. This analysis showed that the mean of our healthy modern human sample sometimes does not conform to perfect bilateral symmetry. This was demonstrated in posterior ala length and facet angle (Table 4) which show significant %DA. Posterior ala length is on average 1 mm greater (%DA is 3.7) on the right side which means that the right ala tends to be posteriorly longer than its left counterpart. On the other hand facet angle is 4.2° larger (%DA = 9.5) on the left side, meaning a more coronal orientation of the left articular facet in our comparative sample.

Landmark analysis of the whole structure showed significant DA and FA. Table 5 presents results of Procrustes ANOVA relative to measurement error as a confounding effect. Magnitude of measurement error is much lower than the magnitude of FA as indicated by mean square and *F* ratio (Klingenberg, 2015) that evaluates that the magnitude of FA is approximately 12 times larger than the measurement error. Mean differences between the original and mirrored configurations are illustrated in Figure 3. Concordantly with the analysis of measurements, asymmetry of the sacrum is more pronounced in

TABLE 7 Wilcoxon rank-sum test of differences between modern human sample and Neandertals

Variable	N (Neandertals)	p (with R1)	p (without R1) ^a
Measurements			
SB	7	NS	NS
S1AP	5	NS	–
S1T	7	NS	–
CAP	3	*	–
CT	6	NS	–
LAL_R	5	*	NS
LAL_L	5	NS	NS
AB_R	3	**	*
FA_R	4	NS	NS
FA_L	4	NS	NS
Indices			
SBi	7	**	*
S1i	5	NS	–
Ci	3	**	–
LALi	3	NS	NS
FAi	4	NS	NS
LALSBi_R	4	*	NS
LALSBi_L	5	*	*
LALS1Ti_R	5	*	NS
LALS1Ti_L	5	*	*

Abbreviations: NS, nonsignificant ($p > .05$); R1, Regourdou 1.

^aVariables that could be affected by pathology in R1 were additionally tested without R1.

* $p < .05$. ** $p < .01$.

the dorsal region. Sacral alae are more symmetric anteriorly while the posterior portion tends to be more developed on the right. Likewise, articular facets are more coronally oriented on the left.

4.2 | Analysis of Neandertal sacra

With regard to the small number of available Neandertal specimens, the Neandertal range of variation was indicated by minimum, maximum, and mean values for each of the linear variables (Figure 4; individual values for Neandertal specimens in Table 6). Most of the Neandertal variation intervals for sacral measurements overlap with modern human variation, but there is a tendency toward wider S1 and greater canal diameters. All Neandertal sacra also have rather short alae. The indices confirm the tendency toward wider S1 relative to sacral breadth and voluminous sacral canal opening. The alae are not markedly asymmetrical and they are relatively short compared to modern sample, which may be due to the assumed male sex of majority of the Neandertal individuals. The FAi also deviates from the mean of healthy modern individuals which is biased by Kebara 2.

Statistical testing confirms observed differences between Neandertal and modern human sacra (Table 7). Significant differences are

observed in variables related to absolute and relative alae dimensions and sacral canal opening even after excluding R1 in cases where R1 could bias the comparison.

This comparison suggests the presence of certain directional differences between Neandertal sacra studied here and the modern sample: all specimens have a larger S1 body relative to sacral breadth, relatively more anteroposteriorly spacious sacral canal and relatively smaller alae, that is, mediolaterally short and anteroposteriorly narrow.

4.3 | Asymmetry of the Regourdou 1 sacrum

The Regourdou 1 sacrum was metrically compared to modern humans (Tables 4 and 6). Due to preservation problems, we were able to compare R1 to the modern sample in only three of the five calculated asymmetry indices given in Table 4. Two of these indices yielded results beyond two SD from the modern human sample: lateral ala length and facet angle, while the third one (anterior ala length) is 1.93 SD from the mean (Table 4).

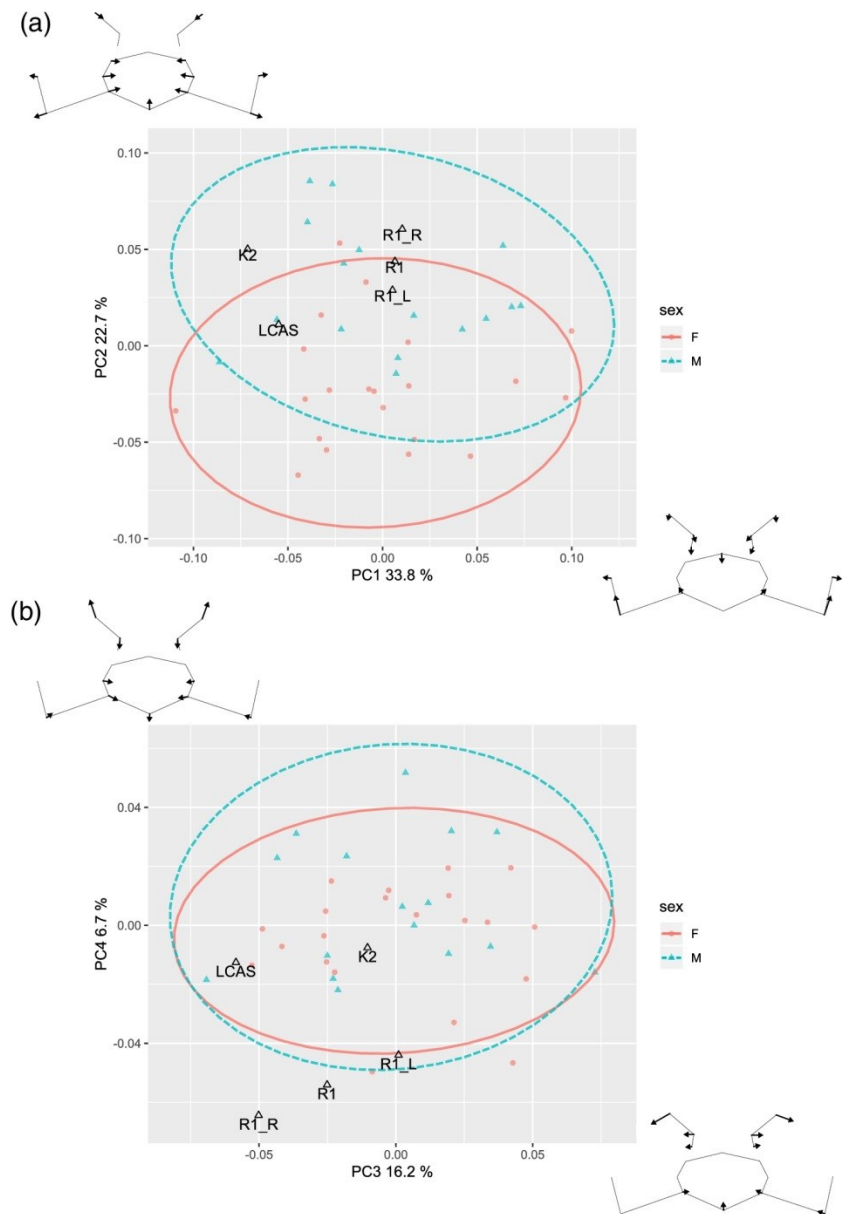
Table 6 compares R1 and other Neandertals to our modern human comparative sample. The R1 sacrum fell outside the 95% confidence interval of the sample for three linear measurements (anteroposterior canal diameter, right lateral ala length, and right facet angle) and four indices (LALi, FAi, right LALSBi), and one index (Ci) is at the limit of the variability (Table 6, Figure 4). The majority of those variables relate to the asymmetry of the alae length or the articular facets orientation. The other measurement is the anteroposterior diameter of the canal which is greater than in the modern sample, and which could also be related to the significantly larger anteroposterior dimension of the canal present in the fifth lumbar vertebra (L5) (Gómez-Olivencia, Arlegi, Barash, Stock, & Been, 2017). Right ala length is significantly smaller than our modern human sample. In contrast, the right facet angle falls far above the modern sample's upper limit. Finally, while not significant, the total sacral breadth slightly deviates toward the lower margin (Figure 4a).

Regarding variables expressing asymmetry (LALi, FAi), the degree of asymmetry in both ala length and facet orientation is far beyond the range observed in healthy modern human sacra (Table 6, Figure 4b). The right ala is very short relative to SB and S1T diameters.

Despite the differences observed between modern and Neandertal sacra affecting the alae and facets, R1 has an even shorter right ala and more asymmetric alae length and facet orientation. Values for R1 are also outside the Neandertal range of variation.

Projected coordinates of landmarks (except landmarks *apR*, *apL*, and *c* due to their absence in fossil specimens) were superimposed using GPA. The PCA was subsequently performed on the Procrustes coordinates and on their asymmetric component to analyze the overall shape of Neandertal sacra relative to modern human variability, and the asymmetry of R1. In the PCA without symmetry control, R1 was represented by three coordinate configurations: the original asymmetric version and two symmetrized versions based on the right

FIGURE 5 Principal component analysis (PCA) of projected landmarks without symmetry control. (a) PC1 and PC2. (b) PC3 and PC4. Main shape changes along PCs illustrate shift from 0 to 0.1 of the given PC. Fossil specimens were aligned to the sample mean and PC scores were computed independently. Regourdou 1 is represented by its original morphology (R1) and two symmetrized configurations based on the right (R1_R) or left (R1_L) side. K2, Kebara 2; LCAS, La Chapelle-aux-Saints 1. Ellipses indicate 95% of variation in the male and female modern samples



or left side. Neandertal specimens K2 and symmetrized LCAS fall within modern human variation for the first four PCs which comprise 79% of total variation (Figure 5a,b) while R1 is within the variation for the first two PCs only. The first two PCs mainly express shape differences in the anterior alar region and relative dimensions of alae and S1 body while PC3 and PC4 reflect orientation of articular facets. Both K2 and LCAS tend to have more negative values along PC1 which means they have less prominent anterior portion of the alae. LCAS also has lower value for PC3 which reflects higher facet angle.

Different configurations change the position of R1 particularly along PC2, reflecting sexual differences in the modern human sample.

As one would expect, the symmetrized configuration based on the longer left ala shifts R1 more into the female variability and vice versa. On the other hand, different versions of R1 move along both the PC3 and PC4 axes, reflecting a greater difference between right and left facet orientation. The R1 original configuration falls outside the modern sample's variation, as does the symmetrized version based on the right side. On the contrary, the left-side mirrored configuration falls at the edge of the sample variation (Figure 4), suggesting this side is closer to the normal morphology.

Performing PCA on the asymmetric component of landmark configurations (Figure 6a,b), R1 falls on the edge of or outside the healthy

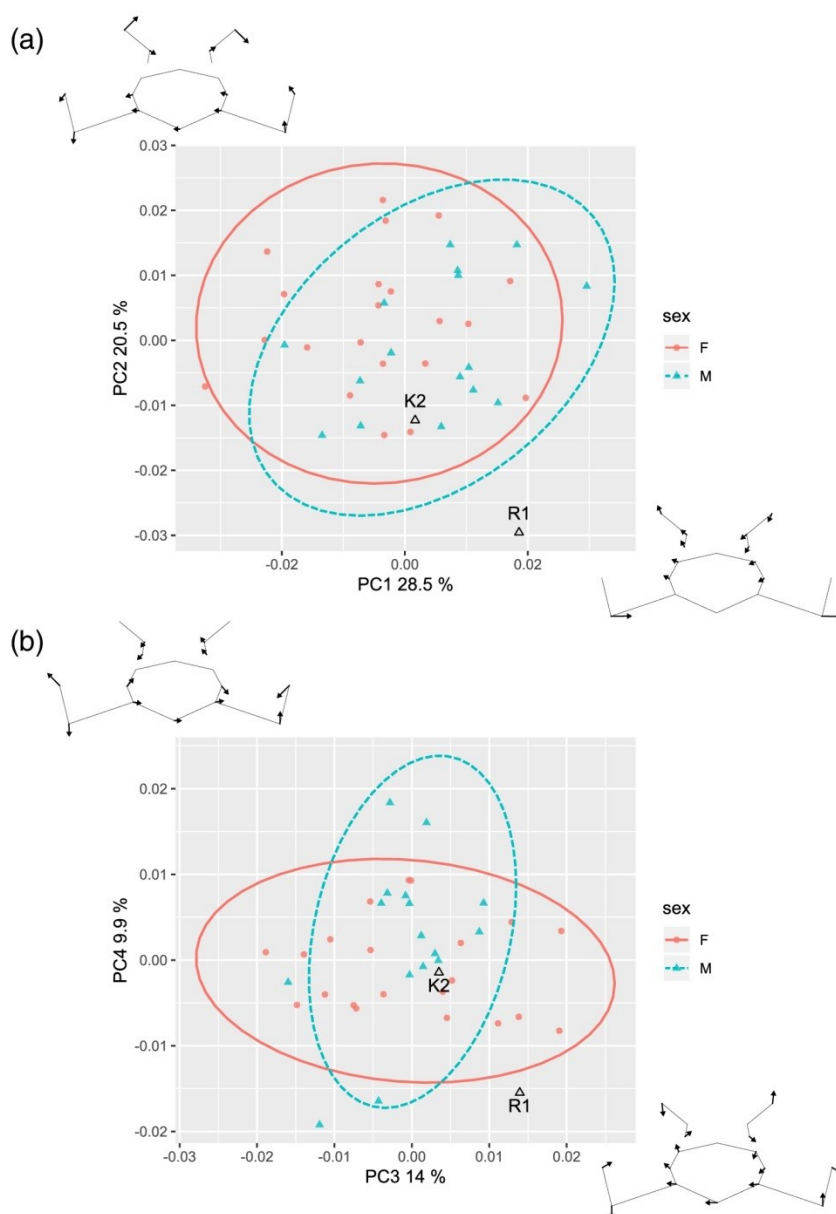


FIGURE 6 Principal component analysis (PCA) of the asymmetric component of projected landmarks. (a) PC1 and PC2. (b) PC3 and PC4. Main shape changes along PCs illustrate shift from 0 to 0.1 of the given PC. K2, Kebara 2; R1, Regourdou 1. Ellipses indicate 95% of variation in the male and female modern sample

modern sample for first four PCs that account for 73% of total variation. In contrast, K2 is again well inside the 95% confidence ellipses of both males and females. The first two PCs reflect the asymmetry in anterior alae and facet orientation, respectively, while PC3 and PC4 reflect mixed effects of alar anteroposterior development and facet orientation.

Comparing the amount of FA in the modern sample with the FA score for R1 and K2, R1 greatly exceeds the sample variation, whereas K2 is close to the mean value (Figure 7).

External morphology of the R1 sacrum has already been described by Meyer et al. (2011). Using virtual imaging methods allowed us to better visualize the object asymmetry. A 3D model of

the R1 sacrum was mirror imaged and superimposed with the original model using landmarks lying on the S1 body (Table 1, Figure 8). The asymmetry in the length of the sacral alae is clearly visible, but the visualization also shows different development of the alae in the superoinferior direction. When the sacral base is positioned horizontally, the shorter right ala rises above the mirrored left ala and thus reaches relatively more cranially, suggesting an asymmetrical alignment of coxal bones in the coronal plane.

Trabecular bone was inspected in the micro-CT scan of R1 sacrum using volume rendering (Figure 8) and cross sections (Supplementary Figure S3). Volume rendering allowed us to see the density of trabecular bone and showed that the trabecular network is

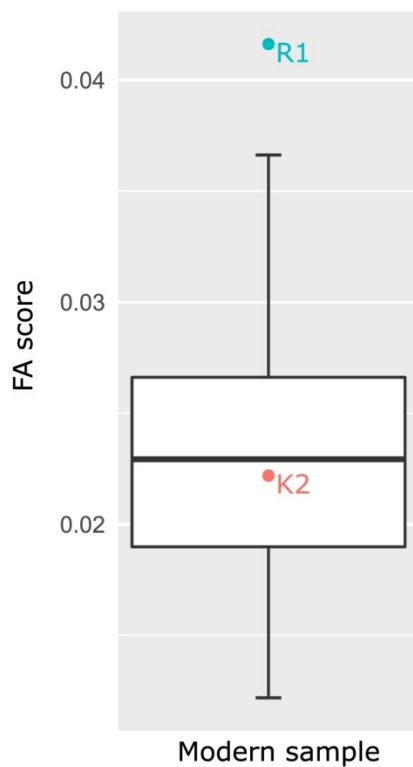


FIGURE 7 Fluctuating asymmetry for landmarks. Boxplot indicates variation for the modern comparative sample. K2, Kebara 2; R1, Regourdou 1

denser on the left side than on the right side. The same pattern was observed in the sagittal and transversal slices of the sacrum (Supplementary Figure S3).

High-resolution imaging allows better observation of the external morphology of the auricular surfaces without the confounding effect of surface coloring (Figure 1). Both auricular surfaces show relatively smooth transition between cranial and caudal arms without great constriction (Nishi et al., 2017). The preserved upper portion of the left auricular surface is very rugose and exhibits conspicuously deep pits. On the other hand, the right auricular surface displays only slight rugosity, but a deep groove caudally. This relief does not correspond to the morphological changes related to age described on the iliac auricular surface (Lovejoy, Meindl, Pryzbeck, & Mensforth, 1985), although the sacral auricular surface does not follow the same changes (Passalacqua, 2009) probably due to differentially thick cartilage (Schunke, 1938). However, greater number of surface irregularities was linked to greater stability of the joint (Vleeming, Volkers, Snijders, & Stoeckart, 1990).

5 | DISCUSSION

In our study, we performed a metric and morphological analysis of the Neandertal sacrum which confirms the presence of some significant

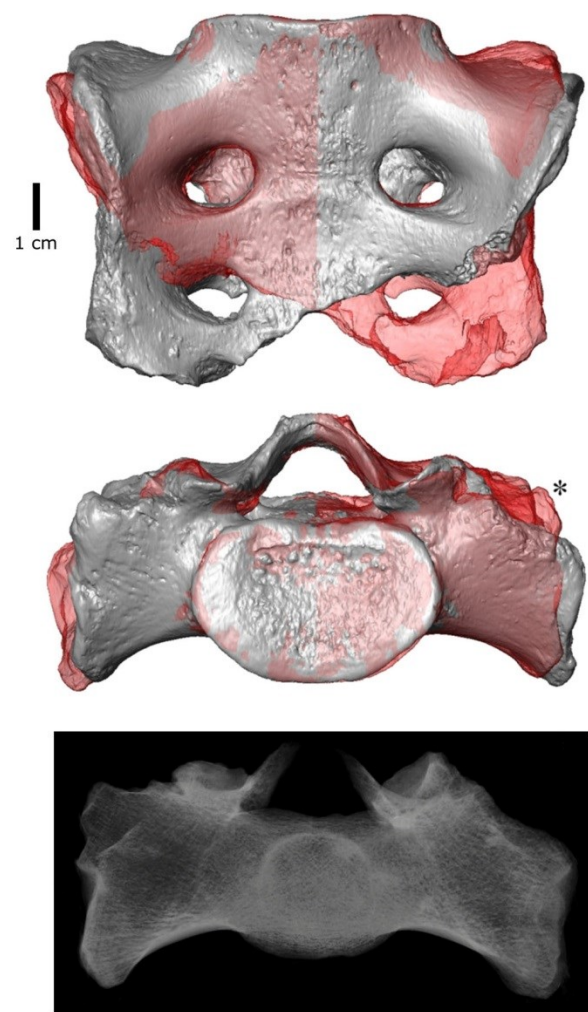


FIGURE 8 Visualization of sacral asymmetry of Regourdou 1. Top and middle: surface comparison (gray = original sacrum, transparent red = mirrored image). An asterisk marks a missing portion of the left ala. Bottom: volume rendering of the micro-CT

differences compared to extant modern humans. We also visualized and quantified the asymmetry of Regourdou 1 sacral alae and articular facets. In comparison with healthy individuals, R1 shows a substantial asymmetry in both mentioned dimensions exceeding the normal variation of the comparative sample. Furthermore, based on our univariate and multivariate comparisons with healthy individuals, the length of the ala is absolutely and relatively very short on the right side. In the discussion, we are going to analyze these results and propose potential interpretations concerning the origin and consequences of this morphology.

5.1 | Biomechanics and sacral asymmetry

Skeletal asymmetry has been studied mostly on limb bones in association with behavioral lateralization. Habitually repeated biomechanical

stress is usually associated with bone growth and therefore structural enlargement of the side experiencing greater loading (Carlson & Judex, 2007; Ruff, Holt, & Trinkaus, 2006; Shaw, Hofmann, Petraglia, Stock, & Gottschall, 2012). Bone functional adaptation is relevant especially for the long bones of upper and lower limbs. However, the interpretation of limb girdle and axial bones asymmetry is more complicated due to different biomechanical functions and development (Auerbach & Raxter, 2008). For example, an opposite pattern to that expected from the biomechanical law has been noted in clavicles, which exhibit enlarged diaphyseal diameters in the context of shorter total length in the dominant upper limb, indicating that different factors influence the clavicle vs. other bones of the arm (Auerbach & Raxter, 2008). Asymmetry in the sacrum has not been extensively studied, but several studies have shown left-side dominance of the sacral dimensions and put the result in relation to pre-dominant right-handedness and crossed asymmetry of lower limbs (Akman et al., 2008; Plochocki, 2002; Tobolsky, Kurki, & Stock, 2016).

The sacrum provides gravity-driven transmission of weight from the upper body to the lower limbs (Pal, 1989) and transmits shock waves leading from the lower limbs during gait (Mizrahi, Verbitsky, & Isakov, 2000). In order to resist shear forces in upright posture, the sacrum is wedged in between the coxal bones, and additional resistance is provided by the *gluteus maximus* muscle and iliosacral ligaments (Barker et al., 2014; Steinke et al., 2010) that generate perpendicular compressive force closure of the sacroiliac joint to overcome gravity (Vleeming et al., 2012). Therefore, the sacrum must resist two different simultaneous pressures: vertical shear and tensile forces of the muscles and ligaments. It has been shown that shear stress in the growth plate promotes degradation of the cartilage, accelerates ossification, and thus causes cessation of growth (Carter, 1987). The sacrum undergoes a high degree of shear stress; therefore, the left-side asymmetry could be caused by earlier cessation of alar growth on the more loaded right side (Plochocki, 2002).

In our analysis, R1 shows left-sided asymmetry in sacral alae which is in concordance with the predominant %DA published elsewhere. However, we did not confirm this type of %DA in our sample. In contrast to other studies analyzing alar asymmetry, we evaluated %DA in relation to intraobserver error and we obtained nonsignificant results except for the posterior ala length which showed right-side asymmetry. Even if %DA in the sacrum exists, the degree of asymmetry is very low in modern humans (our results and Akman et al., 2008; Plochocki, 2002; Tobolsky et al., 2016). It probably originates in the second decade of life during the adolescent growth spurt when the sacroiliac apophyses emerge and fuse (Bollow et al., 1997; Nissinen et al., 2000; Plochocki, 2002). Therefore, the sacrum does not have a long period in which it may be sensitive to lateralized habitual behavior or loading. However, Neandertals and Late Pleistocene humans exhibited stronger asymmetry in the upper limbs than do the majority of extant humans (Sparacello, Villotte, Shackelford, & Trinkaus, 2017; Trinkaus, Churchill, & Ruff, 1994, but see Kubicka, Nowaczewska, Balzeau, & Piontek, 2018). There is no evidence of similarly strong compensatory asymmetry in the lower body (Ruff, Trinkaus, Walker, &

Larsen, 1993; Trinkaus et al., 1994), which given the small number of Neandertal sacra preserved, prevents any assumptions about sacral asymmetry in Neandertals.

On the other hand, the sacrum has a high FA compared to other bones (Storm, 2009; Tobolsky et al., 2016), which implies a greater susceptibility to developmental stress. This is concordant with the fact that the sacrum and lumbosacral junction are regions of frequent developmental abnormalities (Dzupa et al., 2014; Masnicová & Beňuš, 2003). R1 substantially exceeds the range of %DA and even %AA (Table 4). Regarding the short period and rather small amount of growth from apophyseal sacroiliac plates during the second decade of life, a possible origin of sacral asymmetry in the earlier developmental period will now be explored.

5.2 | Development and sacral asymmetry

The mesenchymal template (i.e., paraxial mesoderm) from which the vertebral column originates is formed in the third week of intrauterine development and consists of paired somites that develop simultaneously but independently of each other (Scheuer & Black, 2000). After union of these paired structures, they become precursors of individual vertebrae. Lateral parts of the sacrum are considered developmentally homologous structures to ribs and costal processes of other vertebrae (Scheuer & Black, 2000; Tague, 2007, but see O'Rahilly, Müller, & Meyer, 1990) which are formed from a portion of somites (Barnes, 2012a). Subsequently, a chondrification starts in each blastemal vertebra from two paired centers (Scheuer & Black, 2000). Final ossification starts at the eighth to ninth weeks generally from one center in the vertebral centrum (Barnes, 1994; Scheuer & Black, 2000). During ossification, a sacral ala develops from paired anterior and posterior ossification centers at the level of each of the first three sacral vertebrae. The lateral parts fuse with sacral bodies between 2 and 6 years of age (Scheuer & Black, 2000).

Given the degree of sacral asymmetry in R1 and no evidence of a direct injury on the sacrum, this morphology most likely originated earlier in development (for similar cases see Pfeiffer, 2011; Pitre & Lovell, 2010). Regarding the fact that the period of origin of such a pronounced sacral asymmetry extends from the intrauterine to early postnatal period or even early childhood, two possible explanations can be proposed: a developmental abnormality or an indirect post-traumatic consequence. Unilateral hypoplastic vertebral defects are commonly associated with failure of paraxial mesoderm formation or chondrification (Barnes, 1994, 2012b; Scheuer & Black, 2000); that is, they originate after an insult during the period from the third to eighth weeks of intrauterine life. However, as the asymmetrical appearance is restricted to the sacral alae and is not pronounced in Regourdou 1 S1 body, the morphology could also have originated a few years after birth, which does not rule out a trauma to the lower limbs as a possible cause leading to asymmetric weight transmission. To assess these possibilities, it is helpful to review other abnormalities in the skeleton.

5.3 | Other skeletal abnormalities in the R1 skeleton

A deviation from bilateral symmetry is, apart from the sacrum, also apparent on upper limb bones, vertebrae, sternum, femora, and tali of the R1 individual. Other abnormalities of different types are present on the ribs and femoral shafts.

The asymmetry of upper limb bones of R1 was first studied by Vandermeersch and Trinkaus (1995). They found marked asymmetry in diaphyseal dimensions of the clavicles, humeri, radii, and ulnae with the right side consistently more robust than the left one concluding it was a physiological asymmetry caused by right-hand dominance. The degree of asymmetry was substantial in comparison with modern humans, but it was closer to the lower margin in the Neandertal range (Vandermeersch & Trinkaus, 1995). More evidence of right-handedness in R1 comes from the direction of scratches on the front teeth which is direct evidence of right-hand dominance (Volpato et al., 2012).

Upper limb asymmetry is often attributed to high levels of habitual behavioral lateralization; however, there are also cases of pathologically induced alterations in the diaphyseal properties of upper limbs that can lead to a similar asymmetric appearance (Churchill & Formicola, 1997; Tesorieri, 2016; Trinkaus et al., 1994). Such asymmetry is caused by muscular or neural dysfunction that leads to a secondary effect of a global or localized bone atrophy, and the cause of the primary dysfunction may not be apparent from the skeleton (Churchill & Formicola, 1997; Trinkaus et al., 1994). Resulting limb asymmetry is not always extreme and could therefore be assessed as a sign of handedness (Churchill & Formicola, 1997). However, if the insult occurred during growth, it would also lead to shortening of the impacted limb bones. In addition, the impaired limb would also show periosteal atrophy in the areas of muscular attachments (Ortner, 2003).

Regourdou 1 does not preserve any pair of complete upper limb long bones allowing measurement of their total length, but the bones seem morphologically congruent and do not show any marked discrepancy in length (Vandermeersch & Trinkaus, 1995). In addition, cross-sectional characteristics do not exhibit an abnormal mechanical pattern (Volpato, Couture, Macchiarelli, & Vandermeersch, 2011), and areas of muscular attachment are of similar extent in both upper limbs, indicating that each was capable of normal physical activity with regard to contemporary fossil humans (Vandermeersch & Trinkaus, 1995). Considering these facts, the asymmetry of R1 upper limbs can be considered as physiological.

Three vertebrae exhibit mild scoliotic signs: the spinous process of the seventh cervical vertebra is mildly rotated, and the larger right articular facets of the second thoracic vertebra and spinous process of the ninth thoracic vertebra are twisted to the left (Gómez-Olivencia et al., 2013). Several vertebrae also exhibit mild osteophytes on their articular facets and bodies, especially in the cervical region (Gómez-Olivencia et al., 2013). The sternum is slightly longer on its right side (Gómez-Olivencia, Franciscus, Couture-Veschambre, Maureille, & Arsuaga, 2012).

The first right rib exhibits a prominent bump on its cranial surface close to its dorsal end. In contrast, the seventh right rib shows an area of porous bone propagation inside the compact bone external surface close to the sternal end (Gómez-Olivencia et al., 2018).

The femoral shafts were described as highly asymmetrical in cross-sectional shape, longitudinal curvature, and expression of the *linea aspera*: the left diaphysis is more circular, less curved and the *linea aspera* is more marked (Maureille et al., 2015). Moreover, on the two femoral diaphyses, we observe abnormal relief (in three areas on the right and two on the left) pushing out the surface of the bone. These two pieces look similar and their unusual morphology is probably related to the same origin. Based on their external appearance, it has been considered that these features could represent calcified subperiosteal hematomas (Madelaine et al., 2008; Maureille et al., 2015). While this hypothesis is unlikely, we must nonetheless question if these areas of femoral bone external relief have the same cause(s) as those observed on the two ribs. Bone remodeling is common in metabolic and infectious diseases and uncommon in developmental abnormalities (Aufderheide & Rodríguez-Martín, 1998; Pinhasi & Mays, 2008), which may imply presence of two different defects. Despite its rare occurrence, it can be the case that an individual had more than one disease affecting the skeleton (Ortner, 2008).

The right talocalcaneal articulation has also been described as asymmetric. In particular, it appears that the tali may have differed in the orientation of their heads (Maureille et al., 2015; Pablos et al., 2019; Vandermeersch & Trinkaus, 1995).

5.4 | Possible associations of the skeletal abnormalities and consequences

Sacral asymmetry certainly relates to asymmetrical load dissipation and therefore the mild scoliosis observed in the presacral vertebrae of R1 could be associated with the sacral asymmetry. In addition, the articular facets of S1 show an asymmetric orientation known as facet tropism that occurs relatively often in modern humans (Kalichman, Suri, Guermazi, Li, & Hunter, 2009)—this is in fact true for our comparative sample. Facet joint orientation is critical in maintaining overall stability of the spine (Noren et al., 1991); superior articular facets face dorsomedially in the lumbosacral region, restricting the range of rotation and thus providing stability with respect to shear forces. Normal variation of the facet angle is approximately between 30 and 70° (Mahato, 2011; Noren et al., 1991), and facet tropism occurs when one of the facets is oriented more mediolaterally. It is not clear how facet tropism originates (Samartzis et al., 2016), but it is a probable risk factor for degenerative diseases such as spondylolisthesis and disc herniation (Dai, 2001; Kim et al., 2013; Lai et al., in press; Noren et al., 1991; Schleich et al., 2016). Coronal orientation of one facet causes increased torsional stress because of abnormal rotation of the lumbar spine (Noren et al., 1991). This leads to greater interfacet shear forces in the more sagittally oriented facet (Giles, 1987) leading to degenerative osteoarthritic changes occurring predominantly on this facet (Giles, 1987; Kalichman et al., 2009). Moreover, trabecular bone is

organized in a network that is adaptively remodeling in response to changes in mechanical loading (Chappard, Baslé, Legrand, & Audran, 2008). Therefore, the preserved trabecular structure may contain direct information about the forces that act on the bone. There are two main trabecular bundles in the sacral base that transfer weight from the S1 body and articular facets to the auricular surfaces (Pal, 1989). Asymmetric pattern of trabecular distribution in R1 sacral base indicates that the longer left sacral ala was loaded more than the right.

It was observed that even mild sacral lateral hypoplasia is associated with pelvic obliquity and thus load transfer imbalance (Ortner, 2003; Pfeiffer, 2011). Pelvic obliquity is defined following the Terminology Committee of the Scoliosis Research Society as a "deviation of the pelvis from the horizontal in the frontal plane" (A Glossary of Scoliosis Terms, 1976, pp. 57–58) which goes hand in hand with leg length discrepancy, and importantly, one can be either a cause or a consequence of the other (Gurney, 2002; Winter & Pinto, 1986). Given that the longitudinal growth of long bones is constrained, leg length discrepancy originates during development and may persist into adulthood when the pelvic obliquity is fixed by muscle contractions either above or below the pelvis (Hefti, 2015; Winter & Pinto, 1986) which should be apparent in femoral cross-sectional geometry. The pelvis of R1 after reassembly also shows certain asymmetry (Meyer, 2013; Trinkaus, 2018), which has not been studied in detail due to the fragmentary preservation of coxal bones.

The skeletal abnormalities of R1 do not exclude one of the proposed mechanisms of origin (developmental or traumatic), but we were able to provide reasonable associations between several of the abnormal asymmetries of lower limbs and spine. Unilateral developmental vertebral anomalies have varying degrees of expression from mild hypoplasia to total aplasia (Barnes, 2012b). Lateral vertebral hypoplasia generally affects thoracic or lumbar vertebrae, but it also appears in one or more sacral segments forming an asymmetrically shaped sacrum (Barnes, 2012b). However, regarding the biomechanics in the sacroiliac joint described in Section 4.1, a trauma causing leg length discrepancy could have led to the same effect and thus a traumatic origin in early childhood cannot be excluded, especially due to the state of preservation of the lower limb long bones of R1. Both developmental and traumatic pathologies are well documented in Late Pleistocene individuals, and are in fact quite abundant (Berger & Trinkaus, 1995; Trinkaus, 2011; Trinkaus, 2012, 2018). However, following Berger and Trinkaus (1995), lower limb pathologies are relatively infrequent in the Neandertal fossil record. These authors hypothesize that this bias could result from the necessity for mobility and the fact that most of the Neandertal fossil record comes from caves and rock shelters (Bar-Yosef, 2013): those not able to keep up (in this case due to leg injuries) would be left behind, and thus chances to be incorporated into the fossil record would decrease. Therefore, rather mild defects of lower limbs are found in the Paleolithic record (Trinkaus, 2012) which raises the question about the necessity of provision of care in the Late Pleistocene societies and in this specimen in particular (Spikins et al., in press; Tilley, 2015).

6 | CONCLUSION

We have demonstrated a high degree of sacral asymmetry in the Regourdou 1 Neandertal individual. The right side of its sacrum shows an abnormal morphology that resulted in an asymmetric conformation of the sacral base. Based on our univariate and multivariate comparisons with modern healthy individuals and preserved Neandertal sacra, the asymmetry is caused by a relatively short ala and a high facet angle on the right side of the sacrum. A high degree of alar asymmetry probably originated in early development. An asymmetric sacrum reflects asymmetric load dissipation, indicated by trabecular bone density, and could relate to other morphological abnormalities observed in the skeleton, especially the mild scoliosis of the spine and the asymmetry of the femoral diaphyses. Additional information on other asymmetries on this skeleton will allow us to test our proposed hypotheses.

ACKNOWLEDGMENTS

This research was supported by the Grant Agency of Charles University (no. 10882) and by Irene Levi Sala CARE Archaeological Foundation. Further support comes from the project "NATCH" convention 2016-1R40240-00007349-00007350 of the Région Nouvelle Aquitaine (B.M., C.C.V.), and the ANR (French National Research Agency) projects: LabEx Sciences archéologiques de Bordeaux, no ANR-10-LABX-52, subproject "NéMo" (B.M., C.C.V.). A.G.O. received support by the Research Group IT1418-19 (Eusko Jaurlaritz-Gobierno Vasco), and by the Spanish *Ministerio de Ciencia, Innovación y Universidades* (project PGC2018-093925-B-C33). T.H. received support from the Louisiana Board of Regents LEQSF(2015-18)-RD-A-22. The micro-CT of the sacrum was funded by a Leakey Foundation grant thanks to the generous donation by Gordon Getty and Cole Thompson. The authors would like to thank Jean-Jacques Cleyet-Merle, head of the Musée national de Préhistoire (Les Eyzies-de-Tayac), and Véronique Merlin-Anglade, head of the Musée d'Art et d'Archéologie du Périgord (Périgueux), for the authorization to study the collections conserved at their institutions. Also, the authors would like to thank the curators of anthropological collections of the Sackler Medical Faculty (Tel Aviv) and Musée de l'Homme (Paris) for providing comparative material. Finally, the authors thank Frederic Santos (PACEA) for his statistical help.

ORCID

Rebeka Rmoutilová  <https://orcid.org/0000-0003-2426-4521>

Asier Gómez-Olivencia  <https://orcid.org/0000-0001-7831-3902>

REFERENCES

- Adams, D. C., & Otárola-Castillo, E. (2013). Geomorph: An R package for the collection and analysis of geometric morphometric shape data. *Methods in Ecology and Evolution*, 4(4), 393–399. <https://doi.org/10.1111/2041-210X.12035>
- Akman, S. D., Karakas, P., & Bozkir, M. G. (2008). Bilateral asymmetry in sacrum and handedness. *Neurosurgery Quarterly*, 18(1), 66–68. <https://doi.org/10.1097/WNQ.0b013e31815ca7f5>

- Auerbach, B. M., & Raxter, M. H. (2008). Patterns of clavicular bilateral asymmetry in relation to the humerus: Variation among humans. *Journal of Human Evolution*, 54(5), 663–674. <https://doi.org/10.1016/j.jhevol.2007.10.002>
- Auerbach, B. M., & Ruff, C. B. (2006). Limb bone bilateral asymmetry: Variability and commonality among modern humans. *Journal of Human Evolution*, 50(2), 203–218. <https://doi.org/10.1016/j.jhevol.2005.09.004>
- Aufderheide, A., & Rodríguez-Martín, C. (1998). *The Cambridge Encyclopedia of human paleopathology*. Cambridge: Cambridge University Press.
- Bar-Yosef, O. (2013). Neanderthals and modern humans across Eurasia. In Akazawa T, Nishiaki Y, Aoki K (Eds.), *Dynamics of Learning in Neanderthals and Modern Humans* (Vol. 1, pp. 7–20). Tokyo: Springer Japan.
- Barker, P. J., Hapuarachchi, K. S., Ross, J. A., Sambaiew, E., Ranger, T. A., & Briggs, C. A. (2014). Anatomy and biomechanics of gluteus maximus and the thoracolumbar fascia at the sacroiliac joint. *Clinical Anatomy*, 27(2), 234–240. <https://doi.org/10.1002/ca.22233>
- Barnes, E. (1994). *Developmental defects of the axial skeleton in paleopathology*. Boulder, CO: University Press of Colorado.
- Barnes, E. (2012a). *Atlas of developmental field anomalies of the human skeleton: A paleopathology perspective*. Hoboken, NJ: Wiley-Blackwell.
- Barnes, E. (2012b). Developmental disorders in the skeleton. In A. L. Grauer (Ed.), *A companion to paleopathology* (pp. 380–400). Oxford: Wiley-Blackwell. <https://doi.org/10.1002/9781444345940.ch21>
- Bartucz, L., & Szabó, J. (1940). Die Mussolini-Höhle (Subalyuk) bei Cserépfalu. *Geologica Hungarica: Series Palaeontologica*, 14, 49–105.
- Bates, D., Bolker, B., Walker, S., Singmann, H., Dai, B., Scheipl, F., ... Green, P. (2018). Random effects models in latent class analysis for evaluating accuracy of diagnostic tests. In *Linear mixed-effects models using "eigen" and S4 contact*. <https://doi.org/10.2307/2533043>
- Been, E., Gómez-Olivencia, A., & Kramer, P. A. (2014). Brief communication: Lumbar lordosis in extinct hominins: Implications of the pelvic incidence. *American Journal of Physical Anthropology*, 154(2), 307–314. <https://doi.org/10.1002/ajpa.22507>
- Been, E., Gómez-Olivencia, A., Shefi, S., Soudack, M., Bastir, M., & Barash, A. (2017). Evolution of spinopelvic alignment in hominins. *The Anatomical Record*, 300(5), 900–911. <https://doi.org/10.1002/ar.23559>
- Been, E., Pessah, H., Peleg, S., & Kramer, P. A. (2013). Sacral orientation in hominin evolution. *Advances in Anthropology*, 3(3), 133–141. <https://doi.org/10.4236/aa.2013.33018>
- Berger, T. D., & Trinkaus, E. (1995). Patterns of trauma among the Neanderthals. *Journal of Archaeological Science*, 22(6), 841–852. [https://doi.org/10.1016/0305-4403\(95\)90013-6](https://doi.org/10.1016/0305-4403(95)90013-6)
- Bollow, M., Braun, J., Kannenberg, J., Biedermann, T., Schauer-Petrowskaja, C., Paris, S., ... Hamm, B. (1997). Normal morphology of sacroiliac joints in children: Magnetic resonance studies related to age and sex. *Skeletal Radiology*, 26(12), 697–704. <https://doi.org/10.1007/s002560050314>
- Bonifay, E. (1964). La grotte de Régourdou (Montignac, Dordogne). *Stratigraphie et industrie lithique moustérienne. L'Anthropologie*, 68, 49–64.
- Bookstein, F. (1991). *Morphometric tools for landmark data: Geometry and biology* (1st ed.). Cambridge: Cambridge University Press. <https://doi.org/10.1017/CBO9780511573064>
- Boule, M. (1911). L'homme fossile de la Chapelle-aux-Saints. *Annales de Paléontologie*, 6, 111–172.
- Bräuer, G. (1988). Osteometrie. In R. Knussmann (Ed.), *Anthropologie. Handbuch der vergleichenden biologie des menschen. Begründet von Rudolf Martin* (pp. 160–231). Stuttgart, Germany: Fischer Verlag.
- Carlson, K. J., & Judex, S. (2007). Increased non-linear locomotion alters diaphyseal bone shape. *Journal of Experimental Biology*, 210(17), 3117–3125. <https://doi.org/10.1242/jeb.006544>
- Carter, D. R. (1987). Mechanical loading history and skeletal biology. *Journal of Biomechanics*, 20(11–12), 1095–1109. [https://doi.org/10.1016/0021-9290\(87\)90027-3](https://doi.org/10.1016/0021-9290(87)90027-3)
- Chapman, T. (2017). *Morphometric, functional and biomechanical analysis of a virtual Neandertal in comparison with anatomically modern humans*. (Unpublished doctoral dissertation). Université libre de Bruxelles, Belgium.
- Chappard, D., Baslé, M. F., Legrand, E., & Audran, M. (2008). Trabecular bone microarchitecture: A review. *Morphologie*, 92(299), 162–170. <https://doi.org/10.1016/j.morpho.2008.10.003>
- Churchill, S. E., & Formicola, V. (1997). A case of marked bilateral asymmetry in the upper limbs of an upper palaeolithic male from Barm Grande (Liguria), Italy. *International Journal of Osteoarchaeology*, 7(1), 18–38. [https://doi.org/10.1002/\(SICI\)1099-1212\(199701\)7:1<18::AID-OA303>3.0.CO;2-R](https://doi.org/10.1002/(SICI)1099-1212(199701)7:1<18::AID-OA303>3.0.CO;2-R)
- Dai, L. Y. (2001). Orientation and tropism of lumbar facet joints in degenerative spondylolisthesis. *International Orthopaedics*, 25, 40–42. <https://doi.org/10.1007/s002640000201>
- Dzupa, V., Slepánek, M., Striz, M., Krbec, M., Chmelova, J., Kachlik, D., & Baca, V. (2014). Developmental malformations in the area of the lumbosacral transitional vertebrae and sacrum: Differences in gender and left/right distribution. *Surgical and Radiologic Anatomy*, 36(7), 689–693. <https://doi.org/10.1007/s00276-013-1250-x>
- Fraipont, C. (1927). Sur l'omoplate et le sacrum de l'homme de Spy. *Revue Anthropologique*, 37, 189–195.
- Fraipont, J., & Lohest, M. (1887). La race humaine de Néanderthal ou de Canstadt en Belgique: Recherches ethnographiques sur des ossements humains découverts dans les dépôts quaternaires d'une grotte à Spy et détermination de leur âge géologique. *Archives de Biologie*, 7, 587–757.
- Giles, L. G. F. (1987). Lumbo-sacral zygapophyseal joint tropism and its effect on hyaline cartilage. *Clinical Biomechanics*, 2(1), 2–6. [https://doi.org/10.1016/0268-0033\(87\)90038-6](https://doi.org/10.1016/0268-0033(87)90038-6)
- Gómez-Olivencia, A., Arlegi, M., Barash, A., Stock, J. T., & Been, E. (2017). The Neandertal vertebral column 2: The lumbar spine. *Journal of Human Evolution*, 106, 84–101. <https://doi.org/10.1016/j.jhevol.2017.01.006>
- Gómez-Olivencia, A., Barash, A., García-Martínez, D., Arlegi, M., Kramer, P., Bastir, M., & Been, E. (2018). 3D virtual reconstruction of the Kebara 2 Neandertal thorax. *Nature Communications*, 9(1), 4387. <https://doi.org/10.1038/s41467-018-06803-z>
- Gómez-Olivencia, A., Carretero, J. M., Arsuaga, J. L., Rodríguez-García, L., García-González, R., & Martínez, I. (2007). Metric and morphological study of the upper cervical spine from the Sima de los Huesos site (Sierra de Atapuerca, Burgos, Spain). *Journal of Human Evolution*, 53(1), 6–25. <https://doi.org/10.1016/j.jhevol.2006.12.006>
- Gómez-Olivencia, A., Couture-Veschambre, C., Madelaine, S., & Maureille, B. (2013). The vertebral column of the Regourdou 1 Neandertal. *Journal of Human Evolution*, 64(6), 582–607. <https://doi.org/10.1016/j.jhevol.2013.02.006>
- Gómez-Olivencia, A., Franciscus, R. G., Couture-Veschambre, C., Maureille, B., & Arsuaga, J. L. (2012). The mesosternum of the Regourdou 1 Neandertal revisited. *Journal of Human Evolution*, 62(4), 511–519. <https://doi.org/10.1016/j.jhevol.2012.01.004>
- Gómez-Olivencia, A., Holliday, T., Madelaine, S., Couture-Veschambre, C., & Maureille, B. (2019). The costal skeleton of the Regourdou 1 Neandertal. *Journal of Human Evolution*, 130, 151–171. <https://doi.org/10.1016/j.jhevol.2017.12.005>
- Gunz, P., Mitteroecker, P., Neubauer, S., Weber, G. W., & Bookstein, F. L. (2009). Principles for the virtual reconstruction of hominin crania. *Journal of Human Evolution*, 57(1), 48–62. <https://doi.org/10.1016/j.jhevol.2009.04.004>
- Gurney, B. (2002). Leg length discrepancy. *Gait & Posture*, 15(2), 195–206. [https://doi.org/10.1016/S0966-6362\(01\)00148-5](https://doi.org/10.1016/S0966-6362(01)00148-5)

- Hefti, F. (2015). *Pediatric orthopedics in practice*. Berlin: Springer. <https://doi.org/10.1007/978-3-662-46810-4>
- Kalichman, L., Suri, P., Guermazi, A., Li, L., & Hunter, D. J. (2009). Facet orientation and tropism: Associations with facet joint osteoarthritis and degenerative spondylolisthesis. *Spine*, 34(16), E579–E585. <https://doi.org/10.1097/BRS.0b013e3181aa2acb>
- Kim, H., Chun, H., Lee, H., Kang, K., Lee, C., Chang, B., & Yeom, J. S. (2013). The biomechanical influence of the facet joint orientation and the facet tropism in the lumbar spine. *The Spine Journal*, 13, 1301–1308. <https://doi.org/10.1016/j.spinee.2013.06.025>
- Klingenberg, C. P. (2003). A developmental perspective on developmental instability: Theory, models and mechanisms. In M. Polak (Ed.), *Developmental instability: Causes and consequences*. New York, NY: Oxford University Press.
- Klingenberg, C. P. (2011). MorphoJ: An integrated software package for geometric morphometrics. *Molecular Ecology Resources*, 11, 353–357. <https://doi.org/10.1111/j.1755-0998.2010.02924.x>
- Klingenberg, C. P. (2015). Analyzing fluctuating asymmetry with geometric morphometrics: Concepts, methods, and applications. *Symmetry*, 7(2), 843–934. <https://doi.org/10.3390/sym7020843>
- Klingenberg, C. P., Barluenga, M., & Meyer, A. (2002). Shape analysis of symmetric structures: Quantifying variation among individuals and asymmetry. *Evolution*, 56(10), 1909–1920. <https://doi.org/10.1111/j.0014-3820.2002.tb00117.x>
- Klingenberg, C. P., & Montero, L. R. (2005). Distances and directions in multidimensional shape spaces: Implications for morphometric applications. *Systematic Biology*, 54(4), 678–688. <https://doi.org/10.1080/10635150590947258>
- Kubicka, A. M., Nowaczewska, W., Balzeau, A., & Piontek, J. (2018). Bilateral asymmetry of the humerus in Neandertals, Australian aborigines and medieval humans. *American Journal of Physical Anthropology*, 167(1), 46–60. <https://doi.org/10.1002/ajpa.23601>
- Kujanová, M., Bigoni, L., Velemínská, J., & Velemínský, P. (2008). Limb bones asymmetry and stress in medieval and recent populations of Central Europe. *International Journal of Osteoarchaeology*, 18(5), 476–491. <https://doi.org/10.1002/oa.958>
- Lai, Q., Dai, M., Liu, Y., Zhang, B., Guo, R., Lv, X., ... Zhu, J. (2019). A study of lumbar disc herniation and facet joint asymmetry. *International Surgery*, 103, 87–94. <https://doi.org/10.9738/INTSURG-D-16-00119.1>
- Linstrom, N. J., Heiserman, J. E., Kortman, K. E., Crawford, N. R., Baek, S., Anderson, R. L., ... Dean, B. L. (2009). Anatomical and biomechanical analyses of the unique and consistent locations of sacral insufficiency fractures. *Spine*, 34(4), 309–315. <https://doi.org/10.1097/BRS.0b013e318191ea01>
- Lovejoy, C. O., Meindl, R. S., Pryzbeck, T. R., & Mensforth, R. P. (1985). Chronological metamorphosis of the auricular surface of the ilium: A new method for the determination of adult skeletal age at death. *American Journal of Physical Anthropology*, 68(1), 15–28. <https://doi.org/10.1002/ajpa.1330680103>
- Madelaine, S., Maureille, B., Cavanhié, N., Couture, C., Bonifay, E., Armand, D., ... Vandermeersch, B. (2008). Nouveaux restes humains moustériens rapportés au squelette néandertalien de Regourdou 1 (Regourdou, commune de Montignac, Dordogne, France). *PALEO*, 20(2008), 101–113.
- Mahato, N. K. (2011). Facet dimensions, orientation, and symmetry at L5-S1 junction in lumbosacral transitional states. *Spine*, 36(9), 569–573. <https://doi.org/10.1097/BRS.0b013e3181f6ecb2>
- Martin, R. (1928). *Lehrbuch der anthropologie in systematischer darstellung* (2nd ed.). Jena: Gustav Fischer.
- Masnicová, S., & Beňuš, R. (2003). Developmental anomalies in skeletal remains from the great Moravia and middle ages cemeteries at Devín (Slovakia). *International Journal of Osteoarchaeology*, 13(5), 266–274. <https://doi.org/10.1002/oa.684>
- Maureille, B., Gómez-Olivencia, A., Couture-Veschambre, C., Madelaine, S., & Holliday, T. (2015). Nouveaux restes humains provenant du gisement de Regourdou (Montignac-sur-Vézère, Dordogne, France). *PALEO*, 26, 117–138.
- Maureille, B., Holliday, T. W., Royer, A., Pelletier, M., Couture-Veschambre, C., Discamps, E., ... Turq, A. (2016). New data on the possible Neandertal burial at Regourdou (Montignac-sur-Vézère, Dordogne, France). In Lauwers M, Zémour A, (Eds.), *Qu'est-ce qu'une sépulture? Humanités et systèmes funéraires de la Préhistoire à nos jours : XXXVIèmes Rencontres internationales d'archéologie et d'histoire d'Antibes* (pp. 175–191). Antibes: Editions APDCA.
- Maureille, B., Rougier, H., Houet, F., & Vandermeersch, B. (2001). Les dents inférieures du Neandertalien Regourdou 1 (site de Regourdou, commune de Montignac, Dordogne): Analyses métriques et comparatives. *PALEO*, 13, 183–200. <https://doi.org/10.1097/BRS.0b013e3181aa2acb>
- Meyer, V. (2013). *Apport de la reconstruction virtuelle du bassin Regourdou 1 (Dordogne, France) à la connaissance de l'obstétrique Néandertalienne*. (Unpublished doctoral dissertation). Université Bordeaux 1, France.
- Meyer, V., Brůžek, J., Couture, C., Madelaine, S., & Maureille, B. (2011). Un nouveau bassin néandertalien: Description morphologique des restes pelviens de Regourdou 1 (Montignac, Dordogne, France). *PALEO*, 22, 207–222.
- Milella, M., Zollikofer, C. P. E., & Ponce de León, M. S. (2015). Virtual reconstruction and geometric morphometrics as tools for paleopathology: A new approach to study rare developmental disorders of the skeleton. *The Anatomical Record*, 298(2), 335–345. <https://doi.org/10.1002/ar.23020>
- Mizrahi, J., Verbitsky, O., & Isakov, E. (2000). Shock accelerations and attenuation in downhill and level running. *Clinical Biomechanics*, 15(1), 15–20. [https://doi.org/10.1016/S0268-0033\(99\)00033-9](https://doi.org/10.1016/S0268-0033(99)00033-9)
- Nishi, K., Saiki, K., Imamura, T., Okamoto, K., Wakebe, T., Ogami, K., ... Tsurumoto, T. (2017). Degenerative changes of the sacroiliac auricular joint surface—Validation of influential factors. *Anatomical Science International*, 92(4), 530–538. <https://doi.org/10.1007/s12565-016-0354-x>
- Nissinen, M. J., Heliövaara, M. M., Seitsamo, J. T., Könönen, M. H., Hurmerinta, K. A., & Poussa, M. S. (2000). Development of trunk asymmetry in a cohort of children ages 11 to 22 years. *Spine*, 25(5), 570–574. <https://doi.org/10.1097/00007632-200003010-00007>
- Noren, R., Trafimow, J., Andersson, G. B. J., & Huckman, M. S. (1991). The role of facet joint tropism and facet angle in disc degeneration. *Spine*, 16(5), 530–532.
- O'Rahilly, R., Müller, F., & Meyer, D. B. (1990). The human vertebral column at the end of the embryonic period proper. 4. The sacrococcygeal region. *Journal of Anatomy*, 168, 95–111.
- Ortner, D. (2003). *Identification of pathological conditions in human skeletal remains* (2nd ed.). Amsterdam: Academic Press.
- Ortner, D. (2008). Differential diagnosis of skeletal lesions in infectious disease. In R. Pinhasi & S. Mays (Eds.), *Advances in human paleopathology* (pp. 191–215). Chichester: John Wiley & Sons.
- Pablos, A., Gómez-Olivencia, A., Maureille, B., Holliday, T. W., Madelaine, S., Trinkaus, E., & Couture-Veschambre, C. (2019). Neandertal foot remains from Regourdou 1 (Montignac-sur-Vézère, Dordogne, France). *Journal of Human Evolution*, 128, 17–44. <https://doi.org/10.1016/j.jhevol.2018.11.003>
- Pal, G. P. (1989). Weight transmission through the sacrum in man. *Journal of Anatomy*, 162, 9–17.
- Palmer, A. R., & Strobeck, C. (1986). Fluctuating asymmetry: Measurement, analysis, patterns. *Annual Review of Ecology and Systematics*, 17, 391–421. <https://doi.org/10.1146/annurev.es.17.110186.002135>
- Pap, I., Tillier, A.-M., Arensburg, B., & Chech, M. (1996). The Subalyuk Neandertal remains (Hungary): A re-examination. *Annales Historico-Naturales Musei Nationalis Hungarici*, 88, 233–270.
- Passalacqua, N. V. (2009). Forensic age-at-death estimation from the human sacrum. *J Forensic Sci*, 54, 255–262.

- Peleg, S., Dar, G., Medlej, B., Steinberg, N., Masharawi, Y., Latimer, B., ... HersHKovitz, I. (2007). Orientation of the human sacrum: Anthropological perspectives and methodological approaches. *American Journal of Physical Anthropology*, 133(3), 967–977. <https://doi.org/10.1002/ajpa.20599>
- Pelletier, M., Royer, A., Holliday, T. W., Discamps, E., Madelaine, S., & Maureille, B. (2017). Rabbits in the grave! Consequences of bioturbation on the Neandertal "burial" at Regourdou (Montignac-Sur-Vézère, Dordogne). *Journal of Human Evolution*, 110, 1–17. <https://doi.org/10.1016/j.jhevol.2017.04.001>
- Pfeiffer, S. (2011). Pelvic stress injuries in a small-bodied forager. *International Journal of Osteoarchaeology*, 21(6), 694–703. <https://doi.org/10.1002/oa.1176>
- Pinhasi, R., & Mays, S. (2008). *Advances in human palaeopathology*. Chichester: John Wiley & Sons.
- Pitre, M. C., & Lovell, N. C. (2010). A sacral anomaly from the quaker cemetery, Kingston-upon-Thames, England. *International Journal of Osteoarchaeology*, 20(3), 351–357. <https://doi.org/10.1002/oa.1034>
- Piveteau, J. (1959). Les restes humains de la grotte de Regourdou (Dordogne). *Comptes Rendus de l'Académie des Sciences de Paris, Série D*, 40–44.
- Plavcan, J. M., Meyer, V., Hammond, A. S., Couture, C., Madelaine, S., Holliday, T. W., ... Trinkaus, E. (2014). The Regourdou 1 Neandertal body size. *Comptes Rendus Palevol*, 13(8), 747–754. <https://doi.org/10.1016/j.crpv.2014.07.003>
- Plochocki, J. H. (2002). Directional bilateral asymmetry in human sacral morphology. *International Journal of Osteoarchaeology*, 12(5), 349–355. <https://doi.org/10.1002/oa.633>
- Rak, Y. (1991). The pelvis. In O. Bar-Yosef & B. Vandermeersch (Eds.), *Le squelette moustérien de Kebara 2* (pp. 147–182). Paris: Editions du CNRS.
- RStudio Team. (2016). *RStudio: Integrated development for R*. Boston, MA: RStudio.
- Rueden, C. T., Schindelin, J., Hiner, M. C., DeZonia, B. E., Walter, A. E., Arena, E. T., & Eliceiri, K. W. (2017). ImageJ2: ImageJ for the next generation of scientific image data. *BMC Bioinformatics*, 18(1), 529. <https://doi.org/10.1186/s12859-017-1934-z>
- Ruff, C., Holt, B., & Trinkaus, E. (2006). Who's afraid of the big bad Wolff?: "Wolff's law" and bone functional adaptation. *American Journal of Physical Anthropology*, 129(4), 484–498. <https://doi.org/10.1002/ajpa.20371>
- Ruff, C., Trinkaus, E., Walker, A., & Larsen, C. S. (1993). Postcranial robusticity in homo. I: Temporal trends and mechanical interpretation. *American Journal of Physical Anthropology*, 91(1), 21–53. <https://doi.org/10.1002/ajpa.1330910103>
- Rusk, K. M., & Ousley, S. D. (2016). An evaluation of sex- and ancestry-specific variation in sacral size and shape using geometric morphometrics. *American Journal of Physical Anthropology*, 159(4), 646–654. <https://doi.org/10.1002/ajpa.22926>
- Samartzis, D., Cheung, J. P. Y., Rajasekaran, S., Kawaguchi, Y., Acharya, S., Kawakami, M., ... Williams, R. (2016). Is lumbar facet joint tropism developmental or secondary to degeneration? An international, large-scale multicenter study by the AOSpine Asia Pacific Research Collaboration Consortium. *Scoliosis and Spinal Disorders*, 11(1), 2–9. <https://doi.org/10.1186/s13013-016-0062-2>
- Sawyer, G. J., & Maley, B. (2005). Neandertal reconstructed. *The Anatomical Record*, 283, 23–31. <https://doi.org/10.1002/ar.b.20057>
- Scheuer, L., & Black, S. (2000). *Developmental juvenile osteology*. San Diego, CA: Elsevier Academic Press.
- Schiess, R., Boeni, T., Rühli, F., & Haeusler, M. (2014). Revisiting scoliosis in the KNM-WT 15000 *Homo erectus* skeleton. *Journal of Human Evolution*, 67(1), 48–59. <https://doi.org/10.1016/j.jhevol.2013.12.009>
- Schlager, S. (2016). *Morpho: Calculations and visualisations related to geometric morphometrics*. <https://cran.r-project.org/web/packages/Morpho/index.html>
- Schleich, C., Müller-Lutz, A., Blum, K., Boos, J., Bittersohl, B., Schmitt, B., ... Miese, F. (2016). Facet tropism and facet joint orientation: Risk factors for the development of early biochemical alterations of lumbar intervertebral discs. *Osteoarthritis and Cartilage*, 24(10), 1761–1768. <https://doi.org/10.1016/j.joca.2016.05.004>
- Schunke, G. B. (1938). The anatomy and development of the sacro-iliac joint in man. *The Anatomical Record*, 72(3), 313–331. <https://doi.org/10.1002/ar.1090720306>
- Scolan, H., Santos, F., Tillier, A.-M., Maureille, B., & Quintard, A. (2012). Des nouveaux vestiges néandertaliens à Las Pélénos (Monsempron-Libos, Lot-et-Garonne, France). *Bulletins et Mémoires de La Société d'Anthropologie de Paris*, 24(1–2), 69–95. <https://doi.org/10.1007/s13219-011-0047-x>
- Shaw, C. N., Hofmann, C. L., Petraglia, M. D., Stock, J. T., & Gottschall, J. S. (2012). Neandertal humeri may reflect adaptation to scraping tasks, but not spear thrusting. *PLoS One*, 7(7), 1–8. <https://doi.org/10.1371/journal.pone.0040349>
- Sparacello, V. S., Villotte, S., Shackelford, L. L., & Trinkaus, E. (2017). Patterns of humeral asymmetry among late Pleistocene humans. *Comptes Rendus Palevol*, 16(5–6), 680–689. <https://doi.org/10.1016/j.crpv.2016.09.001>
- Spikins, P., Needham, A., Wright, B., Dytham, C., Gatta, M., & Hitchens, G. (in press). Living to fight another day: The ecological and evolutionary significance of Neanderthal healthcare. *Quaternary Science Reviews Special Issue*, 217, 98–118.
- Steinke, H., Hammer, N., Slowik, V., Stadler, J., Josten, C., Böhme, J., & Spänel-Borowski, K. (2010). Novel insights into the sacroiliac joint ligaments. *Spine*, 35(3), 257–263. <https://doi.org/10.1097/BRS.0b013e3181b7c675>
- Storm, R. A. (2009). *Human skeletal asymmetry: A study of directional and fluctuating asymmetry in assessing health, environmental conditions, and social status in English populations from the 7th to the 19th centuries*. (Unpublished doctoral dissertation). University of Bradford, Bradford, England.
- Tague, R. G. (2000). Do big females have big pelves? *American Journal of Physical Anthropology*, 112(3), 377–393. [https://doi.org/10.1002/1096-8644\(200007\)112:3<377::AID-AJPA8>3.0.CO;2-O](https://doi.org/10.1002/1096-8644(200007)112:3<377::AID-AJPA8>3.0.CO;2-O)
- Tague, R. G. (2007). Costal process of the first sacral vertebra: Sexual dimorphism and obstetrical adaptation. *American Journal of Physical Anthropology*, 132(3), 395–405. <https://doi.org/10.1002/ajpa.20531>
- Tesorieri, M. (2016). Differential diagnosis of pathologically induced upper and lower limb asymmetry in a burial from late medieval Ireland (CE 1439–1511). *International Journal of Paleopathology*, 14, 46–54. <https://doi.org/10.1016/j.ijpp.2016.04.003>
- The Terminology Committee of the Scoliosis Research Society has compiled the present publication. (1976). A Glossary of Scoliosis Terms. *Spine*, 1(1), 57–58.
- Tilley, L. (2015). Care among the Neandertals: La Chapelle-aux-saints 1 and La Ferrassie 1 (case study 2). In *Theory and practice in the bioarchaeology of care* (pp. 219–257). Cham: Springer International Publishing. https://doi.org/10.1007/978-3-319-18860-7_9
- Tobolsky, V. A., Kurki, H. K., & Stock, J. T. (2016). Patterns of directional asymmetry in the pelvis and pelvic canal. *American Journal of Human Biology*, 28(6), 804–810. <https://doi.org/10.1002/ajhb.22870>
- Trinkaus, E. (1983). *The Shanidar Neandertals*. New York, NY: Academic Press.
- Trinkaus, E. (2011). Late Pleistocene adult mortality patterns and modern human establishment. *Proceedings of the National Academy of Sciences of the United States of America*, 108(4), 1267–1271. <https://doi.org/10.1073/pnas.1018700108>
- Trinkaus, E. (2012). Neandertals, early modern humans, and rodeo riders. *Journal of Archaeological Science*, 39(12), 3691–3693. <https://doi.org/10.1016/j.jas.2012.05.039>

- Trinkaus, E. (2018). An abundance of developmental anomalies and abnormalities in Pleistocene people. *Proceedings of the National Academy of Sciences of the United States of America*, 115, 11941–11946. <https://doi.org/10.1073/pnas.1814989115>
- Trinkaus, E., Churchill, S. E., & Ruff, C. B. (1994). Postcranial robusticity in homo. II: Humeral bilateral asymmetry and bone plasticity. *American Journal of Physical Anthropology*, 93(1), 1–34. <https://doi.org/10.1002/ajpa.1330930102>
- Turq, A., Jaubert, J., Maureille, B., & Laville, D. (2008). Le cas des sépultures néandertaliennes du Sud-Ouest: et si on les vieillissait? In B. Vandermeersch, J.-J. Cleyet-Merle, J. Jaubert, B. Maureille, & A. Turq (Eds.), *Première humanité, gestes funéraires des Néandertaliens* (pp. 40–41). Paris: Réunion des Musées Nationaux.
- Vallois, H. V. (1965). Le sternum néandertalien du Regourdou. *Anthropologischer Anzeiger*, 29, 273–289.
- Van Dongen, S., Molenberghs, G., & Matthysen, E. (1999). The statistical analysis of fluctuating asymmetry: REML estimation of a mixed regression model. *Journal of Evolutionary Biology*, 12(1), 94–102. <https://doi.org/10.1046/j.1420-9101.1999.00012.x>
- Vandermeersch, B., & Trinkaus, E. (1995). The postcranial remains of the Régourdou 1 Neandertal: The shoulder and arm remains. *Journal of Human Evolution*, 28(5), 439–476. <https://doi.org/10.1006/jhev.1995.1034>
- Vleeming, A., Schuenke, M. D., Masi, A. T., Carreiro, J. E., Danneels, L., & Willard, F. H. (2012). The sacroiliac joint: An overview of its anatomy, function and potential clinical implications. *Journal of Anatomy*, 221(6), 537–567. <https://doi.org/10.1111/j.1469-7580.2012.01564.x>
- Vleeming, A., Volkers, A., Snijders, C., & Stoeckart, R. (1990). Relation between form and function in the sacroiliac joint. Part II: Biomechanical aspects. *Spine*, 13, 133–136.
- Volpato, V., Couture, C., Macchiarelli, R., & Vandermeersch, B. (2011). Endostructural characterisation of the Regourdou 1 Neandertal proximal arm: Bilateral asymmetry and handedness. In S. Condemi & G.-C. Weniger (Eds.), *Continuity and discontinuity in the peopling of Europe : One hundred fifty years of Neandertal study* (pp. 175–178). Dordrecht: Springer. https://doi.org/10.1007/978-94-007-0492-3_15
- Volpato, V., Macchiarelli, R., Guatelli-Steinberg, D., Fiore, I., Bondioli, L., & Frayer, D. W. (2012). Hand to mouth in a Neandertal: Right-handedness in Regourdou 1. *PLoS One*, 7(8), 3–8. <https://doi.org/10.1371/journal.pone.0043949>
- von Cramon-Taubadel, N., Frazier, B. C., & Lahr, M. M. (2007). The problem of assessing landmark error in geometric Morphometrics: Theory, methods, and modification. *American Journal of Physical Anthropology*, 134, 24–35. <https://doi.org/10.1002/ajpa>
- Wickham, H. (2017). Easily install and load the "Tidyverse." <https://cran.r-project.org/web/packages/tidyverse/tidyverse.pdf>
- Winter, R. B., & Pinto, W. C. (1986). Pelvic obliquity. Its causes and its treatment. *Spine*, 11(3), 225–234.
- Zurmühle, C. A., Milella, M., Steppacher, S. D., Hanke, M. S., Albers, C. E., & Tannast, M. (2017). ArtiFacts: Femoroacetabular impingement—A new pathology? *Clinical Orthopaedics and Related Research*, 475(4), 973–980. <https://doi.org/10.1007/s11999-017-5270-4>

SUPPORTING INFORMATION

Additional supporting information may be found online in the Supporting Information section at the end of this article.

How to cite this article: Rmoutilová R, Gómez-Olivencia A, Brůžek J, et al. A case of marked bilateral asymmetry in the sacral alae of the Neandertal specimen Regourdou 1 (Périgord, France). *Am J Phys Anthropol*. 2019;1–18. <https://doi.org/10.1002/ajpa.23968>

Supplementary information for “A case of marked bilateral asymmetry in the sacral alae of the Neandertal specimen Regourdou 1 (Périgord, France)”

Rmoutilová et al.

Table of contents

Supplementary information: Error of measurement (p. 2–4)

Table S1. Adult Neandertal specimens with preserved parts of the sacrum.

Table S2. Intraobserver error of projected landmarks (in mm). Side of bilateral landmarks is indicated by letters R or L.

Table S3. Intraobserver error of linear measurements (in mm or °). Side of bilateral measurements is indicated by letters R or L.

Table S4. Comparison of sacral measurements for Neandertal specimens measured by us on original and virtual model and published data.

Supplementary information: Correction of taphonomic distortion (p. 5–6)

Figure S1. Correction of the Kebara 2 sacrum.

Figure S2. Correction of the La Chapelle-aux-Saints 1 sacrum.

Supplementary information: Cross-sections of Regourdou 1 sacrum (p. 7)

Figure S3. Cross-sections of Regourdou 1 sacrum.

Supplementary bibliography (p. 8)

Table S1. Adult Neandertal specimens with preserved parts of sacrum.

Specimen	Geography	MIS	Sex	Age	Preservation	Fusion of sacral elements	Description of sacral abnormalities	Reference	Use in our study
La Ferrassie 1	Western Europe	3	M	> 40	very fragmentary	S1-S2 unfused ventrally	-	(Heim, 1976)	-
La Ferrassie 2	Western Europe	3	F	20-30	a fragment of S1 body	-	Uncertain sacralization	(Heim, 1976)	-
LCAS1	Western Europe	3	M	30-40	right portion	-	-	(Boule, 1911; Trinkaus, 2011; Gómez-Olivencia, 2013)	3D scan
Las Palomas 96	Western Europe	3	F	16-20	largely complete without left portion, embedded in breccia	All elements unfused ventrally	-	(Walker et al., 2011)	-
Regourdou 1	Western Europe	4-5	I	20-30	upper portion	Fully fused	(Description in this study)	(references in the main text)	3D scan
Spy 2	Western Europe	5	M		right portion	-	-	(Semal et al., 2009)	metric data
Subalyuk 1	Central Europe	3	F?	young adult	upper portion	Unfused neural arches between S1 and S2; fully fused bodies	Apparent possible asymmetry in sacral alae	(Pap et al., 1996)	metric data
Kebara 2	Mediterranean Levant	3	M	25-40	complete, slightly distorted	S1-S2 unfused ventrally; unfused neural arches between S1 and S2	Presence of dorsal apophyseal facets between S1 and S2; presence of unfused pyramidal sacroiliac apophyseal plates	(Bar-Yosef and Vandermeersch, 1991; Karasik et al., 1998)	3D scan
Shanidar 1	Middle East	3-4	M	> 30	complete, slightly distorted	Fully fused	Deep sacral hiatus	(Trinkaus, 1983)	metric data
Shanidar 3	Middle East	3-4	M	> 30	mainly complete, reconstructed right ala	S1-S2 unfused ventrally	2 last ventral foramina greater on the right side; reduced left 4th dorsal foramen (pinhole)	(Trinkaus, 1983)	metric data
Shanidar 4	Middle East	3-4	M	> 30	lower portion from S2	S2-S3 unfused ventrally; S4-S5 unfused	Deep sacral hiatus	(Trinkaus, 1983)	-

Table S2. Intraobserver error of projected landmarks (in mm). Side of bilateral landmarks is indicated by letters R or L.

Landmark	Median	Minimum	Maximum
pr	0.43	0.13	1.03
mp	0.54	0.19	1.22
lsR	0.54	0.09	2.09
lsL	0.66	0.13	2.18
oaR	0.39	0.05	0.72
oaL	0.42	0.10	1.01
opR	0.72	0.02	2.17
opL	0.67	0.06	2.40
aaR	0.56	0.11	1.38
aaL	0.52	0.07	1.70
alR	0.87	0.11	2.11
alL	0.78	0.17	2.29
apR	0.45	0.11	1.73
apL	0.49	0.08	1.46
pbR	0.30	0.04	0.92
pbL	0.28	0.08	0.78
pmR	0.42	0.07	1.88
pmL	0.54	0.16	3.49
plR	0.35	0.04	1.12
plL	0.32	0.02	1.12
c	0.55	0.07	1.65
Mean	0.51	0.09	1.64

Table S3. Intraobserver error of linear measurements (in mm or °). Side of bilateral measurements is indicated by letters R or L.

Measurement	Median	Relative error (%)	Minimum	Maximum
SB	0.25	0.22	0.02	1.26
S1AP	0.32	1.06	0.01	1.08
S1T	0.40	0.77	0.03	2.52
CAP	0.44	2.33	0.00	1.85
CT	0.25	0.81	0.00	0.92
AB_R	0.36	0.82	0.01	1.50
AB_L	0.36	0.82	0.02	1.37
AAL_R	0.28	0.85	0.03	0.98
AAL_L	0.37	1.17	0.01	1.75
LAL_R	0.34	1.11	0.00	1.83
LAL_L	0.32	0.94	0.00	1.16
PAL_R	0.33	1.06	0.01	1.05
PAL_L	0.40	1.39	0.03	1.19
FA_R	1.44	2.85	0.18	4.68
FA_L	1.27	2.41	0.09	2.77

Table S4. Comparison of sacral measurements for Neandertal specimens measured by us on original and virtual model and published data.

Variable	Regourdou 1			Kebara 2			La Chapelle-aux Saints 1	
	Literature	Original	Virtual	Literature	Original	Virtual	Literature	Virtual
SB	104.0 [†] / 106.0 [‡]	105.2	103.7	122.0 [¶]	121.5	120.8 (118.5)	102.0 [‡] / 100.0 ^{††}	103.3
S1AP	32.0 [‡]	31.9	29.8	33.0 [¶]	31.2	30.4	23.0 [†]	24.5
S1T	51.8 [†]	50.5	49.6	55.0 [¶]	53.4	53.0	50.9 [†] / 48.0 ^{††}	44.4
CAP	-	-	23.2	-	21.8	-	-	22.3
CT	-	-	32.9	-	28.8	30.1	-	31.1
LAL_R	23.0 ^{†,§}	25.7	24.8	33.5 ^{†,§}	35.9	33.7	24.6 ^{†,§} / 26.0 ^{§,††}	28.8
LAL_L	29.0 ^{†,§}	31.7	29.3	-	38.4	36.2 (33.0)	-	-

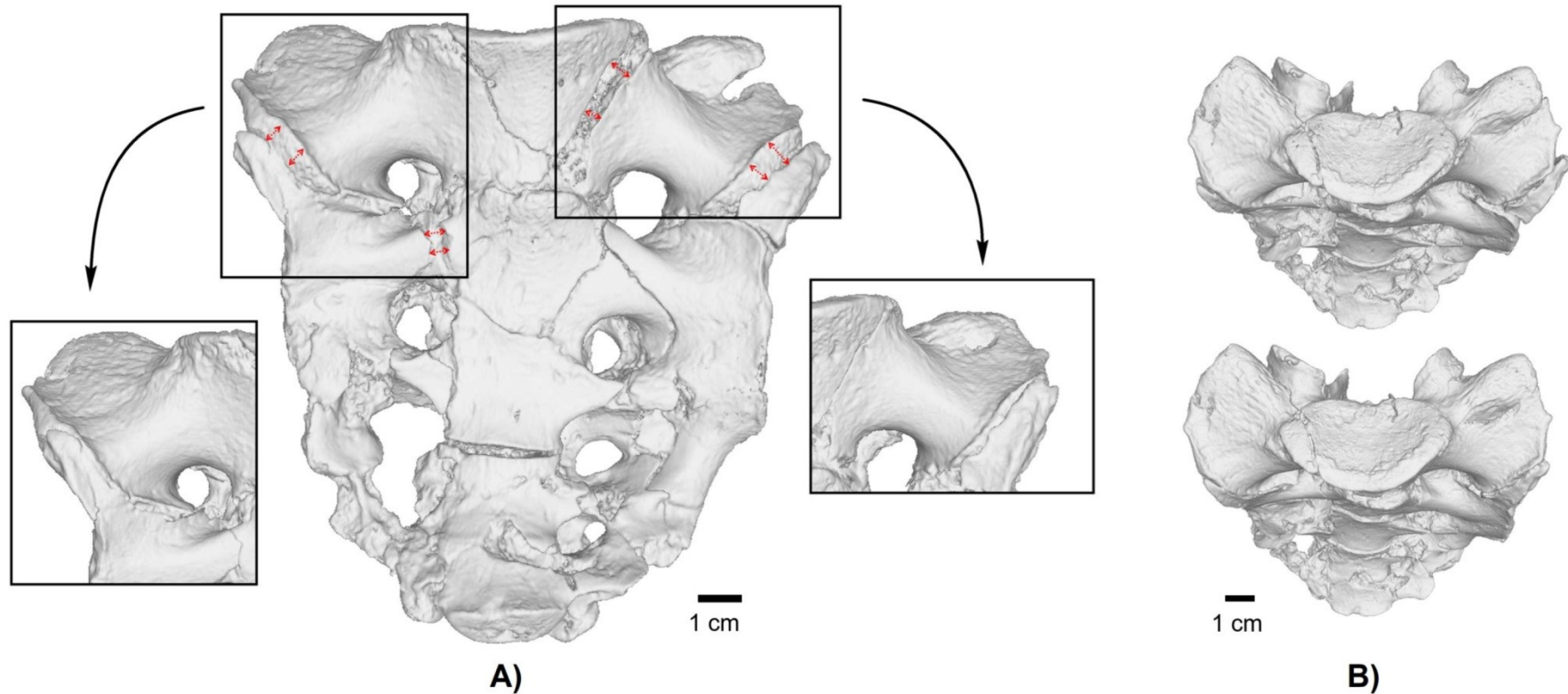
Values after virtual correction of Kebara 2 sacrum are given in parentheses.

[†]Meyer (2013), [‡]Holliday (1995), [§]computed from SB and S1T, [¶]Bar-Yosef and Vandermeersch (1991), ^{††}Trinkaus (2011).

Description: Paleoanthropological specimens are often analyzed using virtual tools (Macchiarelli et al., 2008; Bondioli et al., 2010; Uldin, 2017), but data obtained virtually are usually compared to those acquired on original specimens (e.g., Plavcan et al., 2014; Corron et al., 2017). Therefore, due to further comparisons with published data, several linear dimensions of Neandertal specimens were also measured on original specimens and compared to already published data and to those values measured virtually on 3D models (Supplementary Table S4). Differences between published and our measurements of original specimens ranged between -2.7 and 1.8 mm with a mean difference very close to zero (-0.3 mm). Differences between our measurements of original and virtual specimens ranged between -1.3 and 2.4 mm with a mean difference of 1.1 mm. Absolute mean differences between published data and our own data and between measurements on original vs. virtual specimens did not differ greatly (1.5 and 1.4 mm respectively), but there is a slight bias towards lower values in virtual measurements which tend to be 1 mm smaller than measurements on original specimens. This tendency is expectable regarding the fact that in the virtual approach landmarks are necessarily placed on the surface, but the magnitude is negligible.

For Kebara 2, uncorrected data were used in the evaluation of measurement error between different modes of recording. However, virtual correction (Supplementary Figure S1) noticeably changed values of sacral breadth and length of the left ala (Supplementary Table S4) which is more distorted than the right one corresponding to the severely distorted left hip bone. Both measurements are shorter after virtual correction and the length of the left ala is thus closer to its right counterpart (Supplementary Table S4). The corrected values are used in subsequent analyses.

Figure S1. Correction of the Kebara 2 sacrum. A: Original sacrum with major fissures (red arrows) that served as a guide for the correction. B: a) original sacrum in supero-anterior view, b) corrected sacrum in supero-anterior view, c) superimposed original (grey) and corrected sacrum (transparent red) in superior view.



Description: The Kebara 2 sacrum shows both developmental deformation and taphonomic distortion. There are several elements that remained unfused during ontogenetic development and that were shifted relative to each other due to taphonomic processes which resulted in a distorted shape of the sacral base. The first sacral vertebra (S1) is not fully fused with the rest of the sacrum and there was also a persistent synchondrosis between the lateral masses at this level. On the left side there was an unfused pyramidal apophysis attached to the lateral masses of S1 and S2 (Bar-Yosef and Vandermeersch, 1991). The correction of the sacrum aimed to obtain an image of the sacral base before the taphonomic processes affected its shape. Therefore, the unfused elements affecting the sacral base shape were split into independent pieces and reassembled according to major cracks and gaps. Major differences are on the left side where the ala was more heavily crushed in the antero-posterior direction which corresponds to the taphonomic distortion of the left coxal bone.

Figure S2. Correction of the La Chapelle-aux-Saints 1 sacrum. A: Original sacrum. B: Corrected sacrum.

Description: In LCAS1, the posterior wall of the sacral canal is glued to the rest of the bone and is poorly aligned as described in Gómez-Olivencia (2013). Therefore, this part was aligned correctly along the post-mortem crack in order to capture sacral canal variables.

A missing portion of the promontory in LCAS1 precluded placing the landmark on the promontorium so the position of this landmark was estimated with R package *Morpho* (command *fitLMtps*) (Schlager, 2016).

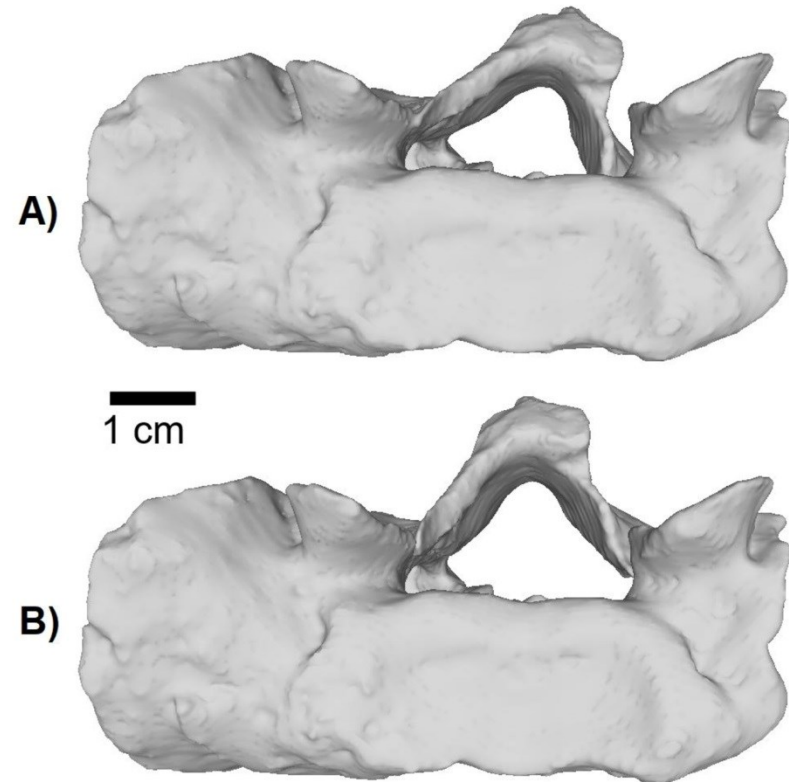
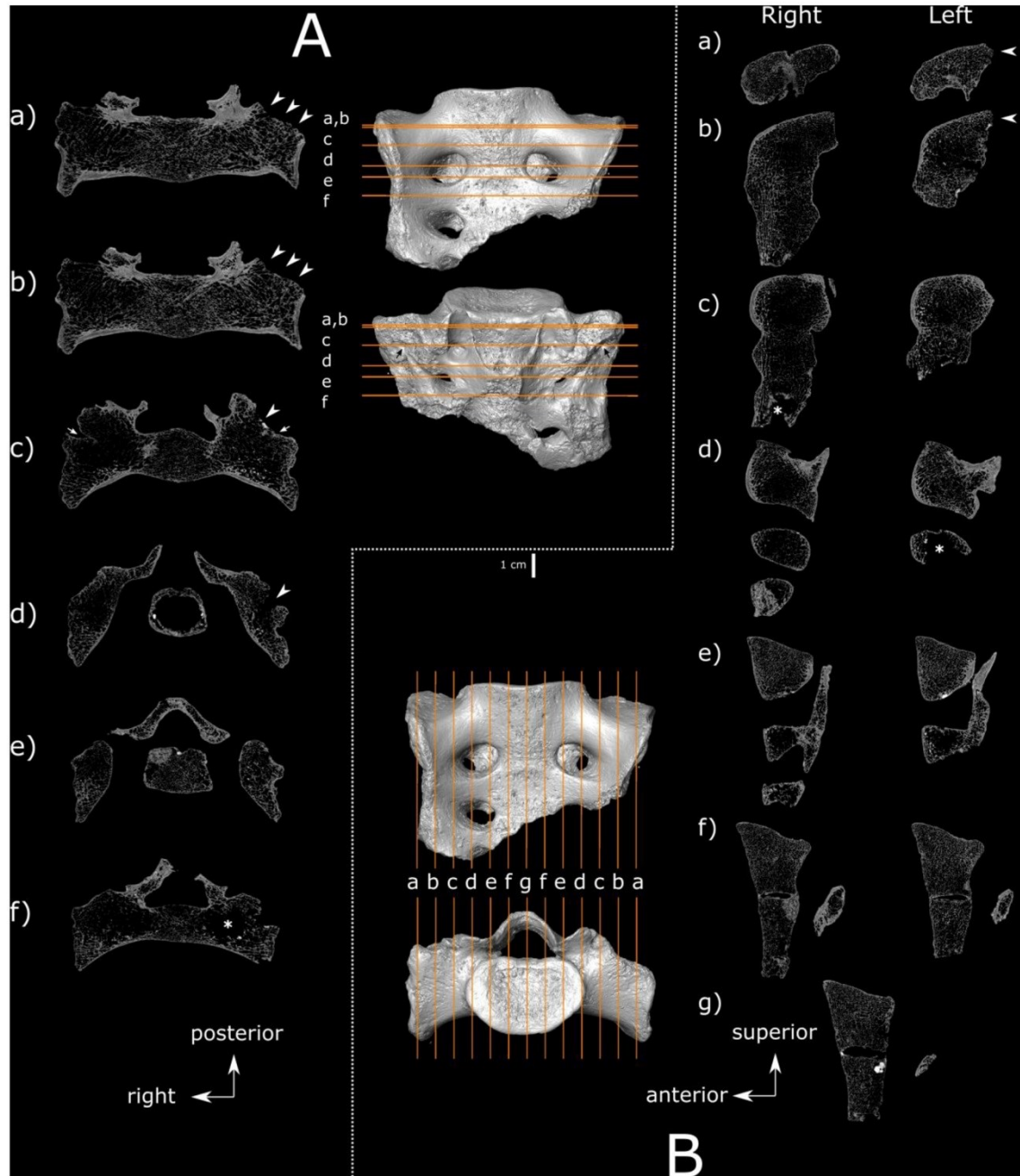


Figure S3. Cross-sections of Regourdou 1 sacrum. A) Transverse slices and B) sagittal slices are indicated by lower case letters. Arrowheads in A) and B) point to the taphonomic erosion of the bone surface; asterisks indicate taphonomic trabecular bone loss. Arrows in the slice c) and the 3D model of A) point to the marked pit for sacro-iliac ligament attachment preserved symmetrically on both sides.



Description: Slices were positioned along the main axes of the sacrum in Avizo. The microCT was resampled according to the slices to maintain the original resolution. Slices in the transverse plane (A) were positioned parallel to the S1-S2 junction (slice d) and slices documenting the taphonomic erosion of the left ala were selected. Slices in the sagittal plane (B) were made in regular intervals symmetrically from the midline (g) across the whole sacral breadth. The slices show asymmetry in trabecular bone density present in the upper portion of the alae: the left ala shows denser trabecular network than the right. The pattern is apparent especially in A) a, b, c, and B) b, c, d.

Supplementary bibliography

- Bar-Yosef, O., & Vandermeersch, B. (1991). *Le Squelette Moustérien de Kébara 2*. Paris: Editions du CNRS.
- Bondioli, L., Bayle, P., Dean, C., Mazurier, A., Puymail, L., Ruff, C., ... Macchiarelli, R. (2010). Technical note: Morphometric maps of long bone shafts and dental roots for imaging topographic thickness variation. *American Journal of Physical Anthropology*, 142(2), 328–334. <https://doi.org/10.1002/ajpa.21271>
- Boule, M. (1911). L'homme fossile de La Chapelle-aux-Saints. *Annales de Paléontologie*, 6, 111–172; 7:21–56, 85–192; 8: 1–70.
- Corron, L., Marchal, F., Condemi, S., Chaumoitre, K., & Adalian, P. (2017). Adéquation, répétabilité et reproductibilité de données ostéométriques obtenues sur os sec, sur des surfaces virtuelles d'os sec et sur des surfaces osseuses d'individus vivants. *Bulletins et Memoires de La Societe d'Anthropologie de Paris*, 29(1–2), 33–53. <https://doi.org/10.1007/s13219-016-0172-7>
- Gómez-Olivencia, A. (2013). Back to the old man's back: reassessment of the anatomical determination of the vertebrae of the Neandertal individual of la Chapelle-aux-Saints. *Annales de Paléontologie*, 99(1), 43–65. <https://doi.org/10.1016/j.annpal.2012.07.002>
- Heim, J. (1976). *Les Hommes Fossiles de La Ferrassie. Tome I. Le Gisement, les Squelettes Adultes (Crâne et Squelette du Tronc)*. Arch. Inst. Paléontol. Humaine (Mémoire 35). Paris.
- Holliday, T. W. (1995). *Body Size and Proportions in the Late Pleistocene Western Old World and the Origins of Modern Humans (Unpublished doctoral dissertation)*. University of New Mexico, Albuquerque.
- Karasik, D., Arensburg, B., Tillier, A. M., & Pavlovsky, O. M. (1998). Skeletal age assessment of fossil hominids. *Journal of Archaeological Science*, 25(7), 689–696. <https://doi.org/10.1006/jasc.1997.0264>
- Macchiarelli, R., Bondioli, L., & Mazurier, A. (2008). Virtual dentitions: touching the hidden evidence. In J. D. Irish & G. C. Nelson (Eds.), *Technique and Application in Dental Anthropology*. Cambridge: Cambridge University Press.
- Meyer, V. (2013). *Apport de la Reconstruction Virtuelle du Bassin Regourdou 1 (Dordogne, France) à la Connaissance de l'Obstétrique Néandertalienne (Unpublished doctoral dissertation)*. Université Bordeaux 1, France, Bordeaux.
- Pap, I., Tillier, A.-M., Arensburg, B., & Chech, M. (1996). The Subalyuk Neanderthal remains (Hungary): a re-examination. *Annales Historico-Naturales Musei Nationalis Hungarici*, 88, 233–270.
- Plavcan, J. M., Meyer, V., Hammond, A. S., Couture, C., Madelaine, S., Holliday, T. W., ... Trinkaus, E. (2014). The Regourdou 1 Neandertal body size. *Comptes Rendus Palevol*, 13(8), 747–754. <https://doi.org/10.1016/j.crpv.2014.07.003>
- Schlager, S. (2016). Morpho: Calculations and Visualisations Related to Geometric Morphometrics.
- Semal, P., Rougier, H., Crevecoeur, I., Jungels, C., Flas, D., Hauzeur, A., ... Van Plicht, J. Der. (2009). New data on the late Neandertals: direct dating of the Belgian Spy fossils. *American Journal of Physical Anthropology*, 138(4), 421–428. <https://doi.org/10.1002/ajpa.20954>
- Trinkaus, E. (1983). *The Shanidar Neandertals*. New York: Academic Press.
- Trinkaus, E. (2011). The postcranial dimensions of the la Chapelle-aux-saints 1 Neandertal. *American Journal of Physical Anthropology*, 145(3), 461–468. <https://doi.org/10.1002/ajpa.21528>
- Uldin, T. (2017). Virtual anthropology – a brief review of the literature and history of computed tomography. *Forensic Sciences Research*, 1790(November), 1–9. <https://doi.org/10.1080/20961790.2017.1369621>
- Walker, M. J., Ortega, J., Parmova, K., Lopez, M. V., & Trinkaus, E. (2011). Morphology, body proportions, and postcranial hypertrophy of a female Neandertal from the Sima de las Palomas, southeastern Spain. *Proceedings of the National Academy of Sciences*, 108(25), 10087–10091. <https://doi.org/10.1073/pnas.1107318108>



Geometric morphometric and traditional methods for sex assessment using the posterior ilium



Rebeka Rmoutilová^{a,b,*}, Ján Dupej^{a,c}, Jana Velemínská^a, Jaroslav Brůžek^{a,b}

^a Department of Anthropology and Human Genetics, Faculty of Science, Charles University, Viničná 7, 128 44 Prague, Czech Republic

^b UMR 5199 PACEA, University of Bordeaux, Bâtiment B8, Allée Geoffroy Saint Hillaire, 33615 Pessac, France

^c Department of Software and Computer Science, Faculty of Mathematics and Physics, Charles University, Malostranské nám. 25, 118 00 Prague, Czech Republic

ARTICLE INFO

Article history:

Received 18 November 2016

Received in revised form 9 February 2017

Accepted 16 March 2017

Available online 18 March 2017

Keywords:

Sex estimation

2D sliding semilandmarks

Auricular surface elevation

Postauricular sulcus

Metric approach

Support vector machine

ABSTRACT

The human hip bone is generally accepted as the most reliable bone for sex estimation in forensic and bioarchaeological disciplines. However, it is seldom completely preserved. The best preserved region is typically around the sacroiliac joint and its auricular surface; it is therefore surprising that this surface has not been involved in standard sexing methods. The aim of this study was to explore the shape and size sexual dimorphism of the auricular surface in detail and to compare its sex estimation accuracy using the geometric morphometric (GM) and traditional methodological approach.

Our sample consisted of 121 specimens from 3 European osteological collections. The GM part of the study was based on 2D sliding semilandmarks that covered the outline of the auricular surface. Furthermore, several linear measurements and visual features (e.g. auricular surface elevation, postauricular sulcus) were chosen to test sex estimation accuracy using support vector machines. Concerning the GM analysis, the most notable sexual differences in the auricular surface outline relate to size. The best accuracy was achieved using form variables reaching 81.0%. Comparable accuracy (80.2%) was achieved using the metric approach, but combined with visual features the accuracy was increased to 93.4%. The GM approach was not very efficient in sexing the auricular surface outline, but the combination of visual features from the posterior ilium and metric variables of the auricular surface could be useful in sex estimation. Therefore, we provide a further testable linear discriminant equation based on this combination of variables.

© 2017 Elsevier B.V. All rights reserved.

1. Introduction

Sex estimation of human skeletal remains is a key step in forensic identification as well as in bioarchaeological studies. The most accurate sex estimation is provided by the hip bone because of the strong selective pressure on female pelvis during the evolutionary process of increasing encephalization [1]. The enlargement of pelvic canal dimensions after acetabular fusion is accompanied with changes in pelvic articulations as a pubic symphysis and sacroiliac joints [2]. This is in concordance with the fact that the highest accuracy of sex determination can be achieved using features of the ischiopubic and sacroiliac hip bone regions [3].

Sacroiliac joint (SIJ) provides a flexible connection between lower limbs and axial skeleton and therefore the upper-body weight is transferred through this articulation to the legs [4,5].

Increased biomechanical loading in males thus causes a great deal of sexual dimorphism in the size of the auricular surface [5–7]. Furthermore, the inferior (i.e. caudal or horizontal) arm of this surface lies along the posterior chord of the greater sciatic notch, which shows important shape differences between the sexes [8–10]. In males, the posterior chord is short in order to reduce the distance between acetabulum and SIJ, favouring bipedal locomotion. On the other hand, the longer posterior chord in females ensures backward position of the sacrum which increases obstetric canal dimensions [2,9]. Moreover, significant sexual dimorphism also exists in the angulation of sacrum [11]. All these indicators suggest that in addition to the size differences, the auricular surface can exhibit some sexual dimorphism in shape.

Auricular features have been studied and described in many forensic monographies [12–15]. Nevertheless, despite a good preservation state of this region compared to the pubis [15–18], the auricular surface is not included in the commonly used sex estimation methods which are based on features from the entire hip bone [3,19,20]. The reason is that a description of morpholog-

* Corresponding author at: Department of Anthropology and Human Genetics, Faculty of Science, Charles University, Viničná 7, 128 44 Prague, Czech Republic.

E-mail address: rebka@seznam.cz (R. Rmoutilová).

ical differences and developing a sexing method are entirely different matters. First, it is necessary to explore the variation of a trait in the population and then to propose a manner of classification which is reproducible and further testable on different samples [21]. Furthermore, it is not possible to reliably determine sex using a single trait [22].

Various visual and metric features of the auricular surface and its surroundings have been explored and tested for sexual dimorphism: auricular surface angle [21,23–27], inferior arm constriction [21,24], auricular surface elevation [2,23,28–30], postauricular sulcus [23,29,31–33], postauricular space [31], iliac tuberosity [31], auricular surface size [26] or length and width of both auricular arms [25,26,28]. Most of the older studies did not reach satisfactory results and some authors even concluded that the features of the auricular region are unreliable indicators of sex [26,30]. Traditional visual and metric assessment is in fact often connected with a higher risk of subjectivity [34] and population specificity [1]. Fortunately, these problems can be at least partially removed by better specified definitions of morphological traits or by using more appropriate, often non-linear, classification methods [28,35,36]. We also encounter this approach in some of the recent studies concerning sexual dimorphism of the auricular surface that achieved considerably higher success than the previous studies [28,29].

Since the 1990s, geometric morphometrics (GM) has found many applications in the study of biological structures [37]. In its basic form, this approach relies on digitizing anatomically homologous points (called landmarks) [38]. However, there are no anatomical landmarks on the outline of auricular surface. Anastasiou and Chamberlain [39] thus verified the sexual dimorphism of the auricular surface, both in shape and size, with geometrically defined points (type 2 or 3 following Bookstein's definition of landmarks [37]). Significant sex differences were found in both shape and size, but the shape component did not contribute very much to the accuracy of sex classification: it reached 87.5% based on the iliac auricular form (shape and size together) compared to 85.9% based solely on the size [39]. Nevertheless, further testing is necessary, particularly on a sample of known sex [39].

The aim of this study was to verify the sexual dimorphism of the auricular surface, in shape and size, by geometric morphometric methods. To that end, sliding semilandmarks were used, that describe the outline of a structure in more detail [40,41]. Simultaneously, several established visual and metric features of the posterior ilium were analysed and both (geometric morphometric and traditional) approaches were compared.

2. Materials and methods

2.1. Materials

The sample consisted of 121 casts of the posterior iliac region from specimens housed in three European osteological collections of known sex and age. The first subsample was composed of 20 females and 28 males from the Coimbra Identified Skeletal Collection (Coimbra, Portugal) which dates to the 19th–20th century [42,43]. The second subsample comprised 15 females and 22 males from the Olivier Documented Collection, Musée de l'Homme, Muséum National d'Histoire Naturelle (Paris, France) which dates to the first half of the 20th century [36,44]. Finally, the third subsample composed of 16 females and 20 males from the Spitalfields Collection, British Museum Natural History (London, United Kingdom) dates to the 18th–19th century [45]. We used a total of 51 females and 70 males of adult age. The exact age was known in 106 individuals (including all females) and ranged from 19 to 96 years. The average age of females and males was 52.0 (sd = 17.8) and 52.6 years (sd = 15.1), respectively.

The casts of the posterior iliac region were analysed to ensure that the visual assessment would not be biased by other sexually dimorphic features from the whole hip bone. High precision condensation dental silicon Reprosil Putty (DENTSPLY DeTrey GmbH, Germany) containing vinyl polysiloxane impression material was used to create moulds of the ventral aspect of the posterior ilium. Subsequently, these imprints ('negative' replicas) were filled with dental gypsum to produce casts that were coloured to gain a natural appearance. Standard procedure for skeletal material replication was followed [46,47] and the used materials were chosen to preserve the properties of the original bone [46,48–50].

2.2. Geometric morphometric approach

2.2.1. 2D imaging

The auricular surface is a relatively flat structure suitable for a two-dimensional analysis [51]. The GM analysis was therefore performed on photographs. They were acquired with a digital camera Canon EOS 600D (Canon Inc. Tokyo, Japan) and a lens EF-S 18–55 mm. The camera was in a fixed position with the focal length of 55 mm and the focal plane 60 cm above the photographed specimen. The cast was placed in a sandbox and photographed in a standardized position. A small 3 cm long and 1.5 cm wide photographic two axis double bubble spirit level was placed on the superior arm (demiface) of the auricular surface which was positioned to be in the horizontal plane (Fig. 1).

The superior arm was chosen because of the relatively flat surface in comparison with the caudal arm [27]. A linear scale was placed directly on the caudal arm so that the landmark locations could be defined in millimetres. A second image of the same cast was subsequently taken in the same position without the linear scale which was finally introduced into the second picture from the previous image.

2.2.2. Semilandmark localisation

Semilandmarks on closed curves were employed in this study due to the lack of anatomical landmarks on the auricular surface [39]. The geometric morphometric procedure was executed in the software Morphome3cs (www.morphome3cs.com) developed in the Department of Software and Computer Science at the Charles University. First, the outline of the auricular surface was manually traced in each image. To initially orient the curves, two points were placed on the top of both arms (Fig. 1) and curves from left-sided specimens were mirrored to the right side. The points served as a base in the floating base registration which was the first step in the superimposition of the curves [38]. The semilandmarks were then placed on the roughly superimposed curves using an iterative process; in its first step, 20 preliminary semilandmarks were automatically placed on the curves at equal curvilinear increments. Next, the semilandmarks were allowed to slide along the curves minimizing the Procrustes distance between a configura-

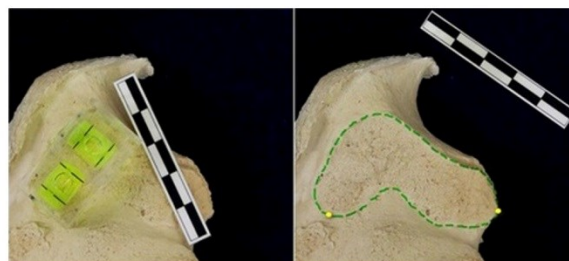


Fig. 1. Acquisition of photographs in standardized position achieved by a spirit level with a 5 cm scale (mediolateral view).

tion of each specimen and the iteratively found sample average [52]. This process ensured a geometrically homologous position of all the semilandmarks [40]. Simultaneously, Generalized Procrustes Analysis (GPA) removed the effect of different position, size and rotation of objects in the coordinate system. The three steps of translation, scaling and rotating thus finally produced shape coordinates [38]. In order to produce form rather than shape, the procedure was repeated, however the specimens were not scaled to unit centroid size [38]. By averaging the aligned coordinates, we obtained mean male and female auricular shape and form.

2.2.3. Size analysis

Centroid size (CS) is a generally accepted measure of size in GM computed as a square root of summed squared distances of each landmark from the centre of the form (centroid) [38]. Except centroid size, traditional measures of size, as surface area and circumference, were computed from the form coordinates to check if CS is appropriate as a measure of size for this structure whose particular shape may result in a bias in the position of the centroid.

2.2.4. Statistical analysis

Shape and form coordinates were further subjected to Principal Component Analysis (PCA) which created a new set of variables called principal components (PCs). The number of PCs included in the statistical testing was determined by the broken-stick rule [53]. Differences between males and females were tested by a non-parametric variant of Hotelling T^2 -test with 10000 permutations.

To analyse the effect of allometry on shape, we fitted a linear model of the shape coordinates on the CS. Residuals of the model were subsequently involved in sex prediction analysis to investigate if the sexual differences persist in the allometric shape.

Differences between population subsamples were tested with Procrustes ANOVA (1000 permutations) with a fixed effect of sex in order to find out if the populations are heterogeneous in shape and form. Population differences in CS of males and females were tested with univariate ANOVA.

The appropriateness of CS was explored by correlation (Pearson correlation coefficient) with other measures of size.

Statistical significance was decided at $\alpha = 0.05$. Statistical software R 3.3.2 (R Foundation for Statistical Computing, Vienna, Austria, 2015) was used in the data analysis and the production of graphical figures. The following R packages were employed: geomorph [54], Morpho [55], Hotelling [56], e1071 [57].

2.3. Traditional approach

Measurements and visual features from the posterior ilium were chosen on the basis of a literature survey. From all the probably sexually dimorphic features listed in the Introduction, only those with a precise definition were selected.

2.3.1. Measurements of the auricular surface

Five measurements and one angle characterizing the auricular surface [26,58] were measured directly on the casts. These variables are described in Table 1 and illustrated in Fig. 2.

The auricular angle has at least three different definitions and can be assessed either metrically or visually [23,26,27]. Due to this inconsistency, some authors claimed that the angle is greater in males [25,26] while others claimed the opposite [21,23,24]. We proceeded according to Ali and MacLaughlin [26] because of a clear definition of the demarking points. From other measurements, only the inferior arm length carries significant sex differences consistently in most of the studies despite a slight variation in the definition [25,26,28]. Nevertheless, all measurements were used to choose the most suitable variables for sex estimation.

Table 1

Definition of metric variables.

	Definition
Inferior arm length (IAL)	Maximal length of the inferior arm measured from the apex of the auricular surface to the posterior inferior iliac spine. [26]
Superior arm length (SAL)	Maximal length of the superior arm measured from the apex to the most superior point of the demifac. [26]
Inferior arm width (IAW)	Computed as the average of the minimum and maximum superoinferior distances measured posterior to the junction with the inferior demifac. [58]
Superior arm width (SAW)	Computed as the average of the minimum and maximum distances measured posterior to the junction with the superior demifac. [58]
Arm distance (AD)	Distance between the most superior point on the border of the superior demifac and the most posterior point of the inferior demifac. [26]
Auricular angle (AA)	Angle at the point of the apex computed from the both arm lengths and arm distance using Cosine rule. [26]

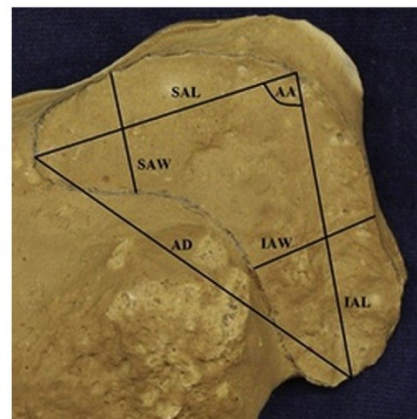


Fig. 2. Auricular surface illustrating metric variables described in Table 1 (medial view of the left iliac bone). IAL = inferior arm length, SAL = superior arm length, IAW = inferior arm width, SAW = superior arm width, AD = arm distance, AA = auricular angle.

2.3.2. Morphological features of the posterior ilium

The auricular surface elevation and postauricular sulcus were evaluated following Wescott's scoring system [29]. The auricular surface elevation is considered as a female trait that emerges in the adolescence as a preadaptation to pregnancy [23,31]. If the elevation is present, the auricular surface noticeably protrudes above the surrounding area (Fig. 3). Otherwise, there is no difference between the auricular surface level and its surroundings. A classical scoring system was used in many studies [21,23,28,30], however the new evaluation system proposed by Wescott [29] dividing the surface elevation into four independent traits may be better adapted and possibly less prone to error. The elevation was therefore scored as follows:

(1) Dorso-superior (DS) elevation

1 – the presence of the dorso-superior auricular surface elevation (female morphology)

0 – the absence of the dorso-superior auricular surface elevation (male morphology)

(2) Dorso-inferior (DI) elevation

1 – the presence of the dorso-inferior auricular surface elevation (female morphology)

0 – the absence of the dorso-inferior auricular surface elevation (male morphology)

(3) Vento-superior (VS) elevation

1 – the presence of the ventro-superior auricular surface elevation (female morphology)

0 – the absence of the ventro-superior auricular surface elevation (male morphology)

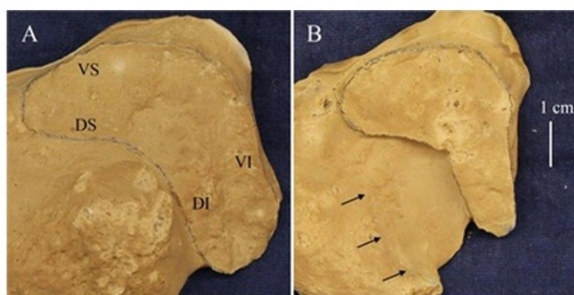


Fig. 3. Absence of the auricular surface elevation and the absence of the postauricular sulcus (A) in the medial view of the left male iliac bone; presence of the auricular surface elevation and the postauricular sulcus (B) in the medial view of the left female iliac bone. Edges indicated in the left image: DS = dorsal superior, DI = dorsal inferior, VS = ventral superior, VI = ventral inferior. Arrows in the right image outline the dorso-superior border of the postauricular sulcus.

1 – the presence of the ventro-superior auricular surface elevation (female morphology)

0 – the absence of the ventro-superior auricular surface elevation (male morphology)

(4) Vetro-inferior (VI) elevation

1 – the presence of the ventro-inferior auricular surface elevation (female morphology)

0 – the absence of the ventro-inferior auricular surface elevation (male morphology)

The postauricular sulcus lies behind the SIJ so it is delimited by the auricular surface on the ventral side and by the iliac tuberosity on the dorsal side (Fig. 3). When well expressed, the groove resembles an imprint of a finger, beginning at the superior arm border, continuing along the inferior arm and terminating superior to the posterior inferior iliac spine [23,31]. The bottom of the sulcus is smooth and the dorsal border formed by the tuberosity is often sharp [29]. When the sulcus is not present the iliac tuberosity rises continuously behind the SIJ and the surface is often not smooth. The postauricular sulcus has a stable scoring system with two (absence/presence) or three (plus undetermined) categories of expression [23,29,31–33]. The postauricular sulcus morphology was scored using two categories:

(5) Postauricular sulcus

1 – the presence of the sulcus (female morphology)

0 – the absence of the sulcus (male morphology)

2.3.3. Statistical analysis

Sex differences in metric variables were analysed using Student's *t*-test. Normality of the data was tested with Shapiro-Wilk test. If the condition of normal distribution was not met in the male or female subsample, then the Wilcoxon test was used to test sex differences. Frequency distribution of morphological variables was analysed with the chi-square test.

ANOVA (or Kruskal-Wallis test if not normal distribution) was used to test population differences in metric variables in male and female sample.

2.4. Intraobserver error

In total, three intraobserver errors were evaluated. First, in the GM part, 10 specimens were photographed on 5 separate occasions to evaluate the intraobserver error in photographing and digitizing landmarks. The outline was marked on the whole set of 50 photographs and form coordinates were computed. Measurement error was evaluated with Procrustes ANOVA and results are summarized in Table 2. They show that the variance (expressed by

mean square) as a result of repeated measurement was significantly smaller in comparison with the inter-individual variance.

Second, for the intraobserver error in the metric assessment all the distances were measured twice by a calliper with 0.1 mm precision. The mean standard error ranged from 0.2 to 0.4 mm in the six measurements. The relative error ranged from 0.3% to 2.8% and was higher in the shorter measurements, such arm widths. For further analysis, the average specimen values were used.

Third, for the visual assessment, 50 randomly chosen specimens were evaluated twice over a period of two weeks. The intraobserver error was evaluated as a percentage of cases where there was a reversal between the two observations. Concerning the auricular surface elevation, a difference in the evaluation occurred in 14.5% of all 200 edges scored (4 edges per specimen). However, the error varied considerably depending on the edge position (Table 3); ventral edges were assessed less reliably than the dorsal ones. The elevation on the ventral side is not apparent as clearly as on the dorsal side due to the steep character of the preauricular surface. A difference in the evaluation of the postauricular sulcus occurred in 8% of cases. High intraobserver error is a typical problem of visual assessment [23,29,30]. However, an error in observation need not result in a difference in sex evaluation. Therefore, the primary data of the 50 specimens in the whole dataset were replaced by the scores obtained in the second observation and sex estimation was recomputed. Despite the high error in observation of visual features, the accuracy of sex estimation did not change significantly when the cross-validation (leave-one-out) scores between both observations were compared using χ^2 test ($\chi^2 = 0.514$, $p = 0.47$).

2.5. Sex prediction

The discrimination power of variables obtained in both geometric and traditional analyses was evaluated using SVM learning model [59]. This algorithm is appropriate for multidimensional data especially when they are not separable by a linear surface, which is a common occurrence in biological data [8]. The mechanism found a hypersurface by maximizing differences between the two groups [60]. Learning model parameters (kernel, cost, γ , variable count) were optimized executing a grid search [61] while searching the best cross-validation (leave-one-out) accuracy. A linear kernel was employed to get the best results in all cases except the form, area and metric variables which required a radial kernel. The cost parameter ranged from 0.1 to 0.5 and the parameter γ from 0.01 to 0.135, depending on the variables. The SVM algorithm was trained and tested on the whole sample. Leave-one-out cross-validation was applied to obtain more objective results of the sex estimation accuracy.

To provide a method immediately available to practitioners and further testable by other researchers, linear discriminant analysis (LDA) was computed for the best combination of variables obtained by SVM.

3. Results

3.1. Geometric morphometric approach

First, homogeneity of the studied sample composed from three different populations was tested. Population differences in females and males were significant in both shape ($F = 2.133$, $p < 0.01$) and form ($F = 4.082$, $p < 0.01$), but an interaction between sex and population was not significant. CS also differed between population samples in females ($F = 4.284$, $p < 0.05$), but not so much in males ($F = 3.099$, $p = 0.05$). Despite the differences among populations,

Table 2

Procrustes ANOVA for auricular form based on repeatedly digitized specimens (N = 10).

Effect	Sum of squares	Mean square	Degrees of freedom	F
Individual	3076.6	478.66	9	17.129**
Error ^a	1117.8	27.94	40	

^a Residual variation due to measurement error.

** P < 0.01.

Table 3

The intraobserver error rate of the auricular surface elevation (N = 50, total number of edges = 200).

	Edge				All edges
	Dorso-superior	Dorso-inferior	Ventro-superior	Ventro-inferior	
Number of scoring differences (%)	3 (6)	4 (8)	10 (20)	12 (24)	29 (14.5)

we decided to use a pooled sample in further analysis because a degree of sexual dimorphism did not differ.

Initially, sex differences in the shape of the auricular surface were analysed. Each of the first 5 PCs accounted for more than 5% of the variation and in total they explained 74% of the total variation. Statistically significant differences were identified between males and females ($t^2 = 4.608$, $p < 0.001$). Both groups were separated only slightly along PC1 (males with lower values than females). PC1 (28%) reflected changes in the region of the auricular apex and the dorsal concavity. The individuals with lower scores (males) along PC1 were narrower in this region, conversely the individuals with more positive values (females) were wider in the apex and dorsal concavity. PC2 (17.8%) was related to the widths of both arms. As PC2 changes, the inferior arm gets narrower while the superior arm gets wider.

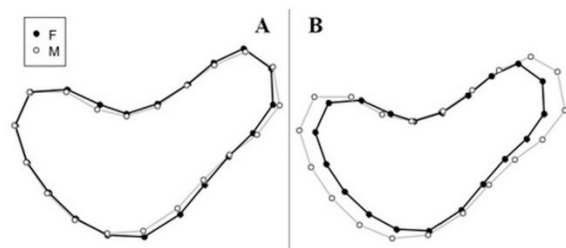
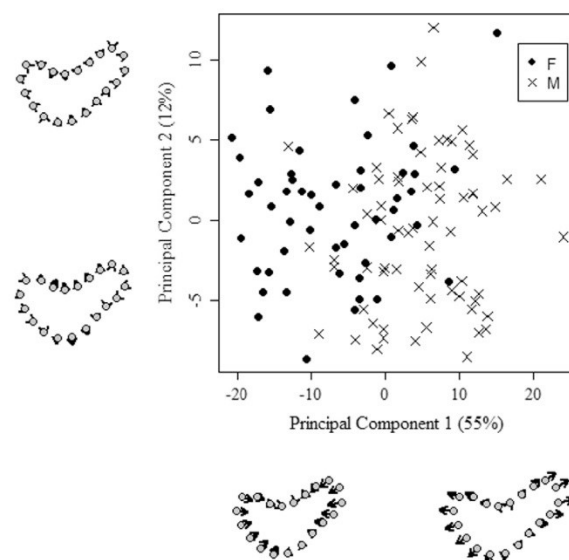
Comparing the average shapes according to sex, there are only slight differences mainly in the region of the apex where females have wider auricular surface than males (Fig. 4a). This corresponds to the effect of PC1.

In contrast to shape, form includes also the size component of a structure. First 4 PCs accounted 82% of the total variation. The permutation Hotelling T^2 -test showed great differences between the sexes ($t^2 = 19.167$, $p < 0.0001$) which were expressed mainly by PC1 (Fig. 5) with better separation of both groups than by PC1 of the shape. PC1 accounted for 55% of variation and expressed general size differences. The auricular surface was larger with positive values of PC1 and vice versa. As the size is ignored in the shape, PC2 of the form expressed very similar effects as PC1 of the shape.

Comparing the average forms (Fig. 4b), the male form was larger than the female one. These differences are reflected by different length and width of both auricular arms.

3.1.1. Size analysis

Correlations between all measures of size were computed to investigate the appropriateness of CS. Both surface area and cir-

**Fig. 4.** Mean shape (A) and form (B) of the auricular surface according to sex.**Fig. 5.** The PCA scatterplot visualizing male and female auricular form accompanied by visualizations of geometry changes according to minimum and maximum values of given PC range.

cumference were highly correlated with CS ($r = 0.95$ and $R^2 = 0.91$; $r = 0.97$ and $R^2 = 0.95$). For comparison, surface area and circumference correlated slightly less with a greater variation expressed by lower value of coefficient of determination ($r = 0.91$ and $R^2 = 0.83$). It is clear from this comparison that CS well represents both traditional measures of size and can be thus safely used as a measure of size for the auricular surface.

3.2. Traditional morphology methods

3.2.1. Measurements

Only 3 of the 6 metric variables showed statistically significant sex differences: inferior arm length (IAL), inferior arm width (IAW) and arm distance (AD) (Table 4). All other variables failed to reveal significant sex differences. These results indicate that especially the inferior arm is significantly longer and wider in males than in females while the superior arm is comparably long and wide between males and females.

Majority of measurements did not show population differences. However, SAL and SAW were significantly different in males and IAW in females (Table 4).

Table 4

Mean measurement values according to sex and test statistics from testing sex and population differences.

Variable	Males	Females	Sex differences	Population differences	
				Females	Males
Inferior arm length (mm)	50.1	44.2	-7.098***	1.968 ^a	0.401
Superior arm length (mm)	38.0	36.4	1440.5 ^a	5.844 ^a	6.626**
Inferior arm width (mm)	18.6	16.7	-3.706***	5.309 ^a	0.511
Superior arm width (mm)	17.5	16.7	-1.527	3.144 ^a	3.220 [†]
Arm distance (mm)	55.5	49.0	-6.791***	1.274	2.255
Auricular angle (°)	76.7	74.2	-1.906	1.938	0.926

* $p < 0.05$.** $p < 0.01$.*** $p < 0.001$.^a Nonparametric form of test was used.

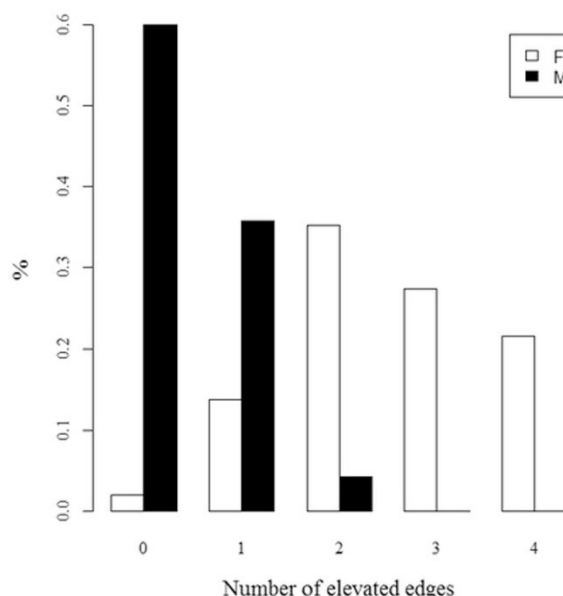
3.2.2. Morphological features

The frequency of elevation was analysed in each of the four surface edges. All surface edges were elevated significantly more often in females than in males (DS: $\chi^2 = 30.106$, DI: $\chi^2 = 49.824$, VS: $\chi^2 = 24.493$, VI: $\chi^2 = 54.547$; $p < 0.0001$ for all edges). The elevation of superior edges was almost never observed in males (in more than 90%). Both inferior edges were elevated more often but it did not exceed 25% of males (Table 5). On the other hand, in females, the correlation with the female morphological trait was considerably weaker; the male morphology (non-elevation) in the DS and VS edges was even slightly more common than the elevation. The elevation considered as the female morphology thus occurred more often in both inferior edges but only in the VI edge the presence exceeded 90% of females (Table 5).

To any given individual, one can assign an elevation score (ranging from 0 to 4) defined simply as the number of elevated edges. No male scored 4 or 3 and only 4.3% of males had 2 edges elevated. Vast majority of males (95.7%) had at most 1 edge elevated (Fig. 6). Approximately a half of the males with 1 elevated edge exhibited the elevation of the VI edge. In females, only 2% did not have elevated any edge of the auricular surface. However, the frequency distribution increased quite sharply from none to 2 elevated edges and then it gradually declined (Fig. 6). The peak of the female distribution was therefore reached for 2 edges elevated. Almost three quarters of females with 2 elevated edges were caused by the DI and VI edge. Altogether, a majority of females (84.4%) had at least two edges elevated in contrast with only 4.3% of males.

Using posterior probability, there is 97.7% chance that an individual with no elevated edge is a male and 100% probability that an individual with 3 or 4 elevated edges is a female. When 1 elevated edge is present, male sex is more probable, but in 2 elevated edges, females already prevail.

In addition, the postauricular sulcus was significantly more frequent in females ($\chi^2 = 58.778$; $p < 0.0001$). The relative percentage of the male morphology in the male sample was almost identical to the relative percentage of the female morphology in the female sample (Table 5).

**Fig. 6.** Percentage of elevated edges in male and female sample.

3.3. Sex prediction of both approaches

Sex prediction was analysed using several different sets of variables. Results are summarized in Table 6.

Initially, prediction was based on the auricular shape, CS and form. Regarding shape, the best classification accuracy with cross-validations achieved 71.9% using 14 PCs. Posterior accuracy was considerably lower in females than in males. Using CS, the accuracy was better, reaching 77.7%. Based on both shape and size (form), the cross-validation accuracy reached 81% using 7 PCs. The posterior accuracy substantially rose in males using form, whereas

Table 5

Frequency distribution of surface elevation (according to separate surface edges) and postauricular sulcus in males (N = 70) and females (N = 51).

Sex	Elevation of separate edges								Postauricular sulcus	
	DS edge		DI edge		VS edge		VI edge		0	1
	0	1	0	1	0	1	0	1		
Males	68	2	62	8	66	4	53	17	60	10
(%)	(97.1)	(2.9)	(88.6)	(11.4)	(94.3)	(5.7)	(75.7)	(24.3)	(85.7)	(14.3)
Females	29	22	13	38	29	22	4	47	8	43
(%)	(56.9)	(43.1)	(25.5)	(74.5)	(56.9)	(43.1)	(7.8)	(92.2)	(15.7)	(84.3)

DS, DI, VS and VI: dorso-superior, dorso-inferior, ventro-superior and ventro-inferior.

Table 6

Sex estimation accuracy (N = 121).

	Correctly assigned (%)		Posterior accuracy (%)	Cross-validation accuracy (%)
	Males	Females		
<i>GM approach</i>				
Shape (14 PCs)	81.4	60.8	72.7	71.9
Form – (7 PCs)	94.3	64.7	81.8	81.0
Centroid size (CS)	88.6	62.8	77.7	77.7
<i>Traditional approach</i>				
Visual (5 variables)	97.1	84.3	91.7	90.9 (93.4 ^{***})
Metric (2 var. [*])	90.0	66.7	80.2	80.2
Visual & metric var. (7 var. [*])	98.6	86.3	93.4	93.4
Visual var. & form (7 PCs)	95.7	88.2	92.6	91.7
LDA ^{***}	97.1	86.3	92.6	91.7

^{*} Inferior arm length and arm distance.^{**} Results in parentheses show how the accuracy changed when the values collected for the intraobserver error were used instead.^{***} Linear discriminant analysis applied to the combination of 7 visual and metric variables.

classification of females improved only slightly. Prediction by shape with allometric effects removed resulted in the prediction accuracy of 60.3%, which indicates that a great deal of shape variation was caused by size.

To assess the importance of visual and metric variables in sex estimation, 3 different sets of variables were analysed: a set of the metric variables, visual variables and both together. The best result (80.2%) using the metric variables was achieved combining only 2 of them (IAL, AD). Visual features (four of the auricular surface elevation and one of the postauricular sulcus) reached the cross-validation accuracy of 90.9%. Finally, using these 2 variables together with all the morphological traits, the accuracy increased to 93.4%. In all three cases, misclassification of females occurred more often.

Linear discriminant analysis was applied to the combination of visual and metric variables and provided an overall posterior accuracy of 92.6% with a bias of 10.8% (more successful classification of males). The final formula for sex estimation using LDA is:

$$\begin{aligned} \text{SCORE}(\text{female}) = & -0.7934(\text{DS} = 1) - 0.8360(\text{DI} = 1) \\ & - 0.4670(\text{VS} = 1) - 1.3754(\text{VI} = 1) \\ & - 0.8127(\text{PS} = 1) + 0.0582(\text{IAL, mm}) \\ & + 0.0363(\text{AD, mm}) - 2.7812 \end{aligned}$$

where the first five variables are the surface elevation edges and postauricular sulcus (values 0 or 1) and the last two variables are the metric ones. Result above zero means a male sex.

4. Discussion

Studies concerning sexual assessment from the posterior ilium often dealt with problems such as high intra- and interobserver error [23], a small testing sample [31], a sample of previously unknown sex [25,39] or a univariate classification approach [26]. Therefore, the posterior ilium morphology was not considered suitable for reliable sex estimation [23,26]. The problem of a lack of objectivity is nowadays often solved by methods of GM [8,39,62]. Following this knowledge, we decided to explore sexual dimorphism of the auricular surface outline with GM methods and to compare it with a traditional approach based on metric and morphological features from the posterior ilium in order to test the sex estimation accuracy.

4.1. Geometric morphometrics and auricular surface outline

In our study, only slight shape differences were found between both sexes, located especially in the region of the auricular apex with females slightly wider in this area than males. However, the

difference of 11.6% in the estimation accuracy between predictions based on shape and allometry-free shape reflects that a great portion of shape variability is probably size-dependent and only correlated with sex. A recent GM study found the same shape differences which were absolutely explained by size [39]. Auricular surface shape is very individually variable [5,63,64] and our results indicate that the sexual differences are rather linked to biomechanics. In addition to the small extent of the sex differences, we do not recommend to evaluate its shape visually.

For the reason that auricular surface lacks any anatomical landmarks sliding semilandmarks were employed in our study. Wilson et al. [65] used evenly spaced semilandmarks to estimate sex from the auricular surface of juvenile ilia. Considering that the female specific traits of the pelvis are usually fully expressed from the adolescence [14,66,67], their success rate 84% [65] was surprisingly high, but dropped to 65% with a use of larger sample [68].

Centroid size provided better sex estimation accuracy than using shape variables indicating that the sexual dimorphism of size is more pronounced in the auricular surface. This is in concordance with Anastasiou and Chamberlain [39] who inferred the small effect of shape from the difference between accuracies based on size (85.9%) and form (87.5%) [39]. In their study, the auricular outline was delimited by 8 geometrical landmarks defined as extreme points relative to the antero-posterior and supero-inferior orientations. Despite the denser representation of the outline with greater number of points, we reached only 77.7% and 81.0% accuracy based on size and form, respectively. The difference might be caused by the used technique or by the fact that their study was based on individuals of unknown sex [39].

4.2. Traditional approach and the posterior ilium

In the traditional part, our results confirmed sexual differences in the inferior arm (length and width) and little to no differences in the superior arm [25,26]. Additionally, the third variable showing significant sexual dimorphism was the measurement (AD) connecting the tops of both arms. Although three variables were significant, only two were important in sex estimation (IAL, AD) reaching 80.2% accuracy. Until now, traditional metric estimations of sex from the auricular surface used only univariate statistics applied on the inferior arm length or surface area. These studies reached 66–71% accuracy [26,28]. Our results indicate that using more than one measurement from the auricular surface can substantially improve the results.

In the morphological assessment of the posterior ilium a high intraobserver error was detected. However, we have already pointed out the difference between the error in observation and

whether it induces a change in sex classification (Section 2.4). The error in observation of the surface elevation and postauricular sulcus was 14.5% and 8%, respectively, but the change in sex classification was much lower and contributed to increase the sex estimation accuracy based on visual approach by 2.5%. It is obvious that a change in scoring of one edge does not necessarily mean a change in sex classification. Using the same description of the elevation, Wescott [29] managed to lower the interobserver error in classification to 2% [29] which is a substantial reduction in comparison with previous studies [23,30].

Using the primary observed morphological data, accuracy of 90.9% was achieved. Only one study exceeded 90% using solely morphological assessment of the posterior ilium [69]. Other studies did not exceed 90% in their success rate with one or more evaluated visual traits from this anatomical area [21,23,28–30]. Only one of them used a classification method (logistic regression) reaching 79.3% accuracy based on the classical definition of the elevation [28]. In Wescott [29], an overall accuracy of 87.1% was reached when 3 or 4 elevated edges were considered as female morphology and other variants as a male one. It is apparent that an involvement of a classification method and a proper definition of morphological traits are important aspects of sex estimation based on traditional approach.

Combining the metric and morphological data provided the best accuracy of 93.4%. A similar success rate was observed in another study combining the inferior arm length, preauricular sulcus and greater sciatic notch evaluation, reaching 94.9% accuracy [28]. These results are encouraging to use combined approach in practice.

As a simple equation cannot be generated from SVM, a formula from LDA was computed to make possible immediate use of this method and facilitate its further testing on different samples.

4.3. Comparison of used approaches

The GM and traditional metric approaches provided surprisingly comparable accuracy (81.0% vs. 80.2%) even though GMs usually improves the accuracy [62,70]. This indicates that both approaches operate on more or less the same information. Although shape was less powerful in sex discrimination than size, its contribution in form is not negligible. It is difficult to analyse pure shape using traditional metric methods, although some shape information is involved when more than one measurement is used. Our metric approach consisted of 2 measurements, but neither of them reflected shape differences localised in the auricular apex as revealed in the GM part. On the other hand, the GM analysis of shape did not show any differences in the length of both arms as identified by the traditional metric analysis. When scaled to the equal size, the difference in the inferior arm length should be apparent as the superior arm is not significantly different between males and females. This discrepancy could possibly be explained by Pinocchio effect which may occur in GM analysis when a large shape change is limited to only a few landmarks [38]. Anastasiou and Chamberlain [39] presented more or less the same intersexual shape differences [39], but the confrontation with traditional metric approach in our study shows that the common superimposition methods may be inappropriate to analyse auricular shape.

A combination of visual and metric variables provided an estimation accuracy of 93.4%. One could object that a combination of the visual features and form variables could provide even higher accuracy because form was slightly better than the metric approach. Therefore, we evaluated this accuracy for illustration (Table 6). The accuracy was not as high as the one obtained with traditional metric methods although sex bias (difference between male and female posterior accuracies) was lowered from 12.3% to 7.5%. Focusing on the efficiency of the traditional and geometric

morphometric approaches, only 2 measurements were sufficient to yield almost the same result as the 7 form variables obtained from PCA. In addition, the traditional metric approach is not as demanding because no special software or equipment is needed. These results support the statement that the GM methods are not going to replace current methods of sex estimation [67]. Due to the failure of auricular shape alone it is preferential to use the traditional technique in sex estimation from the posterior ilium, which can be employed in the field stage of analysis [71].

Whatever data were used, females were determined less accurately than males. This can relate to the amount of morphological variability in males and females, however the pelvic variability is expected to be greater in the male sample [72] because of the stabilizing selection affecting the female pelvis. This issue is, however, still a matter of debate [73,74]. As the SVM correctly estimates the more numerous group [36], the lesser accuracy of sex estimation of females can be caused by properties of the learning algorithm.

4.4. Population specificity of human pelvis

We used a multipopulation sample in our study to ensure that the results are not restricted to one population. Subsamples were not homogenous; they varied in shape, form, CS and some measurements, but there was no variation in sexual dimorphism in the individual subsamples. The subsamples were too small to try sex prediction independently. Furthermore, other studies showed that pooled samples provide better accuracy in predicting sex or stature even though they consist of heterogeneous populations [8,20,75].

Sex estimation methods based on long bones or cranium are known to be population-specific [36,76] because of size differences among populations [77]. Does this fact include the pelvis? By some authors, pelvis is considered as an exception to this rule [12,15], others share an opinion that pelvis is also population specific [50,78–80]. A widespread answer to this problem is a creation of population specific standards [50,78,81], but this approach is questionable in the era of globalization [1] as population affinity cannot be inferred from a single bone with sufficient precision [82]. Despite the evidence of pelvic population specificity, there are tested metric methods that can be considered as population-independent [20,83–86]. These methods work with measurements that cover the whole hip bone sexual dimorphism so all three morpho-functional modules are represented, probably suppressing any specificity [87]. This can be supported by the fact that individual pelvic dimensions are highly variable, but the overall size of pelvic canal remains stable [73]. In other words, a metric method needs to consist of the measurements that capture shape differences reflecting the more spacious pelvic canal in females. That also means that when sex is predicted from a bone fragment, the result must be implicitly less reliable because it is based only on partial pelvic sexual dimorphism [3,87]. This fact can explain the variable sex estimation accuracy achieved from the posterior ilium in previously discussed studies. The variation of results is evident and depends on the degree of sexual dimorphism and used traits. Therefore, such methods are successfully applied on specimens from the same population [21], but a successful method should be efficient also outside its reference population [88]. To solve this problem, the reference sample should be composed of more than one population and further testing should be performed on other samples.

Population specificity has always been attributed especially to metric methods because metric variables are continuous and influenced by size. However, some morphological features are also continuous in their nature and it is the visual assessment that reduces this variability into several discrete categories [89]. Moreover, population specificity can be beside size caused by an overall different

degree of sexual dimorphism [77]. This type of discrepancy is well apparent from shape of the greater sciatic notch whose sex accuracy varies with a population sample used [8,50,79,88,90]. This means that no GM approach can remove the effect of population specificity because, even though the size-related effect is eliminated, differing degrees of sexual dimorphism can influence variation in shape. Only few works analysing population specificity of visual pelvic features exist and they do not provide convincing results [50,91–93]; most of them rather deny population specificity of morphological pelvic traits [91–93].

Concerning the morphological traits used in our study, there is not much literature about their population specificity. It was noted that the absence of the auricular surface elevation on the iliac side can be compensated by the breadth of sacrum which depends on ontogenetic changes that might be population specific [2]. Also, the frequency of elevation was slightly population specific in one observer evaluation [91]. Comparing the frequency of postauricular sulcus with published results, there seems to be no substantial difference among populations of European origin [29], but greater differences were found in comparison with Asian populations [32,33]. Nevertheless, estimating the impact of population specificity on morphological assessment largely depends on the employed definitions of the features and thus on the interobserver error [91].

5. Conclusion

Sexual dimorphism in the auricular surface and posterior ilium was analysed with different methods. The auricular surface outline showed slight shape differences, but the best sex estimation accuracy using geometric morphometric approach was achieved using form (81%). Comparable results (80.2%) were reached with the traditional metric analysis. Considering the efficiency and applicability, the metric approach was more convenient for sex estimation from the auricular surface than the two-dimensional GM approach. Visual assessment of the posterior ilium provided 90.9% accuracy and a combination with the measurements increased the accuracy to 93.4%. A formula obtained with linear discriminant function is proposed for the best combination of variables. Even though a multi-population sample was used in this study, it is necessary to make further testing on other populations.

Acknowledgements

We acknowledge the support from GDR 3592 (Paléobst: Obstétrique et paléo-obstétrique de la lignée humaine) and we thank to the National Museum in Prague for the permission to study the collections in their care. We thank also to the anonymous reviewer for valuable remarks.

References

- [1] J. Brůžek, P. Murail, Methodology and reliability of sex determination from the skeleton, in: A. Schmitt, E. Cunha, J. Pinheiro (Eds.), *Forensic Anthropology and Medicine: Complementary Sciences from Recovery to Cause of Death*, Humana Press, Totowa, New Jersey, 2006, pp. 225–242.
- [2] L.E. St. Hoyme, Sex differentiation in the posterior pelvis, *Collegium Anthropologicum* 8 (1984) 139–154.
- [3] J. Brůžek, A method for visual determination of sex, using the human hip bone, *Am. J. Phys. Anthropol.* 117 (2002) 157–168, <http://dx.doi.org/10.1002/ajpa.10012>.
- [4] G.P. Pal, Weight transmission through the sacrum in man, *J. Anat.* 162 (1989) 9–17.
- [5] A. Vleeming, M.D. Schuenke, A.T. Masi, J.E. Carreiro, L. Danneels, F.H. Willard, The sacroiliac joint: an overview of its anatomy, function and potential clinical implications, *J. Anat.* 221 (2012) 537–567, <http://dx.doi.org/10.1111/j.1469-7580.2012.01564.x>.
- [6] N.A. Ebraheim, T.D. Madsen, R. Xu, J. Mehalik, R.A. Yeasting, Dynamic changes in the contact area of the sacroiliac joint, *Orthopedics* 26 (2003) 711–719.
- [7] N. Krmek, A. Jo-Osvatić, T. Nikolić, V. Krmek, A. Salamon, Anthropological measurement of the sacroiliac joint, *Collegium Anthropologicum* 30 (2006) 811–814.
- [8] J. Velemínská, V. Krajčůček, J. Dupej, J.A. Gómez-Valdés, P. Velemínský, A. Šeřáková, et al., Technical Note: Geometric morphometrics and sexual dimorphism of the greater sciatic notch in adults from two skeletal collections: the accuracy and reliability of sex classification, *Am. J. Phys. Anthropol.* 152 (2013) 558–565, <http://dx.doi.org/10.1002/ajpa.22373>.
- [9] L.D. Hager, Sex differences in the sciatic notch of great apes and modern humans, *Am. J. Phys. Anthropol.* 99 (1996) 287–300, [http://dx.doi.org/10.1002/\(SICI\)1096-8644\(199602\)99:2<287::AID-AJPA6>3.0.CO;2-W](http://dx.doi.org/10.1002/(SICI)1096-8644(199602)99:2<287::AID-AJPA6>3.0.CO;2-W).
- [10] P.L. Walker, Greater sciatic notch morphology: sex, age, and population differences, *Am. J. Phys. Anthropol.* 127 (2005) 385–391, <http://dx.doi.org/10.1002/ajpa.10422>.
- [11] R.G. Tague, Sexual dimorphism in the human bony pelvis, with a consideration of the Neandertal pelvis from Kebara Cave, Israel, *Am. J. Phys. Anthropol.* 88 (1992) 1–21, <http://dx.doi.org/10.1002/ajpa.1330880102>.
- [12] D.A. Komar, J.E. Buikstra, *Forensic Anthropology: Contemporary Theory and Practice*, Oxford University Press, New York, 2008.
- [13] M.Y. Iscan, M. Steyn, *The Human Skeleton in Forensic Medicine*, third ed., Charles C Thomas Publisher, Springfield, USA, 2013.
- [14] R. Pickering, D. Bachman, *The Use of Forensic Anthropology*, second ed., CRC Press, Boca Raton, FL, 2009.
- [15] L. Klepinger, *Fundamentals of Forensic Anthropology*, John Wiley & Sons, Hoboken, New Jersey, 2006.
- [16] T. Waldron, The relative survival of the human skeleton: implications for palaeopathology, in: A. Boddington, A. Garland (Eds.), *Death, Decay and Reconstruction: Approaches to Archaeology and Forensic Science*, Manchester University Press, Manchester, 1987, pp. 55–64.
- [17] N. Telmon, D. Rouge, J. Brugne, A. Sevin, G. Larrouy, L. Arbus, Critères ostéoscopiques d'exploration du vieillissement. L'exemple de la nécropole médiévale de Saint-Étienne de Toulouse, *Bulletins et Mémoires de La Société d'Anthropologie de Paris* 5 (1993) 293–300.
- [18] C.M. Stojanowski, R.M. Seidemann, G.H. Doran, Differential skeletal preservation at Windover Pond: causes and consequences, *Am. J. Phys. Anthropol.* 119 (2002) 15–26, <http://dx.doi.org/10.1002/ajpa.10101>.
- [19] D. Ferembach, I. Schwindesky, M. Stoukal, Recommendation for age and sex diagnoses of skeletons, *J. Hum. Evol.* 9 (1980) 517–549.
- [20] P. Murail, J. Brůžek, F. Houët, E. Cunha, DSP: a tool for probabilistic sex diagnosis using worldwide variability in hip-bone measurements, *Bulletins et Mémoires de La Société d'Anthropologie de Paris* 17 (2005) 167–176.
- [21] V. Novotný, Pohlavní rozdíly a identifikace pohlaví pánevní kosti (Dissertation), Univerzita J. E. Purkyně v Brně, 1981.
- [22] T. Sjøvold, Geschlechtsdiagnose am skelett, in: R. Knußmann (Ed.), *Anthropologie Handbuch Der Vergleichenden Biologie Des Menschen*, Gustav Fischer, Stuttgart, 1988, pp. 444–480.
- [23] J. Brůžek, D. Castex, T. Majó, Évaluation des caractères morphologiques de la face sacro-pelvienne de l'os coxal. Proposition d'une nouvelle méthode de diagnose sexuelle, *Bulletins et Mémoires de La Société d'Anthropologie de Paris* 8 (1996) 491–502, <http://dx.doi.org/10.3406/bmsap.1996.2465>.
- [24] S. Genovés, L'estimation des différences sexuelles dans l'os coxal : différences métriques et différences morphologiques, *Bulletins et Mémoires de La Société d'Anthropologie de Paris* 10 (1959) 3–95.
- [25] M. Valoerdy, D. Hogg, Sex differences in the morphology of the auricular surfaces of the human sacroiliac joint, *Clin. Anat.* 2 (1989) 63–67.
- [26] R.S. Ali, S.M. MacLaughlin, Sex identification from the auricular surface of the adult human ilium, *Int. J. Osteoarchaeology* 1 (1991) 57–61.
- [27] H. Weisl, The articular surfaces of the sacro-iliac joint and their relation to the movements of the sacrum, *Cells Tissues Organs* 22 (1954) 1–14.
- [28] L. Novak, J.J. Schultz, M. McIntyre, Determining sex of the posterior ilium from the Robert J. Terry and William M. Bass collections, *J. Forensic Sci.* 57 (2012) 1155–1160, <http://dx.doi.org/10.1111/j.1556-4029.2012.02122.x>.
- [29] D.J. Wescott, Sexual dimorphism in auricular surface projection and postauricular sulcus morphology, *J. Forensic Sci.* 60 (2015) 679–685, <http://dx.doi.org/10.1111/1556-4029.12737>.
- [30] T. Rogers, S. Saunders, Accuracy of sex determination using morphological traits of the human pelvis, *J. Forensic Sci.* 39 (1994) 1047–1056.
- [31] M.Y. Iscan, K. Derrick, Determination of sex from the sacroiliac joint: a visual assessment technique, *Florida Sci.* 47 (1984) 94–98.
- [32] P. Mahakkanukrauh, P. Duangto, S. Praneatpolgran, P. Singsuwan, Sex determination of iliac bone in a Thai population, *Bull. Chiang Mai Assoc. Med. Sci.* 45 (2012) 61–66.
- [33] D. Gohil, K. Dangar, S. Rathod, K. Jethwa, G. Singal, A study of morphological features of ilium for sex determination in Gujarat state, *J. Res. Med. Dent. Sci.* 2 (2014) 75–78, <http://dx.doi.org/10.5455/jrmds.20142415>.
- [34] S. Nakhaeizadeh, I.E. Dror, R.M. Morgan, Cognitive bias in forensic anthropology: visual assessment of skeletal remains is susceptible to confirmation bias, *Sci. Justice* 54 (2014) 208–214, <http://dx.doi.org/10.1016/j.scijus.2013.11.003>.
- [35] J. Albanese, G. Eklics, A. Tuck, A metric method for sex determination using the proximal femur and fragmentary hipbone, *J. Forensic Sci.* 53 (2008) 1283–1288, <http://dx.doi.org/10.1111/j.1556-4029.2008.00855.x>.
- [36] F. Santos, P. Guyomarch, J. Brůžek, Statistical sex determination from craniometrics: comparison of linear discriminant analysis, logistic regression, and support vector machines, *Forensic Sci. Int.* 245 (2014) 204.e1–204.e8, <http://dx.doi.org/10.1016/j.forsciint.2014.10.010>.

- [37] F. Bookstein, *Morphometric Tools For Landmark Data: Geometry and Biology*, first ed., Cambridge University Press, Cambridge, United Kingdom, 1991, <http://dx.doi.org/10.1017/CBO9780511573064>.
- [38] M. Zelditch, D. Swiderski, H. Sheets, W. Fink, *Geometric Morphometrics for Biologists: A Primer*, Elsevier Academic Press, New York, 2004.
- [39] E. Anastasiou, A.T. Chamberlain, The sexual dimorphism of the sacro-iliac joint: an investigation using geometric morphometric techniques, *J. Forensic Sci.* 58 (2013) 126–134, <http://dx.doi.org/10.1111/j.1556-4029.2012.02282.x>.
- [40] P. Gunz, P. Mitteroecker, Semilandmarks: a method for quantifying curves and surfaces, *Hystrix* 24 (2013) 103–109, <http://dx.doi.org/10.4404/hystrix-24.1-6292>.
- [41] F.L. Bookstein, Landmark methods for forms without landmarks: morphometrics of group differences in outline shape, *Med. Image Anal.* 1 (1997) 225–243, <http://dx.doi.org/10.1109/MMBIA.1996.534080>.
- [42] M.A. Rocha, Les collections ostéologiques humaines identifiées du Musée Anthropologique de l'Université de Coimbra, *Antropologia portuguesa* 13 (1995) 7–38.
- [43] D. Navega, R. Vicente, D.N. Vieira, A.H. Ross, E. Cunha, Sex estimation from the tarsal bones in a Portuguese sample: a machine learning approach, *Int. J. Legal Med.* 129 (2015) 651–659, <http://dx.doi.org/10.1007/s00414-014-1070-5>.
- [44] G. Olivier, *Profil sagittaux et mensuration de crânes de Français*, Paris, 1972.
- [45] T. Molleson, M. Cox, *The Spitalfields Project, Volume 2: The Anthropology*, Council for British Archeology, York, 1993.
- [46] T.D. White, P.A. Folkens, *Human Osteology*, second ed., Academic Press, San Diego, California, 2000.
- [47] T.D. White, P.A. Folkens, *The Human Bone Manual*, Elsevier Academic Press, San Diego, California, 2005, <http://dx.doi.org/10.1016/B978-0-12-088467-4.50022-3>.
- [48] S.W. Hillson, Impression and replica methods for studying hypoplasia and perikymata on human tooth crown surfaces from archaeological sites, *Int. J. Osteoarchaeology* 2 (1992) 65–78, <http://dx.doi.org/10.1002/oa.1390020109>.
- [49] S. Hillson, *Dental Anthropology*, Cambridge University Press, Cambridge, UK, 1996, <http://dx.doi.org/10.1017/CBO9781139170697>.
- [50] M.L. Patriquin, S.R. Loth, M. Steyn, Sexually dimorphic pelvic morphology in South African whites and blacks, *Homo* 53 (2003) 255–262, <http://dx.doi.org/10.1078/0018-442X-00049>.
- [51] S.C. Fox, C. Eliopoulos, I. Moutafi, S.K. Manolis, A simple technique for imaging the human skeleton using a flatbed scanner, *J. Forensic Sci.* 56 (2011) 154–157, <http://dx.doi.org/10.1111/j.1556-4029.2010.01596.x>.
- [52] P. Gunz, P. Mitteroecker, F. Bookstein, Semilandmarks in three dimensions, in: D.E. Slice (Ed.), *Modern Morphometrics in Physical Anthropology*, Kluwer Academic, New York, 2005, pp. 73–98, http://dx.doi.org/10.1007/0-387-27614-9_3.
- [53] P.R. Peres-Neto, D.A. Jackson, K.M. Somers, How many principal components? Stopping rules for determining the number of non-trivial axes revisited, *Comput. Stat. Data Anal.* 49 (2005) 974–997, <http://dx.doi.org/10.1016/j.csda.2004.06.015>.
- [54] D.C. Adams, E. Otárola-Castillo, Geomorph: an R package for the collection and analysis of geometric morphometric shape data, *Methods Ecol. Evol.* 4 (2013) 393–399, <http://dx.doi.org/10.1111/2041-210X.12035>.
- [55] A. Stefan, M.S. Schlager, Morpho: Calculations and Visualisations Related to Geometric Morphometrics, 2016.
- [56] J.M. Curran, Hotelling's T-squared test and variants, 2013.
- [57] D. Meyer, E. Dimitriadou, K. Hornik, A. Weingessel, F. Leisch, C.-C. Chang, et al., e1071: Misc Functions of the Department of Statistics, Probability Theory Group (Formerly: E1071), TU Wien, 2015.
- [58] J.M. Kibii, S.E. Churchill, P. Schmid, K.J. Carlson, N.D. Reed, D.J. de Ruiter, et al., A partial pelvis of *Australopithecus sediba*, *Science* 333 (2011) 1407–1411, <http://dx.doi.org/10.1126/science.1202521>.
- [59] C. Cortes, V. Vapnik, Support vector networks, *Mach. Learn.* 20 (1995) 273–297.
- [60] D. Meyer, Support vector machines: the interface to libsvm in package e1071, FH Technikum, Wien, Austria, 2014, <http://dx.doi.org/10.1007/978-0-387-77242-4>.
- [61] C. Hsu, C. Chang, C. Lin, *A practical Guide to Support Vector Classification*, Taipei, 2010.
- [62] E. Pretorius, M. Steyn, Y. Scholtz, Investigation into the usability of geometric morphometric analysis in assessment of sexual dimorphism, *Am. J. Phys. Anthropol.* 129 (2006) 64–70, <http://dx.doi.org/10.1002/ajpa.20251>.
- [63] C.O. Lovejoy, R.S. Meindl, T.R. Pryzbeck, R.P. Mensforth, Chronological metamorphosis of the auricular surface of the ilium: a new method for the determination of adult skeletal age at death, *Am. J. Phys. Anthropol.* 68 (1985) 15–28, <http://dx.doi.org/10.1002/ajpa.1330680103>.
- [64] O. Bakland, J.H. Hansen, The "axial sacroiliac joint", *Anatomia Clin.* 6 (1984) 29–36, <http://dx.doi.org/10.1007/BF01811211>.
- [65] L.A. Wilson, N. MacLeod, L.T. Humphrey, Morphometric criteria for sexing juvenile human skeletons using the ilium, *J. Forensic Sci.* 53 (2008) 269–278, <http://dx.doi.org/10.1111/j.1556-4029.2008.00656.x>.
- [66] D.M. Mittler, S.G. Sheridan, Sex determination in subadults using auricular surface morphology: a forensic sciences perspective, *J. Forensic Sci.* 37 (1992) 1068–1075.
- [67] M.F. Bilfeld, F. Dedouit, N. Sans, H. Rousseau, D. Roug, N. Telmon, Ontogeny of size and shape sexual dimorphism in the ilium: a multislice computed tomography study by geometric morphometry, *J. Forensic Sci.* 58 (2013) 303–310, <http://dx.doi.org/10.1111/1556-4029.12037>.
- [68] L.A.B. Wilson, H.F.V. Cardoso, L.T. Humphrey, On the reliability of a geometric morphometric approach to sex determination: a blind test of six criteria of the juvenile ilium, *Forensic Sci. Int.* 206 (2011) 35–42, <http://dx.doi.org/10.1016/j.forsciint.2010.06.014>.
- [69] M.Y. Iscan, S.S. Dunlap, Sexing the human sacroiliac joint, *Am. J. Phys. Anthropol.* 60 (1983) 208–209, <http://dx.doi.org/10.1002/ajpa.1330600204>.
- [70] J.A. Gómez-Valdés, M. Quinto-Sánchez, A.M. Garmendia, J. Velemínská, G. Sánchez-Mejorada, J. Brůžek, Comparison of methods to determine sex by evaluating the greater sciatic notch: visual, angular and geometric morphometrics, *Forensic Sci. Int.* 221 (2012) 156.e1–156.e7, <http://dx.doi.org/10.1016/j.forsciint.2012.04.027>.
- [71] F.W. Rösing, M. Graw, B. Marré, S. Ritz-Timme, M.A. Rothschild, K. Röttscher, et al., Recommendations for the forensic diagnosis of sex and age from skeletons, *Homo* 58 (2007) 75–89, <http://dx.doi.org/10.1016/j.jchb.2005.07.002>.
- [72] H.K. Kurki, S. Decrausaz, Shape variation in the human pelvis and limb skeleton: implications for obstetric adaptation, *Am. J. Phys. Anthropol.* 159 (2016) 630–638, <http://dx.doi.org/10.1002/ajpa.22922>.
- [73] H.K. Kurki, Skeletal variability in the pelvis and limb skeleton of humans: does statistical selection limit female pelvic variation?, *Am. J. Hum. Biol.* 25 (2013) 795–802, <http://dx.doi.org/10.1002/ajhb.22455>.
- [74] A. Huseynov, C.P.E. Zollikofer, W. Coudyzer, D. Gascho, C. Kellenberger, R. Hinzpeter, et al., Developmental evidence for obstetric adaptation of the human female pelvis, *Proc. Natl. Acad. Sci.* 113 (2016) 5227–5232, <http://dx.doi.org/10.1073/pnas.1517085113>.
- [75] A.N. Hatza, S.D. Ousley, L.L. Cabo, Estimating stature when ancestry is unknown: What statistical methods work best?, in: *Proceedings of the American Academy of Forensic Sciences XXI*, 2015, pp. 152–153.
- [76] A. Kotěrová, J. Velemínská, J. Dupej, H. Brzobohatá, A. Pilný, J. Brůžek, Disregarding population specificity: its influence on the sex assessment methods from the tibia, *Int. J. Legal Med.* (2016), <http://dx.doi.org/10.1007/s00414-016-1413-5> (in press).
- [77] L. Scheuer, Application of osteology to forensic medicine, *Clin. Anat.* 15 (2002) 297–312, <http://dx.doi.org/10.1002/ca.10028>.
- [78] M.L. Patriquin, M. Steyn, S.R. Loth, Metric analysis of sex differences in South African black and white pelvis, *Forensic Sci. Int.* 147 (2005) 119–127, <http://dx.doi.org/10.1016/j.forsciint.2004.09.074>.
- [79] M. Steyn, E. Pretorius, L. Hutten, Geometric morphometric analysis of the greater sciatic notch in South Africans, *Homo* 54 (2004) 197–206, <http://dx.doi.org/10.1078/0018-442X-00076>.
- [80] K. Rosenberg, A Late Pleistocene human skeleton from Liujiang, China suggests regional population variation in sexual dimorphism in the human pelvis, *Variability Evol.* 10 (2002) 5–17.
- [81] D. Franklin, A. Cardini, A. Flavel, M.K. Marks, Morphometric analysis of pelvic sexual dimorphism in a contemporary Western Australian population, *Int. J. Legal Med.* 128 (2014) 861–872, <http://dx.doi.org/10.1007/s00414-014-0999-8>.
- [82] L. Liebenberg, E.N. L'Abbe, K.E. Stull, Population differences in the postcrania of modern South Africans and the implications for ancestry estimation, *Forensic Sci. Int.* 257 (2015) 522–529.
- [83] M. Steyn, M.L. Patriquin, Osteometric sex determination from the pelvis – Does population specificity matter?, *Forensic Sci. Int.* 191 (2009) 113.e1–113.e5, <http://dx.doi.org/10.1016/j.forsciint.2009.07.009>.
- [84] T. Chapman, P. Lefevre, P. Semal, F. Moiseev, V. Sholukha, S. Lourany, et al., Sex determination using the probabilistic sex diagnosis (DSP: Diagnose sexuelle probabiliste) tool in a virtual environment, *Forensic Sci. Int.* 234 (2014) 189.e1–189.e8, <http://dx.doi.org/10.1016/j.forsciint.2013.10.037>.
- [85] S. Mestekova, J. Bruzek, J. Velemínska, K. Chaumoitre, A test of the DSP sexing method on CT images from a modern French sample, *J. Forensic Sci.* 60 (2015) 1295–1299, <http://dx.doi.org/10.1111/1556-4029.12817>.
- [86] J.P. Macaluso Jr., Sex determination from the acetabulum: test of a possible non-population-specific discriminant function equation, *J. Forensic Leg. Med.* 17 (2010) 348–351, <http://dx.doi.org/10.1016/j.jfm.2010.06.001>.
- [87] J. Brůžek, Fiabilité des fonctions discriminantes dans la détermination sexuelle de l'os coxal. Critiques et propositions, *Bulletins et Mémoires de La Société d'Anthropologie de Paris* 4 (1992) 67–104.
- [88] S.M. MacLaughlin, M.F. Bruce, Population variation in sexual dimorphism in the human innominate, *Hum. Evol.* 1 (1986) 221–231.
- [89] V. Novotný, The principle of equifinality and the evolution of sexual dimorphism of the human pelvis, in: *International Congress of Anthropological and Ethnological Sciences*, Zagreb, Zagreb, 1988.
- [90] P.N. González, V. Bernal, S. Ivan Perez, G. Barrientos, Analysis of dimorphic structures of the human pelvis: its implications for sex estimation in samples without reference collections, *J. Archaeol. Sci.* 34 (2007) 1720–1730, <http://dx.doi.org/10.1016/j.jas.2006.12.013>.
- [91] G.A. Listi, The impact of racial metric variation in the os coxae on the morphological assessment of sex, *J. Forensic Sci.* 55 (2010) 1157–1161, <http://dx.doi.org/10.1111/j.1556-4029.2010.01428.x>.
- [92] A. Kiales, M.W. Kenyhercz, K.E. Stull, K.A. McCormick, S.J. Call, Worldwide population variation in pelvic sexual dimorphism, *Am. J. Phys. Anthropol.* 159 (2016) 193, <http://dx.doi.org/10.1002/ajpa.22955>.
- [93] S.R. Rennie, M. Clegg, S. Gonzalez, Geographic and temporal variation in morphological sexing traits of the pelvis, *Am. J. Phys. Anthropol.* 159 (2016) 266–267, <http://dx.doi.org/10.1002/ajpa.22955>.



Contents lists available at ScienceDirect

Journal of Forensic and Legal Medicine

journal homepage: www.elsevier.com/locate/yjflm

Research Paper

Impact of 3D surface scanning protocols on the *Os coxae* digital data: Implications for sex and age-at-death assessmentAnežka Kotěrová^{a,*}, Vlastimil Králík^b, Rebeka Rmoutilová^{a,c}, Lukáš Friedl^{d,e}, Pavel Růžička^b, Jana Velemínská^a, François Marchal^f, Jaroslav Brůžek^{a,c}^a Department of Anthropology and Human Genetics, Faculty of Science, Charles University, Viničná 7, Prague, 128 43, Czech Republic^b Department of Mechanics, Biomechanics and Mechatronics, Faculty of Mechanical Engineering, CTU in Prague, Technická 4, Prague, 166 07, Czech Republic^c Laboratoire PACEA, UMR 5199, CNRS, Université Bordeaux, CS 50023, Pessac, 33615, France^d Department of Anthropology, University of West Bohemia, Plzeň, 30614, Czech Republic^e Interdisciplinary Center for Archaeology and Evolution of Human Behaviour (ICAEHB), Faculdade das Ciências Humanas e Sociais, Universidade do Algarve, Campus Gambelas, 8005-139, Faro, Portugal^f UMR 7268 ADES, Aix-Marseille University, EFS, CNRS, Faculté de Médecine Secteur Nord, 13344, Marseille Cedex 15, France

ARTICLE INFO

Keywords:

Laser scanning
Structured light technology
RedLux profiler
Biological profile
Age and sex estimation
Os coxae

ABSTRACT

The 3D imaging technologies have become of paramount importance for example in disciplines such as forensic anthropology and bioarchaeology, where they are being used more and more frequently. There are several new possibilities that they offer; for instance, the easier and faster sharing of data among institutions, the possibility of permanent documentation, or new opportunities of data analysis. An important requirement, however, is whether the data obtained from different scanning devices are comparable and whether the possible varying outputs could affect further analyses, such as the estimation of the biological profile. Therefore, we aimed to investigate two important questions: (1) whether 3D models acquired by two different scanning technologies (structured light and laser) are comparable and (2) whether the scanning equipment has an effect on the anthropological analyses, such as age-at-death estimation and sex assessment.

3D models of *os coxa* ($n = 29$) were acquired by laser (NextEngine) and structured light (HP 3D Structured Light Scanner PRO 2) scanners. The resulting 3D models from both scanners were subjected to age-at-death analyses (via the quantitative method of Stoyanova et al., 2017) and sex analyses (via Diagnose Sexuelle Probabiliste 2 of Brůžek et al., 2017). Furthermore, high quality scans of a small sample ($n = 5$) of pubic symphyseal surfaces with the RedLux Profiler device were acquired as reference surfaces to which the outputs from both scanners were compared. Small deviations between surfaces were more evident in more rugged surfaces (in areas of depression and protrusion). Even though small differences from the reference surfaces were found, they did not have a significant effect on the age and sex estimates. It never resulted in the opposite sex assignment, and no significant differences were observed between age estimates (with the exception of those with the TPS/BE model).

1. Introduction

The 3D imaging technologies, i.e. surface scanning (both, laser and structured light), as well as computed tomography (CT) scanners and micro-CT scanners have become widely used in anatomical research over the last few years.¹ All of these devices make it possible to obtain 3D models of desired objects. Surface scanning, contrary to CT scanning, offers several practical advantages, for instance, the higher portability of most devices, texture capture options, low cost, and rapid post-processing. Furthermore, they can be operated without

certification since there is no radiation involved during the scanning process.^{2–4} On the other hand, internal structures remain hidden.⁴ Scanning technologies based on visible light have spread to many different disciplines: e.g. to forensic science,^{5,6} anthropology and paleoanthropology,^{2–4,7} anatomy and morphology,^{8–11} and paleontology and archaeology.^{8,12,13} They have allowed for new applications and brought additional advantages. It is now possible, for instance, to create and archive digital copies of skeletal remains as 3D models in the virtual environment. Such digital osteological collections are invaluable for researchers for several reasons. First, they represent the possibility

* Corresponding author. Department of Anthropology and Human Genetics, Charles University, Viničná 7, Prague 2, 128 43, Czech Republic.
E-mail address: koterova@natur.cuni.cz (A. Kotěrová).

<https://doi.org/10.1016/j.jflm.2019.101866>

Received 1 June 2019; Received in revised form 30 August 2019; Accepted 3 September 2019

Available online 05 September 2019

1752-928X/ © 2019 Elsevier Ltd and Faculty of Forensic and Legal Medicine. All rights reserved.

of permanent storage or documentation and conservation of bones, which are then accessible even though the real remains are no longer available or do not exist anymore. Virtual storage can serve not only as a repository, but also enables easier and faster sharing of data among researchers and institutions (e.g. Refs. 1,3,4,8,12,14–16). The reduced need for physical manipulation with human remains is certainly a great advantage¹⁵ since the preservation of dry bones varies as they are constantly being used for scientific purposes.¹⁷ Virtual models could be used for teaching and research, as well as for 3D printing, which can be used for exhibition purposes^{10,18,19} or as demonstrative evidence in court.^{20,21} Last but not least, digital technologies enable us to virtually reconstruct damaged skeletal remains, e.g. incompletely preserved fossil remains.^{22–24}

Traditional methods of biological profile estimation that use a morphometric or visual approach are usually used for defining the biological profile of an individual in bioarchaeology as well as in forensic anthropology (e.g. Refs. 25,26). However, virtual bone models have become of paramount importance and are commonly used, for instance, to measure metric variables in order to estimate sex.^{27,28} The consistency between the dimensions taken directly from dry bones and from their virtual representations,^{28–31} and even from their printed replicas,²⁰ has been proven repeatedly. Sex and stature estimates via linear measurements taken from virtual data obtained with two different laser scanners showed only a very small deviation from traditionally obtained data in one recent study.³² Moreover, bones in the virtual environment can undergo analyses that cannot be performed on dry bones, e.g. quantitative analyses of the surface with the use of geometric morphometrics.

For example, geometric morphometric tools are used for sex estimation^{33–35} and ancestry assessment.^{36,37} To estimate age-at-death, pelvic articulations (the pubic symphysis, the auricular surface, and the acetabulum) are often used since their surfaces undergo changes with aging and, recently, these surfaces have begun to be evaluated quantitatively.^{38–42} Such analyses tend to be more objective than traditional visual methods based on scoring as they allow for the evaluation of the morphological variation of the skeletal remains independent of the human eye and experience of the researcher.¹⁸

Villa et al.⁴³ raised an important question as to whether the results of surface quantification used for age estimation from different laser scanners are comparable. The precision and repeatability of measurements among different scanning devices are necessary in order to ensure the reliability of the biological profile estimation methods. We have extended this question to another parameter of biological profile – sex estimation (besides age estimation) and, in contrast to the original study where only laser scanners were used, both laser and structured light scanners were compared.

The aims of the present study are twofold. The first is to compare 3D models of *os coxae* made by two different surface scanners (NextEngine laser scanner and HP 3D Structured Light Scanner Pro S2) with a reference sample derived from a RedLux Profiler device. Second, we aimed at assessing whether the scanning equipment has an effect on the age-at-death estimation (via the quantitative method of Stoyanova et al., 2017) and sex assessment (via DSP2 - Diagnose Sexuelle Probabiliste of Brůžek et al., 2017).

2. Material

The skeletal sample used in the present study originates from the cemetery of the second church in the Mikulčice settlement (9th–10th century AD), South Moravia, Czech Republic. This sample represents a medieval population of Central Europe that belonged to the Great Moravian Empire.⁴⁴ We used 18 adult individuals, of which 11 had well preserved *os coxae* on both sides, and seven individuals who had only the left or right bone well preserved. Altogether, 29 *os coxae* were used in this study. Only individuals with well-preserved articular surfaces (pubic symphysis and auricular surface) were selected. Even if we do

not know the real age or sex of individuals, we can compare the resulting estimates with each other when they are derived from surface models digitized with different scanning technologies (HP 3D SLS, NextEngine and RedLux).

3. Methods

3.1. Digitization of skeletal material

A small sample of pubic symphyses ($n = 5$) was digitized with the use of a RedLux Profiler contactless metrology device (RedLux Ltd., Southampton, UK).^{45,46} Samples were selected to include both smooth and significantly billowed symphyses. The scanned surface of key areas was utilized as a reference surface to compare the resolution and quality of scans obtained by commonly used scanners. The whole surface of *os coxae* ($n = 29$) was then digitized with two different scanning devices: the NextEngine 3D scanner Ultra HD and the HP 3D Structured Light Scanner PRO S2. The scanning process as well as the post-processing procedures of all three scanners are described in the following sections.

3.1.1. RedLux

The pubic symphyses of five selected *os coxae* were digitized using the RedLux profiler, which is a device designed for very precise surface measurements using a confocal sensor. Due to limited space capacity resulting from the technical arrangement of the measuring device, the physical casts of these five pubic symphyses needed to be obtained. As a casting material, the two-component Addition Cure Molding Rubber was used, which is known under the trade designation MM242R.⁴⁷ This material shows negligible volumetric change (linear shrinkage of 0.09%) and excellent quality and accuracy of surface reconstruction. It is also necessary to ensure thorough venting, using a desiccator and vacuum pump so that no air bubbles affect the volumetric change. Venting was carried out for a minimum of 10 min at 150 mbar vacuum. The resulting symphyseal cast for one selected sample is shown in Fig. 1.

The casts were scanned using a highly accurate RedLux profiler device. The instrument was equipped with two high-precision movable linear axes and two rotary ones. The rotary sections carry the sample and the linear sections carry the sensor. With this sensor, the lens error, commonly known as chromatic aberration, is used to measure the distance to an object. By combining the sensor signal with the knowledge of the exact position of all 4 stages, 3D representation of the surface can be created. The instrument has the capability to measure the entire surface in a single procedure. The accuracy of the resulting point cloud is given by the resolution of 2 linear axes, the resolution of the two rotational axes and the resolution of the probe. The resolution of each linear axis is 100 nm, the resolution of each rotary axis is 10 arc seconds and the resolution of the probe is 20 nm. A detailed description of the



Fig. 1. Symphyseal cast of sample no. 390.

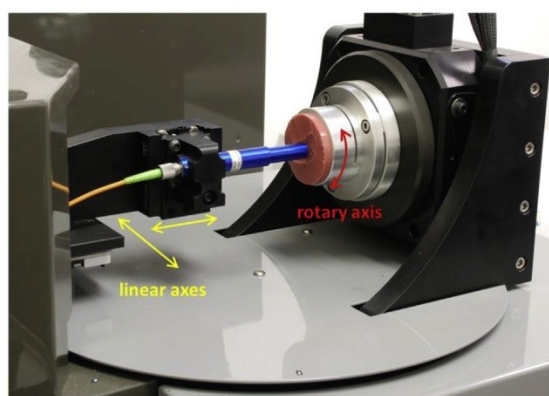


Fig. 2. Arrangement of the RedLux measuring device.

RedLux profiler device can be found in Ref.⁴⁸ The arrangement of the measuring device is shown in Fig. 2.

Since the measurement of a surface with a RedLux profiler is a free-form surface measurement task, it is important to scan the surface with a sufficiently dense point cloud to capture the real scanned surface with all its irregularities. Throughout all of the performed measurements, the point cloud density was 540 individual points per one rotation of the measured sample in the vertical plane; within every single rotation, the measured sample was shifted by approximately 0.1 mm in the horizontal plane. More than 120,000 points were obtained for each sample using a RedLux profiler device. The resulting point cloud for the selected sample is shown in Fig. 3.

As it is shown in Fig. 3, the point coverage on the sample surface is irregular due to the used scanning method. For a subsequent comparison with the HP 3D Structured Light Scanner Pro S2 and the NextEngine laser scanner, it was necessary to obtain a regular network of points. First, the co-ordinate data collected from the RedLux profiler were interpolated using Matlab's function *scatteredInterpolant* (The Mathworks, Inc.). This function is included in the basic Matlab package and performs interpolation on 3D sets of points that have no structure among their relative locations (scattered data set).

Interpolation step $\Delta = 0.025$ mm and a 'natural' interpolation method was chosen for both directions, specifying the density of the net. A detailed description of this function can be found in the Matlab software.⁴⁹ The mesh representation of the surface is shown in Fig. 3.

3.1.2. NextEngine and HP 3D structured light scanner PRO S2

The whole sample of *os coxae* was digitized by two different surface scanners. We used the laser scanner NextEngine 3D Ultra HD and the HP 3D Structured Light Scanner PRO S2 (previously known as DAVID SLS 2) with a maximum resolution of 0.1 mm and 0.05 mm, respectively. These two scanners represent different scanning technologies: laser and structured light. Since the aim of this study is to compare the resulting 3D models from different surface scanners in terms of their

surface representation and their possible impact on sex and age estimation, 3D models were created under the optimal conditions for the particular scanner.

The entire surface of *os coxae* was scanned to facilitate the creation of the osteological collection. The whole *os coxae* were used to estimate sex. However, only isolated pubic symphyseal surfaces were used for age-at-death estimation. The scanning process as well as the post-processing (aligning multiple scans of each bone together to form a final polygonal mesh) were performed in the integrated software of each scanner (ScanStudio HD and David LaserScanner v.3.10.4, respectively). In the case of HP 3D Structured Light Scanner PRO S2 (hereinafter HP 3D SLS), the calibration was done with the 120 mm pattern, which is ideal for objects of a size similar to an *os coxae*. The scanning procedure was performed against a black background and the scanned *os coxae* were manually rotated from both the ventral and dorsal sides to create a solid model. In the case of the NextEngine scanner, a dedicated rotational device was used to fix the bone and rotate it in front of the scanner so that each individual scan overlapped with the previous one and the next. The final scan was automatically assembled from these individual scans using the ScanStudio HD software. Each bone was attached to the device at two points: one along the iliac crest and the other just in front of the ischial tuberosity. Both points were selected to minimize the areas where the laser beam does not reach, thus, ensuring that if there is a fraction of the surface to be reconstructed, such an area is very small. These contact areas with the rotational device might have been approximately 1 mm² each.

The final 3D models were saved in the stl format. Each mesh had to be simplified (consistent simplification on 3 million faces) in order to facilitate manipulation. Subsequently, the 3D models from the NextEngine 3D scanner had to be scaled (in MeshLab software⁵⁰) to obtain the same dimensions as the models from the HP 3D SLS. The models of the whole *os coxae* were used for sex estimation, while the articular surfaces of pubic symphysis that we isolated from the rest of the bone (in MeshLab software) served as input data for age-at-death estimation.

3.2. Comparison of resulting 3D surfaces

Once the mesh representation of the pubic symphyseal surface was created, it became important to calculate the distribution of deviations between the actual and reference surfaces. Both surfaces were overlapped using the *local best fit* feature implemented in the commercially available GOM Inspect software.⁵¹ The function minimizes differences (square error) through all of the used points and the software tries to align the point sets so the differences are zero or as close to zero as possible. The resulting deviations were assessed with descriptive statistics (mean, standard deviation, median, and interquartile range) for all samples.

3.3. Biological profile assessment

3.3.1. Sex estimation

Linear dimensions derived from 3D surface models taken with two

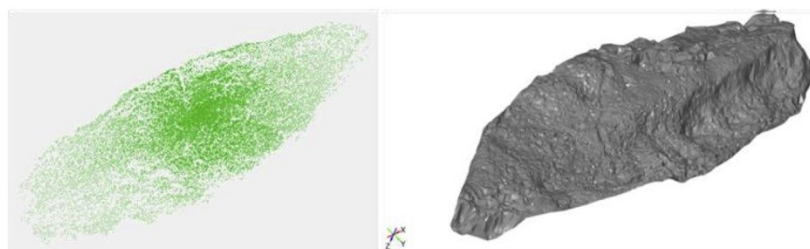


Fig. 3. left: Cloud of points (left), mesh representation of surface (right), sample no. 359.

Table 1
Os coxae measurements in DSP2.

	Variable	Name	Reference
1	PUM	Acetabulo-symphyseal pubic length	81
2	SPU	Cotylo-pubic width	82
3	DCOX (M1)	Coxal length	83
4	IIMT (M15.1)	Greater sciatic notch height	83
5	ISMM	Ischium post-acetabular length	84
6	SCOX (12)	Iliac or coxal breadth	83
7	SS	Spino-sciatic length	82
8	SA	Spino-auricular length	82
9	SIS (M14.1)	Cotylo-sciatic breadth	83
10	VEAC (M22)	Vertical acetabular diameter	83

different scanners and dimensions directly from dry *ossa coxa* served as the input data for the DSP2 (Diagnose Sexuelle Probabiliste 2) sex determination method.^{52,53} The DSP2 method is based on linear discriminant analysis and posterior probabilities. The output of this sex determination tool is the probability of being male or female (sex is determined if the posterior probability is ≥ 0.95). Ten variables (or a number, at least four, that could be measured for a given bone depending on its preservation) were measured according to the definitions (Table 1) described in the software interface. The variables were first measured on dry bones with appropriate measuring instruments (sliding caliper, friction divider, and pelvimeter). Second, the measurements on the 3D models were carried out in the Morphome3cs software⁵⁴ in the virtual environment. Additionally, ten randomly chosen *ossa coxa* were measured twice over a period of four weeks (for all three types of acquisition) for intra-observer error. All the measurements were taken by two researchers (AK and RR), both trained in pelvic osteometry with approximately the same experience. Apart from the intra-observer error calculated for linear variables, the inter-observer error between the two equally trained observers was calculated as well.

To verify the accuracy of the measured dimensions within each type of data taken by one observer (intra-observer error), we calculated the technical error of measurement (TEM) and the relative TEM (rTEM) expressed as a percentage. Both statistical characteristics are commonly used to evaluate intra-observer precision.^{27,30,55–57} The inter-observer error was computed for measurements taken on dry bones and on 3D models acquired with both scanners. A paired *t*-test was applied to assess whether there were significant differences between the two observers.

3.3.2. Age-at-death estimation

The age-at-death of our sample was estimated with the use of a recent computational method of Stoyanova et al.^{40,41} This fully quantitative evaluation of pubic symphyseal surfaces is based on the mathematical evaluation of the flatness of the surface, the curvature of the ventral margin of the pubic symphysis and their combination. The flatness of the surface is captured by the TPS/BE (Thin Plate Spline/Bending Energy) analysis and the SAH-Score (described in detail in Ref. 39). The last computational method captures the curvature of the ventral margin (VC) of the pubic symphysis. These analyses are incorporated into the “forAge” software. A detailed description can be found in the original study.⁴¹

The isolated articular surfaces of the pubic symphyses (from the reference sample as well as from both compared samples) were simplified to 15,000 faces and saved in the ply format before loading to the forAge software to estimate the age-at-death. All the isolated pubic symphyseal surfaces ($n = 29$) from the NextEngine, the HP 3D SLS, and the small sample ($n = 5$) from the RedLux were subjected to this quantitative analysis. The 3D models digitized with HP 3D SLS and NextEngine were compared using a paired *t*-test. The small sample ($n = 5$) of pubic bones digitized with RedLux was also compared with

other samples. The differences within the corresponding individuals between RedLux and HP 3D SLS and RedLux and NextEngine, respectively, were evaluated with a paired one-sample *t*-test.

4. Results

4.1. Comparison of resulting 3D surfaces

Examples of three isolated pubic symphyseal surfaces digitized with the three scanning devices are shown in Fig. 4.

Visualization has been made in the form of color-coded maps of scatters of deviations between the reference and compared scans. This comparison was performed for all 5 selected pubic symphyseal surfaces, both for the HP 3D Structured Light Scanner Pro S2 and the NextEngine laser scanner. The color scale bar on the map of deviations shows both positive and negative dimensional changes. The positive scale (red color) means that the compared surface is above the reference surface and the negative scale (blue color) indicates that the compared surface is below the reference one. The gray color refers to the surface where no data were available from the compared scanners (HP 3D SLS and NextEngine).

An example of color-coded maps for selected surfaces is shown in Fig. 5. It can be seen that the largest and the smallest deviations from the reference surfaces are in the areas of depressions or protrusions. This is more evident on surfaces that are more rugged (e.g. pubic symphysis no. 390). It shows that scans acquired by HP 3D SLS and NextEngine are smoothed out and do not capture as much detail as the reference surface obtained with the RedLux profiler. This is due to the resolution of the particular scanning technology.

The descriptive statistics of the resulting deviations are summarized in Table 2. The graphical comparison of the examined scanners is shown in Fig. 6 for all the samples in the form of box plots. The deviations from the reference surface were slightly larger for the NextEngine than for the HP 3D SLS. In the case of the NextEngine scanner, the interquartile range is higher for all samples, as is the standard deviation, except for sample no. 383. Contrary to the NextEngine results, there are more places where no data are available in the scans from the HP 3D SLS, particularly in the major depressions. From Table 2 and Fig. 6, it can also be seen that the value of the percentage difference of IQR is related to the degree of the billowing of the surface. The percentage difference of IQR is significantly higher in the samples which are more corrugated, such as sample no. 390, where a relatively large lateral billowing is evident (Fig. 5).

4.2. Sex estimation

For the manual DSP method as well as for virtual DSP performed on both 3D models (HP 3D SLS and NextEngine), comparisons of estimated sexes (and agreement) between two observers were performed. The results of agreement in estimating male, female, and undetermined sex (N/A) of the two researchers are shown in Tables 3–5. Some differences between the observers were found (these variations concerned three individuals); however, the opposite sex was never assigned to the same individual (rather, such an individual was assigned N/A).

4.2.1. Intra and inter-observer error of measurements

Results of intra-observer error are presented in Table 6. With the measurements on dry bones, the average TEM values were 0.80 mm and 0.62 mm, respectively. TEM values for dry bones ranged between 0.32 and 1.35 mm with rTEM 0.35%–3.09% for the first researcher; for the second researcher, from 0.45 to 1.01 mm, rTEM 0.20%–2.07%. The lowest average TEM values were reached by both researchers coincidentally in the case of HP 3D SLS (0.62 and 0.56 mm, respectively). The intra-observer error of the Researcher 1 ranged between 0.35 and 1.24 mm for all ten dimensions and the rTEM ranged between 0.21% and 2.85%; for Researcher 2, between 0.24 and 0.88 mm with rTEM

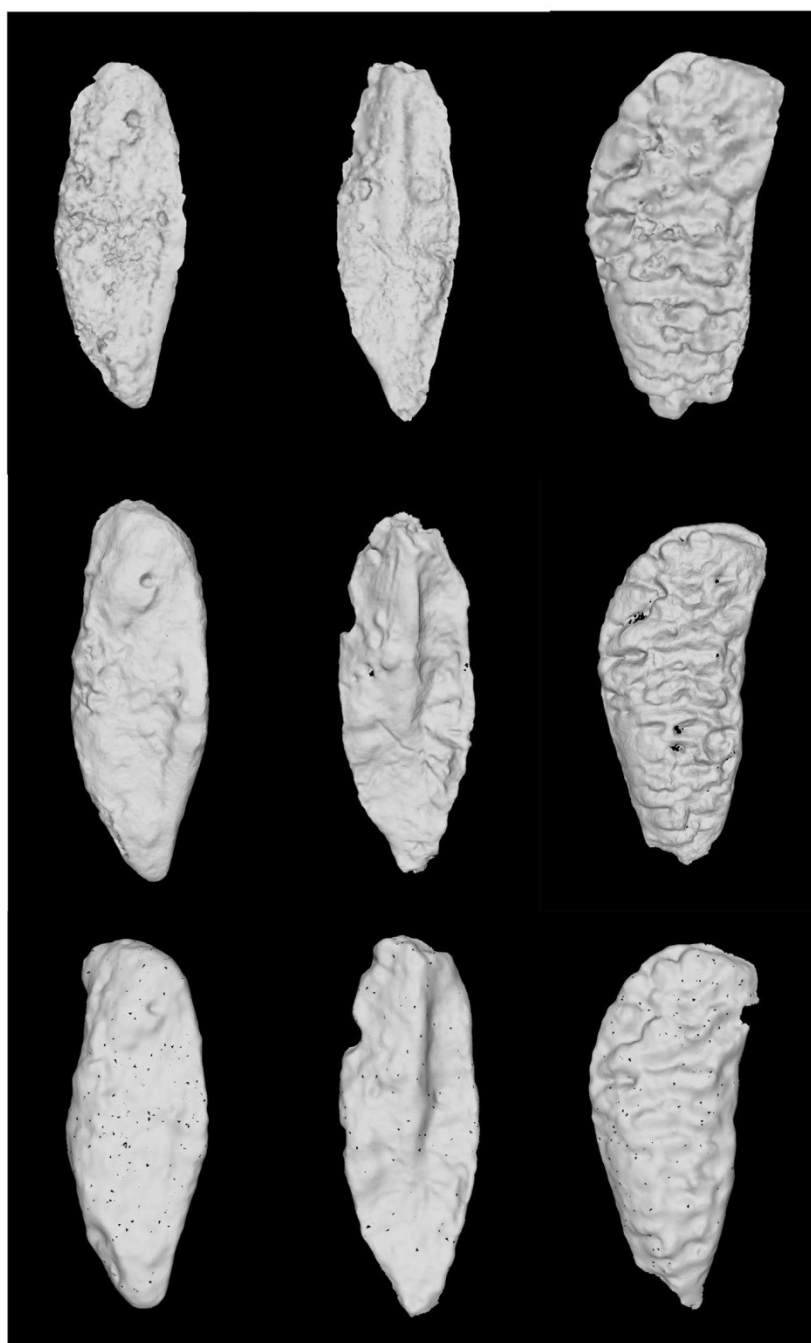


Fig. 4. Examples of digitized surfaces of isolated pubic symphyses. Models derived from RedLux (upper row), HP 3D SLS (middle row) and NextEngine (lower row).

from 0.19% to 2.22%. The average intra-observer error for NextEngine was very similar to the previous results (0.72 mm and 0.57 mm, respectively). The error for Researcher 1 was between 0.26 and 1.38 mm, r TEM 0.20%–2.36%; the TEM of Researcher 2 ranged from 0.12 to 1.19 mm, with r TEM of 0.07%–1.95%.

The results of inter-observer error for the variables measured directly on dry bones, on 3D models digitized with HP 3D SLS, and NextEngine, respectively, are shown in Table 7. Significant differences between the two researchers when dry bones were measured were

found for IIMT, ISMM, SCOX, SS, and VEAC). The DSP variables measured on the 3D models from the HP 3D SLS scanner were statistically different between the two researchers in IIMT, ISMM, SCOX, SS, SIS, and VEAC. Inter-observer differences were also found for the 3D measurements derived from NextEngine, namely for PUM, DCOX, SS, and VEAC.

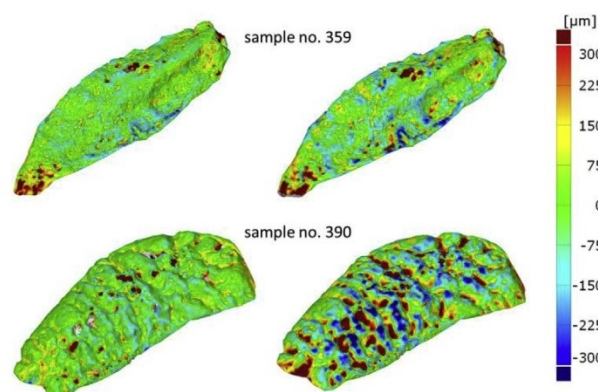


Fig. 5. Color-coded maps of the resulting deviations (sample no. 359 and 390); left: HP 3D SLS vs. reference surface; right: NextEngine laser scanner vs. reference surface. (For interpretation of the references to color in this figure legend, the reader is referred to the Web version of this article.)

4.3. Age estimation

A paired *t*-test was applied to reveal the potential differences between the estimated ages derived from the 3D models of the isolated pubic symphyses from the NextEngine and the HP 3D SLS. The results are provided in Table 8. The differences in the estimated ages were not statistically significant. The only exception was the TPS/BE regression model. Thus, the null hypothesis was not rejected for any of the models, except for the TPS/BE model. These results can be interpreted as a negligible effect of the scanning technologies on age estimation in this study. The sample of isolated pubic symphyseal surfaces derived from the RedLux Profiler ($n = 5$) was also subjected to the age-at-death analysis. We did detect differences between HP 3D SLS and RedLux for the SAH model, and between NextEngine and Redlux in the SAH and SAH + VC models. The null hypothesis was not rejected in all other cases (see Table 9).

5. Discussion

5.1. Scanning – problem of compatibility

Many researchers travel around the world and study osteological collections to design new methods or to validate already existing ones. Scanning technologies are already used in biological and forensic anthropology and have become of paramount importance (e.g. Refs. 4,7,58). Some of the greatest benefits are the digital storage and sharing of osteological remains. The digital material can come to researchers or it can be publicly available under certain conditions. However, research institutions are equipped with different scanning devices that may

produce varying outputs.

Therefore, it is necessary to verify that the outputs from different devices are comparable to each other (and under what settings) and that they do not affect further analyses such as the estimation of the biological profile. The comparability of outputs from different devices is especially important in age-at-death estimation since minor changes on the joint surface may influence the final estimate significantly. However, the consistency of outputs from different devices for biological profile estimation needs to be tested. This has not yet been sufficiently explored, except for a few exceptions, such as the aforementioned study of Villa et al.⁴³

To test the effect of the scanning device on the forensic methods of biological profile estimation, we chose sex and age-at-death estimation. For sexing, the method called DSP is well established; its reliability has been proven and it guarantees objectivity (e.g. Refs. 27,28,59,60). The forAge software is one of the few age estimation approaches using the mathematical quantification of bone surface that has been published so far. The repeatability of the method was tested with excellent results⁶¹ and its use is suitable for individuals under 40 years of age.⁶²

The advantages and disadvantages of both scanners (NextEngine and HP 3D Structured Light Scanner PRO S2) and the technologies represented by them should be discussed to help future users assess them for their research goals. Both scanning technologies are used on skeletal remains. However, laser scanning technology is generally preferred among anthropologists.^{18,63} One of the most often used scanners is the NextEngine laser scanner (e.g. Refs. 7,10,39,64–66), which was also used for the development of one method of age estimation that we tested in our study.^{40,41} Although less attention has been paid to HP 3D SLS, its use is now on the rise. HP 3D SLS was used or tested in many studies on human and animal bones, as well as for other purposes.^{19,67–74} Both tested scanners are commercially available, and belong to the low-cost category of scanners (under \$ 3,000), which makes them accessible to a great number of users. Moreover, the cost vs. performance ratio very often makes them the first choice. In terms of the time needed to acquire and post-process scans, the HP 3D SLS outperforms the NextEngine scanner, mainly because the laser technology is more time-consuming than other technologies.^{4,15} Both scanners are characterized by high portability, and can be easily carried to various collections around the world. Also, both scanners are able to capture texture and provide a 3D textured mesh as an output, which is often a great benefit.⁷

Nonetheless, both NextEngine and HP 3D SLS have some limitations. Although laser and white light scanners are commonly used on skeletal remains, they are limited in scanning dark or transparent objects, or objects reflecting light (e.g. tooth enamel).^{7,75,76} Systems using blue light (e.g. HP 3D SLS) should reduce this limitation⁷; however, one of the authors (A.K.), who routinely operates the HP 3D SLS, has experienced similar issues (problems capturing very dark areas on objects). In the case of the HP 3D SLS, constant ambient light during scanning is recommended, and a generally darker room is better suited for scanning.

Table 2

Results of quantitative comparison between measured samples (HP 3D SLS vs. Reference sample^a and NextEngine vs. Reference sample).

No. of individual	Scanner	Mean value for normal distribution	Median	Standard deviation	Interquartile span	Percentage difference IQR
352	HP 3D	26	2	154	147	+50
	NextE	26	4	204	220	
359	HP 3D	8	−8	118	104	+35
	NextE	7	−4	146	140	
382	HP 3D	14	6	113	114	+24
	NextE	13	0	138	141	
383	HP 3D	15	5	187	122	+51
	NextE	26	15	174	184	
390	HP 3D	14	0	126	88	+141
	NextE	21	2	202	212	

^a Reference samples were acquired with the RedLux Profiler.

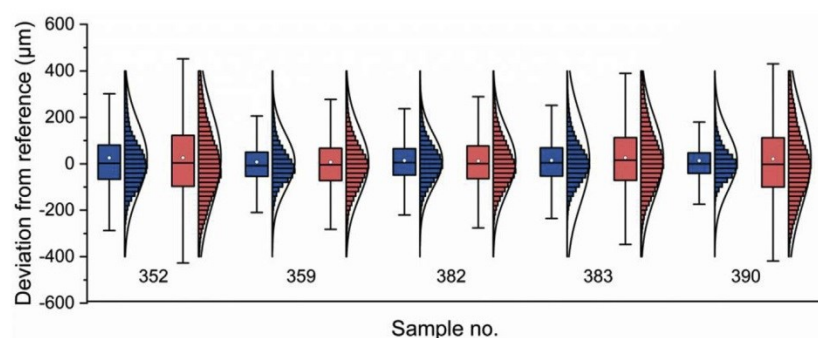


Fig. 6. Deviation from the reference sample (Redlux scan) for the HP 3D SLS (blue) and NextEngine laser scanner (red). On each box, the central mark is the median, the white point is the mean value for normal distribution μ , the edges of the box are the 25th and 75th percentiles, and the whiskers extend to the most extreme data points not considered outliers. (For interpretation of the references to color in this figure legend, the reader is referred to the Web version of this article.)

Table 3

Agreement between researchers in estimating sex with the use of DSP on dry bones. Shaded cells correspond to the number of individuals in which the two researchers agreed.

		Researcher 1			
		Male	Female	N/A	Total
Researcher 2	Male	15	0	0	15
	Female	0	13	0	13
	N/A	1	0	0	1
Total		16	13	0	29

Table 4

Agreement between the researchers in estimating sex with the use of the DSP on virtual models from HP 3D SLS. Shaded cells correspond to the number of individuals in which the two researchers agreed.

		Researcher 1			
		Male	Female	N/A	Total
Researcher 2	Male	15	1	0	16
	Female	0	11	0	11
	N/A	0	1	1	2
Total		15	13	1	29

Table 5

Agreement between the two researchers in estimating sex with the use of the DSP on virtual models from NextEngine. Shaded cells correspond to the number of individuals in which the two researchers agreed.

		Researcher 1			
		Male	Female	N/A	Total
Researcher 2	Male	15	0	0	15
	Female	0	12	0	12
	N/A	1	0	1	2
Total		16	12	1	29

It has to be emphasized that the quality of 3D models could be affected by post-processing. Simplification is often required to reduce file size and to fasten data processing and manipulation to virtual data.^{4,77} Even though in the case of smoothing procedures the positive or negative effect on mesh topology depends on the algorithm used, the decimation procedure always leads to loss of information, which affects mesh topology and measurement. By increasing the mesh triangle size, the accuracy of measurement is negatively affected.^{77,78} The amount of decimation should be defined with regards to the type of object and the purpose for which it is to be used.^{4,77} In this paper, the only post-processing step performed was decimation, in order to enable better manipulation on the computer during analysis. Since the whole *osssa coxa* was scanned, in the case of HP 3D SLS and NextEngine, simplification was applied to all the models equally to enhance the possibility of manipulation with minimum information loss. These models were then

decimated once more due to the forAge software properties. The reference models using Redlux needed to be simplified only once in order to estimate age. Other post-processing procedures (e.g. hole filling, smoothing) were not performed to prevent the quality of the scan from being negatively affected. Therefore, the dimensions in our study could not be affected by different post-processing procedures. However, it would be of great benefit for future studies if somebody tested to what extent the surface could be simplified without losing too much information or obtaining inaccurate or imprecise estimates.

In our study, we worked with the assumption that different scanner operators or different scanning protocols do not affect the resulting 3D models or their geometric properties.⁷⁸ However, all the virtual data were acquired by experienced operators to ensure the consistency of scanned data. All the data were taken under the optimal conditions of each scanner. Since it would be complicated to compare scanning devices with each other, such an approach seemed the most reasonable to us. Moreover, it was also used in the study by Villa et al.⁴³

5.2. Comparison of tested devices

Even the visual inspection of the final 3D models revealed that the Redlux scanner captures much more detail than the other two low-cost scanners.

Our results indicate that the NextEngine laser scanner captured fewer details (it smoothed the surface the most and had the largest information loss) than the HP 3D Structured Light Scanner when compared to the reference scans from the Redlux Profiler. Singh et al.⁷⁹ report that structured light technology is more accurate in comparison to laser technology when used to calculate surface area and volume. Results of another study¹⁵ indicate that structured light technology captured external structures better than other technologies (including laser technology). It should be noted here that these differences, as found in our study, are relatively small and their impact on further analyses (biological profile analyses) would be negligible. Our analyses of sex and age estimation confirm this notion.

5.3. Influence of different scanning devices on the linear measurement and sex assessment

Both observers estimated the sex of all individuals almost uniformly irrespective of the scanning technology. The intra-observer and inter-observer errors of the linear measurements were evaluated. According to Camison et al.,⁸⁰ who divided *r*TEM values into five categories (< 1% = excellent, 1–3.9% = very good, 4–6.9% = good, 7–9.9% = moderate, and > 10% = poor), the intra-observer error of both researchers in most cases fell into the “excellent” category and the rest into “very good” (the highest value reached 3.09%). Nevertheless, our results of inter-observer error show some statistically significant differences between the two observers, which may not be due to different scanners, as their results never led to the opposite classification.

Table 6

The intra-observer precision of measured variables used for DSP.

Variable	Researcher 1						Researcher 2					
	dry bones		HP 3D SLS		NextEngine		dry bones		HP 3D SLS		NextEngine	
	TEM	rTEM	TEM	rTEM	TEM	rTEM	TEM	rTEM	TEM	rTEM	TEM	rTEM
PUM	1.19	1.58	1.24	1.64	1.38	1.84	0.56	0.74	0.82	1.07	1.17	1.51
SPU	0.89	3.09	0.80	2.85	0.67	2.36	0.56	1.97	0.63	2.22	0.46	1.57
DCOX	0.77	0.35	0.49	0.23	1.11	0.51	0.45	0.20	0.83	0.38	1.19	0.55
IIMT	1.35	2.91	0.91	2.05	0.78	1.76	0.94	2.07	0.88	2.02	0.85	1.95
ISMM	1.25	1.14	0.57	0.52	1.31	1.16	0.47	0.43	0.67	0.60	0.55	0.49
SCOX	0.57	0.35	0.35	0.21	0.33	0.20	0.55	0.34	0.30	0.19	0.12	0.07
SS	0.43	0.57	0.43	0.58	0.26	0.35	0.60	0.81	0.24	0.33	0.47	0.63
SA	0.68	0.84	0.53	0.67	0.40	0.50	1.01	1.25	0.38	0.48	0.42	0.52
SIS	0.32	0.80	0.40	1.03	0.38	0.97	0.49	1.24	0.43	1.11	0.26	0.66
VEAC	0.54	0.95	0.52	0.91	0.58	1.00	0.60	1.07	0.45	0.81	0.24	0.43
mean	0.80		0.62		0.72		0.62		0.56		0.57	

TEM = technical error of measurement; rTEM = relative technical error of measurement; the measurement unit of TEM is given in mm; rTEM expressed as a percentage.

Table 7

Results of measurement differences (used for sex estimation with the DSP) on dry bones, 3D models made with HP 3D SLS and NextEngine between two researchers.

Variable	N	Max difference (mm)	Mean difference (mm)	SD	p-value
Dry bones					
PUM	29	4.00	1.22	4.99	0.05
SPU	28	4.00	1.34	3.06	0.11
DCOX	27	4.00	0.98	9.18	0.53
IIMT	28	4.50	1.79	6.79	< 0.005
ISMM	29	3.50	1.07	5.98	< 0.001
SCOX	15	3.00	0.83	6.27	0.01
SS	28	3.50	1.70	3.64	< 0.001
SA	28	4.50	1.70	4.34	0.12
SIS	29	2.00	0.45	2.9	0.27
VEAC	29	3.50	0.97	2.99	0.02
HP 3D SLS					
PUM	29	5.00	1.66	4.88	0.18
SPU	28	3.30	1.04	3.01	0.22
DCOX	27	6.49	2.18	8.49	0.21
IIMT	28	5.24	1.79	6.86	0.02
ISMM	29	5.00	1.01	5.99	< 0.01
SCOX	15	3.81	1.11	6.49	0.04
SS	28	3.32	0.96	3.66	< 0.001
SA	28	4.10	0.97	4.61	0.89
SIS	29	1.01	0.51	2.93	< 0.01
VEAC	29	4.97	1.90	3.07	< 0.001
NextEngine					
PUM	29	7.76	2.51	4.63	< 0.001
SPU	28	3.49	1.16	3.14	0.07
DCOX	27	7.46	2.13	9.25	0.01
IIMT	28	4.88	1.49	7.08	0.22
ISMM	29	2.60	0.82	6.21	0.83
SCOX	15	5.18	0.97	6.60	0.20
SS	28	2.85	1.19	3.67	< 0.001
SA	28	3.01	0.98	4.68	0.51
SIS	29	2.09	0.54	2.75	0.44
VEAC	29	4.31	2.39	3.32	< 0.001

Here, our results could be interpreted in a way that is similar to the study of Mullins and Albanese³²: that even significant differences (in the observer) need not affect the estimates or utility of this type of data. To the best of our knowledge, this is the first study testing the DSP method on virtual models acquired by surface scanners. Previously, the method was tested only on 3D models acquired with CT scanning (e.g. Refs. 27,28,60).

Table 8

Results of a paired t-test between the estimated ages based on models from HP 3D SLS and NextEngine.

Regression model	p-value
TPS/BE ^a	0.01
SAH ^b	0.07
VC ^c	0.10
TPS/BE + VC ^d	0.27
SAH + VC ^e	0.41

P-values are shown for a two-tailed test.

^a Thin plate spline/Bending energy.

^b Slice and Algee-Hewitt score.

^c Ventral curvature.

^d Combination of TPS/BE and VC (multivariate model).

^e Combination of SAH score and VC (multivariate model).

Table 9

Results of a paired t-test for differences between estimated ages derived from the HP 3D SLS vs. RedLux and between NextEngine vs RedLux.

Regression model	HP 3D SLS vs. RedLux	NextEngine vs. RedLux
	p-value	
TPS/BE ^a	0.74	0.41
SAH ^b	0.04	0.03
VC ^c	0.30	0.18
TPS/BE + VC ^d	0.87	0.99
SAH + VC ^e	0.05	0.03

P-values are shown for a two-tailed test.

^a Thin plate spline/Bending energy.

^b Slice and Algee-Hewitt score.

^c Ventral curvature.

^d Combination of TPS/BE and VC (multivariate model).

^e Combination of SAH score and VC (multivariate model).

5.4. Effect of the scanning device on delicate surface changes in the age-at-death estimation

Although the comparison of captured surfaces from both low-cost scanners showed slightly better outputs for the HP 3D SLS, there was almost no effect detected on the quantitative methods of age estimation (the only exception was the TPS/BE model). We can conclude that other scanning technologies (at least structured light, here represented by the HP 3D SLS) can be used to estimate age using the method of Stoyanova

et al. ^{40,41}

When compared to the outputs obtained with the Redlux, significant differences in one out of five models were found in the case of HP 3D SLS and two out of five with NextEngine. However, it was not assumed in our study that Redlux should be used to estimate age-at-death through quantitative methods. This device was selected only as a reference for comparing two low cost scanners as its routine use in anthropology would be too expensive and impractical.

Larger deviations between the captured surfaces are more evident on more billowed surfaces, e.g. sample no. 390, which was obviously a very young individual (with a partially unfused iliac crest). Therefore, further investigation is needed to clarify whether the effect of different scanners is more obvious in more billowed surfaces, typical for younger individuals.

6. Conclusion

The two tested scanning technologies, structured light and laser represented by HP 3D SLS and NextEngine, respectively, showed only small surface deviation from the reference sample in our study. The structured light technology seems to be more accurate (captures slightly more detail) than the laser technology. Nevertheless, no significant impact on age and sex estimates was observed, except for the TPS/BE model in age estimation. Thus, it appears that the type of scanner does not have a significant effect on the estimate of the biological profile under optimal scanning settings. However, we encourage further investigation, especially in the case of age-at-death estimation, where even subtle changes to the articulation surface are evaluated. Both the existing as well as future analyses of these surfaces could be sensitive to the different 3D representations acquired with various devices.

Declarations of interest

None.

Acknowledgments

We would like to thank the Department of Anthropology at the National Museum in Prague for providing the osteological material.

This research has been supported by the research grant Charles University Grant Agency No. 642218 and partially by IRN Bipedal Equilibrium, CNRS, France.

References

- Villa C, Buckberry J, Lynnerup N. Evaluating osteological ageing from digital data. *J Anat*. 2016;2016:12544. <https://doi.org/10.1111/joa.12544>.
- Friess M. Calvarial shape variation among Middle Pleistocene hominins: an application of surface scanning in paleoanthropology. *CR Palevol*. 2010;9:435–443. <https://doi.org/10.1016/j.crpv.2010.07.016>.
- Kuzminsky SC, Gardiner MS. Three-dimensional laser scanning: potential uses for museum conservation and scientific research. *J Archaeol Sci*. 2012;39:2744–2751. <https://doi.org/10.1016/j.jas.2012.04.020>.
- Friess M. Scratching the surface? The use of surface scanning in physical and paleoanthropology. *J Anthropol Sci*. 2012;90:1–25. <https://doi.org/10.4436/jass.90004>.
- Thompson TJU, Norris P. A new method for the recovery and evidential comparison of footwear impressions using 3D structured light scanning. *Sci Justice*. 2018;58:237–243. <https://doi.org/10.1016/j.scjus.2018.02.001>.
- Naether S, Buck U, Raess B, Thali M. Crime scene reconstruction using 3-D scanning and medical imaging technologies. *Sci Justice*. 2010;50:35. <https://doi.org/10.1016/j.scjus.2009.11.037>.
- Slizewski A, Friess M, Semal P. Surface scanning of anthropological specimens: nominal-actual comparison with low cost laser scanner and high end fringe light projection surface scanning systems. *Quartar*. 2010;57:179–187.
- Vigiano D, Thanassoulas T, Di-Cesare C, et al. A low-cost system to acquire 3D surface data from anatomical samples. *Eur J Anat*. 2015;19:343–349.
- Aung SC, Ngim RCK, Lee ST. Evaluation of the laser scanner as a surface measuring tool and its accuracy compared with direct facial anthropometric measurements. *Br J Plast Surg*. 1995;48:551–558. [https://doi.org/10.1016/0007-1226\(95\)90043-8](https://doi.org/10.1016/0007-1226(95)90043-8).
- Cantín M, Muñoz M, Olate S. Generation of 3D tooth models based on three-dimensional scanning to study the morphology of permanent teeth. *Int J Morphol*. 2015;33:782–787.
- Gibelli D, Pucciarelli V, Poppa P, et al. Three-dimensional facial anatomy evaluation: reliability of laser scanner consecutive scans procedure in comparison with stereo-photogrammetry. *J Cranio-Maxillo-Fac Surg*. 2018;46:1807–1813. <https://doi.org/10.1016/j.jcms.2018.07.008>.
- Adams JW, Olah A, McCurry MR, Potze S, Wilson BA. Surface model and tomographic archive of fossil primate and other mammal holotype and paratype specimens of the Ditsong National Museum of Natural History, Pretoria, South Africa. *PLoS One*. 2015;10:1–14. <https://doi.org/10.1371/journal.pone.0139800>.
- Mpherron SP, Gernat T, Hublin J. Structured light scanning for high-resolution documentation of in situ archaeological finds. *J Archaeol Sci*. 2009;36:19–24. <https://doi.org/10.1016/j.jas.2008.06.028>.
- Guydish M, Henson K. Using digitized Native American skeletal remains to conduct osteological analyses. *Proc W Va Acad Sci*. 2017;89.
- Mathys A, Brecko J, Semal P. Comparing 3D digitizing technologies: what are the differences? *Digital Heritage International Congress (DigitalHeritage)*. IEEE; 2013:201–204.
- Errickson D. Shedding light on skeletal remains: the use of structured light scanning for 3D archiving. In: Errickson D, Thompson T, eds. *Human Remains: Another Dimension*. Academic Press; 2017:93–101.
- Ferreira MT, Ross AH, Cunha E. A reflection on the maintenance of identified skeletal collections state of preservation. *Rev Med Leg*. 2017;8:186. <https://doi.org/10.1016/j.medleg.2017.10.017>.
- Errickson D, Grueso I, Griffith SJ, et al. Towards a best practice for the use of active non-contact surface scanning to record human skeletal remains from archaeological contexts. *Int J Osteoarchaeol*. 2017;27:650–661. <https://doi.org/10.1002/oa.2587>.
- Klein S, Avery M, Adams G, Pollard S, Simske S. From scan to print: 3D printing as a means for replication. *NIP & Digital Fabrication Conference. Society for Imaging Science and Technology*. 2014; 2014:417–421.
- Carew RM, Morgan RM, Rando C. A preliminary investigation into the accuracy of 3D modeling and 3D printing in forensic anthropology evidence reconstruction. *J Forensic Sci*. 2018;64:342–352. <https://doi.org/10.1111/1556-4029.13917>.
- Chase RJ, LaPorte G. The next generation of crime tools and challenges: 3D printing. *Natl Inst Justice*. 2017;279:49–57.
- Rmoutilová R, Guyomarc'h P, Velemínský P, et al. Virtual reconstruction of the upper palaeolithic skull from Zlatý Kůň, Czech republic: sex assessment and morphological affinity. *PLoS One*. 2018;13:e0201431.
- Weber G, Schäfer K, Prossinger H, Gunz P, Mitteroecker P, Seidler H. Virtual anthropology: the digital evolution in anthropological sciences. *J Physiol Anthropol Appl Hum Sci*. 2001;20:69–80.
- Benazzi S, Gruppioni G, Strait DS, Hublin JJ. Technical Note: virtual reconstruction of KNM-ER 1813 Homo habilis cranium. *Am J Phys Anthropol*. 2014;153:154–160. <https://doi.org/10.1002/ajpa.22376>.
- Langley-Shirley N, Tersigni-Tarrant MA. *Forensic Anthropology A Comprehensive Introduction*. second ed. Boca Raton: CRC Press; 2017.
- Nikita E. *Osteoarchaeology: A Guide to the Macroscopic Study of Human Skeletal Remains*. London: Academic Press; 2017.
- Mestekova S, Bruzek J, Velemínská J, Chaumoitre K. A test of the DSP sexing method on CT images from a modern French sample. *J Forensic Sci*. 2015;60:1295–1299. <https://doi.org/10.1111/1556-4029.12817>.
- Chapman T, Lefevre P, Semal P, et al. Sex determination using the probabilistic sex diagnosis (DSP: Diagnose sexuelle Probabiliste) tool in a virtual environment. *Forensic Sci Int*. 2014;234:189–e1. <https://doi.org/10.1016/j.forsciint.2013.10.037>.
- Citardi MJ, Herrmann B, Hollenbeak CS, Stack BC, Cooper M, Bucholz RD. Comparison of scientific calipers and computer-enabled CT review for the measurement of skull base and craniomaxillofacial dimensions. *Skull Base*. 2001;11:5–11. <https://doi.org/10.1055/s-2001-12781>.
- Corron L, Marchal F, Condesi S, Chaumoitre K, Adalian P. Evaluating the consistency, repeatability, and reproducibility of osteometric data on dry bone surfaces, scanned dry bone surfaces, and scanned bone surfaces obtained from living individuals. *BMSAP*. 2017;29:33–53. <https://doi.org/10.1007/s13219-016-0172-7>.
- Verhoff MA, Ramsthaler F, Krähahn J, et al. Digital forensic osteology-Possibilities in cooperation with the Virtopsy*project. *Forensic Sci Int*. 2008;174:152–156. <https://doi.org/10.1016/j.forsciint.2007.03.017>.
- Mullins RA, Albanese J. Estimating biological characteristics with virtual laser data. *J Forensic Sci*. 2018;63:815–823. <https://doi.org/10.1111/1556-4029.13621>.
- Musilová B, Dupe J, Velemínská J, Chaumoitre K. Exocranial surfaces for sex assessment of the human cranium. *Forensic Sci Int*. 2016;269:70–77. <https://doi.org/10.1016/j.forsciint.2016.11.006>.
- Abdel Fatah EE, Shirley NR, Jantz RL, Mahfouz MR. Improving sex estimation from crania using a novel three-dimensional quantitative method. *J Forensic Sci*. 2014;59:590–600. <https://doi.org/10.1111/1556-4029.12379>.
- Bulut O, Petaros A, Hizliol I, Wärmänder SKTS, Hekimoglu B. Sexual dimorphism in frontal bone roundness quantified by a novel 3D-based and landmark-free method. *Forensic Sci Int*. 2016;261:162.e1–162.e5. <https://doi.org/10.1016/j.forsciint.2016.01.028>.
- Cavaignac E, Li K, Faruch M, et al. Three-dimensional geometric morphometric analysis reveals ethnic dimorphism in the shape of the femur. *J Exp Orthopaedics*. 2017;4:13. <https://doi.org/10.1186/s40634-017-0088-2>.
- Murphy RE, Garvin HM. A morphometric outline analysis of ancestry and sex differences in cranial shape. *J Forensic Sci*. 2018;63:1001–1009. <https://doi.org/10.1111/1556-4029.13699>.
- Villa C, Buckberry J, Cattaneo C, Frohlich B, Lynnerup N. Quantitative analysis of the morphological changes of the pubic symphyseal face and the auricular surface and implications for age at death estimation. *J Forensic Sci*. 2015;60:556–565. <https://doi.org/10.1111/1556-4029.12689>.
- Slice DE, Algee-Hewitt BFB. Modeling bone surface morphology: a fully quantitative

- method for age-at-death estimation using the pubic symphysis. *J Forensic Sci.* 2015;60:835–843 <https://doi.org/10.1111/1556-4029.12778>.
40. Stoyanova D, Algee-Hewitt BFB, Slice DE. An enhanced computational method for age-at-death estimation based on the pubic symphysis using 3D laser scans and thin plate splines. *Am J Phys Anthropol.* 2015;158:431–440 <https://doi.org/10.1002/ajpa.22797>.
 41. Stoyanova DK, Algee-Hewitt BFB, Kim J, Slice DE. A computational framework for age-at-death estimation from the skeleton: surface and outline analysis of 3D laser scans of the adult pubic symphysis. *J Forensic Sci.* 2017;62:1434–1444 <https://doi.org/10.1111/1556-4029.13439>.
 42. San-Millán M, Rissech C, Turbón D. Shape variability of the adult human acetabulum and acetabular fossa related to sex and age by geometric morphometrics. Implications for adult age estimation. *Forensic Sci Int.* 2017;272:50–63 <https://doi.org/10.1016/j.forsciint.2017.01.005>.
 43. Villa C, Gaudio D, Cattaneo C, Buckberry J, Wilson AS, Lynnerup N. Surface curvature of pelvic joints from three laser scanners: separating anatomy from measurement error. *J Forensic Sci.* 2015;60:374–381 <https://doi.org/10.1111/1556-4029.12696>.
 44. Poláček L. Das Hinterland des frühmittelalterlichen Zentrums in Mikulčice. Stand und Perspektiven der Forschung. In: Poláček L, ed. *Das Wirtschaftliche Hinterl. Der Frühmittelalterlichen Zentren.* Int. Tagungen Mikulčice VI, Archeologický Ústav Akademie Věd ČR. 2008;257–298 Brno.
 45. Nawabi DH, Nassif NA, Do HT, et al. What causes unexplained pain in patients with metal-on metal hip devices? A retrieval, histologic, and imaging analysis. *Clin Orthop Relat Res.* 2014;472:543–554 <https://doi.org/10.1007/s11999-013-3199-9>.
 46. Cook RB, Shearwood-Porter NR, Latham JM, Wood RJK. Volumetric assessment of material loss from retrieved cemented metal hip replacement stems. *Tribology Int.* 2015;89:105–108 <https://doi.org/10.1016/j.triboint.2014.12.026>.
 47. ACC SILICONES LTD. *Technical Data Sheet.* 2017;2017 https://acc-silicones.com/products/moulding_rubbers/MM242R.
 48. Tuke M, Taylor A, Roques A, Maul C. 3D linear and volumetric wear measurement on artificial hip joints-Validation of a new methodology. *Precis Eng.* 2010;34:777–783 <https://doi.org/10.1016/j.precisioneng.2010.06.001>.
 49. The MathWorks, Inc. *MATLAB R2015b [software].* 2015;2015.
 50. Cignoni P, Callieri M, Corsini M, Dellepiane M, Ganovelli F, Ranzuglia G. *MeshLab: An Open-Source Mesh Processing Tool.* 6th Eurographics Italian Chapter Conference. 2008;2008:129–136.
 51. GOM GmbH. *GOM Inspect 2016 [software].* 2016;2016.
 52. Murail P, Bruzek J, Houët F, Cunha E. DSP: a tool for probabilistic sex diagnosis using worldwide variability in hip-bone measurements. *BMSAP.* 2005;17:167–176.
 53. Brůžek J, Santos F, Dutailly B, Murail P, Cunha E. Validation and reliability of the sex estimation of the human os coxae using freely available DSP2 software for bioarchaeology and forensic anthropology. *Am J Phys Anthropol.* 2017;164:440–449 <https://doi.org/10.1002/ajpa.23282>.
 54. Morphome3cs II. *CGG MFF UK.* 2015;2015 <http://www.morphome3cs.com/>.
 55. Lottering N, Reynolds MS, MacGregor DM, Meredith M, Gregory LS. Morphometric modelling of ageing in the human pubic symphysis: sexual dimorphism in an Australian population. *Forensic Sci Int.* 2014;236:195.e1–e11 <https://doi.org/10.1016/j.forsciint.2013.12.041>.
 56. Stomfai S, Ahrens W, Bammann K, et al. Intra- and inter-observer reliability in anthropometric measurements in children. *Int J Obes.* 2011;35:45–51 <https://doi.org/10.1038/ijo.2011.34>.
 57. Machado MPS, Costa ST, Freire AR, et al. Application and validation of Diagnose Sexuelle Probabiliste V2 tool in a miscegenated population. *Forensic Sci Int.* 2018;290:351.e1–351.e5 <https://doi.org/10.1016/j.forsciint.2018.06.043>.
 58. Carew RM, Erickson D. Imaging in forensic science: five years on. *J For Radiol Imag.* 2019;16:24–33 <https://doi.org/10.1016/j.jofri.2019.01.002>.
 59. Quatrehomme G, Radoman I, Nogueira L, du Jardin P, Alunni V. Sex determination using the DSP (probabilistic sex diagnosis) method on the coxal bone: efficiency of method according to number of available variables. *Forensic Sci Int.* 2017;272:190–193 <https://doi.org/10.1016/j.forsciint.2016.10.020>.
 60. Rodríguez Paz A, Banner J, Villa C. Validity of the probabilistic sex diagnosis method (DSP) on 3D CT-scans from modern Danish population. *Rev Med Leg.* 2018 <https://doi.org/10.1016/j.medleg.2018.08.002>.
 61. Kim J, Algee-Hewitt BFB, Stoyanova DK, Figueroa-Soto C, Slice D. Testing reliability of the computational age-at-death estimation methods between five observers using three-dimensional image data of the pubic symphysis. *J Forensic Sci.* 2018;64:507–518 <https://doi.org/10.1111/1556-4029.13842>.
 62. Kotěrová A, Velemínská J, Cunha E, Brůžek J. A validation study of the Stoyanova et al. method (2017) for age-at-death estimation quantifying the 3D pubic symphyseal surface of adult males of European populations. *Int J Leg Med.* 2018;133:603–612 <https://doi.org/10.1007/s00414-018-1934-1>.
 63. Erickson D, Thompson T, Rankin B. *An Optimum Guide for the Reduction of Noise Using a Surface Scanner for Digitising Human Osteological Remains.* 2015;2015 https://guides.archaeologydataservice.ac.uk/g2gp/CS_StructuredLight.
 64. Algee-Hewitt BFB, Wheat AD. The reality of virtual anthropology: comparing digitizer and laser scan data collection methods for the quantitative assessment of the cranium. *Am J Phys Anthropol.* 2016;160:148–155 <https://doi.org/10.1002/ajpa.22932>.
 65. Gualdi-Russo E, Zaccagni L, Russo V. Giovanni Battista Morgagni: facial reconstruction by virtual anthropology. *Forensic Sci Med Pathol.* 2015;11:222–227 <https://doi.org/10.1007/s12024-015-9665-9>.
 66. Shearer BM, Sholts SB, Garvin HM, Wärmländer SKTS. Sexual dimorphism in human browridge volume measured from 3D models of dry crania: a new digital morphometrics approach. *Forensic Sci Int.* 2012;222:e1–400. e5 <https://doi.org/10.1016/j.forsciint.2012.06.013>.
 67. Tambusso PS, McDonald HG, Fariña RA. Description of the stylohyal bone of a giant sloth (*Lestodon armatus*). *Palaeontol Electron.* 2015;18:1–10 <https://doi.org/10.26879/506>.
 68. Maté-González M, Aramendi J, González-Aguilera D, Yravedra J. Statistical comparison between low-cost methods for 3D characterization of cut-marks on bones. *Remote Sens.* 2017;9:873 <https://doi.org/10.3390/rs9090873>.
 69. Edwards J, Rogers T. The accuracy and applicability of 3D modeling and printing blunt force cranial injuries. *J Forensic Sci.* 2017;1–9 <https://doi.org/10.1111/1556-4029.13627>.
 70. Viciano J, López-Lázaro S, Pérez-Fernández Á, Amores-Ampuero A, D'Anastasio R, Jiménez-Triguero JM. Scheuermann's disease in a juvenile male from the late Roman necropolis of Torrenueva (3rd-4th century CE, Granada, Spain). *Int J Paleopathol.* 2017;18:26–37 <https://doi.org/10.1016/j.ijpp.2017.04.003>.
 71. Porter ST, Roussel M, Soressi M. A simple photogrammetry rig for the reliable creation of 3D artifact models in the field: lithic examples from the early upper paleolithic sequence of les cottés (France). *Adv Archaeol Pract.* 2016;4:71–86 <https://doi.org/10.7183/2326-3768.4.1.71>.
 72. Massinon M, Dumont B, De Cock N, Salah SOT, Lebeuf F. Study of retention variability on an early growth stage herbaceous plant using a 3D virtual spraying model. *Crop Prot.* 2015;78:63–71 <https://doi.org/10.1016/j.cropro.2015.08.018>.
 73. Secher JJ, Darvann TA, Pinholt EM. Accuracy and reproducibility of the DAVID SLS-2 scanner in three-dimensional facial imaging. *J Cranio-Maxillo-Fac Surg.* 2017;45:1662–1670 <https://doi.org/10.1016/j.jcms.2017.07.006>.
 74. Yravedra J, Aramendi J, Maté-González MÁ, Courtenay LA, González-Aguilera D. Differentiating percussion pits and carnivore tooth pits using 3D reconstructions and geometric morphometrics. *PLoS One.* 2018;13:e0194324 <https://doi.org/10.1371/journal.pone.0194324>.
 75. Zaimovic-Uzunovic N, Lemes S. Influences of surface parameters on laser 3D scanning. *IMEKO Conference Proceedings: International Symposium on Measurement and Quality Control.* 2010;2010.
 76. Perrone RV, Williams JL. Dimensional accuracy and repeatability of the NextEngine laser scanner for use in osteology and forensic anthropology. *J Archaeol Sci Rep.* 2019;25:308–319. <https://doi.org/10.1016/j.jasrep.2019.04.012>.
 77. Veneziano A, Landi F, Profico A. Surface smoothing, decimation, and their effects on 3D biological specimens. *Am J Phys Anthropol.* 2018;166:473–480 <https://doi.org/10.1002/ajpa.23431>.
 78. Sholts SB, Wärmländer SKTS, Flores LM, Miller KWP, Walker PL. Variation in the measurement of cranial volume and surface area using 3d laser scanning technology. *J Forensic Sci.* 2010;55:871–876 <https://doi.org/10.1111/j.1556-4029.2010.01380.x>.
 79. Singh R, Baby B, Suri A, Anand S. Comparison of laser and structured light scanning techniques for neurosurgery applications. *3rd International Conference on Signal Processing and Integrated Networks (SPIN).* IEEE; 2016:301–305 <https://doi.org/10.1109/SPIN.2016.7566708>.
 80. Camison L, Bykowski M, Lee WW, et al. Validation of the Vectra H1 portable three-dimensional photogrammetry system for facial imaging. *Int J Oral Maxillofac Surg.* 2018;47:403–410 <https://doi.org/10.1016/j.ijom.2017.08.008>.
 81. Novotný V. Sex determination of the pelvic bone: a systems approach. *Anthropologie.* 1986;XXIV:197–206.
 82. Gaillard J. Détermination sexuelle d'un os coxal fragmentaire. *Bull Mem Soc Anthropol Paris.* 1960;2:255–267.
 83. Braüer G. Osteometrie. In: Knussmann R, ed. *Anthropol. Handb. Des Vergleichenden Biol. Des Menschen, Band 1.* Stuttgart: Gustav Fischer Verlag; 1988:160–232.
 84. Schulte-Ellis F, Schmidt D, Hayek L, Craig J. Determination of sex with a discriminant analysis of new pelvic bone measurements: Part I. *J Forensic Sci.* 1983;28:169–180.

A method of sexing the human os coxae based on logistic regressions and Bruzek's nonmetric traits

Frédéric Santos¹  | Pierre Guyomarc'h²  | Rebeka Rmoutilova^{1,3}  | Jaroslav Bruzek^{1,3}

¹Université de Bordeaux – CNRS – MCC,
UMR 5199 PACEA, Pessac, France

²Université Aix Marseille – CNRS – EFS, UMR
7268 ADES, Marseille, France

³Department of Anthropology and Human
Genetics, Faculty of Science, Charles
University, Prague, Czech Republic

Correspondence

Frédéric Santos, Université de Bordeaux, UMR
5199 PACEA, Bâtiment B8, Allée Geoffroy
Saint-Hilaire, CS 50023, Pessac Cedex 33615,
France.
Email: frederic.santos@u-bordeaux.fr

Funding information

Grantová Agentura České Republiky, Grant/
Award Number: GAČR 14-22823S; Grantová
Agentura, Univerzita Karlova, Grant/Award
Number: GAUK 1088217

Abstract

Objectives: This study aims at proposing a visual method for sexing the human os coxae based on a statistical approach, using a scoring system of traits described by Bruzek (2002). This method is evaluated on a meta-population sample, where the data were acquired by direct observation of dry bones as well as computed tomography (CT) scans. A comparison with the original Bruzek's (2002) method is performed.

Materials and methods: Five hundred and ninety two ossa coxae of modern humans are included in the reference dataset. Two other samples, composed respectively of 518 ossa coxae and 99 CT-scan images, are both used for validation purposes. The individuals come from five European or North American population samples. Eleven trichotomic traits (expressing female, male, or intermediate forms) were observed on each os coxae. The new approach employs statistical processing based on logistic regressions. An R package freely available online, PELVIS, implements both methods.

Results: Both methods provide highly reliable sex estimates. The new statistical method has a slightly better accuracy rate (99.2%) than the former method (98.2%) but has also a higher rate of indeterminate individuals (12.9% vs. 3% for complete bones).

Conclusion: The efficiency of both methods is compared. Low error rates were preferred over high ability of reaching the classification threshold. The impact of lateralization and the asymmetry of observed traits are discussed. Finally, it is shown that this visual method of sex estimation is reliable and easy to use through the graphical user interface of the R package.

KEYWORDS

hip bone, identification, innominate, morphoscopy, sex estimation

1 | INTRODUCTION

The assessment of biological sex from the skeleton is highly important and has implications in various subfields of physical anthropology, as stated by each study and textbook that focuses on estimating the parameters of an individual's biological profile using both metric and visual methods (e.g., Dirkmaat, 2012; Nikita, 2017). The use of visual methods is convenient hence popular and is most often used to estimate sex from the skull (e.g., Langley, Dudzik, & Cloutier, 2018; Lewis & Garvin, 2016) or parts of the pelvis such as the pubis

(e.g., Gómez-Valdés et al., 2017; Klaes, Ousley, & Vollner, 2012) or the sciatic notch (Walker, 2005). However, visual methods that use scoring of morphological traits of the whole os coxae (Bruzek, 2002; Ferembach, Schwidetzky, & Stloukal, 1980) have not yet provided posterior probabilities for sex estimates.

It is well-known that due to its inherent functions, the most reliable anatomical bony part for sex estimation is the os coxae. The os coxae can be described as an integrated unit consisting of two principal modules: a sacro-iliac module and an ischio-pubic module. Modularity helps to understand the evolvability and plasticity of organismal

form (Esteve-Altava, 2017) and, consequently, the sexual dimorphism and its variation.

The os coxae is more sexually dimorphic than any other bone, and no significant intraindividual relationships between pelvic and cranial sexual measurements have been observed (Best, Garvin, & Cabo, 2017). For these reasons, in the assessment of sex, the pelvis is preferred over the skull and other parts of the skeleton. The pelvis and especially the ossa coxae show a broadly similar pattern of sexual dimorphism across different geographical regions, and this general pattern of pelvic sexual dimorphism appeared in early modern humans, approximately at least 100–150 thousand years ago (Betti, 2014; Bruzek & Murail, 2006; Bruzek, Santos, Dutailly, Murail, & Cunha, 2017; Hager, 1989, 1996; Rosenberg & Trevathan, 2002).

Errors in sexing influence subsequent analyses, for example, an error in sex estimation can lead to wrong biological or social interpretations in an attempt to explain spurious results. As noted recently by Berg and Kenyhercz (2017), over the last 30 years, myriad new methodological or statistically based research articles have been published, but only a small number of these methods are easily applicable. In contrast to metric methods, morphological methods are relatively fast and easy to use after proper training; they do not require any specialized equipment but tend to be more subjective, and they have primarily been limited to the use of nonstatistical approaches with no quantifiable measure of certainty. Many nonmetric sex estimation techniques are available for the skull and postcranial elements; however, few of these techniques are accompanied by thorough statistical evaluation. Exceptions include the method of estimating sex according to nonmetric traits of the mandible (Berg & Kenyhercz, 2017) or the skull (Walker, 2008) and the modifications of the Phenice (1969) method, which uses the visually evaluated features of the pubis (Klares et al., 2012). Spreadsheets for sex estimation based on the last two publications are available at <http://math.mercyhurst.edu/~sousley/Software/>, and an R-Shiny application, MorphoPASSE, has also been developed by Klares and Cole (2018). However, it must be noted that each of the three Phenice's traits that are used in the Klares et al.'s method is located on the pubic bone; thus, while this method is often referred to as using the "pelvis," the three traits do not account for sexual dimorphism in the ilium or ischium (Lesciotto & Doershuk, 2018).

Bruzek's method (Bruzek, 2002) for estimating sex from the os coxae is used in a number of studies, ranging from paleoanthropology (e.g., Bruzek, Franciscus, Novotny, & Trinkaus, 2006; Hammond, Royer, & Fleagle, 2017; Samsel, Knüsel, & Villotte, 2016; Trinkaus, 2016) to bioarchaeology (e.g., Debono & Mafart, 2006; Linderholm & Kjellström, 2011; Roksandic, Djurić, Rakočević, & Seguin, 2006; Ščesnaité-Jerdiakova et al., 2015; White & Folkens, 2005), and is presented in several forensic anthropology manuals (e.g., Black & Ferguson, 2011; Dirkmaat, 2012; Işcan & Steyn, 2013). However, this method does not provide a probability for sex estimation.

For a method to be confidently employed in a particular setting (i.e., on specific population or groups), the method must be validated with different samples (e.g., Garvin, Sholts, & Mosca, 2014; Kenyhercz, Klares, Stull, McCormick, & Cole, 2017; Lewis & Garvin, 2016). Despite the

popularity of this method for estimating sex from the os coxae, there is a lack of studies evaluating its accuracy across a variety of samples.

The aim of this article is to introduce a new sex estimation method combining the visual assessment proposed by Bruzek (2002) and a statistical framework delivering posterior probabilities. An application on fragmentary skeletal remains is also considered as well as an effect of laterality on the sex estimate. Finally, the method is tested on a material obtained from CT-scans in order to extend possibilities of future testing studies.

2 | MATERIALS AND METHODS

2.1 | Samples

Coxal data of 592 adult individuals of known sex from five skeletal population samples were collected and scored blindly by one of the authors (J.B.) between 1986 and 2006. Five hundred and eighteen individuals could be measured on both left and right bones, and the coxal data were available on only one side for 74 individuals, for a total of 1,110 ($= 2 \times 518 + 74$) ossa coxae. Consequently, we chose 592 ($= 518 + 74$) out of those 1,110 ossa coxae to build our reference sample, all of them belonging to distinct individuals. If both sides were available for a given individual, we selected only the left bone by convention; otherwise, the only present side was included. In total, the reference dataset is composed of 579 left ossa coxae and 13 right ossa coxae. The 518 right ossa coxae which were not included in the reference sample will be used as a test sample to discuss the impact of lateralization on sex estimation. These datasets can be accessed on Zenodo (Bruzek, Rmoutilova, Guyomarc'h, & Santos, 2019) or through the R package PELVIS described below.

The reference sample is further described in Table 1. Data for two out of the five population samples were already used as a reference material in the original method published by Bruzek (2002). These samples are: the Tamagnini Collection ($n = 240$ ossa coxae) housed in Coimbra, Portugal and the Olivier Collection ($n = 160$) curated at the Musée de l'Homme, Paris, France. Three additional population samples were added in this article: the Hamann-Todd Collection ($n = 160$) from the Cleveland Museum of Natural History, Cleveland; the Terry Collection ($n = 411$) from the Smithsonian Institution, Washington, DC and the Spitalfields Collection ($n = 74$) from the Christ Church Spitalfields crypt at the Natural History Museum, London, England.

All samples include adult individuals of comparable ages, the average age being slightly over 50 years in each population sample (Table 1).

To extend the applicability of this method in the scope of virtual anthropology, 3D models of hip bones were also segmented from CT-scans. The virtual sample consisted of a random selection of 99 abdominal CT-scans (49 males and 50 females) acquired at the CHU Hôpital Nord in Marseille, France. The CT-scans, already used in a previous study by Mestekova, Bruzek, Velemínska, and Chaumoitre (2015), were anonymized and collected after approval was obtained from the ethics committee of the Faculty of Medicine in Marseille. Patients with skeletal disorders were excluded. Both hip bones from each patient were used; therefore, the virtual sample consisted of 198 ossa coxae.

TABLE 1 Description of the reference meta-population sample

	Coimbra	HamTodd	London	Paris	Terry
Number of females	66 (64)	57 (55)	43 (41)	32 (29)	106 (104)
Number of males	54 (52)	56 (54)	30 (30)	48 (44)	100 (99)
Mean age (and standard deviation) in years	54.4 (19.2)	54.2 (20.1)	55.7 (16.9)	53 (11.5)	50.7 (18.9)
Age range (years)	(19–96)	(21–89)	(19–92)	(30–80)	(19–95)
Age-at-death period	Early 20th century	1910–1940	1,729–1852	Early 20th century	19th and 20th century

In the first two rows, the number of complete ossa coxa (i.e., having no missing observation among the 11 visual traits) is indicated between brackets. Short codes for the collections: [Coimbra] Tamagnini collection (Coimbra, Portugal), [HamTodd] Hamann-Todd collection (Cleveland, OH), [London] Spitalfields (London, England), [Paris] Olivier collection (Paris, France), [Terry] Terry collection (Washington, DC).

The acquisition was performed with a Siemens© Sensation 64 cardio scanner (Erlangen, Germany). The acquisition parameters were as follows: detector collimation, 64 9 0.6 mm; gantry rotation, 0.5 s; pitch, 1.5 mm per gantry rotation; tube voltage, 120 kV; and tube current, 36–350 mAs. The ossa coxae were segmented semi-automatically in the software TIVMI (<http://projets.pacea.u-bordeaux.fr/TIVMI>) by HMH 3D (Dutailly, Coqueugnot, Desbarats, Gueorguieva, & Synave, 2009). The segmented 3D models were subsequently visually evaluated following the current method.

2.2 | Description of visual criteria

A trichotomic evaluation is proposed for all 11 traits (for technical details see Table 1 and figs. 1–5 included in Bruzek, 2002; and Figure 1 from the present text).

2.2.1 | Sacroiliac module (A, B, C)

A. Entire aspect of the preauricular surface (PrSu). The principle of assessment is to identify two negative relief structures, the preauricular groove (Zaaier, 1866) and the paraglenoid groove (Löhr, 1894) in a topologically complex situation. The aim of the evaluation is to define a sexual form of individual morphology of the preauricular area. This character is described in Novotny (1981) and Bruzek (2002).

1. PrSu1: Development of a negative relief on the preauricular surface. Scoring: (F) well-delimited deep depression, which refers to the groove depth and is similar to the “GP-type” as defined by Houghton (1974); (i) intermediate form “I cannot decide;” (M) smooth surface or very slightly negative relief corresponding to an absence of groove, which is similar to “GL-type” as defined by Houghton (1974) for the groove of ligament.
2. PrSu2: Aspect of grooves or pitting. Scoring: (f) closed circumference of pit(s) or groove(s) when a depression is present; (i) intermediate form “I cannot decide;” (m) absent depression or open circumference of depressions.
3. PrSu3: Development of a positive relief. Scoring: (f) lack of positive relief or tubercle; (i) intermediate form “I cannot decide;” (m) tubercle present or clear protuberance.

B. Entire aspect of the greater sciatic notch (GrSN), also as defined by Novotny (1981) and Bruzek (2002). The evaluation of the sexual form of the greater sciatic notch is according to the mutual relationship of the proportions of both chords (anterior and posterior), defined by the entire width and depth of the sciatic notch.

4. GrSN1: Proportion of the length of sciatic notch chords. Scoring: (f) posterior chord segment (AC) longer than or equal to the anterior chord (CB); (i) intermediate form “I cannot decide;” (m) posterior chord (AC) shorter than the anterior chord (CB).
5. GrSN2: Form of contour notch chords. Scoring: (f) symmetry of chords contours in the basal portion of the sciatic notch relative to its depth; (i) intermediate form “I cannot decide;” (m) symmetry of chords contours in the basal portion of the sciatic notch relative to its depth.
6. GrSN3: Retroversion of the posterior notch chord relative to the line from point A perpendicular to the sciatic notch breadth. Scoring: (f) lack of retroversion, contour (outline) of the posterior chord does not cross the perpendicular line; (i) intermediate form “I cannot decide;” contour tangent the perpendicular; (m) contour of posterior chord crosses the perpendicular line.

C. Form of the composite arch. This character was originally designed by Genoves (1959).

7. CArc: Relation between outline of the sciatic notch and outline of the auricular surface. Scoring: (F) double curve; (O) intermediate form “I cannot decide;” (M) single curve.

2.2.2 | Ischiopubic module (D, E)

D. Entire morphology of the inferior pelvis in caudal view (InfP). It is described in Novotny (1981) and Bruzek (2002).

8. InfP1: Shape of *margo inferior ossis coxae*. Scoring: (f) external eversion; (i) intermediate form “I cannot decide;” (m) direct course of its medial part.
9. InfP2: Development of the phallic ridge or phallic crest (*crista phallica*) is a sexually dimorphic crest on the caudal aspect of the *ramus inferior ossis pubis*, serving for the insertion of *crus penis/clitoridis* (Kachlik, Musil, & Baca, 2018). This ridge is defined as the hill where the cruses of the penis hold at the

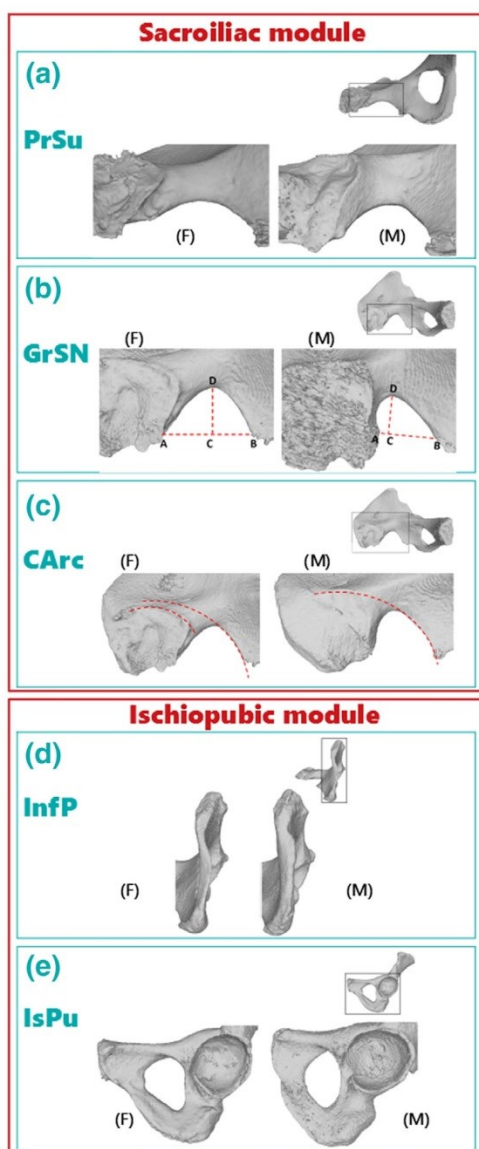


FIGURE 1 Evaluation of the five characters spread over two modules of the human os coxae, from CT images segmentation. (a) Preauricular surface (PrSu). "F" = female morphology (f-f-f after Bruzek, 2002; corresponding to the combination {PrSu1 = f, PrSu2 = f, PrSu3 = f} after this study). "M" = male morphology (m-m-m after Bruzek, 2002; corresponding to the combination {PrSu1 = m, PrSu2 = m, PrSu3 = m} after this study). (b) Greater sciatic notch (GrSN). "F" = female morphology (f-f-f after Bruzek, 2002; corresponding to the combination {GrSN1 = f, GrSN2 = f, GrSN3 = f} after this study). "M" = male morphology (m-m-m after Bruzek, 2002; corresponding to the combination {GrSN1 = m, GrSN2 = m, GrSN3 = m} after this study). (c) Composite arch (CArc). "F" = female morphology. "M" = male morphology. (d) Inferior pelvis (InfP). "F" = female morphology (f-f-f after Bruzek, 2002; corresponding to the combination {InfP1 = f, InfP2 = f, InfP3 = f} after this study). "M" = male morphology (m-m-m after Bruzek, 2002; corresponding to the combination {InfP1 = m, InfP2 = m, InfP3 = m} after this study). (e) Ischiopubic proportion (IsPu). "F" = female morphology. "M" = male morphology

outer part of the ischiopubic ramus (Ulucam, Alicioglu, Cikmaz, Yilmaz, & Sut, 2009). Scoring: (f) lack of the phallic ridge or presence of only a little mound; (i) intermediate form "I cannot decide;" (m) clear presence of the phallic ridge.

10. InfP3: Inferior pelvis general aspect. Scoring: (f) gracile aspect; (i) intermediate form "I cannot decide;" (m) robust aspect.

E. Ischiopubic proportion (IsPu). Practically, this ratio is assessed by a visual inspection only and corresponds to the ischiopubic index (Schultz, 1930; Washburn, 1948).

11. IsPu: Visual relationship between pubis and ischium lengths. Scoring: (F) pubis visually longer than ischium; (O) intermediate form; (M) ischium visually longer than pubis.

2.3 | Reminder of the original visual method for sexing the human os coxae

The original method suggested by Bruzek (2002) proceeds through the two following steps:

Step 1. From the scoring of the 11 original trichotomic traits, derive five main variables—namely, "characters" in what follows—summarizing the morphology of each os coxae area. Those five characters are "PrSu" (entire aspect of the preauricular surface), "GrSN" (entire aspect of the greater sciatic notch), "CArc" (form of the composite arch), "InfP" (entire morphology of the inferior pelvis) and "IsPu" (ischiopubic proportion). The two characters "CArc" and "IsPu" are the direct transcription of the corresponding trait value, "F," "O," or "M." For each group of three traits associated with a given pelvic area, the value of their character is derived based on a strict majority rule: when at least two trait values indicate either "F" or "m," these are used as a basis to determine the corresponding character value or sexual form. For instance, a triplet {PrSu1 = "f," PrSu2 = "f," PrSu3 = "m"} corresponds to a character value PrSu = "F."

Step 2. From the sequence of five characters, derive a final sex estimate again using a majority rule: the morphology ("F" or "M") which is in strict majority prevails, regardless of the number of intermediate morphologies. For instance, a set of values {F, F, O, M, O} for the five character values corresponds to a female sex estimate. If there are as many female as male morphologies (e.g., a set of values {F, M, F, O, M}), the individual remains indeterminate (no sex assigned).

These steps are illustrated in Figure 2.

2.4 | Introducing logistic regression models

In this section, we introduce a new method that makes use of logistic regression to derive a statistical sex estimate from the 11 original traits, thereby providing a posterior probability for the classification. The algorithm used to produce a sex estimate for a given individual involves the following steps:

Step 1. Filter the whole dataset to keep only the individuals with no missing values for the traits used to describe the individual to be determined, such that the learning dataset used to build logistic

FIGURE 2 Summary of the original Bruzek (2002) method for sex estimation, based on visual traits, and trait values used for logistic regression models

Traits	Trait values	Step 1:		Step 2:	
		Derive the five characters		Bruzek 2002 sex estimate	
PrSu1	"f", "i", or "m"	PrSu =	<div> " F " if # "f" ≥ 2 </div>	<div> Female if # "F" > # "M" </div> <div> Male if # "F" < # "M" </div> <div> Indet. if # "F" = # "M" </div>	
PrSu2	"f", "i", or "m"		<div> " M " if # "m" ≥ 2 </div>		
PrSu3	"f", "i", or "m"		<div> " 0 " otherwise </div>		
GrSN1	"f", "i", or "m"	GrSN =	<div> " F " if # "f" ≥ 2 </div>		
GrSN2	"f", "i", or "m"		<div> " M " if # "m" ≥ 2 </div>		
GrSN3	"f", "i", or "m"		<div> " 0 " otherwise </div>		
CArc	"F", "0", or "M"	CArc: direct retranscription of the trait			
InfP1	"f", "i", or "m"	InfP =	<div> " F " if # "f" ≥ 2 </div>		
InfP2	"f", "i", or "m"		<div> " M " if # "m" ≥ 2 </div>		
InfP3	"f", "i", or "m"		<div> " 0 " otherwise </div>		
IsPu	"F", "0", or "M"	IsPu: direct retranscription of the trait			
Used as inputs for logistic regression models		Used as inputs for Bruzek 2002 method			

regression models will be composed of complete cases only. By such, the number of remaining individuals will always be greater than 572—the number of complete bones within the reference meta-population sample—which ensures, for each possible combination of traits, a large amount of data from which the model learns.

Step 2. Using this learning sample, build a logistic regression model where the sex is the dependent variable, and the predictors are all the traits that could be observed on the target individual.

Step 3. From this model, select the best subset of predictors (ranging possibly from one to all of them), using a classical stepwise algorithm implemented in the R package MASS (Venables & Ripley, 2002) that aims to minimize the Bayesian information criterion (BIC). To get more reliable sex estimates, the classical value of 95% is considered as the posterior probability threshold to reach for an individual to be classified: below this value, estimates are considered indeterminate. In that way, the best model can be evaluated in both its ability to provide few indeterminate individuals (hereafter, "% indeterminate") and its rate of correct sex estimation among individuals that reach the classification threshold (hereafter, "% accuracy"). Both rates are estimated using a 10-fold cross-validation on the learning sample.

Step 4. Use this optimal model to deliver a sex estimate for the target individual, and the associated posterior probability.

This protocol allows for the use of a specific model for each individual, depending on which traits are missing.

2.5 | Presentation of the R-Shiny application for calculating a statistical sex estimate

To facilitate the sex estimation with the former Bruzek's (2002) method and to implement the new mathematical model described above, a package for the R statistical software (R Core Team, 2019) has been created, called PELVIS. It can be freely downloaded and installed from CRAN (Comprehensive R Archive Network) or from GitLab (<https://gitlab.com/f.santos/pelvis>), and then runs natively on all operating systems. PELVIS has a graphical user interface coded using the R package shiny (Chang, Cheng, Allaire, Xie, & McPherson,

2018) such that the analysis can be done through a browser window, as shown on Figure 3.


Detailed technical information about installing and using PELVIS is available online as supporting information, along with a dataset allowing to test the application.

2.6 | Design of the study

As there are 11 initial traits, 2047 (i.e., $2^{11}-1$) possible combinations of traits can be used as an input to obtain a sex estimate, depending on which traits could be observed. All of these possibilities cannot be tested extensively, but several models which make use of sets of traits that are anatomically consistent (i.e., that correspond to usual schemes of state of preservation) can be evaluated. Three situations are considered in this article: the case of complete bones (with all 11 traits as initial inputs), the case of preservation of the sacroiliac complex only (with the traits related to preauricular surface, greater sciatic notch and composite arch as initial inputs), and the case of preservation of the ischiopubic complex only (with the traits related to the inferior pelvis and ischiopubic proportions as initial inputs). These situations are studied using the whole dataset of 592 ossa coxae from five population samples. For the logistic regression models, the results are given after leave-one-out cross-validation: each of the ossa coxae is removed from the learning dataset when its corresponding model is built, so that we can properly estimate the predictive accuracy of the model in future (new) data.

Finally, the 198 ossa coxae scored from CT-scans are studied separately as a validation sample: the logistic regression models applied on those bones were learned on the main meta-population sample.

All the statistical analyses were performed with R 3.5.3 (R Core Team, 2019). Along with the R package PELVIS freely available online, we also provide as Supporting Information online the R code used in this study to improve the replicability of all the results—figures and tables—presented hereafter. To promote an open and reproducible research in biological anthropology (Martin, 2019), this study follows the guidelines given by Nuijten (2019).


PELVIS — A visual method for sexing the human os coxae based on Bruzek's nonmetric traits.

Data input: manual editing
Data input: from text file

Name of the unknown individual

Presacral surface (P_{Su1})
Development of negative relief on presacral surface (P_{Su1})

Aspects of grooves or pitting (P_{Su2})
I, pits or grooves with closed circumference

Development of positive relief on presacral surface (P_{Su3})
I, intermediate form

Great sciatic notch (G_{SN})
Proportion of length of sciatic chords (G_{SN1})

Form of contour notch chords (G_{SN2})
I, symmetry relative to depth in basal portion of sciatic notch

Contour of posterior notch chord relative to line from point A to sciatic notch breadth (G_{SN3})
m, contour of posterior chord crosses perpendicular line

Composite arch (C_{Ar})
Relation between outline of sciatic notch and outline of auricular surface

Inferior pelvis (InIP)
Characterization of mango inferior axis coxae (InIP1)

Phallic ridge (InIP2)
f, lack of the phallic ridge or presence of only little mound

Iscchio-public ramus aspect (InIP3)
f, gracile aspect

Ischiopubic proportion (IsPu)
Relation between pubis and ischium lengths

Ischiopubic ratio (IsPu2)
f, Ischium longer than pubis

Compute sex estimate

Please note that posterior probabilities are rounded to the third decimal place.

Results

Show
10 entries

	P _{Su1}	P _{Su2}	P _{Su3}	G _{SN1}	G _{SN2}	G _{SN3}	C _{Ar}	InIP1	InIP2	InIP3	InIP	IsPu	Sex estimate (Bruzek 2002)	Statistical sex estimate (2019)	Prob(F)	Prob(M)	Selected predictors in LR model	10-fold CV accuracy (%)	Index, rate in CV (%)
Indiv01	f	f	i	F	f	m	F	F	NA	f	f	0	F	F	1	0	PSu2, G _{SN1} , C _{Ar} , InIP3, IsPu	99.2	12.24

Showing 1 to 1 of 1 entries

[Download the complete table \(CSV file\)](#)

FIGURE 3 Graphical user interface of the R-shiny application PELVIS. Through the first tab ("manual editing" of trait values), an example of sex estimation is given for an individual using 10 out of 11 possible traits

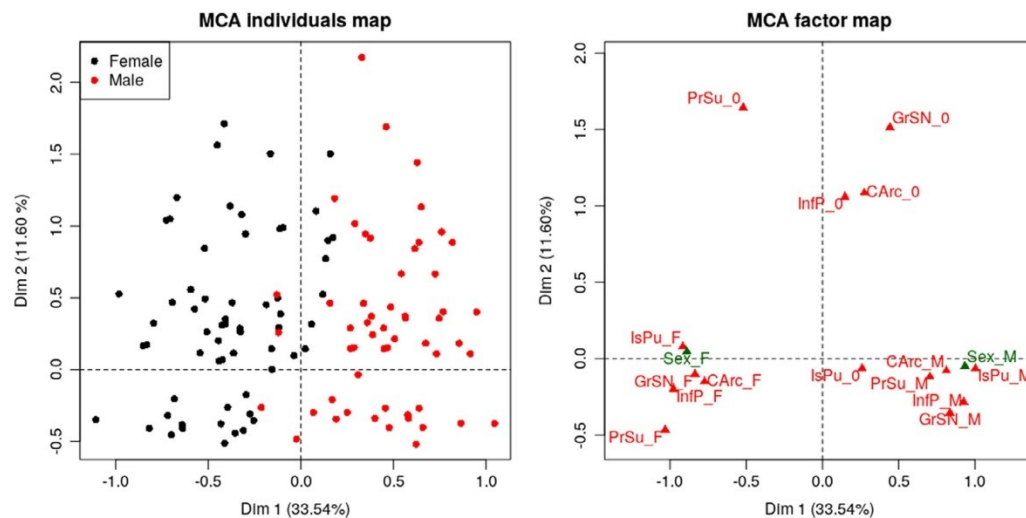


FIGURE 4 Multiple correspondence analysis of the 572 complete ossa coxae from the reference sample, using the five characters (PrSu, GrSN, CArc, InfP, IsPu) coded as trichotomic factors ("F," "0," or "M"). The true sex of the individuals is included as a supplementary variable

3 | RESULTS

3.1 | Descriptive statistics

A multiple correspondence analysis (MCA) was performed on the 572 complete bones from the reference meta-population sample using the five characters PrSu, GrSN, CArc, IsPu, and InfP as the input variables, thereby enabling illustration of their strong discriminant power when considered together (Le, Josse, & Husson, 2008). The first axis clearly opposes female individuals associated with all extreme female morphologies and the male individuals associated with all extreme male morphologies (Figure 4).

However, the MCA factor map also suggests that for some characters, the intermediate morphologies are not evenly distributed between females and males. Most occurrences (59 out of 74, i.e., 80%) of the intermediate shape of the preauricular surface ("PrSu_0") were recorded on female individuals, whereas the occurrences of the intermediate shape of the ischiopubic proportions ("IsPu_0") were more frequent on male individuals (65 out of 106, i.e., 61%). This is also the case for some of the 11 trichotomic traits, such as PrSu2, the intermediate shape of which is considerably more frequent within females (77% within the whole reference dataset), or GrSN3, the intermediate shape of which is more frequent within males (75%). All of these trends, which were not taken into account in the original Bruzek's (2002) method, can be exploited by logistic regression models.

3.2 | Sex classification accuracy and error rate

An example of an R-Shiny output for calculating a statistical sex estimate is presented in Figure 3.

For the meta-population sample, the results for both methods are reported in Table 2. As expected in Figure 4, the original Bruzek's method provides a low error rate when considering all possible traits—

that is, complete bones—, since only 10 out of 572 ossa coxae are misclassified (seven female and three male bones). Although slightly higher, the error rate remains satisfying when restricting the input data to specific pelvic areas, thus proving the applicability of the Bruzek method on various population samples, even when sexing incomplete bones.

The method based on logistic regression models delivers results that differ noticeably. The error rate is lowered in all situations but at the cost of a clear increase in the rate of indeterminate individuals. However, the sex estimates are particularly reliable, since the error rate remains constantly below 1.5% in the three studied cases.

The two methods perform consistently for each of the five population samples: no clear differences in classification accuracy were noted from one collection to another, as shown in Table 3 for the case of complete bones. Similar results are obtained when considering the sacroiliac or ischiopubic modules independently.

However, a careful inspection of misclassified individuals reveals that most classification errors using the sacroiliac module consist of females misclassified as males (Table 4). This trend is not exceptionally strong but it is consistent in both methodological approaches.

These methods were also tested on data acquired through CT-scans, and their respective performances remain nearly identical to those obtained by direct observation, as shown in Table 5. The CT-scan observations provided indeterminate rates close to those observed on Table 2 (above 10% for statistical sex estimates). Regarding the utility of a method to be tested on various population samples, these results encourage future studies to use data from virtual material. This kind of data has a great advantage because it can provide information on present populations.

3.3 | Exploration of asymmetry in the recorded traits

Strong levels of directional asymmetry for certain traits could lead to an increase in the classification error rate (Đurić, Rakočević, & Đonić,

TABLE 2 Results of sex assessment for the reference meta-population sample

	Number of bones	Complete bone 572	Sacroiliac module 589	Ischiopubic module 574
Original Bruzek (2002) method	Correct sex estimates	545	515	515
	Indeterminate estimates	17	44	43
	Classification errors	10	30	16
	% accuracy	98.20%	94.50%	96.99%
	% indeterminate	2.97%	7.47%	7.49%
Statistical sex estimate (2019)	Traits selected in LR model	PrSu2, GrSN1, CArc, InfP3, IsPu	CArc, PrSu2, GrSN1, GrSN2	IsPu, InfP1, InfP2
	Correct sex estimates	494	406	466
	Indeterminate estimates	74	178	101
	Classification errors	4	5	7
	% accuracy (LOOCV)	99.20%	98.78%	98.52%
	% indeterminate (LOOCV)	12.94%	30.22%	17.60%

The three columns correspond to three sets of traits initially used as inputs for both methods, that is, Bruzek, 2002 and the probabilistic method based on logistic regressions. ("Complete bones" = all traits; "Sacroiliac module" = {CArc, GrSN1, GrSN2, GrSN3, PrSu1, PrSu2, PrSu3}; "Ischiopubic module" = {IsPu, InfP1, InfP2, InfP3}. "% indeterminate": Percentage of cases that do not reach the classification threshold; "% accuracy": Percentage of correct classification among cases that reach the classification threshold for posterior probability).

TABLE 3 Results of sex assessment per population sample, using the 572 complete bones from the meta-population sample

		Coimbra	HamTodd	London	Paris	Terry
Original Bruzek (2002) method	% accuracy	99.09%	99.07%	97.06%	97.22%	97.97%
	% indeterminate	5.17%	0.92%	4.23%	1.37%	2.96%
Statistical sex estimate (2019)	% accuracy (LOOCV)	98.02%	100%	100%	98.51%	99.42%
	% indeterminate	12.93%	12.84%	12.68%	8.22%	14.78%

"% indeterminate": Percentage of cases that do not reach the classification threshold; "% accuracy": Percentage of correct classification among cases that reach the classification threshold for posterior probability).

True sex\estimated sex	Original Bruzek's (2002) method			Statistical sex estimate (2019)		
	Female	Indeterminate	Male	Female	Indeterminate	Male
Female	254	30	20	208	92	4
Male	10	14	261	1	86	198

TABLE 4 Sex estimation of 589 ossa coxae with no missing values for all the traits related to the sacroiliac module (CArc, PrSu1, PrSu2, PrSu3, GrSN1, GrSN2, GrSN3)

Sex estimates are produced using only those traits. ("indeterminate": Individuals that did not reach the classification threshold of 0.95 for posterior probability).

2005) by introducing a systematic bias on one side, which is not related to sex. Bilateral asymmetry of all traits and characters was evaluated with Cohen's Kappa (Cohen, 1968; Gamer, Lemon, & Singh, 2012), and the results are presented in Table 6. All traits from the ischiopubic complex exhibit a low level of asymmetry, whereas some traits from the sacroiliac complex show a relatively high asymmetry.

GrSN3 shows the highest level of asymmetry. Among the 518 individuals for whom both left and right ossa coxae could be observed, 62 individuals had a strong asymmetry for this trait, that is, female morphology on one side and male morphology on the other side. These individuals are not specific to a given population sample, nor do they present extreme age or stature values, but most of them (47 out of 62) are men (extensive results not presented). However, for both sexes, in most cases (39 out of 62), the right side exhibits a female

form, whereas the left side has a male form. This may suggest a component of directional asymmetry for this trait, whether related to the biomechanics of locomotion or to genetic factors. Interestingly, this trait is not selected among the best predictors in logistic regression models presented in Table 2 after the stepwise algorithm, and its level of asymmetry, by introducing some noise, could be part of the explanation.

Similar but weak observations can be made on other traits recorded on the sacroiliac complex. A single trait, GrSN1, seems to have a more complex pattern of asymmetry, since the presence of a strong asymmetry ("f"/"m") was more frequent within females but without being directional, whereas strong asymmetry was rare within male individuals but possibly directional, with the female shape being generally observed on the right bone.

TABLE 5 Results of sex assessment for the 198 complete and virtually reconstructed ossa coxae (CT-scans, Marseille)

Original Bruzek (2002) method	Correct sex estimates	189
	Indeterminate estimates	5
	Classification errors	4
	% accuracy	97.93%
	% indeterminate	2.53%
Statistical sex estimate (2019)	Traits selected in LR model	IsPu, CArc, PrSu2, InfP3, GrSN1
	Correct sex estimates	174
	Indeterminate estimates	23
	Classification errors	1
	% accuracy	99.43%
	% indeterminate	11.62%

All available traits were initially used as inputs for both methods. The logistic regression model was learned on the 572 complete bones from the meta-population sample. ("% indeterminate": Percentage of cases that do not reach the classification threshold; "% accuracy": Percentage of correct classification among cases that reach the classification threshold for posterior probability).

3.4 | Impact of lateralization on classification results

Since the reference meta-population sample includes a large majority of left bones, it is necessary to evaluate if this choice does impact or not on the ability to produce accurate sex estimates for right bones with the statistical models implemented in PELVIS. We conducted an experiment by selecting on one hand only the 579 left bones among the 1,110 available ossa coxae, and using it as a training sample for logistic regression models. On the other hand, the remaining 531 right bones were used as a test sample in order to evaluate the impact of lateralization on sex estimation. The right bones were estimated using the same algorithm implemented in PELVIS, and the results are presented in Table 7.

As previously shown, a reasonable amount of ossa coxae remain indeterminate (14.3%), but only four out of the 531 right bones were misclassified (0.8%). Lateralization seems to have no impact on the classification results, as this error rate has a similar magnitude as the one obtained in Table 2 for left bones in a leave-one-out cross-validation.

Furthermore, the original Bruzek (2002) method, when applied to the same bones, gives a similar number of left and right bones in the misclassified ossa coxae (10 left bones and 9 right bones, extensive results not presented).

4 | DISCUSSION

A reliable sex estimation of the skeleton is of major importance in bioarchaeology and forensic anthropology. In the adult skeleton, sex

TABLE 7 Sex estimation of 531 right ossa coxae using 579 left ossa coxae as training sample

True sex\sex estimate	Female	Indeterminate	Male
Female	243	21	2
Male	2	57	206

Logistic regression models are used, following the method implemented in the PELVIS R package. ("indeterminate": Individuals that did not reach the classification threshold of 0.95 for posterior probability).

estimation is usually a first step in creating a biological profile because most of the methods currently used for the estimation of ancestry, stature, and age are sex-specific (Klaes et al., 2012; Scheuer, 2002). The accuracy and reliability of the sex estimation from the skeleton depends on the skeletal element, the method proposed, and the degree of sexual dimorphism inherent to the population's morphology. For these reasons, in certain instances, metric methods are better than morphological (visual or nonmetric) ones. However, a recent survey of forensic anthropologists and bioarchaeologists has shown that the methods employed vary considerably with practitioner, and morphoscopic methods are preferred only when both types of methods cannot be used (Klaes, 2013).

Nevertheless, there are several methods that use only a limited portion of the os coxae to estimate sex; these methods use the pubic bone (Klaes et al., 2012; Phenice, 1969), the morphology of the sciatic notch, and the posterior ilium (Ali & MacLaughlin, 1991; Bruzek, Castex, & Majo, 1996; Işcan & Derrick, 1984). The only method that uses the whole hip bone to visually estimate sex was proposed by Bruzek (2002). However, shortcomings of nonmetric methods in general, as summarized by Bruzek (2002), include a high degree of observer subjectivity, a lack of consistency in the evaluation of traits, and a strong dependence on the previous experiences of the observer. To these drawbacks, "one could add that most nonmetric methods generally avoid the use of statistical methods for classification, which often optimize correct classification rates" (Klaes et al., 2012, p. 104).

4.1 | Accuracy rate and definitions of accuracy

This article proposes a statistical approach that provides a quantitative sex estimation based on visual traits of the os coxae. When estimating sex from the skeleton, accuracy is the most common indicator of a method's success. Equally important as method accuracy is a risk of error. The error rate in sex estimation naturally depends on the observation of a single trait. This may be influenced by the observation itself (observer's overall impression or gestalt) but also by the number of evaluated categories of each trait.

After Best et al. (2017), "each anthropologist has his/her own way of dealing with this particular problem, and its solution is based on

TABLE 6 Assessment of the symmetry of the variables using 518 left and right ossa coxae from the five population samples

	PrSu1	PrSu2	PrSu3	PrSu	GrSN1	GrSN2	GrSN3	GrSN	CArc	IsPu	InfP1	InfP2	InfP3	InfP
κ	0.80	0.85	0.67	0.85	0.70	0.69	0.50	0.75	0.76	0.91	0.93	0.88	0.97	0.95

The values indicated are Cohen's kappa with quadratic weighting scheme.

experience, the amount and types of analyses conducted, and familiarity and confidence in the methods used; all of these solidify to form a sort of “gestalt” in the mind of the anthropologist. A gestalt is the unwritten criteria needed to assign a sex category or other determination to a set of unknown remains.” It seems, as a study of sex estimation from the skull showed, that morphoscopic features are evaluated very quickly to provide a “gestalt” assessment (Berg & Tersigni-Tarrant, 2014). This “gestalt” effect also operates unconsciously even when using verbal definitions of categories in visually scored characters (Lewis & Garvin, 2016). For these reasons, it is rather difficult to quantify the part of observer experience when assessing the accuracy and reliability of a method (Novotny, 1981). Both new and experienced observers should achieve the same level of accuracy in determining the sex of an individual (Bruzek & Murail, 2006).

It should be noted that the definition of “accuracy” adopted in this article differs from the one adopted in several previous studies, that is, the percentage of correctly classified individuals among the whole sample. Unlike most other classical methods of sex estimation (e.g., Kales et al., 2012; Phenice, 1969; Walker, 2008), Bruzek’s revised method—as well as DSP2 (Bruzek et al., 2017)—provides three possible outputs: an “indeterminate” output is added to the classical female and male estimates. The notion of “indeterminate” sex estimate is not taken into account in most methods; consequently the accuracy is usually reported as the ratio between the number of individuals correctly estimated and the total number of individuals. Since the revised Bruzek’s method does not guarantee to provide a sex estimate for all individuals, two different rates had to be jointly reported to evaluate its efficiency: (a) “% indeterminate,” the rate of individuals that do not reach the classification threshold, and (b) “% accuracy,” defined as the rate of individuals correctly estimated among nonindeterminate individuals (Tables 2–3, 5). Of note, the traditional estimate of accuracy rate (i.e., the percentage of correctly classified individuals among the whole sample) can still be retrieved from our indicators by calculating $(\% \text{ accuracy}) \times (100 - \% \text{ indeterminate})$.

4.2 | Scoring system

There are different views on the number of categories in the scoring of morphoscopic features; they range from dichotomous (Phenice, 1969) or trichotomous categories (Bruzek, 2002; Novotny, 1981) to a higher number of ordinal categories (Kales et al., 2012; Walker, 2008). Both low and high numbers of categories increase the risk of error. However, biological sex is categorical and noncontinuous (i.e., dichotomous) in nature, and as such, an “ambiguous” category is a representation of an “I don’t know” group, rather than a characteristic class of a sample (McFadden & Oxenham, 2016). The presence of this category is necessary because it reduces the risk of misclassification.

For this reason, another method of evaluation was suggested by Novotny (1981), who replaced a descriptive or ordinal evaluation of characters with trichotomy based on binary scoring (*yes* or *no*) and an intermediate category (*I cannot decide*). This principle was used by Bruzek (2002) and is also preserved in this study. This approach probably reduces the observer’s subjectivity during the evaluation of

selected traits, contrary to the ordinal scoring in which it is difficult to decide between two neighboring categories, for example, “well-developed concavity,” “slight concavity,” and “no concavity.”

4.3 | Comparison between original and revised Bruzek’s methods

The difference between the original Bruzek (2002) method and the new method implemented in the R-Shiny application is not in the visual evaluation of characters but in their further processing. The original method employed and redefined complex variables such as PrSu, GrSN, and InfP based on a combination of individual sub-variables. Therefore, in the case of the preauricular surface (PrSu), the resulting character value is given by combining the results of the evaluations of PrSu1, PrSu2, and PrSu3 according to the principle of majority that corresponds to the sex. In contrast, the method based on logistic regression takes all 11 primary variables separately and combines them in the logistic regression, which also provides posterior probability estimates.

The R-Shiny application implements both methods, since they seem to be complementary. The approach with statistical sex estimates is very accurate but clearly more prudential. Logistic regressions lead to slightly lower classification error than the original method but also to more indeterminate estimates. Conversely, the original Bruzek’s method enables a satisfactory sex estimate even for those individuals remaining indeterminate when using logistic regressions. Indeed, among the 74 ossa coxae (32 female and 42 male bones) remaining indeterminate after applying a logistic regression model on complete bones in leave-one out cross-validation, only 14 of them are still indeterminate when using Bruzek’s (2002) method, and six are misclassified (extensive results available as Supporting Information online). Interestingly, the individuals remaining indeterminate in one method or the other do not necessarily correspond, which indicates that the original method can provide a useful trend when the statistical models do not allow to conclude.

Finally, despite the presence of a moderate amount of asymmetry for certain traits, laterality does not affect the classification results. As shown in Table 7, the statistical models learned on left bones ensure an accurate sex estimation of right bones. Additionally, left bones and their right counterparts were numbered similarly among classification errors using the original Bruzek (2002) method. Consequently, it is confirmed that both methods provide reliable results regardless of laterality. The use of several traits showing a high level of sexual dimorphism makes it possible to dampen any asymmetry-related idiosyncrasy possibly presented by one of them.

4.4 | Future directions

The R package presented in this article, PELVIS, will be maintained by the corresponding author and is likely to receive regular updates. Several improvements and developments can be considered for the future of this package and this method. Two improvements can be considered for the traits used in Bruzek’s method. The first one could

be the inclusion of Phenice (1969) traits. The second, as discussed above, would consist in testing and evaluating a wider five-step scale ("F," "F?," "I," "M?," "M") than the current trichotomic scheme ("f," "i," "m") to determine which rating is better.

Finally, some more research effort is planned as concerns the statistical processing of the observed traits. In a recent article, Konigsberg and Frankenberg (2019) expressed some concerns on the traditional approach using logistic regression for sex estimation from visual traits. In this important contribution, Konigsberg and Frankenberg's remarks were directed to Kales et al.'s (2012) method, but the discussion they initiated is also valuable to provide future directions for improving Bruzek's method. Among the comments they made on Kales et al.'s method, two of them (the absence of variable selection in logistic regression models, and the difficulty to apply a different logistic regression model on each given bone depending on the trait values that could be taken on it) are natively addressed in our R package PELVIS in a fully automatized way. However, we do agree with Konigsberg and Frankenberg (2019), and with Kales, Ousley, and Vollner (2019, p. 2), that the use of modern machine learning techniques should be tested in search for a better classification accuracy; although we already noted in a previous study (Santos, Guyomarc'h, & Bruzek, 2014) that using modern classifiers involves an increase in complexity and execution time which is not always paid off by a similar increase in classification accuracy. For the present study, we performed simulations using modern classifiers such as random forests on Bruzek's morphoscopic data, that did not allow any improvement compared to logistic regressions (both results and R code are provided as Supporting Information online). The rather simple approach by logistic regression is competitive here, given the level of sexual dimorphism observed for Bruzek's nonmetric traits. Nonetheless, we are still testing other recent statistical methods, and some new tools are likely to be made available in the R package PELVIS if a substantially better classification accuracy can be achieved. In all cases, a new short validation study will be performed and submitted along with any major change made in PELVIS. As noted by Kales et al. (2019, p. 2), "analytical methods will continue to improve, and we should adjust and adapt accordingly."

5 | CONCLUSIONS

Generally, visual sex estimation using the os coxae produces highly accurate classifications, although the approach is considerably more subjective than the morphometric assessment of sex (Johnstone-Belford, Flavel, & Franklin, 2018). The Bruzek (2002) method is widely used by the bioarchaeology community in Europe and gained a more global acceptance in the forensic practice during the last few years. To overcome the population-specificity of sex estimation methods and strengthen the method by providing statistics of reliability, this study proposed a new tool to estimate the sex of an individual from scoring visual traits of the os coxae through models based on a meta-population of more than a thousand individuals of known sex. Scoring of these traits on CT-scan reconstructed models provided similar

results to the scoring of physical bones. The improved Bruzek method has an accuracy rate of more than 99% with an average rate of 13% indeterminate results on complete bones. Although the level of indeterminacy is higher than the metric method, the level of certainty in sexing is still optimal.

ACKNOWLEDGMENTS

The authors would like to thank Radka Firlova for the segmentation of the CT-scans, and Élodie Bernardeau for the logo design of the R-Shiny application. This work was supported by Charles University Grant Agency (GAUK No. 1088217) and the Czech Science Grant Foundation (GAČR No. 14-228235).

DATA ACCESSIBILITY

The data that support the findings of this study are openly available in Zenodo at <https://doi.org/10.5281/zenodo.2586897>, reference number 2589917.

ORCID

Frédéric Santos  <https://orcid.org/0000-0003-1445-3871>

Pierre Guyomarc'h  <https://orcid.org/0000-0002-9419-9270>

Rebeka Rmoutilova  <https://orcid.org/0000-0003-2426-4521>

REFERENCES

- Ali, R. S., & MacLaughlin, S. M. (1991). Sex identification from the auricular surface of the adult human ilium. *International Journal of Osteoarchaeology*, 1(1), 57–61. <https://doi.org/10.1002/oa.1390010108>
- Berg, G. E., & Kenyhercz, M. W. (2017). Introducing human mandible identification [(hu)MANid]: A free, web-based GUI to classify human mandibles. *Journal of Forensic Sciences*, 62(6), 1592–1598. <https://doi.org/10.1111/1556-4029.13479>
- Berg, G. E., & Tersigni-Tarrant, M. A. (2014). *Sex and ancestry determination: assessing the 'gestalt'*. Proceedings of the 66th Annual Scientific Meeting of the American Academy of Forensic Sciences; 2014 Feb 17–22; Seattle, WA. Colorado Springs, CO: American Academy of Forensic Sciences.
- Best, K. C., Garvin, H. M., & Cabo, L. L. (2017). An investigation into the relationship between human cranial and pelvic sexual dimorphism. *Journal of Forensic Sciences*, 63, 990–1000. <https://doi.org/10.1111/1556-4029.13669>
- Betti, L. (2014). Sexual dimorphism in the size and shape of the os coxae and the effects of microevolutionary processes. *American Journal of Physical Anthropology*, 153(2), 167–177. <https://doi.org/10.1002/ajpa.22410>
- Black, S., & Ferguson, E. (2011). *Forensic anthropology: 2000 to 2010*. Boca Raton, FL: CRC Press.
- Bruzek, J. (2002). A method for visual determination of sex, using the human hip bone. *American Journal of Physical Anthropology*, 117, 157–168. <https://doi.org/10.1002/ajpa.10012>
- Bruzek, J., Castex, D., & Majo, T. (1996). Évaluation des caractères morphologiques de la face sacro-pelvienne de l'os coxal. Proposition d'une nouvelle méthode de diagnose sexuelle. *Bulletins et Mémoires de la Société d'Anthropologie de Paris*, 8, 491–502.

- Bruzek, J., Franciscus, R. G., Novotny, V., & Trinkaus, E. (2006). The assessment of sex. In E. Trinkaus & J. Svoboda (Eds.), *Early modern human evolution in Central Europe: The people of Dolní Věstonice and Pavlov* (pp. 46–62). New York, NY: Oxford University Press.
- Bruzek, J., & Murail, P. (2006). Methodology and reliability of sex determination from the skeleton. In A. Schmitt, E. Cunha, & J. Pinheiro (Eds.), *Forensic anthropology and medicine*. Totowa, NJ: Humana Press.
- Bruzek, J., Rmoutilova, R., Guyomarc'h, P., & Santos, F. (2019). Supporting data for: A method of sexing the human os coxae based on logistic regressions and Bruzek's nonmetric traits [Data set]. *Zenodo*. <http://doi.org/10.5281/zenodo.2589917>
- Bruzek, J., Santos, F., Dutailly, B., Murail, P., & Cunha, E. (2017). Validation and reliability of the sex estimation of the human os coxae using freely available DSP2 software for bioarchaeology and forensic anthropology. *American Journal of Physical Anthropology*, 164(2), 440–449. <https://doi.org/10.1002/ajpa.23282>
- Chang, W., Cheng, J., Allaire, J. J., Xie, Y., & McPherson, J. (2018). Shiny: Web application framework for R. R package version 1.2.0. <https://CRAN.R-project.org/package=shiny>
- Cohen, J. (1968). Weighted kappa: Nominal scale agreement with provision for scaled disagreement or partial credit. *Psychological Bulletin*, 70, 213–220.
- Debono, L., & Mafart, B. (2006). Sex determination from fragmented hip bones using the Bruzek method: Experience in a historic necropolis in Provence (France). *Anthropologie (Brno)*, 44(2), 167–172.
- Dirkmaat, D. C. (2012). *A companion to forensic anthropology*. Hoboken, NJ: Blackwell Publishing Ltd.
- Đurić, M., Rakočević, Z., & Đonić, D. (2005). The reliability of sex determination of skeletons from forensic context in the Balkans. *Forensic Science International*, 147(2–3), 159–164. <https://doi.org/10.1016/j.forsciint.2004.09.111>
- Dutailly, B., Coqueugniot, H., Desbarats, P., Gueorguieva, S., & Synave, R. (2009). 3D surface reconstruction using HMM algorithm. IEEE International Conference on Image Processing (ICIP09), pp. 2505–2508.
- Esteve-Altava, B. (2017). In search of morphological modules: A systematic review. *Biological Reviews*, 92(3), 1332–1347. <https://doi.org/10.1111/brv.12284>
- Ferembach, D., Schwidetzky, I., & Stloukal, M. (1980). Recommendations for age and sex diagnoses of skeletons. *Journal of Human Evolution*, 9, 517–549.
- Gamer, M., Lemon, J., & Singh, I. (2012). irr: Various coefficients of inter-rater reliability and agreement. R package version 0.84. <https://CRAN.R-project.org/package=irr>
- Garvin, H. M., Sholts, S. B., & Mosca, L. A. (2014). Sexual dimorphism in human cranial trait scores: Effects of population, age, and body size. *American Journal of Physical Anthropology*, 154(2), 259–269. <https://doi.org/10.1002/ajpa.22502>
- Genoves, S. (1959). L'estimation des différences sexuelles dans l'os coxal: différences métriques et différences morphologiques. *Bulletins et Mémoires de la Société d'Anthropologie de Paris*, 10, 3–95.
- Gómez-Valdés, J. A., Garmendia, A. M., García-Barzola, L., Sánchez-Mejorada, G., Karam, C., Baraybar, J. P., & Kales, A. (2017). Recalibration of the Kales et al. (2012) method of sexing the human innominate for Mexican populations. *American Journal of Physical Anthropology*, 162, 600–604. <https://doi.org/10.1002/ajpa.23157>
- Hager, L. D. (1989). *The evolution of sex differences in the hominid bony pelvis*. Berkeley, CA: University of California.
- Hager, L. D. (1996). Sex differences in the sciatic notch of great apes and modern humans. *American Journal of Physical Anthropology*, 99, 287–300.
- Hammond, A. S., Royer, D. F., & Fleagle, J. G. (2017). The Omo-Kibish I pelvis. *Journal of Human Evolution*, 108, 199–219. <https://doi.org/10.1016/j.jhevol.2017.04.004>
- Houghton, P. (1974). The relationship of the pre-auricular groove of the ilium to pregnancy. *American Journal of Physical Anthropology*, 41(3), 381–389. <https://doi.org/10.1002/ajpa.1330410305>
- Işcan, M., & Derrick, K. (1984). Determination of sex from the sacroiliac joint: A visual assessment technique. *Florida Scientist*, 47(2), 94–98.
- Işcan, M. Y., & Steyn, M. (2013). *The human skeleton in forensic medicine*. Springfield, IL: Charles C Thomas Publisher.
- Johnstone-Belford, E., Flavel, A., & Franklin, D. (2018). Morphoscopic observations in clinical pelvic MDCT scans: Assessing the accuracy of the Phenice traits for sex estimation in a Western Australian population. *Journal of Forensic Radiology and Imaging*, 12, 5–10. <https://doi.org/10.1016/j.jofri.2018.02.003>
- Kachlik, D., Musil, V., & Baca, V. (2018). Contribution to the anatomical nomenclature concerning lower limb anatomy. *Surgical and Radiologic Anatomy*, 40(5), 537–562.
- Kenyhercz, M. W., Kales, A. R., Stull, K. E., McCormick, K. A., & Cole, S. J. (2017). Worldwide population variation in pelvic sexual dimorphism: A validation and recalibration of the Kales et al. method. *Forensic Science International*, 277, 259–e1. <https://doi.org/10.1016/j.forsciint.2017.05.001>
- Kales, A. R. (2013). *Current practices in forensic anthropology for sex estimation in unidentified, adult individuals*. Proceedings of the 65th Annual Meeting of the American Academy of Forensic Sciences; February 18–23; Washington, DC. Colorado Springs, CO: American Academy of Forensic Sciences.
- Kales, A. R., & Cole, S. J. (2018). *MorphoPASSE: The morphological pelvis and skull sex estimation database manual. Version 1.0*. Topeka, KS: Washburn University.
- Kales, A. R., Ousley, S., & Vollner, J. (2019). Response to multivariate ordinal probit analysis in the skeletal assessment of sex (Konigsberg and Frankenberg). *American Journal of Physical Anthropology*, 149(1), 104–114. <https://doi.org/10.1002/ajpa.23830>
- Kales, A. R., Ousley, S. D., & Vollner, J. M. (2012). A revised method of sexing the human innominate using Phenice's nonmetric traits and statistical methods. *American Journal of Physical Anthropology*, 169(2), 388–389. <https://doi.org/10.1002/ajpa.22102>
- Konigsberg, K. W., & Frankenberg, S. R. (2019). Multivariate ordinal probit analysis in the skeletal assessment of sex. *American Journal of Physical Anthropology*, 169(2), 385–387. <https://doi.org/10.1002/ajpa.23832>
- Langley, N. R., Dudzik, B., & Cloutier, A. (2018). A decision tree for non-metric sex assessment from the skull. *Journal of Forensic Sciences*, 63(1), 31–37. <https://doi.org/10.1111/1556-4029.13534>
- Le, S., Josse, J., & Husson, F. (2008). FactoMineR: An R package for multivariate analysis. *Journal of Statistical Software*, 25(1), 1–18. <https://doi.org/10.18637/jss.v025.i01>
- Lesciotto, K. M., & Doershuk, L. J. (2018). Accuracy and reliability of the Kales et al. (2012) Morphoscopic pelvic sexing method. *Journal of Forensic Sciences*, 63, 214–220. <https://doi.org/10.1111/1556-4029.13501>
- Lewis, C. J., & Garvin, H. M. (2016). Reliability of the Walker cranial nonmetric method and implications for sex estimation. *Journal of Forensic Sciences*, 61(3), 743–751. <https://doi.org/10.1111/1556-4029.13013>
- Linderholm, A., & Kjellström, A. (2011). Stable isotope analysis of a medieval skeletal sample indicative of systemic disease from Sigtuna Sweden. *Journal of Archaeological Science*, 38(4), 925–933. <https://doi.org/10.1016/j.jas.2010.11.022>
- Löhr, P. (1894). Ueber den Sulcus praeauricularis des Darmbeins und ähnliche Furchen anderer Knochen. *Anatomischer Anzeiger*, 9, 521–536.
- Martin, M. A. (2019). Biological anthropology in 2018: Grounded in theory, questioning contexts, embracing innovation. *American Anthropologist*, 121, 417–430. <https://doi.org/10.1111/aman.13233>
- McFadden, C., & Oxenham, M. F. (2016). Revisiting the Phenice technique sex classification results reported by MacLaughlin and Bruce (1990). *American Journal of Physical Anthropology*, 159, 182–183. <https://doi.org/10.1002/ajpa.22839>
- Mestekova, S., Bruzek, J., Velemínska, J., & Chaumoitre, K. (2015). A test of the DSP sexing method on CT images from a modern French

- sample. *Journal of Forensic Sciences*, 60, 1295–1299. <https://doi.org/10.1111/1556-4029.12817>
- Nikita, E. (2017). *Osteoarchaeology: A guide to the macroscopic study of human skeletal remains*. Cambridge, MA: Academic Press.
- Novotny, V. (1981). *Pohlavni rozdíly a identifikace pohlaví panevní kosti (Sex differences and identification of sex in pelvic bone)*. (PhD Thesis). University of Purkyne, Brno.
- Nuijten, M. (2019). Practical tools and strategies for researchers to increase replicability. *Developmental Medicine and Child Neurology*, 61, 535–539. <https://doi.org/10.1111/dmcn.14054>
- Phenice, T. W. (1969). A newly developed visual method of sexing the os pubis. *American Journal of Physical Anthropology*, 30(2), 297–301.
- R Core Team (2019). *R: A language and environment for statistical computing*. Vienna, Austria: R Foundation for Statistical Computing.
- Roksandic, M., Djurić, M., Rakočević, Z., & Seguin, K. (2006). Interpersonal violence at Lepenski Vir Mesolithic/Neolithic complex of the iron gates gorge (Serbia-Romania). *American Journal of Physical Anthropology*, 129(3), 339–348. <https://doi.org/10.1002/ajpa.20286>
- Rosenberg, K., & Trevathan, W. (2002). Birth, obstetrics and human evolution. *BJOG: An International Journal of Obstetrics & Gynaecology*, 109, 1199–1206. <https://doi.org/10.1046/j.1471-0528.2002.00010.x>
- Samsel, M., Knüsel, C. J., & Villotte, S. (2016). Réévaluation du sexe et de l'âge au décès du sujet azilien Le Peyrat 5, Saint-Rabier (Dordogne, France). *Bulletins et Mémoires de la Société d'Anthropologie de Paris*, 28 (3–4), 213–220. <https://doi.org/10.1007/s13219-016-0162-9>
- Santos, F., Guyomarc'h, P., & Bruzek, J. (2014). Statistical sex determination from craniometrics: Comparison of linear discriminant analysis, logistic regression, and support vector machines. *Forensic Science International*, 245, 204.e1–204.e8. <https://doi.org/10.1016/j.forsciint.2014.10.010>
- Ščēsnaite-Jerdiakova, A., Pliss, L., Gerhards, G., Gordina, E. P., Gustiņa, A., Pole, I., Zole, E., Kimsis, J., Jansone, I., & Ranka, R. (2015). *Morphological characterisation and molecular sex determination of human remains from the 15th–17th centuries in Latvia*. Proceedings of the Latvian Academy of Sciences. Section B. Natural, Exact, and Applied Sciences. (Vol. 69, No. 1–2, pp. 8–13). De Gruyter Open.
- Scheuer, L. (2002). Application of osteology to forensic medicine. *Clinical Anatomy*, 15(4), 297–312.
- Schultz, A. H. (1930). The skeleton of trunk and limbs of higher primates. *Human Biology*, 2, 303–348.
- Trinkaus, E. (2016). The sexual attribution of the La Quina 5 Neandertal. *Bulletins et Mémoires de la Société d'Anthropologie de Paris*, 28(3–4), 111–117. <https://doi.org/10.1007/s13219-016-0159-4>
- Ulucam, E., Alicioglu, B., Cikmaz, S., Yilmaz, A., & Sut, N. (2009). The morphometric analysis of crista phallica in identification of sexes. *International Journal of Morphology*, 27, 977–980. <https://doi.org/10.4067/S0717-95022009000400002>
- Venables, W. N., & Ripley, B. D. (2002). *Modern applied statistics with S*. New York, NY: Springer.
- Walker, P. L. (2008). Sexing skulls using discriminant function analysis of visually assessed traits. *American Journal of Physical Anthropology*, 136 (1), 39–50. <https://doi.org/10.1002/ajpa.20776>
- Walker, P. L. (2005). Greater sciatic notch morphology: Sex, age, and population differences. *American Journal of Physical Anthropology*, 127(4), 385–391. <https://doi.org/10.1002/ajpa.10422>
- Washburn, S. L. (1948). Sex differences in the pubic bone. *American Journal of Physical Anthropology*, 6, 199–207.
- White, T. D., & Folkens, P. A. (2005). *The human bone manual*. Amsterdam; Boston, MA: Elsevier Academic.
- Zaaijer, T. (1866). Untersuchungen über die Form des Beckens javanischen Frauen. *Naturrk Verhandl Holland Maatsch Ventensch Haarlem*, 24, 1–42.

SUPPORTING INFORMATION

Additional supporting information may be found online in the Supporting Information section at the end of this article.

How to cite this article: Santos F, Guyomarc'h P, Rmoutilova R, Bruzek J. A method of sexing the human os coxae based on logistic regressions and Bruzek's nonmetric traits. *Am J Phys Anthropol*. 2019;1–13. <https://doi.org/10.1002/ajpa.23855>

Supporting information (Appendix S1 to S3) to the paper Santos et al. (2019) concern the use of the R application and can be found online <https://onlinelibrary.wiley.com/doi/full/10.1002/ajpa.23855>. Likewise, the raw data are available here <https://doi.org/10.5281/zenodo.2586897>.